University of Strathclyde
Department of Pure and Applied Chemistry

RESPONSIVE EMULSIFIERS BASED ON PEPTIDE SELF-ASSEMBLY

by

INÊS PIMENTEL MOREIRA

A thesis submitted to the Department of Pure and Applied Chemistry, University of Strathclyde, in part fulfillment of the regulations for the degree of Doctor of Philosophy in Chemistry.

2017

Declaration

This thesis is the result of the author's original research. It has been composed by the author and has not been previously submitted for examination which has led to the award of a degree.

Signed:

Date:

Believe you can and you are halfway there.

Theodore Roosevelt

Acknowledgements

First of all, I would like to thank my supervisors, Dr. Tell Tuttle and Prof. Rein Ulijn, for giving me the exceptional opportunity to be part of their groups, for their guidance, constant advice and encouragement throughout this research project.

I am grateful to Dr. Dimitrios Lamprou. Thanks also go to Margaret Mullin from the University of Glasgow for the help with TEM and SEM, Dr. Tong Wang from City University of New York with TEM and Gillian Robb with fluorescence microscopy. Thank you to the technicians of the analytical facilities at the Chemistry Department of the University of Strathclyde and to Isabel Scott for all the help with paper-work matters. Results were obtained using the EPSRC funded ARCHIE-WeSt High Performance Computer (www.archie-west.ac.uk; EPSRC grant no. EP/K000586/1).

I also need to acknowledge the financial support by the EC 7th Framework Programme Marie Curie Actions and all SMARTNET members for the knowledge exchange. Thanks to Dr. Mikel Morvan, Dr. Patrick Moreau and Dr. Roberto Company for hosting me in their team at Laboratoire du Futur, Solvay, in Bordeaux. My 3-month placement was a very positive professional experience. Thanks to Laura for welcoming me there and embracing me in her group of friends. To Vânia, Jorge, Serhii, Matija, Tomasz (thanks for the good time and help while in Glasgow), Philip, Kars, Nishant, Marco, Ana Catarina: we had a great time during all the meetings and I feel lucky to have been part of such a nice group.

I would also like to thank all the past and present members of the Tuttle and Ulijn groups for helpful discussions at group meetings, conferences and coffee breaks. The good environment and fun times in and outside the lab were essential. In particular, thanks to Meghan for being my initial mentor in synthesis, to Dan for making me laugh when scripting, to Krystyna for being so kind and for the good chats, to Babis for his support during my stay in NYC, to Flo for the chococino company and to Gary for being my emulsions pal and help with the co-assembled submission scripts.

Thank you Mari for all the shared special moments along this journey, which included hosting me in my first weeks in Glasgow, the travelling, the eating and the good talks. To Iván, thanks for all your help from the beginning, even before I arrived, and for being able to gather everyone as a group, even being Iván. Ana, thanks for your invaluable friendship, for your hug and for always being there for a chat about anything and everything. My stay in Glasgow was an incredibly good experience thanks to my Glasgow Family, who was essential to make me feel at home throughout these 3 years. Kiko, Paula, Davide, Andreia, Laura, Miguel, together with the aforementioned: I will never forget our international dinners, games, hikings and trips around Scotland!

Muito obrigada to my amazing family and friends from Portugal for encouraging me to embrace this challenge, for always being present during my physical absence and for the quality short time when visiting. To both Mariana and Sophia, thanks for the support, it is incredible how distance can make friendship stronger.

Most importantly, I am incredibly grateful to my parents, Teresa and Benjamim, and my sister Rita, my models to follow in life. Your love and support brought me where I am today. Thank you for, more than me, believing I could do it and for the constant encouraging words throughout this whole experience.

Nuno, my thank you is not enough… Your patience, kindness and cheerfulness were key. You have been with me through all the good and bad moments, and I would have never done it without you. It is rewarding to know I am sharing my life with you.

The Author

Publications

- **Moreira, Inês P.**; Sasselli, Ivan R.; Cannon, Daniel A.; Hughes, Meghan; Lamprou, Dimitrios A.; Tuttle, Tell; Ulijn, Rein V. Enzymatically activated emulsions stabilised by interfacial nanofibre networks. *Soft Matter*, **2016**, 12 (9), 2623-2631.

As first author of this article, I was responsible for performing all experimental and computational work, along with manuscript preparation and submission, with help from others in different techniques. The work carried out is discussed in Chapter 3 of this thesis.

- **Moreira, Inês P.**; Piskorz, Tomasz K.; van Esch, Jan H.; Tuttle, Tell; Ulijn, Rein V. Biocatalytic self-assembly of tripeptide gels and emulsions. *Langmuir,* **2017**, 33 (20) 4986-4995.

As first author of this article, I was responsible for performing all experimental and computational work, along with manuscript preparation and submission, with help from the second author in logP calculations for validation of parameterisation. The work carried out is discussed in Chapter 4 of this thesis.

- **Moreira, Inês P.**; Scott, Gary; Ulijn, Rein V.; Tuttle, Tell. Computational prediction of tripeptide-dipeptide co-assembly. *Chem Comm*, **2017**, Manuscript in preparation.

As first author of this article, I was responsible for performing all experimental and computational work, with help from the second author in calculation submission scripts. The work carried out is discussed in Chapter 5 of this thesis.

- Ulijn, Rein; Tuttle, Tell; **Moreira, Inês**; Scott, Gary; McKnight, Paul John; Ruck, Martin Edwin. Stable Emulsions. PCT Int Appl., **2015**, 46 pp. Patent application.

As a co-author of this patent application, I was responsible for performing some of the experimental and computational work referenced. The work in this is also related to the Chapter 3 of this thesis.

- Sasselli, Ivan R.; **Moreira, Inês P.**; Ulijn, Rein V.; Tuttle, Tell. Molecular Dynamics Simulations Reveal Disruptive Self-Assembly in Dynamic Peptide Libraries. Submitted to *Organic and Biomolecular Chemistry* in May 2017.

As a co-author of this article, I performed some experimental tests. The work carried out here is not directly related with this thesis.

Conferences

1. MGMS M3 Modelling Molecules and Materials (20-22nd August 2014), Poster – 'Self-assembly and molecular simulation of aromatic dipeptide amphiphiles at oil/water interfaces'

2. Nanopeptide 2015 (2-4th March 2015), Poster – 'Enzymatically triggered emulsifiers based on aromatic peptide amphiphiles – Interactions and Interface Behaviour'

3. Scotchem Computational Chemistry (26th June 2015), Poster – 'Enzymatically Triggered Interfacial Nanofibre Networks as On-demand Stabilised Emulsions'

4. Active and Adaptive Materials (22-23rd October 2015), Poster – 'Enzymatically activated emulsions stabilized by interfacial self-assembled structures'

5. MRS Spring Meeting (28th March-1st April 2016), Oral presentation – 'Enzymatically Activated Emulsions Stabilized by Interfacial Self-Assembled Structures'

6. Conference on Gels, Formulations and Supramolecular Materials (9-10th June 2016), Poster – 'Responsive emulsifiers achieved by enzyme-triggered self-assembly of simplistic short peptides'

7. Bio | Nano | Med Colloquium (23-24th June 2016), Poster – 'Responsive emulsifiers achieved by enzyme-triggered self-assembly of simplistic short peptides'

Abbreviations

3D	Three-Dimensional
AA	All-Atom
AFM	Atomic Force Microscopy
AP	Aggregation Propensity / Alkaline Phosphatase
CD	Circular Dichroism
CG	Coarse-Grained
CHARMM	Chemistry at HARvard Macromolecular Mechanics
DFT	Density Functional Theory
DIPEA	N,N-Diisopropylethylamine
DNA	Deoxyribonucleic Acid
Fmoc	9-fluorenylmethoxycarbonyl
FTIR	Fourier Transform Infrared Spectroscopy
HBTU	O-Benzotriazole-N,N,N',N'-tetramethyl-uronium-hexafluoro-phosphate
HPLC	High Performance Liquid Chromatography
LJ	Lennard-Jones

LMWG	Low Molecular Weight Gelator
MAXE	Maximum Error
MD	Molecular Dynamics
MINE	Minimum Error
MM	Molecular Mechanics / Molar Mass
MS	Mass Spectroscopy
MUE	Mean Unsigned Error
NAMD	Nanoscale Molecular Dynamics
NMR	Nuclear Magnetic Resonance
PBC	Periodic Boundary Conditions
QM	Quantum Mechanics
RNA	Ribonucleic Acid
RT	Room Temperature
SASA	Solvent-Accessible Surface Area
SDS	Sodium Dodecyl Sulphate
SEM	Scanning Electron Microscopy
TEM	Transmission Electron Microscopy
TLC	Thin Layer Chromatography
VMD	Visual Molecular Dynamics
WAXS	Wide-Angle X-ray Scattering
XRD	X-ray Diffraction

Abstract

The molecular self-assembly of aromatic peptide amphiphiles has raised interest through the last decades due to the possibility to form different nanostructures in aqueous medium, depending on the sequence, kinetics and established non-covalent interactions. Enzyme-triggered self-assembly gives an extra spatiotemporal control over the assembling process when initiating, *e.g.*, fibre formation and consequent gelation under physiological unchanged conditions. The development of natural alternative types of emulsifiers is critical and more recently sought within the cosmetic/food industries. Peptides can act as surfactants if they are designed to present an amphiphilic nature, and can also be switchable if designed to respond to stimuli, which would be attractive for different applications.

An alkaline phosphatase is used to transform phosphorylated precursors into self-assembling aromatic-capped dipeptide amphiphiles, providing a route to trigger self-assembly of nanofibrous networks and hydrogels in aqueous medium. The same mechanism is proven for unprotected tripeptides, where the kinetic control, tuned by the amount of enzyme used, is shown to play a key role in dictating the morphology of the nanofibrous networks produced and consequent hydrogel stiffness.

When the aromatic dipeptide amphiphiles or amphiphilic tripeptides are used in biphasic systems, nanofibrous networks are shown to self-assemble preferentially at the aqueous/organic interface or vicinity, thereby stabilising the oil-in-water droplet

dispersions. Alkaline phosphatase is shown to be active in aqueous-organic solvent systems, in approximately the same extent as in aqueous buffer. Different experimental and computational techniques are used to obtain further insight on the supramolecular interactions responsible for the self-assembly process, in both aqueous and biphasic systems. The ability of on-demand emulsification is shown by the addition of the enzyme to the biphasic de-emulsified mixture after storage for different times, proving these two kinds of peptidic systems can be used as responsive emulsifiers. In addition, the possibility of controlling the emulsification extent by taking advantage of the dephosphorylation kinetics and consequent formation of different stabilising fibrous networks is shown.

The use of a non-covalent trigger for the formation of a specific structure can also be attractive for various applications. The possibility of achieving innovative functional materials through co-assembly of tripeptides and dipeptides is also studied. A computational screening approach has been developed for the creation of design rules to produce hydrogelators and better emulsifiers.

In this work, the possibility of on-demand emulsification when using biocatalytically-triggered self-assembly of short peptide amphiphiles was shown for the first time. The time control and tuning over the emulsifying ability extent was also proved. Additionally, design methods allow for the identification of promising candidates for numerous types of materials. Co-assembled tripeptides and dipeptides can be carefully designed to give rise to hydrogels and effective emulsifiers, which can be highly attractive for different applications.

Table of Contents

List of Figures

List of Tables

1 Introduction

1.1 Project Motivation

Self-assembly is a bottom-up method that spontaneously produces larger ordered systems based on simple building blocks.[1] Peptide based nanostructures that undergo self-assembly have been exploited in recent years for diverse applications. This increased interest is due to the possibility of producing different architectures depending on the molecular structure of the starting materials and on the kinetics of formation. The understanding of the non-covalent interactions responsible for self-assembly to occur is key and can be obtained by a combination of experimental and computational techniques. It has been proven that the hydrophobic effect, H-bonding and π-stacking are the most prevalent, with the relative importance of each of these dependent on the peptide sequence.[2]

A variety of stimuli can be used to trigger self-assembly, which gives further control over the process. Enzymes have been employed to convert non-assembled precursors into self-assembling molecules. By using an enzymatically-triggered assembly, kinetically trapped structures are normally achieved, which can be controlled by changing the enzyme concentration.[3]

Surfactants are extensively used in a range of detergent, cosmetic and food industries. Although they are effective, some of them are toxic, non-biocompatible and present undesirable environmental impact. Some alternatives of surfactants have been studied and used throughout the years, with some recent examples focused on the development of peptidic surfactants based on naturally occurring building blocks.[4] In addition, effort has also been dedicated to the development of switchable emulsifiers. The ability of controlling the surfactant activity until needed, create foam or get removed from the product stream after it is no longer needed can be highly attractive for different applications.[5] It would be advantageous to design responsive simpler emulsifiers based on enzyme-triggered self-assembly of short peptides. The ability to control emulsification under constant and physiological conditions can be promising for different cosmetics and the food industry.

1.2 Project Aims

The main aims of this research project are to develop responsive emulsifiers as alternatives to traditional surfactants. The ability of short peptide molecules to stabilise emulsions on-demand upon enzyme-triggered self-assembly is assessed. Specifically, the objectives are to:

i) Study the feasibility of enzymatically triggered self-assembly of different amphiphilic peptides to stabilise oil-in-water emulsions

ii) Understand the supramolecular interactions present in the final self-assembled structures by using experimental and computational techniques

iii) Assess the possibility of controlling the emulsification extent under kinetic control, by varying the enzyme concentration

iv) Elucidate the structure/function relationships by altering molecular structure and peptide sequence, using modified and unmodified short peptide amphiphiles

v) Evaluate the possibility of creating new hydrogelators and emulsifiers through co-assembly of short peptides

1.3 Layout of the Thesis

This thesis is divided into different chapters. It begins with an extensive literature review, which covers the relevant background and is divided into four subsections. The first two are related to each other and focus, in gradually increased detail, on biocatalytically triggered self-assembly of short peptide nanostructures. The diversity of building blocks that can be used for the self-assembly of different peptide-based architectures is discussed, along with the supramolecular interactions responsible for assembly and gelation. The enzyme-

triggered self-assembly is then reviewed, focusing on different systems that use kinetic and/or thermodynamic control. The third subsection focuses on emulsions, traditionally used surfactants and emulsification alternatives, including stimuli-responsive emulsifiers. The last section of literature review presents an introduction to molecular dynamics simulations of these peptidic systems.

The following chapters are experimental chapters. Each of these is presented separately with its own Introduction, Results & Discussion and Materials & Methods to allow for a more organised story of the overall research. The first experimental chapter (Chapter 3) investigates the enzymatically triggered 9-fluorenylmethoxycarbonyl (Fmoc)-peptide amphiphiles and their use as responsive emulsifiers. Alkaline phosphatase enzyme is used for the biocatalytic formation of hydrogelator Fmoc-tyrosyl-leucine-OH (Fmoc-YL) from its phosphorylated precursor in water. Extensive experimental characterisation and atomistic molecular modelling of Fmoc-YL and Fmoc-Y*p*L are described in order to gain further insight on the supramolecular interactions responsible for their preferred assemblies. The enzymatically triggered self-assembly is then studied in a biphasic system of chloroform and water, to assess the ability of Fmoc-YL to self-assemble at the interface, forming an entangled nanofibrous network that stabilises oil-in-water emulsions on-demand.

Chapter 4 focuses on the assessment of unmodified simple tripeptides to undergo enzyme-triggered self-assembly that can be more attractive for cosmetics and food applications. The gelator H-lysyl-tyrosyl-phenylalanine-OH (KYF) is produced upon the addition of alkaline phosphatase to its non-assembling phosphorylated precursor. Different enzyme concentrations were used, for which the supramolecular interactions, mechanical and morphological properties were assessed to evaluate the kinetic control over the final assembled structures. Coarse-grained simulations of KYF and KY*p*F are also carried out to compare behaviours and correlate the supramolecular interactions and final properties of the materials. This system is then employed in a rapeseed oil/water mixture to evaluate the capability of emulsion stabilisation by the formation of nanofibres and/or viscosity increase. In addition to time-control, the ability to use the kinetic control to tune emulsion stability by using different enzyme concentrations is assessed.

In Chapter 5, the possibility of creating new functional peptidic materials that can be useful for various applications through co-assembly is studied using a coarse-grained molecular dynamics screening approach. The screening and design of hydrogelators is carried out by computationally simulating all possible dipeptides in the presence of a non-capped tripeptide H-aspartyl-phenylalanyl-phenylalanine-OH (DFF), which was previously shown to form bilayers and aqueous solutions. The use of a non-covalent trigger for the formation of specific supramolecular structures is attractive as it avoids the need to chemically modify the peptides. The generation of design rules for the production of more effective emulsifiers that form interfacial nanofibrous networks *via* the cooperative co-assembly between DFF and dipeptides is then carried out, which can be highly useful for different applications.

To finalise, an overall conclusion highlights the main findings within the reported research. Further work guidelines to be carried on the continuation of this project are also presented. These include a preliminary experimental test, which is carried out following Chapter 5, of hydrogelators and emulsifiers, in order to verify if desired co-assembled materials can be designed through MD simulations.

2 Literature Review

2.1 Peptide Nanostructures

Peptide based materials have been increasingly researched throughout the last decades in numerous different areas, such as tissue engineering, drug delivery, optical and electronic devices, cell scaffolding, among others.[6-7] The use of peptides as building blocks presents some advantages over conventional polymeric materials. Peptides are naturally occurring molecules that are able to spontaneously fold into specific structures.[8-10] Since intramolecular interactions are responsible for the secondary, tertiary and quaternary structure of peptides and proteins, different functions can be achieved.[11] Peptide nanostructures present a large range of chemical and structural properties that can thus be manipulated by designing the peptide sequence. Peptides can also present attractive features in the creation of smart biomaterials that are responsive to environmental stimuli.[12-14]

2.1.1 Building Blocks of Peptides

Peptides are naturally occurring chains of amino acids, the simplest ones being dipeptides, consisting of just 2 amino acids, tripeptides, *etc*. Amino acids are sometimes called "the building blocks of life", since they are the basic components of proteins in nature that are shared amongst all living systems. All amino acids present a common structure (Figure 2.1), differing between each other in the chemical nature of the side chain (R). The latter is what endows peptide nanostructures with a rich chemical diversity.[15] A carboxyl, an amine group and a specific side chain compose the naturally occurring amino acids, except proline, which presents a five-membered nitrogen-containing ring and glycine, whose side chain is a hydrogen atom. Apart from glycine, which is achiral, all the others exist in nature in the L-conformation (Figure 2.1a).

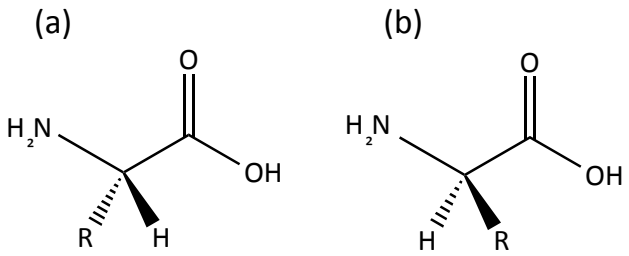

Figure 2.1. Chemical structure of L-amino acid (a) and D-amino acid (b) configurations, where R represents the side chain.

The 20 gene-encoded amino acids can be grouped in different categories based on their R-group charge, hydrophilicity/hydrophobicity, H-bonding capability, which is presented in Figure 2.2, together with their names and one-letter abbreviations. There are some exceptional cases of amino acids that cannot be grouped in any of the categories – glycine, proline and cysteine. As already mentioned and shown in Figure 2.2, glycine is achiral because it is the simplest building block since the side group is a hydrogen atom, presenting minimum steric hindrance and thus offering high flexibility. Due to its high steric flexibility, glycine is frequently found in beta-turns, along with proline. Proline presents a distinctive cyclic side chain, turning it more rigid in comparison with the other amino acids. However, since it lacks the amide H to form hydrogen bonds, proline tends to induce folding, by creating a bend in peptide chains. In addition, cysteine has a highly reactive thiol side chain that is responsible for the formation of covalent disulphide bonds between cysteines in close vicinity and thus cross-linking by oxidation.

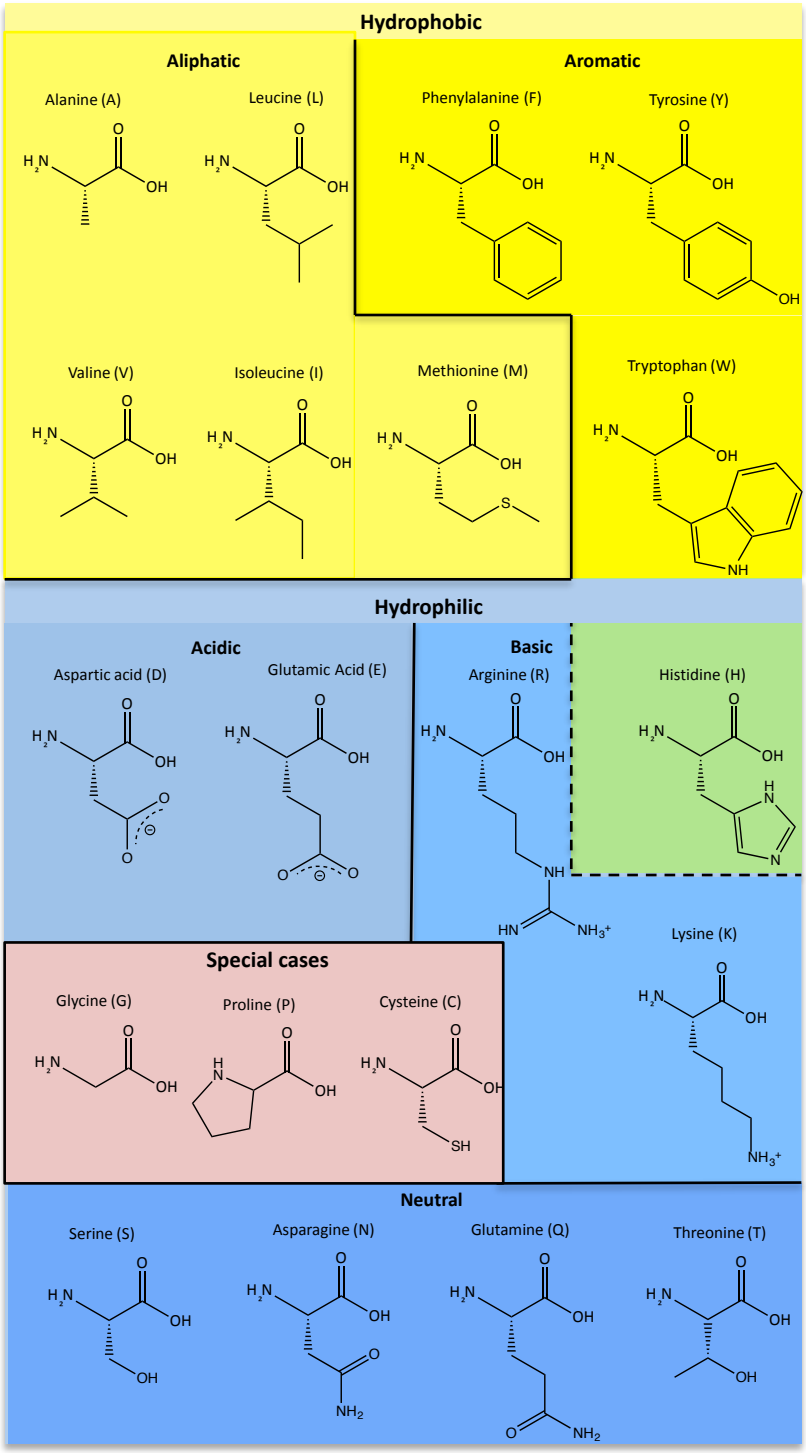

Figure 2.2. Chemical structures, names and one-letter abbreviations of the 20 amino acids in their L form, grouped based on their side chain properties.

2.1.2 Peptide design

The amino acids are able to create a peptide chain by covalently linking the amino functional group of one and the carboxyl group of the other, forming an amide (peptide) bond (Figure 2.3).[16] Formation of this linkage releases water, through a so-called condensation reaction. However, this reaction does not occur spontaneously, since the amino acids need an activation agent to create a positive dipole on the carbon, that then receives the electron from the lone pair of the next amino acid's -NH. The order of the amino acids within a polypeptide is known as the primary structure. The primary sequence is conventionally denoted from the N-terminus to the C-terminus.

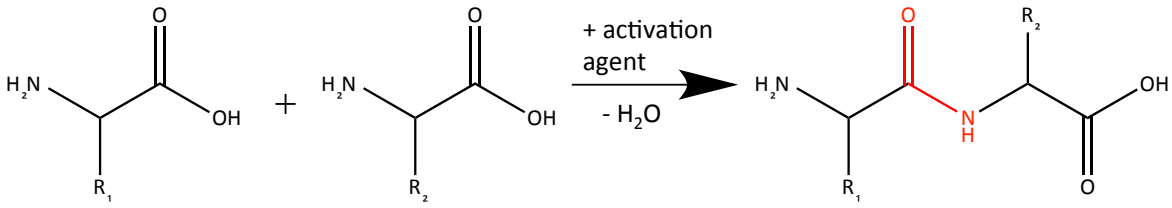

Figure 2.3. Schematic representation of the condensation reaction between two amino acids to form a dipeptide. The amide bond is coloured in red.

The linking of amino acids to achieve protein biosynthesis in living cells is a complex process that is carried out in the ribosomes and is called translation. For this protein formation to occur, messenger RNA (mRNA) molecules specify the order of the amino acids to be coupled and transfer RNA (tRNA) molecules carry them to specific codons in the ribosome. The ribosome is a ribozyme that catalyses the amide bond formation by binding two tRNA substrates, one with the increasing peptide chain and the other with the adding single amino acid *via* a high-energy ester linkage to their 3'-hydroxyl.[17]

Although some chemical polypeptide synthesis techniques were previously exploited, it was not until the pioneer Merrifield discovered the possibility of solid phase peptide synthesis (SPPS)[18] that peptide synthesis met the increasing requirements of efficiency and simplicity. This is a multistep method that consists of the addition of a protected amino acid to a growing peptide chain that is covalently bound to a solid insoluble particle, allowing

for the quick filtration and washing of the immobilised formed peptide, followed by chemical cleavage of the formed peptide off the solid support purification.

The synthesis of peptides, by taking advantage of the chemical diversity of the amino acid building blocks, may give rise to nanomaterials that adopt the constituent amino acids' properties. Given that amino acids are the natural building blocks of peptides and proteins, which form the structural and functional basis of the living world, it seems reasonable that these same peptides (or simpler versions thereof) can also self-assemble and produce stable nanostructures for materials and nanotechnology applications. Different nanostructures are formed depending on the use of di-, tri- or bigger peptides and on the sequence of the amino acids used, which can be tailor made for specific functions and applications.[19]

2.2 Self-assembly and Gelation

Molecular self-assembly was described in 1991 by Whitesides and co-workers as the spontaneous organisation of molecules into stable patterns or structures without human intervention.[1, 20-21] Static self-assembly occurs in systems that are at equilibrium and that spontaneously reorder without requiring energy input, while dynamic self-assembly processes are actively controlled and rely on energy input to form ordered structures.[21] Mimicking nature, molecular self-assembly is a bottom-up autonomous process of forming ordered structures based on molecular building blocks. It presents several advantages over the conventional top-down approaches of nanoscale fabrication, which involves carving a large material to give rise to nanoscale materials that can reach miniaturisation limits.[22] Synthesis of nanomaterials with strictly controlled size, shape and surface from nanoscale building blocks allows the achievement of specific desired functions.[23]

One specific class of self-assembled materials are supramolecular or polymeric gels. Gels have been defined in several different ways over time. Nowadays, a gel is considered to be any system that forms a continuous 3-dimensional entangled solid network within a liquid phase or gas.[24] The formation of the solid network prevents the remaining liquid or gas from flowing, resulting in a macroscopically solid system. Based on this definition, there

are several ways of classifying gels, depending on the physical state of the bulk phase and on the chemical properties of the components. A chemical gel is one in which the 3D network is based on covalent crosslinking, while a physical gel is formed through non-covalent interactions. Depending on whether the liquid is water or an organic solvent, they are called hydrogelators or organogelators, respectively.

Supramolecular gels are a type of physical gels formed through non-covalent interactions of small organic compounds in water or organic solvents.[25-26] This behaviour is based on the ability of the so-called low molecular weight (LMW) gelator molecules – that present a molecular weight of less than 2000 Da – to self-assemble and immobilise the solvent within the 3D fibrous network.[27] Since this self-assembly is established by non-covalent interactions, network formation and hence gelation of physical supramolecular gels are usually dynamic and thermoreversible.[24] These are actually advantageous in comparison with the traditional polymer networks cross-linked by covalent bonds that are irreversible and static.

Small molecules that are able to form gels in aqueous solvents comprise an expanding area of research.[28] As already mentioned, certain peptide chains have the ability to undergo bottom-up molecular self-assembly into larger peptidic structures, giving rise to several possible nanostructures. When 3D entangled networks of fibrils or tape-like aggregates are formed in a scaffolding way that confers rigidity to the solution, a gel is formed.[29] The entanglement extent and the nanostructure morphology define the properties of the material.[30-31] The detailed understanding of the supramolecular interactions present in the final arrangement of a self-assembled structure remains a big challenge.[19] However, much progress has been made in recent years with design rules emerging, as detailed in the next section.

2.2.1 Supramolecular Interactions

In a peptide self-assembly process, the supramolecular chemistry is regulated by weak non-covalent interactions, which comprise a large range of attractive and repulsive contributions.[19, 32-33] While 200 to 460 kJ.mol^{-1} is necessary to break a single covalent bond, weak, non-covalent interactions are often considered to be reversible, as they only need 4-

30 kJ.mol^{-1} to be disrupted.[32-34] Even though they are weak individually, these interactions have a very significant influence on the supramolecular ordering of peptide nanostructures, since they stabilise the assemblies in a sustained manner. These non-covalent interactions can be hydrogen bonding, π-π stacking, van der Waals forces, electrostatic interactions and hydrophobic/solvophobic effects: the most important in self-assembly of peptide nanostructures are explained below.

2.2.1.1 Hydrogen bonding

H-bonding interactions are based on the attraction between an electronegative atom and a hydrogen covalently linked to a highly electronegative atom.[34] This interaction is normally considered to be 10% covalent due to the overlap of orbitals, with the remaining 90% electrostatic[32] due to a dipole-dipole interaction.[33] In this hydrogen bonding process, the atom linked to the hydrogen (X) is known as the hydrogen bond donor and is usually fluorine, oxygen or nitrogen, while the other with a lone pair of electrons (A) is the acceptor, usually oxygen or nitrogen (Figure 2.4).

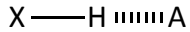

Figure 2.4. Schematic representation of a hydrogen bond between the donor (X) and the acceptor (A).

The normally occurring hydrogen bonds present an average donor-acceptor distance (X-A) between 2.2 and 4 Å.[35] The typical hydrogen bonds occurring in peptide backbones between N-H and O=C have an approximate distance of 1.8 Å, measured from the hydrogen atom of the NH to the carbonyl oxygen (Figure 2.5). It has been shown that the average distance of this backbone-backbone H-bond in a β-sheet configuration is smaller than in α-helices (2.06 Å).[36] Hydrogen bonding interactions can also occur between a side chain and the backbone or between two side chains. One example would be a H-bond formed between the –OH hydrogen donor of tyrosine side chain and any backbone oxygen acceptor. Besides, any acceptor of a side chain of these amino acids can link with a donor of another side chain. Specific host-guest dipolar and hydrogen bonding interactions are much more significant in the case of non-polar solvents.

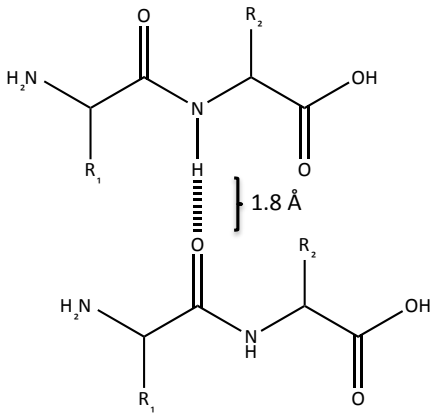

Figure 2.5. Schematic representation of the recurrent H-bonds and distance between peptide backbones.

2.2.1.2 Aromatic interactions

π-stacking interactions are attractive non-covalent interactions based on π-conjugated electrons between aromatic rings. These are important interactions in peptide self-assembly, when the peptides present aromatic moieties (constituted by F, Y or W amino acids), and/or N-terminal capping aromatic group. This type of interaction can occur in different conformations – parallel, T-shaped and displaced parallel (Figure 2.6).

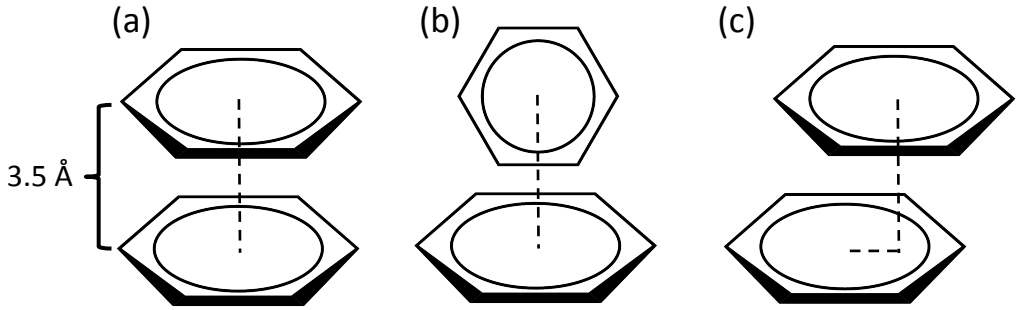

Figure 2.6. Schematic representation of different π-stacking orientations: (a) Parallel; (b) T-shaped; (c) Displaced Parallel and respective distances.

The relative orientation of the two residues is determined by the dispersion interactions between the two aromatic groups depending on the π-conjugated electrons. Parallel orientation of π-stacking (Figure 2.6a) is the less common in naturally occurring interactions due to the repulsion given by the negatively charged pi-systems. The T-shaped

orientation (Figure 2.6b) occurs when an edge is facing a face instead of face-to-face. Strictly, the T-shaped orientation should not be considered as π-stacking as it is seen as a weak form of H-bonding between one aromatic ring and the other, since there is no stacking of the electron surfaces.[33] Displaced parallel orientation (Figure 2.6c), *i.e.*, the parallel orientation with the rings not above one another, was shown to be the most stable conformation when studies of several known proteins were carried out.[37] Studies of dimers (isolated pairs) of aromatic amino acids gave insight on how they preferentially stack their aromatic rings, with a displaced parallel orientation as the configuration most commonly found in nature. It is not surprising that each dimer aromatic interaction has a distinct character, based on their different electrostatic potentials. Phenylalanine is known to have the largest tendency to self-interact, while the other aromatic amino acids have more tendency to form hetero arrangements.[38]

2.2.1.3 Van der Waals forces

Van der Waals forces are weak interactions that occur when two uncharged atoms are close enough to make their surrounding electron clouds influence each other.[32] Two dipoles can be formed by random and small variations on the electrons around one nucleus, creating a transient electric dipole in the atom. These two dipoles are weakly attracted to each other, bringing the nuclei closer.[32] The electron clouds then start to repel each other, as the nuclei are brought closer. When these attraction and repulsion forces are equal, the atom is said to be in van der Waals contact. Van der Waals forces can have two components: attractive forces (London dispersion) that dominate at longer distances; and repulsive forces (Steric repulsion), which are more prevalent at very short distances.

2.2.1.4 Electrostatic interactions

These are the strongest non-covalent interactions and they are also important for peptide self-assembly since the negatively and positively charged amino acids (D, E, R, H and K, as present in Figure 2.2) can interact between each other through electrostatic interactions. These interactions occur between charges following Coulomb's law (Equation 2.1): the force (F) of ionic interactions in a solution depends on the magnitude of the charges (Q), the distance between the charged groups (r) and the Coulomb's constant (k).

$$F = \frac{kQ_1Q_2}{{r_{1,2}}^2} \qquad \text{(Equation 2.1)}$$

It can be concluded that the interaction between two molecules 1 and 2 is stronger when they come together, since F increases with a lower distance. At physiological conditions (pH 7-8), there is an equal mixture of weak acid and anionic forms of an amino acid and the zwitterions are present (Figure 2.7b). This occurs because the pK_a value of the amino group $-NH_3^+$ is 9-11 and of the carboxylic group -COOH is 1.5-2.5 in the different amino acids. In peptides, where the N- and C-termini are further away from each other than in an amino acid, the pK_a values become closer (7.5-8 for the amine and 3-4 for the acid terminus).[39] Therefore, peptides in solution can form strong electrostatic interactions, substantially contributing to peptide self-assembly. The self-assembly process can be detectable by pK_a shifts, when pK_a values vary depending on the environment. This happens *e.g.*, when at pH above 2.5 the carboxylic acid composing the C-terminus of a peptide chain is still protonated, when it usually gets deprotonated at that pH value – the apparent pK_a value.[40] The proximity of molecules with the same charge varies the tendency to be protonated and so it can suggest self-assembly is happening. The use of pH-sensitive peptides to trigger self-assembly will be discussed in more detail in Section 2.2.3.1.

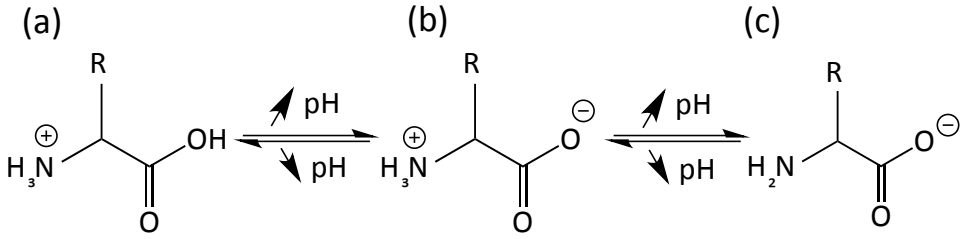

Figure 2.7. Acid/base equilibrium of the amino and acid groups of a general amino acid.

Salt bridges are the result of a combination of hydrogen bonding and electrostatic interactions and are commonly found in proteins but also, more generally, in supramolecular chemistry.[41] The typical distance between the heavy atoms of a carboxylate and a cationic amino group participating in a salt bridge at the ionic strength present in pH 8 buffers is usually around 4 Å.[34, 42]

2.2.1.5 Hydrophobic effect

Hydrophobic effect is a major driving force for aqueous self-assembly processes, with the amphiphilic molecules arranging in a way that hydrophobic residues face the interior and hydrophilic parts the exterior, since they tend to interact with the polar solvent. However, the strength of hydrophobic interactions is not due to any intrinsic attraction between nonpolar residues or repulsive forces between polar and nonpolar moieties. Instead, it is driven by a thermodynamic preference of water to interact with hydrophilic residues or to minimise the number of water molecules to surround hydrophobic moieties of the solute.[32] The process of dissolving a nonpolar solute in a polar solvent like water is unfavourable ($\Delta G > 0$). The disruption of H-bonds between water molecules leads to a small change in enthalpy, which can be negative, positive or zero depending on the formation of new H-bonds with the solute. However, the entropy of the system is highly decreased upon the addition of a nonpolar solute, where the neighbouring water molecules organise in a cage-like manner depending on the surface area of the solute.[32] In this case, the solute is hydrophobic.[34] The solvent in use cannot be ignored since it plays an important role in supramolecular chemistry. As already mentioned, hydrophobic or solvophobic effects are of extreme importance for polar solvents, in particular water, since molecules compete for binding sites, especially for hydrogen bonding.[33]

Most of these self-assembly processes − in particular those involving peptides − are developed in water, which in bulk possess high entropy due to little order. Entropic contributions are vital, since when solute molecules cluster together, fewer solvent cages are needed and water molecules are freed-up, increasing the entropy of the system in a way to turn the association of hydrophobic molecules in water spontaneous.[32]

Molecular self-assembly of peptides is thus driven by a combination of many weak non-covalent interactions such as H-Bonding, π-stacking and the hydrophobic effect that tend to form and stabilise nanostructures. The hydrophobic amino acids tend to the interior of the assemblies and the hydrophilic ones face the solvent due to the hydrophobic effect. However, hydrogen bonds play a key role in determining the directionality and supramolecular structure within the peptide based systems. In a peptide chain, the amide

and carbonyl groups of the backbone allow for H-bonding, while other types of interactions that might occur for each case are governed by the specific side chains of the building blocks. In addition, the hydrophobic amino acids that present an aromatic side chain are able to form π-stacking between them or with other coupled large aromatic groups, producing a stacked nanostructure where the aromatic hydrophobic moieties are placed in the interior.

2.2.2 Amphiphilic Peptides as LMWG

Aromatic interactions are critical for the molecular self-assembly of fibrillar peptide nanostructures to provide order and directionality. One common approach in peptide self-assembly is to use a short peptide chain, usually between one and five amino acids, capped at the N-terminus with a large synthetic aromatic group in order to exploit extra aromatic interactions.[2] By using these aromatic peptide amphiphiles, the amphiphilicity required to drive molecular self-assembly is balanced to enable structure formation *via* H-bonding and π-stacking. Aromatic peptide amphiphiles based on fluorenylmethoxycarbonyl-peptides have first been studied by Vegners in 1995, where Fmoc-LD was shown to form a thermoreversible gel.[43] 9 years later another work on Fmoc (9-fluorenylmethoxycarbonyl) peptides was published, by Xu's group.[44] Xu and co-workers first introduced a new type of Fmoc-peptide hydrogels that respond to a biological ligand-receptor interaction. By discovering the ability of Fmoc-AA to undergo or disrupt gelation upon binding to its ligand vancomycin,[45] they achieved experimental flexibility and higher control on gel formation and materials' properties.

Aromatic dipeptides have been discovered to self-assemble into nanotubes by Gazit's group. In a reductionist way, they discovered diphenylalanine (FF) to be the simplest building block to form amyloid fibrils, that are associated with several different diseases such as Alzheimer's disease, diabetes mellitus, among others.[9, 46-48] Amyloid fibril formation is a common natural process in which cellular proteins self-assemble into larger and ordered protein structures. FF, a short peptide that comprises the aromatic core of the β-amyloid polypeptide, was found to efficiently self-assemble into peptide nanostructures. The self-assembly was believed to happen due to a combination of hydrophobic effect,

which led to hydrogen bonding and aromatic stacking interactions between their phenyl rings, giving rise to stable peptide nanotubes and fibres, depending on the directionality and prevalence of interactions.[46, 49-50] Later on, some modifications in the N- and C-terminus of FF were done to study the possible electrostatic role in the self-assembly process, resulting in the discovery of Fmoc-FF as an effective hydrogelator.[48] Fmoc-dipeptides, including Fmoc-FF were also simultaneously but independently discovered by our group to form stable hydrogels at physiological conditions, useful for cell culture.[51] After aromatic peptide amphiphiles emerged as self-assembling systems, they have been the object of study since they form stable self-supporting hydrogels that can be useful for cell culturing, optoelectronics, antimicrobial agents, amongst many others applications.[11, 52-55]

Some aromatic moieties that were successfully capped at the N-terminus are phenyl, naphthalene[56-57], fluorene[58-62], pyrene[58] (Figure 2.8) among others. The fluorene aromatic group (Figure 2.8c) is probably the most commonly used in research, as it was the first example used and has been shown to be the most consistent facilitator of gelation.[54, 63]

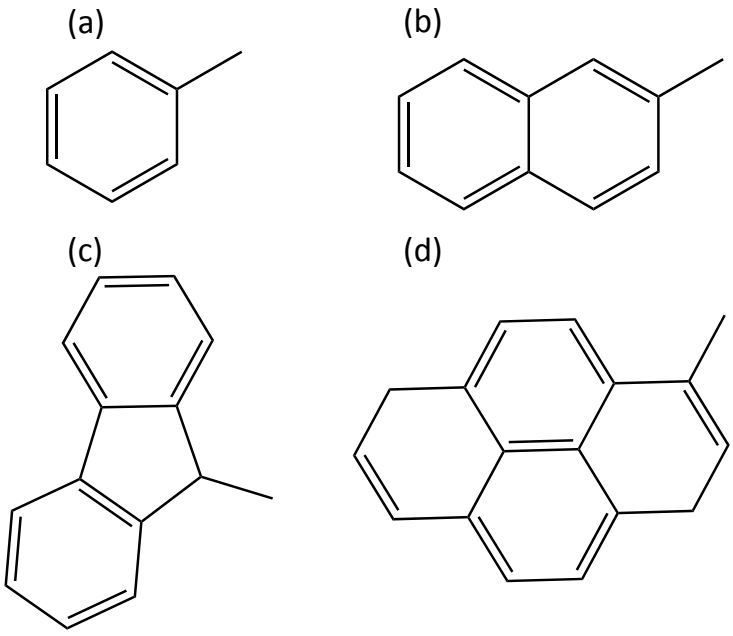

Figure 2.8. Aromatic moieties for N-terminus modification: (a) Phenyl; (b) Naphthalene;(c) Fluorene; (d) Pyrene.

There are several criteria to be considered upon the design of an aromatic peptide amphiphile, with each part influencing in the final supramolecular structure formed. In Figure 2.9, an Fmoc-dipeptide is represented to show the different parts on the design of an aromatic (di)peptide amphiphile.

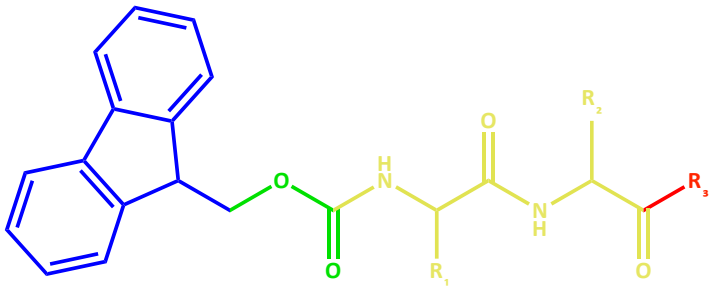

Figure 2.9. Chemical structure of an aromatic dipeptide amphiphile. Blue – Aromatic moiety at N-terminus; Green – linker; Yellow – Dipeptide; Red – C-terminus.

Substantial morphological and structural changes have been shown for different amino acid sequences and aromatic moieties used,[53, 57, 63-64] since the occurring interactions for each case (see Section 2.2.2.1) will vary. Apart from the aromatic group and the peptide chain, the linker segment between them (green in Figure 2.9) was also shown to be determinant for the relative orientation of the peptidic and aromatic segments in the final produced nanostructures.[58, 63] In fact, a study from Flemming *et al.*[63] showed that the linker between the peptide and the fluorenyl aromatic group makes a significant difference to the self-assembly and hydrogelation of the systems. Specifically, they demonstrated that more rigid linkers are preferential, with short linkers limiting the conformation and aromatic stacking interactions, thus giving priority to the methoxycarbonyl link in the Fmoc group, instead of carbonyl, methylcarbonyl or ethylcarbonyl linkers. Also, the chemical nature of the C-terminus (in red on Figure 2.9) is an important parameter that influences the balance between protonated and ionised forms.[2] The free C-terminus confers a negative charge to the aromatic peptide amphiphiles and the pH changes the ratio of acid to conjugate base, which affects the aqueous solubility of the system. Since the aggregation and gelation are determined by the solubility and charge of the aromatic peptide amphiphiles, the self-assembly of the gelator can be triggered by pH adjustments.[40] The use of variations in pH

or ionic strength, as a self-assembly stimulus, as well as ionisation and pK_a shifts are further discussed in Section 2.2.3.1.

These modified peptidic molecules are commonly referred to as aromatic peptide amphiphiles, to distinguish them from peptide amphiphiles which contain an aliphatic tail.[65-66] These two classes of peptide amphiphiles have very different mechanisms of self-assembly, since aliphatic peptide amphiphiles present a linear hydrophilic head/hydrophobic tail that directs into spherical and cylindrical micelles, while in aromatic peptide amphiphiles the directional stacking of hydrophobic fragments gives rise to more tunable interactions and produce a greater variety of nanostructures.[2] Even though these aromatic peptide amphiphiles provide an extra π-stacking possibility, short peptides based on alpha amino acids only can also be designed to take advantage of a hydrophilic/hydrophobic balance. The latter will be simply called dipeptides, tripeptides or short peptides from now on to avoid confusion and, in conjunction with aromatic peptide amphiphiles, they are all considered amphiphilic peptides.

2.2.2.1 Modes of self-assembly of amphiphilic peptides

By using different combinations of peptide chains capped at the N-terminus (Figure 2.10a), it is possible to design aromatic peptide amphiphiles to drive a combination of hydrophobic effect, π-stacking interactions and hydrogen bonding, giving rise to a specific final structure. The self-assembly of these LMWGs is established by the alignment of hydrophobic and hydrophilic parts of the molecules, as already discussed.[67] The supramolecular stacking arrangement can either follow parallel, antiparallel or interlocked anti-parallel conformations (See Figure 2.10b). Based on these supramolecular interactions (as well as kinetic contributions), tubes[68], fibres[69-70], tapes[3], spheres[71] and leaf-like structures[72] can be produced (Figure 2.10c). Several studies have been published on the self-assembly of Fmoc-peptide amphiphiles and formation of stable hydrogels.[3, 20, 31, 58, 68, 73-75]

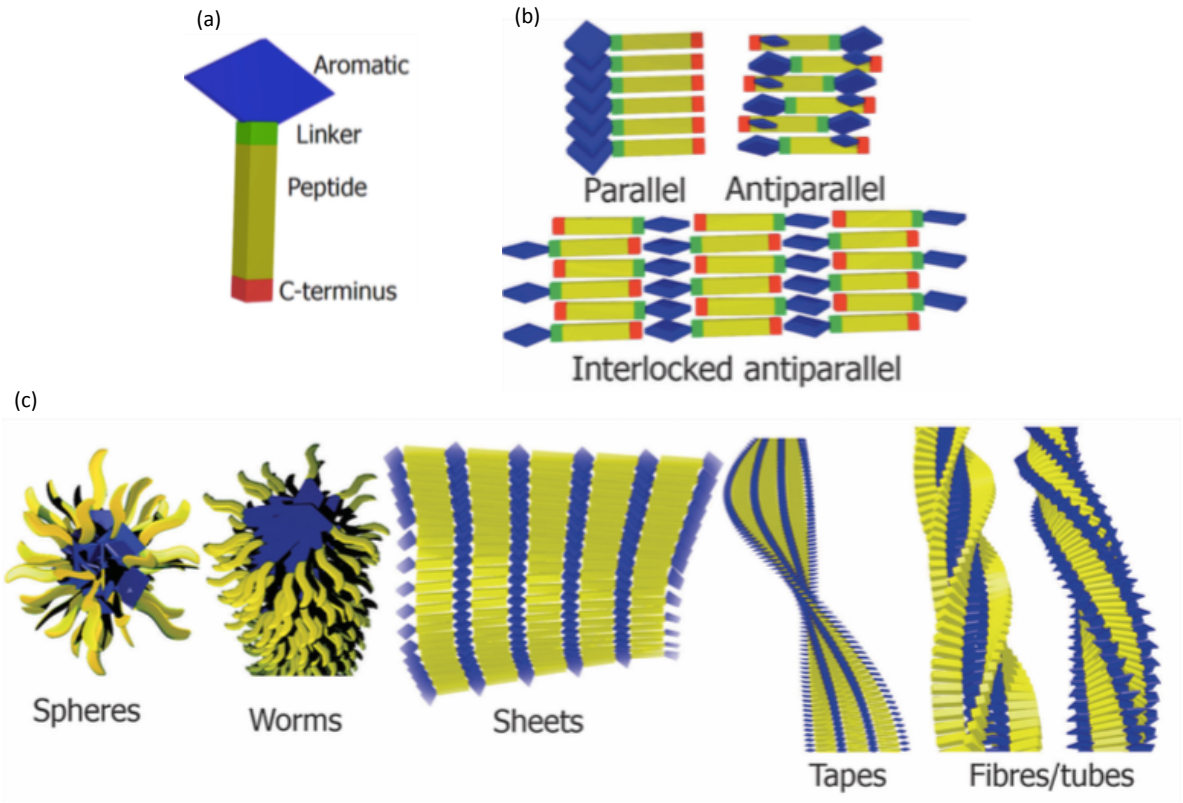

Figure 2.10. Schematic representation of (a) an aromatic peptide amphiphile; (b) Possible established conformations; (c) Possible supramolecular nanostructures formed. Figure adapted from Ref.[2] with permission from the Royal Society of Chemistry.

As shown in Figure 2.10b, when the Fmoc-(di)peptide possesses only one aromatic group (the fluorenyl), the most favourable way to self-assemble is in a parallel or interlocked-anti-parallel conformation. When a parallel arrangement occurs, the Fmoc hydrophobic moieties undergo aromatic interactions, and the peptidic amide groups link between each other by hydrogen bondings. Also the carboxyl groups of the C-terminus are able to interact between them and/or with water. In turn, if the used (di)peptide has an aromatic group as one of the amino acid side chains, an antiparallel conformation is possible to occur, since aromatic interactions can happen between the Fmoc N-termini and between that sidechain aromatic ring of adjacent molecules (Figure 2.10b). However, this is a prerequisite for the antiparallel conformations, as demonstrated by Yang and co-workers, where the peptidic part of the gelator can compete with the Fmoc groups for aromatic stacking interactions.[76] The interlocked antiparallel conformation represents a distinct antiparallel conformation

where the adjacent Fmoc groups stack between each other, also having a contribution from peptide chain H-bonding interactions (Figure 2.10b).

However, since backbone distance between hydrogen bonded peptide chains are usually of 4.2-4.8 Å length and aromatic interactions cover distances of around 3.5 Å, it is difficult to simultaneously optimise H-bonding and π-stacking in both conformations. This can possibly explain the twisted formed nanotubes or nanofibres found in many Fmoc-peptide amphiphiles studies, where the aromatic groups are closer together in the core and the peptidic chain slightly increases distance in each "layer", resulting in a twisted structure.

The assignment of the established conformations usually comes from evidence of H-bonding or π-stacking interactions. Fluorescence spectroscopy is normally used to assess the changes in the aromatic environment, where specific emission bands can elucidate about the presence of aromatic interactions.[58, 61, 77-78] A redshift in the spectrum when monitored over time often points to self-assembly (Figure 2.11a) of the aromatic peptide amphiphiles. The presence of H-bonding between peptide chains is normally taken from Fourier Transform Infra Red (FTIR) spectroscopy, where bands in specific areas are associated with the formation of a β-sheet type H-bonding network (Figure 2.11b for Fmoc-YL).[46, 74, 79] This, in combination with other techniques, can sometimes be assigned to antiparallel conformation.

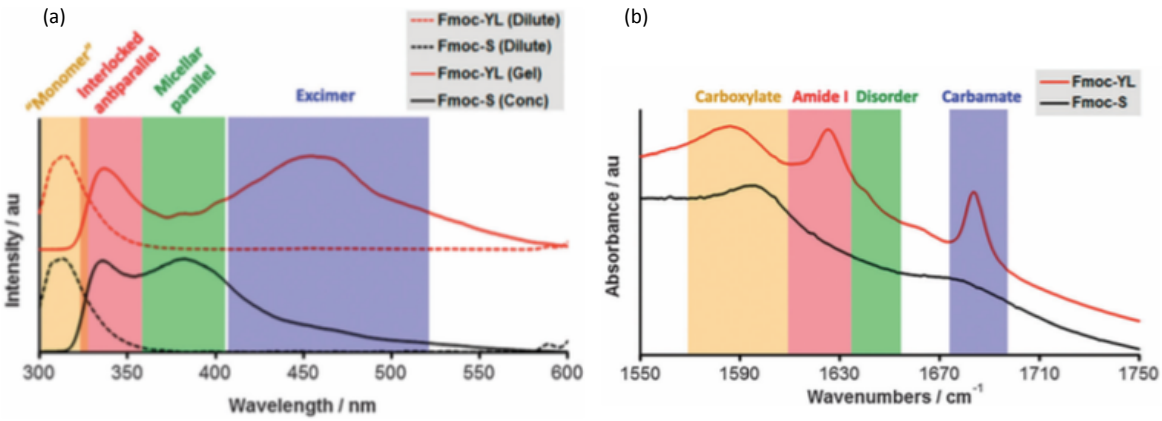

Figure 2.11. (a) Typical fluorescence emission spectra for Fmoc-peptide amphiphiles; (b) Typical IR amide I spectra for Fmoc-peptide amphiphiles. Both Figures adapted from Ref. [2] with permission from the Royal Society of Chemistry.

Haixia Xu *et al.* explain that π-stacking and H-bonding are both key interactions on the formation of π-π interlocked anti-parallel β-sheets of, for example, Fmoc-FF and Fmoc-L_3.[75] To support these claims, they developed Molecular Dynamics (MD) models and experimental methods in order to have further insight on the formed structures and on the interactions' distances. The group demonstrated β-sheet formation at around 4.7 Å between Fmoc-L_3 molecules (peptide backbones) and of π-stacking at around 3.6 Å between Fmoc moieties, with concordant values from experimental and MD simulations. In addition, they provided evidence that these fibrous interlocked anti-parallel nanostructures allow intermolecular electron delocalization. When the polar carboxylic acid tends to the non-polar environment where π-stacking occurs, this contrary behaviour is possibly driven by a mechanism of electronic transport.[75]

β-sheet-like hydrogen bonding is commonly found in self-assembling Fmoc-peptide amphiphiles and it has been hypothesised in many studies to help drive self-assembly and stabilise the supramolecular nanostructures. However, Eckes and co-workers demonstrated both experimentally and computationally that β-sheet like hydrogen bonding is not critical for the self-assembly of Fmoc-short peptides to occur.[80] Since Fmoc-dialanine is known to self-assemble into fibrous-like structures and the β-sheet H-bondings between the amide groups were thought to be the main interaction responsible for this, a depsipeptide with ester bonds instead of amide bonds has been used to compare and test if the β-sheet-like hydrogen bonding between amide groups is actually required. They concluded that it is not as important as hydrophobic and/or aromatic stacking interactions since the depsipeptide of Fmoc-AA, Fmoc-ALac, experienced self-assembly and hydrogelation.[80] Besides, although β-sheet like hydrogen bonds were previously assumed as anti-parallel, Flemming and co-workers demonstrated by Infrared (IR) Spectroscopy and DFT calculations that it is not possible to conclude if Fmoc-AA form parallel or anti-parallel β-sheet conformation based on FTIR data alone.[74]

Self-assembly into supramolecular structures has also been proven for some unmodified short peptides, which inherently present biocompatible properties. In addition to the dipeptides (FF, FW) that contain aromatic amino acids,[46, 49, 51] tripeptides have also been shown to self-assemble into nanostructures.[81-82] Marchesan *et al*. showed the conversion

from non-assembling tripeptides FFV, VFF and LFF to hydrogelators formed by fibrils when the stereochemistry of the N-terminal amino acid is changed from its natural to its D form.[81, 83] In fact, a screening of all the possible dipeptides[84] and tripeptides[85] gave further insight into what exactly is needed for increased aggregation propensity and self-assembly potential. Some examples of Fmoc-(short) peptide amphiphiles and unmodified short peptides are summarised in Table 2.1, where the different structures and responsible supramolecular interactions are presented, most of the times based on evidence from fluorescence and IR spectroscopy as presented previously (Figure 2.11).

It is possible to conclude that, depending on the chemical structures, conditions and methods of self-assembly, many different interactions can prevail, defining the final formed structures. It is possible to observe from Table 2.1 that the existence, number and position of aromatic groups in a peptide chain, apart from the Fmoc moiety, has a significant influence on the structure of the self-assembled compound.

Table 2.1. Examples of achieved structures of amphiphilic peptides as reported by the authors. When the symbol "–" is present, the property was not mentioned/not assessed in the cited article.

Fmoc-peptide	Observed structure	Imaging method	Evidence of π-stacking	Evidence of H-bonding	Macroscopic Appearance	Reference
FF	Nanotubes	TEM/SEM	✔	✔	Solution	46, 50
Fmoc-Y	Fibrous network	AFM	✔	–	Gel	78
Fmoc-AA	Fibrous network	TEM	–	✔	Gel	51, 74, 80
Fmoc-FF	Fibrous network	TEM/CryoSEM	✔	✔	Gel	51, 53, 68
Fmoc-GG	Fibrous network	CryoSEM	✔	–	Gel	45, 51
Fmoc-FP	Spheres	TEM	–	✖	Solution	53
Fmoc-FG	Fibrous	TEM	–	✖	Gel	53

	network					
Fmoc-GF	Microtubes	TEM/SEM	–	✖	Solution	[53]
Fmoc-YL	Fibrous network	AFM	✔	✔	Gel	[3, 58]
Fmoc-YT	Fibrous network	TEM	✔	✔	Viscous solution	[59]
Fmoc-YS	Fibrous network	TEM	✔	✔	Gel	[59]
Fmoc-YN	Fibrous network	TEM	✔	✔	Gel	[59]
Fmoc-YQ	Spheres	TEM	✖	✖	Solution	[59]
Fmoc-L_3	Nanotubes	TEM/AFM	✔	✔	Gel	[75]
Fmoc-RGD	Nanotubes	TEM	–	✖	Solution	[53]
Fmoc-RGDF	Fibrous network	TEM	–	✔	Gel	[53]

FFF	Nanoplates	TEM/SEM	–	✔	–	[86]
^{D}VFF	Nanotapes	CryoTEM/ AFM	✔	✔	Gel	[81]
KFG	Vesicles/ Nanotubes	AFM/TEM	✔	✔	–	[82]
KYF	Fibrous network	TEM	–	✔	Gel	[85]

2.2.3 On-demand self-assembly of amphiphilic peptides

Some amphiphilic peptide systems experience spontaneous self-assembly when placed in the reaction medium (water or buffer), without the need for an external stimulus. For these, it is difficult to control nucleation or structure growth and kinetically trapped structures are likely to be formed instead of thermodynamic structures. This results in poor reproducibility because many defects occur in the resulting structures.[87] Even though the production of different nanostructures from the same building blocks can be highly attractive, to allow this, control over the process is necessary.[3] Hence, researchers have exploited several ways of activating and controlling the assembly process, by coupling an additional 'activating' step to the self-assembly, that is usually kinetically controlled. These exploit the modification of non-active precursors into self-assembling molecules. A number of chemical and physical means have been used as a trigger for self-assembly systems: changes in pH, as already mentioned, but also changes in ionic strength, temperature, light or the use of enzymes (discussed in Section 2.2.4).

2.2.3.1 pH as a stimulus for self-assembly

Changing the pH of the medium is a very common and simple way of controlling self-assembly in pH sensitive hydrogels.[51, 68, 88-89] It consists of changing the protonated/deprotonated state of the pH-sensitive groups, endowing neutralisation of the charges of the system. Even though side chains of the amino acids can be used for this purpose, the unprotected C-terminus of the sequence is the most commonly exploited group for a pH trigger of self-assembly. As the free acid C-terminus usually presents a negative charge, pH adjustments can easily control the solubility and charge of the system, which consequently determine if self-assembly and hydrogelation processes occur (Figure 2.12a).

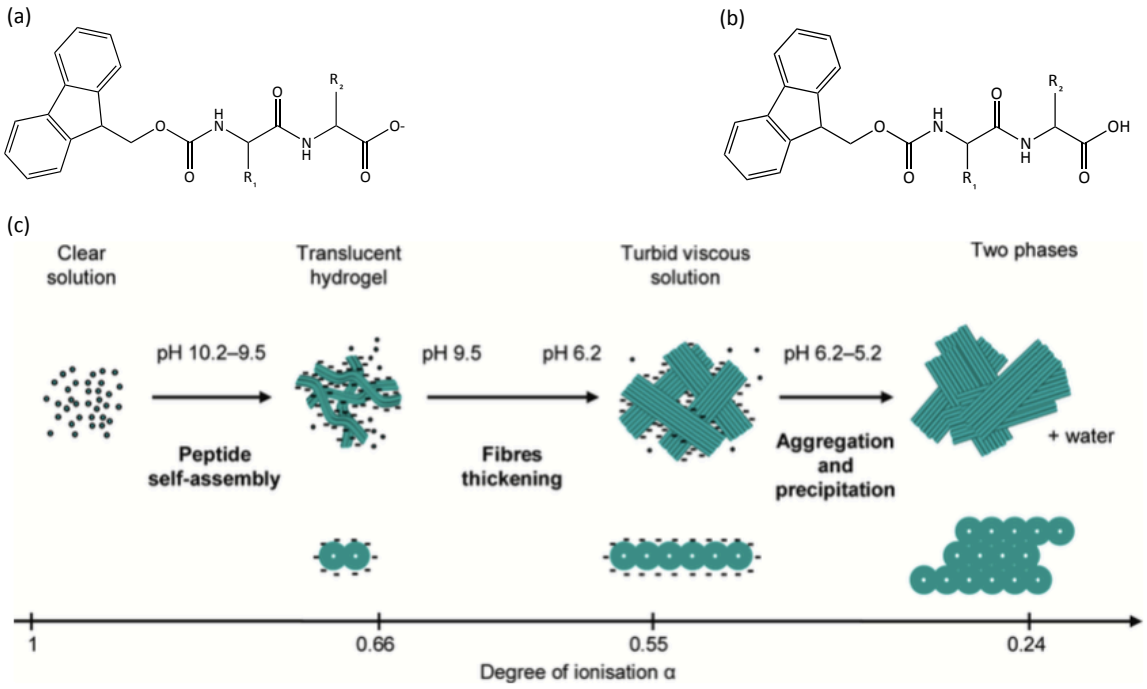

Figure 2.12. Chemical representation of a generic Fmoc-dipeptide (a) deprotonated and (b) protonated; (c) Schematic representation of the self-assembly of Fmoc-FF throughout the pH range. Figure adapted with permission from Tang, C. *et al*., *Langmuir* 2009, *25* (16), 9447-9453.[40] Copyright (2009) American Chemical Society.

The majority of aqueous self-assembly experiments are carried out using aqueous buffers in a way to ensure the pH stability and the equal mixture of weak acid and anionic forms of the compound when the pH = pK_a of the acidic group. The deprotonated state of a generic Fmoc-dipeptide in Figure 2.12a is unable to self-assemble due to charge repulsion, but when the pH of the medium is decreased and the protonated state in Figure 2.12b is formed, self-assembly can be initiated. Although self-assembly would be expected to only occur at low pH, below the pK_a of the acid group in dilute solutions (approximately 3.5), there are many cases of gelation at physiological pH. One example of this is Fmoc-FF (a highly hydrophobic derivative), which has been shown to self-assemble when gradually decreasing from pH 9 to neutral pH.[68] It is known that dramatic pK_a shifts can occur in protein and peptide self-assembly, especially in hydrophobic environments.[90] By performing titration experiments, Tang and co-workers were able to achieve further insight over the self-assembly and precipitation processes of Fmoc-FF molecules depending on the

pH and degree of ionisation (Figure 2.12c).[40] They stated that self-assembly occurred upon lowering pH due to dramatic pK_a shifts of ~ 6.4 and ~ 2.2 pH units. The first pK_a transition was attributed to the self-assembly of both protonated and non-protonated forms into fibrils while the second resulted in further neutralisation, at which precipitation of the peptide occurs due to ribbon aggregation and phase separation. In subsequent studies, they demonstrated the existence of a single apparent pK_a transition for Fmoc-FG, Fmoc-GG and Fmoc-GF, correlating it to the hydrophobicity (logP) and flexibility of the Fmoc-dipeptide under study.[91] These changes in the resulting structures are the reason why pK_a shifts can be used as a predictive tool for critical assembly.

2.2.3.2 Ionic strength as a stimulus for self-assembly

Changes in the ionic strength of the system can be used to screen charge effects. Dissolved salts are dissociated in water to form a cation and an anion, and each of them may be surrounded by a water shell, which disturbs the adjacent structure of water and therefore the hydrophobic effect.[34] The hydration of the building blocks is increased for these ionic-responsive hydrogels, due to the presence of mobile counter-ions (such as Na^+), responsible for balancing the fixed charges on the structure. As a result, it is possible to control self-assembly by changing the ions, water organisation and thus modifying the strength of the hydrophobic effect.[15, 92] Some significant changes in the hydrogel properties and supramolecular structures were detected when using different ions that have a different tendency to order water.[93] This can be explained by the Hofmeister effect, which is influenced by the impact on water organisation, the degree of hydration of ions in water, the involved cation and specific interactions between ions and solutes.[34] Due to these reasons, there is an increased interest in varying conditions to impact on the hydrophobic effect and to utilise these variations to form the desired final structures.

2.2.3.3 Temperature as a stimulus for self-assembly

Varying the temperature to control self-assembly is also a widely-used method. As non-covalent intermolecular interactions are broken at high temperatures, one way to control self-assembly is by heating the aqueous solvent and subsequently cooling it, as self-assembly is initiated when the temperature slowly decreases. Gel-solution transition

temperature (T_{gel}) is the temperature above which the supramolecular network breaks down and a gel is transformed into a solution. As a result of this, hydrogels can be prepared *via* a heat-cool cycle, which is a reversible process that does not affect significantly the final properties of the nanostructures. Increasing the temperature subsequently increases the solubility of the gelator by disruption of the H-bonds between water molecules, which increases the entropy due to less order and fewer hydrogen bonds between water molecules. Thermodynamic factors are thus interlinked and influence the gelation process, where this can be seen as a metastable kinetically trapped state.

Different thermoreversible hydrogels have been developed throughout the years by using, *e.g.*, poly(N-isopropyl-acrylamide) (PNiPAM).[94-95] Many Fmoc-peptide amphiphiles have been found to undergo gelation upon heating and cooling down again. Tang and co-workers used heating up to 75-80 °C followed by cooling and developed rheological studies in function of temperature of Fmoc-FG due to the unusual behaviour of gel formation above the apparent pK_a.[91] They showed that viscous solutions at 25 °C became relatively strong gels upon heating to 80 °C, but were not so stable as precipitation started to occur after cooling it to 4 °C.[91] In turn, Pappas *et al.* studied the behaviour of Fmoc-FL and Fmoc-YL systems upon heating, showing increased order and gel state retention for the first and disorder, leading to disruption and gel dissolution for the latter.

2.2.3.4 Light as a stimulus for self-assembly

Light is also a possible stimulus that may be used to control self-assembly of aromatic peptide amphiphiles, requiring light sensitive aromatic groups instead of Fmoc. Azobenzene (Azo) and derivatives are the most common aromatic residues used for the production of photoresponsive supramolecular hydrogels.[96] The c*is*-to-*trans* conformational switching of the phenyl rings change the stacking and assembly properties under UV irradiation. It was demonstrated that, upon a light irradiation process, a non-assembling precursor turns into a hydrogelator[97] and reversible photoresponsive gel/solution transitions can be achieved.[98] Sahoo and co-workers showed transition of ambient light stable *trans*-Azo-YF-NH_2 into its cis-isomer when irradiated with UV light, which then hydrolyses enzymatically into its amino acid derivatives, undergoing gel dissolution (the *trans* isomer

is not hydrolysed due to favourable self-assembly of the peptide).[99] Also, Raeburn *et al.* demonstrated the conversion of LMWG into a hydrogel upon UV irradiation as a new approach of lowering the pH of the solution below the apparent pK_a, enabling self-assembly into fibrous networks.[97] In their case, the gelator itself was not UV-responsive, but they used a photoacid generator (PAG) to allow UV-triggered gelation of a number of dipeptide conjugates such as Fmoc-LG but also 2Nap-AA and 2Nap-FF, *etc*.[97] This self-assembly trigger is seen as advantageous since light can be focused to a particular zone, giving rise to targeted gelation instead of a bulk solution gelation.[97]

2.2.4 Biocatalytic self-assembly of amphiphilic peptides

As already mentioned, there is a substantial interest in developing systems that use an external stimulus to assemble on-demand, which enables better control of the process under constant physiological conditions. Since scientists are seeking to mimic biology's approaches to achieve a more controllable bottom-up nanostructure production, enzymatic catalysis has emerged as an attractive trigger.

There are several advantages of using the catalytic activity of enzymes to initiate self-assembly of amphiphilic peptides. These are mainly related with the fact that enzymes operate under constant environmental conditions, which sets them apart from most other self-assembly triggers,[100] except for light. In contrast to the previously presented on-demand self-assembly of peptide nanostructures, the enzymatic trigger does not require changes in conditions during the course of the reaction (except for the addition of the enzyme itself), although in some cases temporary heating is used to facilitate the enzymatic conversion.[3, 59, 101] Since enzymes are biological molecules that operate at constant controlled temperature and pH conditions, these systems can be used at physiological conditions for biomedical applications.[3, 20, 56, 69, 102] Also, the expression levels of some enzymes are affected by diseases, showing higher activity for specific diseases.[103] Since these enzymes can be disease markers, a combination of their detection and spatial/temporal drug delivery is highly attractive for therapeutic purposes. The mechanism of enzyme-triggered self-assembly of aromatic peptide amphiphiles gains special interest upon the possibility of reaching spatiotemporal control.[100]

Bing Xu's group was the first to exploit biocatalytic self-assembly of Fmoc-peptide amphiphiles using an alkaline phosphatase to dephosphorylate Fmoc-tyrosine phosphate (Fmoc-Y*p*) under basic conditions, forming a hydrogel.[61] Since then, hundreds of studies have been published on the use of different enzymes for self-assembly formation and control.[104]

Enzymatic conversion from non-assembling precursors into self-assembled building blocks is usually based on the fact that self-assembling molecules are amphiphilic and the hydrophobic/hydrophilic balance dictates the self-assembly tendency. It is actually the chemical addition or removal of a hydrophobic or hydrophilic group that results in the self-assembling motif. This unit is then able to interact through non-covalent interactions to form self-assembled nanostructures.[100, 105] The coupling of biocatalysis and molecular self-assembly can be achieved in different ways. The two most common approaches are the enzymatic hydrolysis/removal of a charged or steric group that precludes self-assembly to occur due to electrostatic repulsion[3, 55, 61-62, 101, 106] (black blocks in Figure 2.13a), or the condensation (reversed hydrolysis) of amino acid derivatives to produce peptide amphiphiles (See Figure 2.13b).[20, 60]

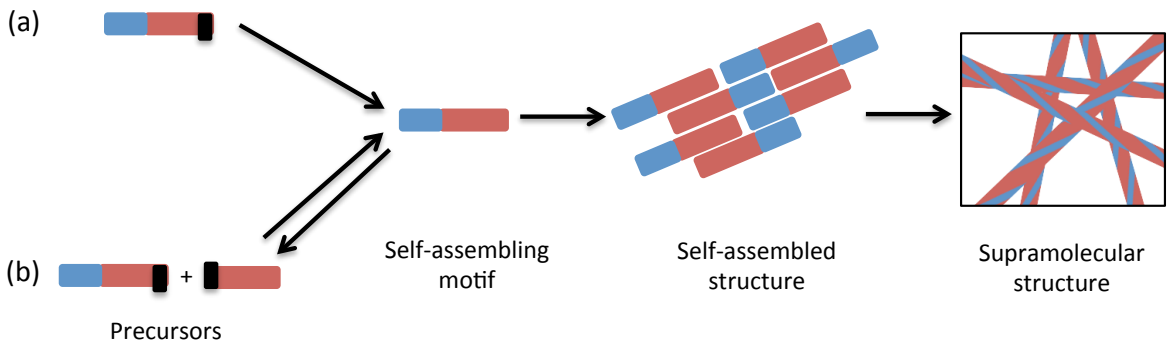

Figure 2.13. Schematic representation of the two modes of action of enzyme-triggered self-assembly into entangled fibrous networks: (a) Hydrolysis by cleavage of blocking group, represented in black; (b) Reversed hydrolysis by condensation of amino acids.

The first scenario is focused on the use of enzymes that break covalent bonds such as hydrolases (phosphatase, esterase, amidase, lactamase, protease and subtilisin). In particular, phosphatase triggered self-assembly (following route (a)) is relevant for the

production of Fmoc peptide hydrogelators, giving rise to supramolecular hydrogels.[55, 61-62, 78, 102, 106-107] As already mentioned, the phosphate moieties on the Fmoc peptides prohibit molecular self-assembly to occur.

Alkaline phosphatase is a hydrolase enzyme that naturally exists in cells, tissues and organs and plays important roles in intra- and intercellular signalling,[108] being responsible for the protein activity and signal transduction[103] by removing phosphate groups from different types of molecules such as proteins and peptides. The activity levels of phosphatases are affected in case of diabetes, cancer or multiple sclerosis.[103] In this context, it soon became the enzyme of choice to control the hydrophobic/hydrophilic balance, converting a non-assembling precursor that is soluble in weak alkaline aqueous solutions, such as phosphate buffer, into a more hydrophobic hydrogelator compound.[109] This hydrogelator aggregates as a result of non-covalent interactions, allowing for self-assembly to occur and for the production of a supramolecular hydrogel.[109]

The second case (See Figure 2.13b) comprises a condensation reaction by enzymes such as thermolysin and chymotrypsin. A thermodynamically driven self-assembly process has been extensively used in different Fmoc-peptide amphiphiles.[101, 110] In particular, Dynamic Combinatorial Libraries (DCL) have been studied, by putting distinct and competing building blocks into a system and allowing for the dynamic interchange to happen until the equilibrium is reached and the preferred thermodynamic state is achieved.[20, 111-114] Since the self-assembly into supramolecular structures is the driving force for the condensation to occur, the percentage of final structures corresponds to the tendency for the formation of self-assembled structures.

The two represented ways of enzymatically controlled self-assembly have very different mechanisms of action, taking place under kinetic or thermodynamic control, respectively, as explained further in the next section.

2.2.4.1 Kinetic versus Thermodynamic control

Enzyme-triggered self-assembled systems can follow different pathways depending on the system and the enzymatic reaction that initiates self-assembly,[100, 115] where the two main

cases are represented in Figure 2.14. In the former case (route a), both the enzymatic reaction and the self-assembly process are favoured to occur spontaneously (See Figure 2.14a) and the enzymatic reaction is largely irreversible (*i.e.*, it has a large equilibrium constant in favour of the products). These two factors mean that the rate of formation of the self-assembling structure and consequent gelation are dictated by the enzymatic reaction rate (kinetic control). The dramatic reduction of dynamics of the supramolecular structure upon gelation leads to kinetic locking, since reorganisation is unfavourable at the conditions used. Since the catalysis is the only determining step, the kinetically trapped supramolecular structures may correspond to a local minima in the free-energy landscape (self-assembled structure 1), preventing relaxation towards the global thermodynamic minimum (self-assembled structure 2).[3, 116-117] However, it is possible to unlock these kinetically trapped metastable states by performing a heat-cool cycle.[3] By supplying energy in the form of heat, the supramolecular interactions are disrupted and the gels broken, reverting the monomers to their initial state and allowing them to reorganise upon gradual cooling.[3] The reversibility of some reactions can be attractive to drive the self-assembly in the direction that favours the formation of the most thermodynamically stable nanostructures.[20, 60, 118]

The enzymatic reaction rate can be controlled by the concentration of catalyst added, having self-assembled supramolecular structures formed more quickly at higher enzymatic concentrations. Even though it has been proven that the final composition of the samples is not affected, morphological and mechanical properties of the nanostructures are, however, influenced by the enzyme concentration used.[119] In fact, the supramolecular organisation can be changed by tuning the catalyst concentration, which is beneficial for the generation of reproducible structures with controlled degrees of order. A wide range of hydrogels with different mechanical properties have been prepared when using an enzymatic approach to kinetically control the self-assembly process.[3, 62, 106, 119] Surprisingly, when increasing the enzyme amount, more ordered supramolecular structures and more stable gels were achieved.[3, 120] This counterintuitive behaviour where faster enzyme-triggered self-assembly gives rise to fewer defects was further studied and attributed to the enzyme cluster formation and nucleation mechanism.[121]

Thornton and colleagues showed evidence for the kinetically controlled structure formation of alkaline phosphatase-triggered self-assembly process of Fmoc-Y, instead of just characterising the final structures.[78] By studying the mechanism and kinetics of dephosphorylation, they showed the formation of temporary aggregates prior to fibre formation and gelation.[78] They have also shown evidence that the mechanical properties of assembling nanomaterials can be tuned by varying conditions as enzyme concentration, giving control over the molecular order.[62] Hirst *et al.* showed the importance of the combination between kinetically-controlled self-assembly systems and localised nucleation and growth mechanism to produce local thermodynamic minima structures.[3] When a hydrogel is formed by this method, the structure is locked under kinetic control, making it unfavourable for the system to reorganise the self-assembled units. They used the enzyme subtilisin to catalyse the hydrolysis of Fmoc-peptide-methyl esters to Fmoc-peptide hydrogelators and demonstrated its ability to form non-equilibrium supramolecular structures that self-assemble in a quicker way. Thornton and colleagues also defended the advantage of the arrested dynamics that arises from the "locking" of the supramolecular structure when gelation happens for precisely controlling the self-assembly kinetic system and the achievement of specific desired nanostructures.[78] Abul-Haija *et al.* developed a system of Fmoc-FY*p* pre-gelator and a surfactant-like amino acid or peptide that is phosphatase responsive and thus kinetically controlled.[106] They studied the one-step co-assembly of gelator/surfactant peptide-based systems triggered by phosphatase action that show on-demand transformation from micelles into co-assembled nanofibres that can display the surfactant head group at the surface. They found out that Fmoc-FY/T and Fmoc-FY/RGD formed more ordered structures and stiffer gels when increasing phosphatase concentration, while the opposite effect was observed for the Fmoc-FY/S system, which permits the conclusion that this depends on the chemical structures and self-assembly process.[106]

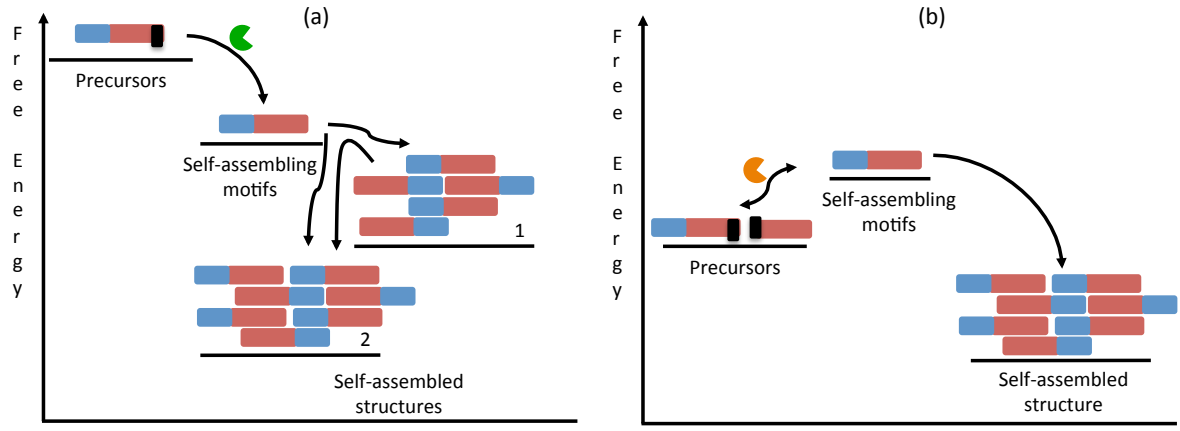

Figure 2.14. Free energy diagram of (a) Enzyme-triggered self-assembly under kinetic control; (b) Enzyme-triggered self-assembly under thermodynamic control.

On the second case (route b), the enzymatic reaction of bond making is thermodynamically unfavoured but the process is facilitated by the low free energy contribution of the self-assembly step (See Figure 2.14b), allowing the process to occur. Due to this, the self-assembling motifs can be converted back to their precursors in a fully reversible reaction. This is an attractive feature, as it comprises full reversibility providing opportunities for constant defect repairing of the supramolecular structures.[100] It is possible to reduce defects and to eventually form the thermodynamically favoured supramolecular structure by developing a biocatalytic system that undergoes thermodynamically driven self-assembly. This approach is only applicable when the desired structure represents the global equilibrium state and, sometimes, they represent just the local thermodynamic minima. This is the reason why the formation of non-equilibrium supramolecular structures is also important and complements the thermodynamic approach. By these ways, highly selective supramolecular nanostructures with few defects can be designed for any application such as drug delivery, three-dimensional cell culture, imaging and antimicrobial nanomaterials, among others.

2.2.4.2 Other types of biocatalytic self-assembly

In addition to these, there are other arising ways of using biocatalytically-triggered self-assembly, where the objective is to mimic nature's systems that display dynamic instability

and not always follow equilibrium.[122] This is exactly the main difference between a Man-made system and many of nature's active assembling systems, where assembly requires energy input and breakdown is equilibrium-driven. There is rising interest in achieving systems that are not permanent and can be reconfigurable, reaching the dynamic self-assembly, introduced by Whitesides.[21]

The dis-assembly of a hydrogel network can also be enzymatically controlled and can be useful for many applications such as controlled drug release.[56] It occurs in the opposite way to the self-assembly, by conversion of hydrogelators into precursors where transitions of the overall macroscopic structure from a hydrogel into a solution are observed.[15] The enzyme catalyses either a reaction of addition of a blocking group to the hydrogel monomers (causing steric hindrance or electrostatic repulsion which prevents self-assembly), a reaction of covalent bond cleaving or one that exploits any chemical changes in functional groups that modifies the charge balance. It almost never depends on energy input, except in the work of phosphatase/kinase developed by Xu's group to regulate supramolecular hydrogelation.[109] They demonstrated that dephosphorylation catalysed by phosphatase gave rise to a hydrogelator and then the formed hydrogel was broken by the activity of kinase that phosphorylated it again in the presence of a phosphate donor (ATP), re-forming a solution.[56] A single enzyme is hardly ever used to control assembly and dis-assembly since the reactions are usually irreversible,[56] which is solved in nature by the counteractive and cooperative work of a pair of enzymes to regulate protein functions.[109] Phosphatase and kinase are two well-known antagonist enzymes that regulate signal transduction in a cell and can also regulate formation and disruption of supramolecular hydrogels by catalysing assembly and dis-assembly. Since the phosphatase activity follows a favoured reaction and the kinase an unfavoured one, the cooperative action of the two is overall thermodynamically controlled. However, it can operate away from equilibrium by adding ATP fuel, favouring the system to the hydrolysis reaction when the fuel runs out. This enzymatic switch has been stated to be very promising for the design and application of biomaterials in different therapies.

Debnath and co-workers developed a non-equilibrium biocatalytic self-assembled system with dynamic instability that actually relies on the assembly by kinetic control and

disassembly by thermodynamic control using a single enzyme – chymotrypsin.[122] By using an activated acid (methyl ester), they were able to create a temporary high-concentration of the gelator that can then be hydrolysed forming nanofibres with dynamic instability, mimicking natural dynamic self-assembled systems. The system could undergo self-assembly, with the amide bond formed by transacylation catalysed by chymotrypsin, and be reassembled several times by adding more methyl ester to temporarily drive the system away from equilibrium. Pappas *et al.* reported on the transient supramolecular reorganisation of Fmoc-dipeptide amphiphiles when using ultrasound energy, that revert back to the initial structures when the sound is switched off.[123] The transitions in the balance between H-bonding and π-stacking interactions were sequence dependent: Fmoc-FL undergoes a reconfiguration from tapes to coiled fibres; and Fmoc-YL reconfigures from straight fibres to spherical aggregates under high frequency oscillating pressure waves. All together, these examples show that dynamic out-of-equilibrium systems are achievable.

2.3 Emulsions and Surfactants

Emulsions are metastable dispersions of one liquid in an immiscible liquid medium in the form of droplets.[124-125] Even though not all emulsions are constituted by water in one phase and an oil in the other, this is the normally used nomenclature. Emulsions can be classified according to their type and size. According to the former, they can be oil-in-water or water-in-oil, depending if oil droplets are dispersed in a water continuous phase or if water droplets are dispersed in oil medium, respectively.[126] Based on the latter, they can be considered as microemulsions, miniemulsions, macroemulsions and nanoemulsions, where the size acts more as a guide and the thermodynamics of formation is what actually distinguishes them. Microemulsions (droplet size < 100 nm) are thermodynamically stable, being formed spontaneously ($\Delta G_{form} \leq 0$), whereas the others are kinetically stable.[126] When placed together in a container, water and oil form two separate layers since that is the most stable state, minimising the contact area between phases and the free energy.[127] In order to form an emulsion and disperse one phase into the other, energy needs to be brought to the

system, except in the case of microemulsions. The dispersion of one phase into droplets is thus achieved by agitation/homogenisation. The free energy per unit area denotes the amount of work necessary to expand the interface and is usually called interfacial or surface tension γ.[128] A solid-liquid system is termed suspension, whereas a liquid-liquid system is an emulsion.[127] An interface corresponds to the boundary between two phases. When one of the phases is gaseous (gas-liquid and gas-solid), the interface is called the surface and the work required to change its shape is called surface tension. However, and because the focus of this thesis will be on liquid-liquid interfaces, the term interfacial tension will be used throughout this thesis regardless of the nature of the two phases.

The thermodynamics upon emulsion formation, or free energy of formation, can be expressed by Equation 2.2:

$$\Delta G_{form} = \Delta A \gamma_{1,2} - T\Delta S_{conf} \qquad \text{(Equation 2.2)}$$

where ΔA is the change in interfacial area, $\gamma_{1,2}$ the interfacial tension between phases 1 and 2 at temperature T and ΔS_{conf} the configurational entropy change. In order to lower the energy necessary for emulsification and disperse two immiscible liquids, the free energy for creating a new area of interface $\Delta A \gamma_{1,2}$ needs to be decreased. Since the droplets are constantly moving and tend to merge together to re-establish phase-separated layers, a third component is needed to lower the interfacial tension - a surfactant. For the emulsion to form spontaneously (microemulsion), ultra-low interfacial tension is needed (~10^{-4} to 10^{-2} $mN.m^{-1}$), which is only achieved when adding a second surfactant.[129-130]

Surfactant is a commonly used contraction that stands for "surface active agent", which means being active at surfaces. Surfactants are organic molecules known for adsorbing at interfaces and surfaces, in order to decrease the free energy of the boundary between the two immiscible phases. Surfactant adsorption at water-oil interfaces is a key property for emulsion formation due to their ability to increase the interfacial area between two immiscible phases.[127, 131] Surfactants are commonly used within the cosmetics, food, coating, petrochemical, detergency and pharmaceutical industries, but also in scientific processes that involve biological systems and purification.[132-133]

Surfactants are amphiphilic molecules, since they have a polar head group and a hydrophobic tail (See Figure 2.15). This amphiphilic nature explains their tendency for the interfaces, where the polar heads tend to be in contact with water and the hydrophobic tail in an apolar environment. This tail generally consists of one or more carbon chains, which may be linear or branched. The physicochemical properties of surfactants can be highly influenced by the chain length of the surfactant tail, the degree of chain branching and the position of the head group. The surfactants are classified by the polar head, and can thus be ionic, anionic, non-ionic or zwitterionic. The latter class relates to the surfactants that present both anionic and cationic charges at normal conditions.

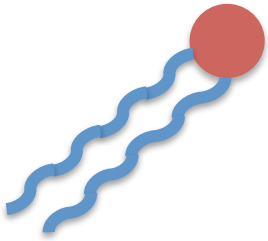

Figure 2.15. Schematic representation of a surfactant.

Since the created interactions to form a self-assembled monolayer depend on the structure of the surfactant and on the nature of the phases,[134] there is no universally good surfactant. The choice of surfactant will therefore depend on the desired application, knowing that it should have high solubility in the continuous phase of the required type of emulsion. This is known as the Bancroft rule, which states that water soluble surfactants tend to stabilise O/W emulsions, while oil soluble surfactants stabilise W/O emulsions.[135] This rule opposes the one applied when no surfactant is used, where the type of emulsion depends on the volume fraction of each phase.

A surfactant can either undergo adsorption to the water/oil interface or aggregate in solution, giving rise to the so-called micelles. Micelles are formed with the hydrophobic tails facing the interior and the hydrophilic heads the water phase (Figure 2.16). These are, therefore, highly water soluble aggregates that do not present surface activity.[134] This micellisation process is seen as a competitive alternative to the adsorption at interfaces. Since it also results from the hydrophobic effect, avoiding the hydrophobic tails of

monomers to contact with water, it also reduces the free energy of the system.[127] The concentration of surfactant in water at which micelles start to form is called the critical micelle concentration (CMC), this is a defining characteristic of a surfactant.

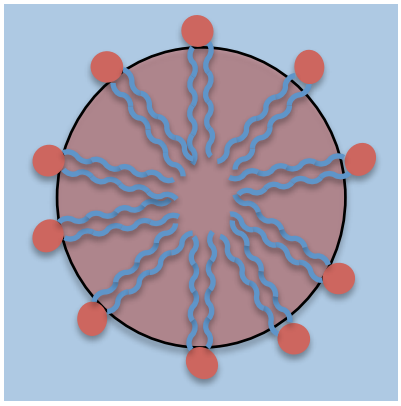

Figure 2.16. Schematic representation of a micelle.

2.3.1 Emulsion stability and measurement

The production of emulsions or foams requires the formation of droplets, the size of which is controlled by different factors.[134] The homogenisation/agitation method, which is responsible for the movement of liquids in a specific flow regime, is key for the emulsification process.[136] The disruptive forces, created by homogenisers and dependent on hydrodynamic conditions, are then responsible for the creation of droplets and their size. However, after homogenisation, droplets move quickly and collide frequently, trying to coalesce to minimise the interfacial area.[137-138]

In addition to the adsorption of the surfactant molecules at the oil-water interface to reduce the interfacial tension, its presence is also essential as to form a self-assembled monolayer[132] and prevent the droplets from coalescence. The stronger the tendency of the surfactant to accumulate at the interface, the denser the packing and hence, the larger the reduction of the interfacial tension. If the concentration of the surfactant is not high enough to cover the droplet interface, the droplets are likely to merge with their neighbours.[139]

Emulsion instability may involve a combination of different mechanisms that lead to emulsion disruption.[140] These major forces of instability can affect each other and are schematically represented in Figure 2.17.

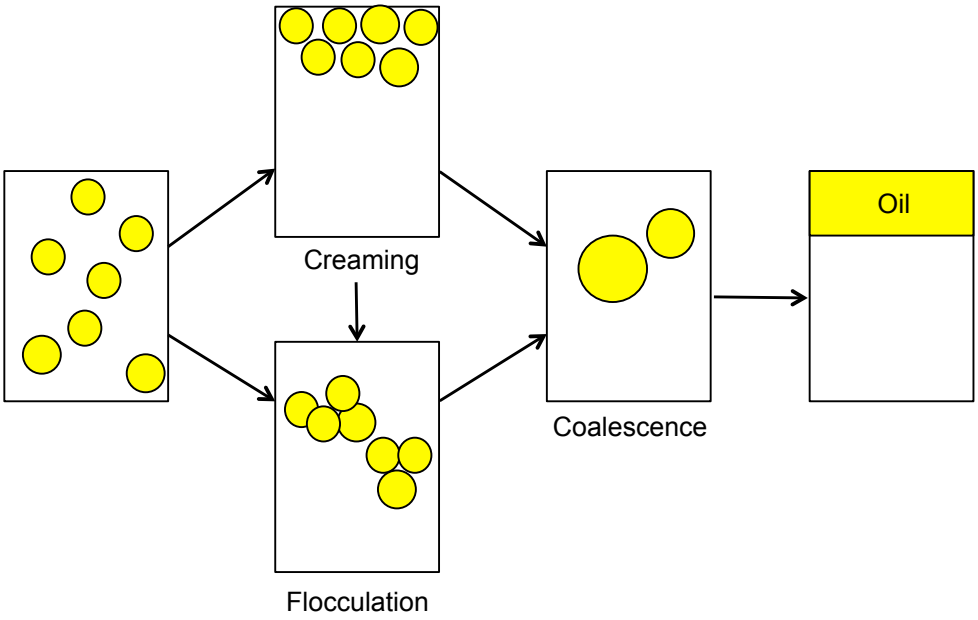

Figure 2.17. Schematic representation of the different instability phenomena responsible for emulsion break-down.

Creaming (or sedimentation) is normally a reversible process by which droplets undergo gravitational separation and move upwards (or downwards, if their density is higher than the density of the continuous phase) to form a packed layer. The creaming rate (v) in dilute emulsions can be explained by Stokes' equation (Equation 2.3).

$$v = \frac{d^2(\rho_d - \rho_c)g}{18\eta} \qquad \text{(Equation 2.3)}$$

where d represents the droplet diameter, ρ_d the droplet density, ρ_c the density of the continuous phase, g the gravitional acceleration and η the viscosity of the continuous phase. From this, it is clear that there are three ways to decrease creaming rate and thus increase emulsion stability due to creaming: (i) by reducing the droplet size; (ii) by overlapping the densities; or (iii) by increasing the viscosity of the medium.

Flocculation occurs when two or more droplets "stick" together to form an aggregate, but the individuality of each droplet is remained. Coalescence happens when two or more droplets merge together, creating a single larger droplet. Coalescence of droplets is normally caused by one of the other phenomena (as in Figure 2.17), usually occurring before complete emulsion break-down and layer separation.

Unlike microemulsions, that are thermodynamically stable and present a high degree of dynamics, allowing for variations, macroemulsions are inherently unstable systems that tend to disruption.[136] The development of long-term stable emulsions is highly desired in many fields including food industry, but this is still in process. Since emulsions are thermodynamically unstable, the kinetic stability is of great importance. In fact, emulsion instability processes can take place over a long period of time, which allows for the emulsions to remain in a metastable state that is kinetically stable.[140]

The measurement of emulsion stability can be challenging but there are some methods in the literature to measure the stability. Since creaming in emulsions is normally a slow process, accelerated tests are usually employed, such as centrifugation of the emulsion, heating of the emulsion or application of ultrasound energy. There are only a few reported methods to measure flocculation, as the most commonly used are the ones that measure coalescence, which precedes phase separation. Coalescence of emulsion droplets causes several changes with time, such as the average droplet size, number of droplets, turbidity, and viscosity, among others. Since no macroemulsion is permanently stable, it is normal to compare the time it takes for properties to change. Thus, emulsion stability is usually measured by following the changes over time of any of the above mentioned properties. In fact, an emulsion is judged to be more stable than another one if it undergoes changes in a more slowly manner. While this latter approach is more accurate than an empirical approach, it is not assured that the changes are only occurring due to coalescence.[136] The most efficient way of measuring emulsion stability is thus to analyse the evolution of the droplet size with time since instability phenomena either affect or are affected by the diameter increase.[137]

2.3.2 Alternative emulsification processes

Although traditional surfactants are adequate to stabilise emulsions, they are not always biocompatible or biodegradable, which may be limiting for some applications. There is a constant concern about the ecological impact of surfactants, since the majority of them used in households and different industries ultimately go into the sewers. Besides the legislation on this, the formulation of surfactants can play an important role, since the surfactant structure has a significant influence on the rate of biodegradation.[128] Dermatological effects of surfactants that are frequently used in cosmetics formulations are also subject of much concern. Anionic surfactants are more skin irritating than non-ionics, for example, and some of them, such as nonylphenol and nonylphenol ethoxylates, present high toxicity.[141] Moreover, some surfactants are known to present limited stability towards temperature, pH and salts.[142] In addition to traditional surfactants, several other different types of emulsifiers have been investigated over the last decades.

As already mentioned, it is usually the covering monolayer that prevents the droplets to undergo coalescence.[128] Surface active polymers or copolymers have been highly exploited in the last decades.[127] They can be designed in different ways that allow the orientation of the molecule so that the hydrophilic moieties face the polar environment, reducing the interfacial tension.[127] The formation of micelles is usually favoured as they have a relatively low CMC value when compared to low molecular weight surfactants. In fact, polymeric surfactant-based micelles have been used by some authors as drug delivery systems. However, the quick diffusion to the new interface is the reason why low molecular weight surfactants are preferred over high molecular weight polymers, proteins and liquid crystals to stabilise emulsions.[128] One of the clear trends in current surfactant formulation are to synthesise surfactants from natural sources.[143] Natural products that have always been seen as possible hydrophilic head groups are sugars or amino acids, while fatty acids are the immediate choice for the hydrophobic tail of surfactants.[128] However, many other approaches have already been developed and investigated (Figure 2.18).

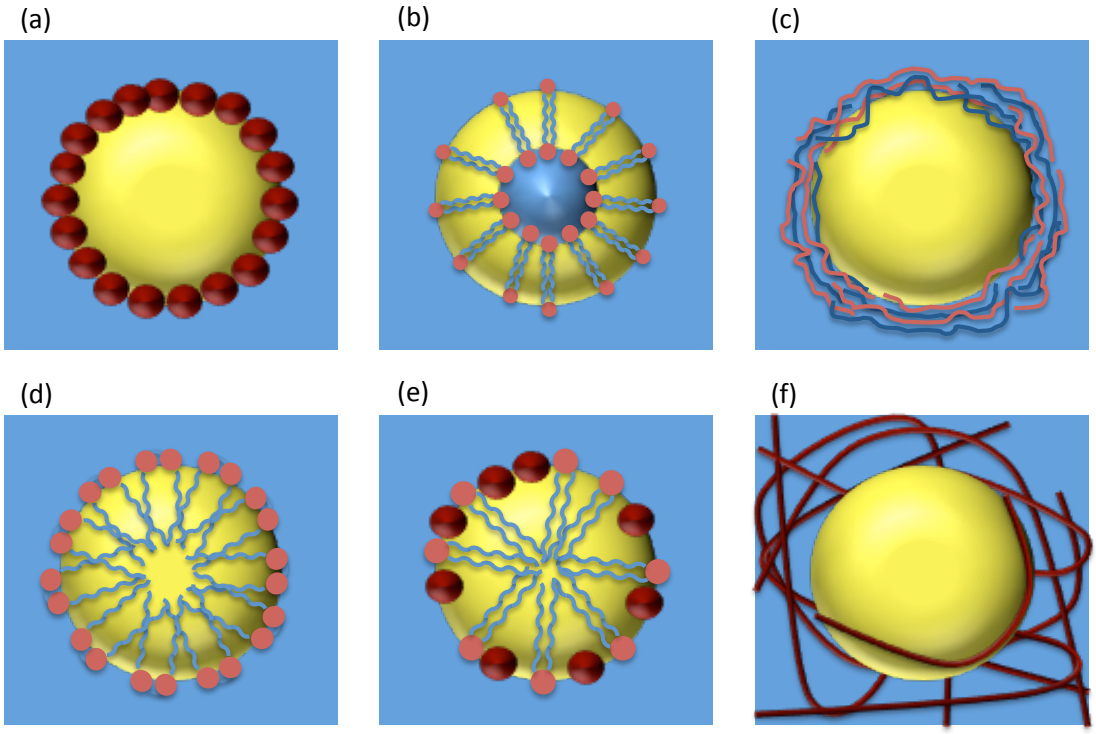

Figure 2.18. Different emulsification processes: (a) Pickering emulsions; (b) Bolaamphiphiles; (c) Layer-by-layer microcapsules; (d) Gemini surfactants; (e) Combination between surfactants and particles; (f) Gelled emulsions.

Pickering emulsions (Figure 2.18a), emulsions stabilised with solid particles, have gathered increasing interest, where solid nanoparticles are used instead of surfactants.[144-145] These solid-stabilised emulsions were given this name since Pickering observed that colloidal particles situated at the oil-water interface could stabilise emulsions of oil and water.[146]Furthermore, Pickering emulsions have high resistance to coalescence and preserve the properties of a classical emulsion stabilised by surfactants.[145, 147] Besides, an approach that combines peptide self-assembly and Pickering emulsions to make and emulsify microparticles was shown, that can be used to immobilise enzymes, allowing them to be used in organic media.[148]

Bolaamphiphiles differ from typical surfactants since they have two hydrophilic heads connected by a hydrophobic section.[149] They are very attractive for encapsulation and drug transport, since they have the ability to carry both polar and nonpolar molecules, depending

on the formulation.[150] As represented in Figure 2.18b, where an aqueous core is formed, polar molecules can be transported.

Microcapsules produced by several different methods have recently been considered for application in the pharmaceutical field, as emulsion stabiliser agents. Layer-by-Layer-based microcapsules (Figure 2.18c) made of polyelectrolytes and fluorescein have advantageous properties, such as a high loading capacity, good biocompatibility, high stability to environmental stress and stimulus-responsive behaviour.[151]

Gemini surfactants, which are dimeric surfactants containing two hydrophobic tails and two head groups connected with a linker, also arise as possible emulsifiers (Figure 2.18d). The spacer can be either hydrophilic or hydrophobic, rigid or flexible, and connects the two molecules by the head groups, or in close vicinity to them.[127] There has been considerable research interest since they present very low CMC values and are efficient lowering the surface tension.[128]

Additionally, the use of a combination of surfactant and particles for stabilisation of water-in-oil or oil-in-water emulsions has attracted significant attention (Figure 2.18e).[152-153] Oil-in-water emulsions stabilised by dual emulsifiers were proven to be very stable – when adding surfactant molecules to a nanoparticle system initially led to particle flocculation and then surfactant adsorption decreased the interfacial tension.[152] Also the opposite process of adding a particles' system to a surfactant-based emulsion increased their efficiency as emulsifiers, due to synergic interactions between them at the emulsion droplet interface and in the bulk.

The use of interpenetrating networks achieved by the orthogonal self-assembly of low molecular weight gelators and surfactant micelles has been studied thoroughly as it allows for the formation of more distinct architectures.[154-155] In addition to gelling binary water/surfactant systems, the gelation of microemulsions has also been studied.[156-157] Gelled emulsions can be used to delay or prevent droplet coalescence (Figure 2.18f). These can be formed by gelation of the aqueous phase by *e.g.*, hydrophilic polymers.[158-159] The formation of a gel matrix where droplets are embedded prevents the emulsion to undergo coalescence or creaming. The rheological properties of these gel-type emulsions have been

proven to depend on the volume ratio and interaction between the matrix and the droplets.[160] The stiffness of the gels increased when the droplet-adsorbed protein interacts with the casein gel matrix.[161-162] In-situ gelation of the polymer/protein at the interface or at the continuous phase can also occur upon emulsification or after the process,[163-164] when using self-assembling systems.

When adsorbed to an interface, proteins in general can have their helical structures destroyed, as the molecules rearrange according to the hydrophilic/hydrophobic constitution. The denaturation of proteins when non-covalent interactions are broken and the chain is re-formed can turn them into water insoluble. The formed insoluble monolayer can then exhibit a specific gel-like interfacial rheological behaviour.[165] The same happens when proteins undergo thermal denaturation: above certain temperatures, viscosity of the continuous phase is increased and gelation can occur. These mechanisms may decrease the tendency of de-emulsification due to the reduced droplet mobility.[166] Moreover, proteins have been shown to form a protective interfacial layer that may form electrostatic repulsion forces between droplets and prevent their coalescence,[159] which is commonly used in food industry.[142] The formation of ordered structures at the interface between two immiscible liquids has been demonstrated to increase the mechanical strength of the interfacial layer in question. Hermanson and co-workers also discovered the ability of recombinant engineered protein C_{16} that mimics ADF-14 (from Araneus Diadematus Fibroin) spider-silk protein to adsorb at the interface between water and oil.[167] After adsorption, the protein self-assembles at the surface of the emulsion droplets, forming a mechanically stable microcapsule able to encapsulate drugs.

2.3.2.1 Surfactant-like amphiphilic peptides

Surfactant-like peptides have been exploited for some different applications such as membrane protein stabilisation,[168] drug and gene transport,[169] among others.[12] Peptides can be finely adjusted to be amphiphilic, and there are many possible options depending on the chosen constituent amino acids (Figure 2.2), as already explored in Section 2.1.2. Peptide amphiphiles composed of a hydrophobic alkyl tail (C_{16}-VVVAAAKKK ($C_{16}V_3A_3K_3$) have been combined with alginate to form microcapsules with self-assembled peptide

nanostructures at the surface of the shells.[170] When in comparison with larger proteins, the design and synthesis ease enable surfactant-like peptides for oil/water emulsion stabilisation as an attractive class of emulsifiers.

The degree of hydrophobicity and the length of the nonpolar tail can be controlled by choosing the amino acids to use for each application.[149] Designed peptides of one to two hydrophilic (charged) amino acids as the polar head and four or more consecutive hydrophobic amino acids as the tail have been proven to undergo self-assembly in water and form nanotubes and nanovesicles.[4, 169, 171] However, the previously mentioned studies have been challenged because of difficulty in reproducing the structures.[172] Surfactant-like peptides have been designed by mimicking the structure of traditional surfactants.[169] A_6D, V_6D, V_6D_2 and L_6D_2 have been developed and studied,[171, 173] by using an acetylated N-terminus of the varying hydrophobic tail and the uncapped C-terminus for the polar head, which was the negatively charged aspartic acid for all tested (Figure 2.19).

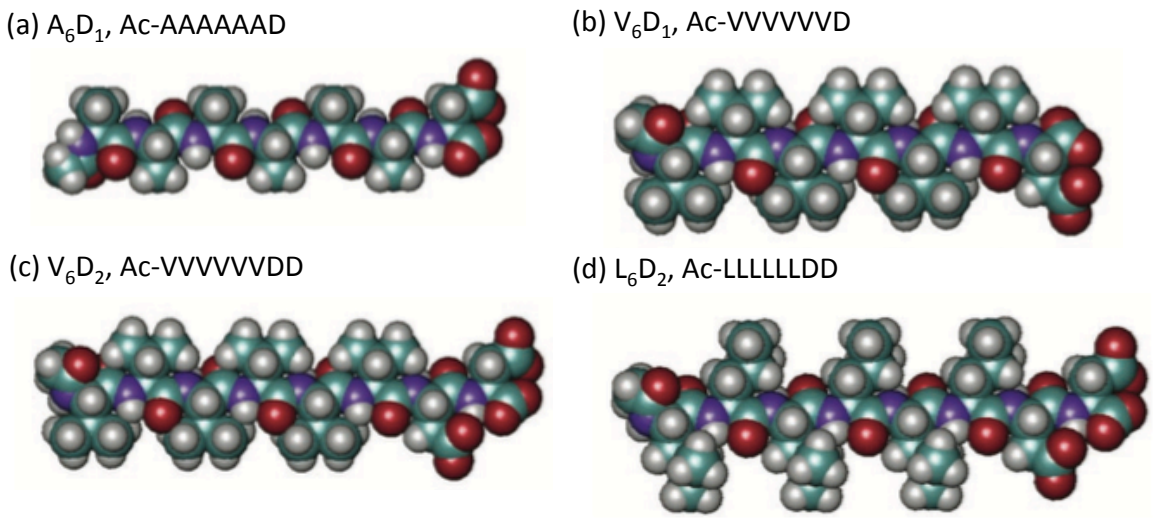

Figure 2.19. Modelled surfactant peptides: (a) A_6D_1; (b) V_6D_1; (c) V_6D_2; (d) L_6D_2. The green represents carbon, the red oxygen, the blue nitrogen and the white hydrogen atoms. Figure adapted with permission from S. Vauthey *et al.*, *Proceedings of the National Academy of Sciences* 2002, *99* (8), 5355-5360.[171] Copyright (2002) National Academy of Sciences, U.S.A.

Polypeptides have been shown to form microemulsions of oil-in-water upon the self-assembly into stable microcapsules.[174] Some peptides that present hydrophilic and

hydrophobic side chains have been exploited as surfactants by Middelberg's group, taking into account the ability of polypeptides to lower interfacial tension and enhance the stability of emulsions.[5, 175-180] 21-mer and 28-mer helical peptides (Lac21 and Lac28, respectively) were first investigated as biosurfactants and are known to adsorb at the oil/water interface, reducing the interfacial tension.[180] The so-called pepfactants (long chain (21-mer) peptide surfactants) are specifically designed for the stabilisation of emulsions where Lac21 (Figure 2.20a), AM1 (Figure 2.20b) and AFD4 (Figure 2.20c) are carefully studied.[178] AM1 differs from the well-known Lac21 by the replacement of two internal sites with metal-binding histidine residues, and AFD4 presents additional histidine residues. They have a seven-residue repeating motif with hydrophobic moieties spaced of 3 or 4 residues apart, which allows for the formation of α-helices.[178]

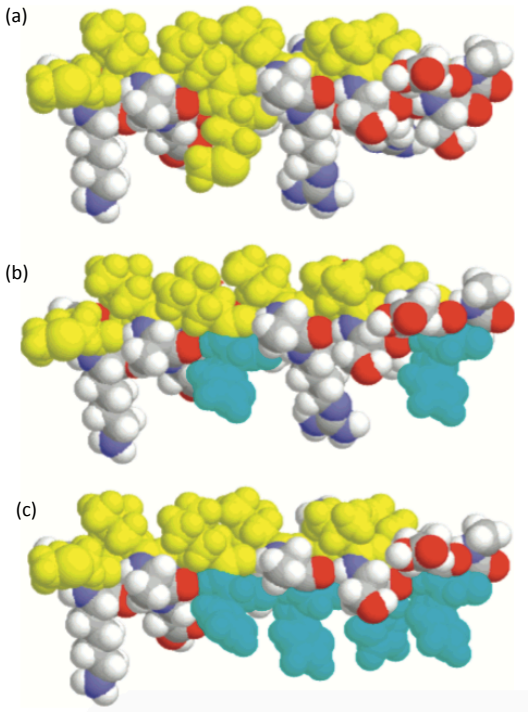

Figure 2.20. Modelled surfactant peptides: (a) Lac21; (b) AM1; (c) AFD4. The hydrophobic residues are represented in yellow and metal-binding histidine residues in blue. Figure adapted with permission from A. F. Dexter and A. P. J. Middelberg, *The Journal of Physical Chemistry C* 2007, *111* (28), 10484-10492.[178] Copyright (2007) American Chemical Society.

When a short peptide chain is used and the N-terminus capped with *e.g.*, an Fmoc group (aromatic peptide amphiphiles), a molecule with surfactant properties is formed due to the hydrophobic and hydrophilic parts.[181] Aromatic peptide amphiphiles (discussed in Section 2.2.2.) can thus present a potential use in the formation of oil-in-water or water-in-oil emulsions. Recently, our group demonstrated that Fmoc- (and pyrene-) dipeptide amphiphiles, when in a biphasic system, can self-assemble into nanofibrous networks at the aqueous/organic interface, upon brief shaking by hand, resulting in the ability to stabilise emulsions (Figure 2.21a).[79] Instead of the traditional surfactant adsorption, these emulsifiers undergo self-assembly based on non-covalent interactions. The fibrous-stabilised emulsions were demonstrated to possess higher stability towards temperature and salts when compared to a commonly used surfactant (sodium dodecyl sulfate, SDS), which adsorbs to the interface.[79] Along this line, carefully designed simple short peptides such as tripeptides were also assessed as emulsifiers. Depending on the designed sequence, they were shown to be able to stabilise O/W emulsions either by forming more traditional monolayer-type structures at the interface or by self-assembling into interfacial nanofibrous networks (Figure 2.21b).[182]

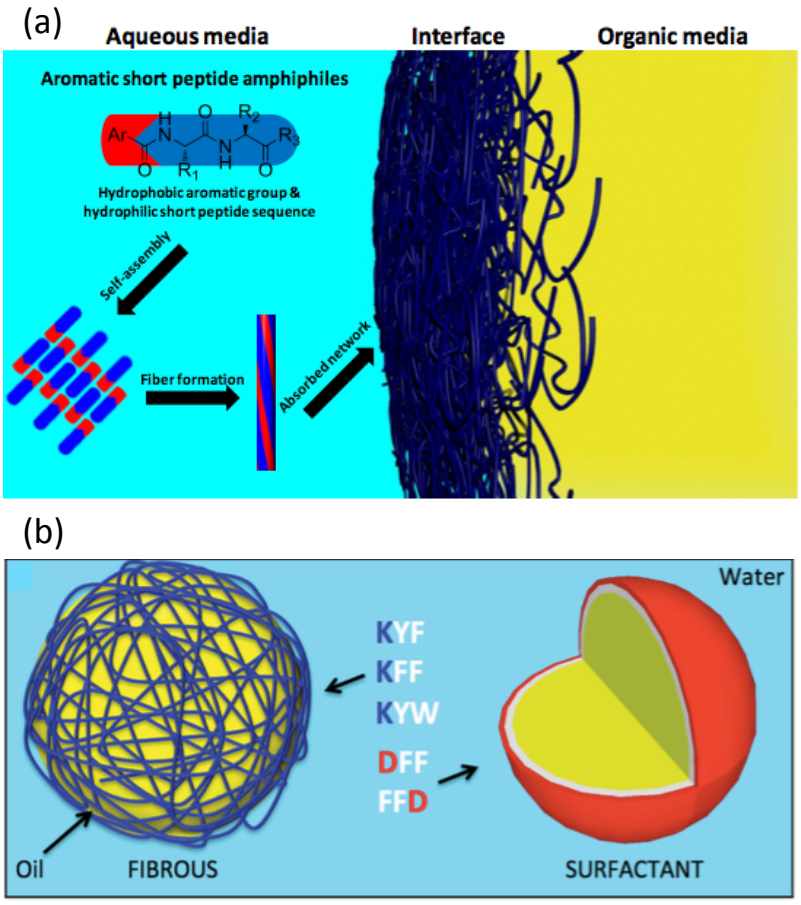

Figure 2.21. (a) Schematic representation of the self-assembly and entanglement of fibrous networks of aromatic dipeptide amphiphiles at chloroform/water interface, stabilising the droplets. Figure adapted from S. Bai, C. Pappas *et al*., *ACS nano* 2014, *8* (7), 7005-7013.[79] Copyright (2014) American Chemical Society; (b) Schematic representation of the surfactant-type emulsification as opposed to the interfacial nanofibrous droplet stabilisation when using distinct tripeptides. Figure adapted from reference [182] by permission of John Wiley & Sons, Inc. Copyright 2000 by John Wiley & Sons, Inc.

2.3.3 Stimuli-responsive emulsifiers

Stimuli-responsive emulsifiers have become very attractive in the latest decades.[183] Whilst the ability of an emulsion to withstand a range of environmental conditions is attractive, it is beneficial to have control over the (de)formation process (*i.e.* triggered emulsification). Emulsions, suspensions and foams are desired or non-wanted in different industrial processes, depending on the specific application.[184] Temporary emulsions are of interest in different areas: cleaning and degreasing of equipment; Enhanced Oil Recovery (EOR),[185-

[186] where oil is more easily labilised when the oil/water interfacial tension is reduced; within the biomedical field,[127] *e.g.*, drug delivery applications;[187] and for cosmetics products, when emulsions should separate upon use.[188] In addition, switchable surfactants are attractive in the way their activity can be delayed until needed, they can be recovered for use afterwards and removed from the product stream.[131] Most of the effort has focussed on switching-off the surfactant when emulsion stability is no longer needed.[189] However, the development of an efficient method of promoting either formation or coalescence of emulsions at a specific desired stage is beneficial, which has not been yet satisfactorily resolved. Besides the development of cleavable surfactants able to reduce the oil/water interfacial tension, much effort has been put on the achievement of properties that enable the surfactant diffusion to the newly created interface. Cleavable surfactants may be irreversibly converted, while switchable surfactants can interconvert from emulsion to a de-emulsified two-phase system and *vice-versa* when applying different stimuli.[131] For the switchable surfactants, it is possible to re-form emulsions by applying an appropriate trigger, and it is possible to break an emulsion stabilised by either of the surfactants, which may find applications, *e.g.*, in the biomedical field.

Switchable surfactants of many designs have been developed, differing mostly in the kind of trigger. The most used triggers are light,[190-192] temperature,[193-195] pH,[196-198] magnetic field,[199] CO_2/N_2.[131, 147, 189] The inversion of the emulsion type (from O/W to W/O) has been proven when using polymers by changing pH,[200] temperature,[194] light,[191] *etc*. However, enzymes can be highly attractive as triggers, if biocompatible physiological conditions need to be maintained. It has been shown in our group that it is possible to use enzymes to break water-in-oil emulsions that are produced by droplet microfluidic at physiological conditions. Bai *et al*. demonstrated the action of a protease such as thermolysin as a de-emulsifier, which can be explained by catalysis of the peptide bond hydrolysis of the surfactants used, causing the disassembly of the created nanofibrous networks and hence coalescence.[79] Besides, droplet microfluidics has also been used to produce stabilised water-in-oil droplets by a biocatalytic self-assembly of aromatic dipeptide amphiphiles.[201] It was also demonstrated that enzymes not only play a vital role in the catalysis of self-assembly and formation of particles but also in destabilising the emulsion droplets when they adsorb to the particles, promoting particle transfer from oil to water phase.

The use of peptides that rely on weak non-covalent interactions for self-assembly would allow the production of switchable emulsifiers that reorganise their structure by changing environmental conditions. The previously presented 21-residue peptide AM1, based on the amphiphilic peptide Lac21, was first reported as a stimuli-responsive surfactant that rearranges at a fluid-fluid interface upon a change in pH or presence/absence of a metal ion, regulated by the addition to the bulk aqueous solution of the metal-binding histidine residue or of a chelating agent that sequesters it.[198, 202] The previously presented pepfactants were demonstrated to stabilise foams and emulsions at fluid-fluid interfaces in a stimuli-responsive manner by changing the bulk solution conditions.[5, 198] When the film state is converted to a detergent state by a change in the bulk solution composition, the emulsion undergoes rapid coalescence. Even though this concept of switchable emulsifiers is highly desirable for different applications, its research is still in its infancy. To our knowledge, there are no studies on the use of simple aromatic peptide amphiphiles for the on-demand production and control of the emulsification ability.

2.4 Computational modelling of self-assembly

Computational modelling, in addition to experimental data, can be very helpful in providing insight into chemical systems at various levels, including molecular self-assembly processes.[203] Molecular dynamics (MD) has been extensively used to model biomolecular systems in order to understand the interactions and behaviour of the molecules throughout time. MD simulations were conceived and started to be performed in the 1950s but it was not until 1976 that the first MD simulation of a protein was reported.[204-205] Since then, the growth of computing power allowed the use of much larger simulations and systems, and there has been a dramatically increased interest to make the most stable and accurate simulations since then.[206] In fact, van Gunsteren asserts that the steady and rapid increase of the computing power is the main driving force behind the development of biomolecular modelling, followed by the progression of modelling methods.[203] Due to the highly dynamic nature of the systems and the significant conformational changes occurring throughout the time in a biomolecular self-assembly

process, MD simulations based on Molecular Mechanics (MM) are much more favourable than those based on Quantum Mechanics (QM) methods.[207]

MD methods provide the opportunity to understand the behaviour of biomolecular systems over time, when intermolecular interactions are altered and structural changes occur while the conformational energy landscape accessible to proteins is explored. Force field methods, also known as MM methods, only express the energy of the system as a function of nuclei positions. This simplifies the calculations, thus allowing the use of MD methods with large systems such as proteins, lipid bilayers, DNA, among others.

2.4.1 Principles of Molecular Dynamics

Molecular dynamics (MD) is a deterministic method that assumes the present positions and velocities of the atoms to predict the next ones, following a classical physical representation. These MD simulation methods are based upon a simplistic model of interactions that follows the Born-Oppenheimer approximation,[208] which separates the motion of nuclei and electrons within a molecule. Molecules are described in a "ball and spring" fashion in MM methods.[209] Successive configurations of the system are created by integrating Newton's equations of motion at every time step, usually ~1 fs.[210] The force F of each particle is assumed to be the same at that time step and is calculated by the derivative of the potential energy variations V, taking into account the position of the particle. Using this force, the acceleration of the atom, with mass m, is calculated, which gives its motion. By doing this, a series of space points in time (a trajectory) is defined until the end of the simulation.[209]

By using a force field where the potential energy is a function of the parameters that are related to both bonded and non-bonded atoms, it is possible to obtain a picture of the intra- and intermolecular forces within a system. Equation 2.4 expresses a class I force field, which is defined by the sum of terms, but its accuracy can be improved by the incorporation of higher-order terms.[209-210]

$$V(r^N) = \sum_{bonds} \frac{k_b}{2}\left(l_i - l_{i,0}\right)^2 + \sum_{angles} \frac{k_\theta}{2}\left(\theta_i - \theta_{i,0}\right)^2 + \sum_{torsions} \frac{V_n}{2}(1 + \cos n\omega - \gamma) + \sum_{i=1}^{N} \frac{q_i q_j}{4\pi\varepsilon r_{ij}} + \sum_{j=i+1}^{N} 4\varepsilon_{ij}\left[\left(\frac{\sigma_{ij}}{r_{ij}}\right)^{12} - \left(\frac{\sigma_{ij}}{r_{ij}}\right)^{6}\right] \quad \text{(Equation 2.4)}$$

$V(r^N)$ represents the potential energy, function of the positions (r) of N particles (or atoms). The number of parameters characterises the force field. The first term in Equation 2.4 is a Hooke's law formula that denotes the interaction between pairs of bonded atoms, where the energy increases with the square of the displacement from the reference bond length l_0. The second relates to the change in energy according to the angle θ between three atoms, also varying with the deviation from the reference angle. They are both modelled by a harmonic potential where the potential energy is directly proportional to the force constant (k) and dependent on the bond stretching and angle distortion, respectively. Since a large energy barrier would need to be overcome to deviate them from the reference value, these first two terms (bonds and angles) are normally called hard terms, as they do not change significantly throughout the simulation. The third term in the equation is a torsional potential that accounts for the potential energy penalties when a bond rotates, represented by the rotational angle ω. γ represents the phase factor, n the multiplicity and V_n is normally referred to as the "barrier" height, which can be misleading since other terms, such as non-bonded, contribute to the barrier height when a bond is rotated. Also out-of-plane bending terms can be incorporated in a force field, treating the four atoms that are not bonded in the sequence 1-2-3-4 as an "improper" torsion angle. Finally, the last terms are related to non-bonded forces occurring in atoms separated by more than three bonds, where electrostatic and van der Waals interactions are the most relevant for the understanding of molecular structures.[210] Electrostatic interactions are modelled by Coulomb's law, describing the interactions between pairs of point charges, based on the unequal distribution of charge within a molecule. The parameters q_i and q_j represent the partial charges of the two atoms at a distance r_{ij}. The energy is inversely proportional to the medium permittivity (ϵ_0). In turn, a Lennard-Jones (LJ) potential is used for van der Waals interactions, quantifying the energetic influence when van der Waals forces are present. This LJ 12-6 potential consists of two adjustable parameters: the collision diameter σ, which is the

distance between two particles for which the potential is zero; and the well depth ε, which is the depth of the energy minima.

This way, MD generates successive configurations of the system by integrating Newton's laws of motion, specifying the positions and velocities of the particles in the system over time.[210] Besides the energy equations, some algorithms need to be added to MD simulations to mimic the environmental conditions that occur experimentally. Different ensembles such as constant NVT and NPT can be employed, where there is a constant number of atoms (N), temperature (T) and volume (V) or pressure (P). Periodic Boundary Conditions (PBC) are normally used to multiply the system periodically in every direction, to give an infinite bulk phase. In this way, interactions between molecules in a system and the virtual neighbouring ones through the box opposing walls are made possible. As depicted in Figure 2.22, the blue particle is able to interact with the red particle across the boundaries of the box when PBC are used, which would otherwise not occur.

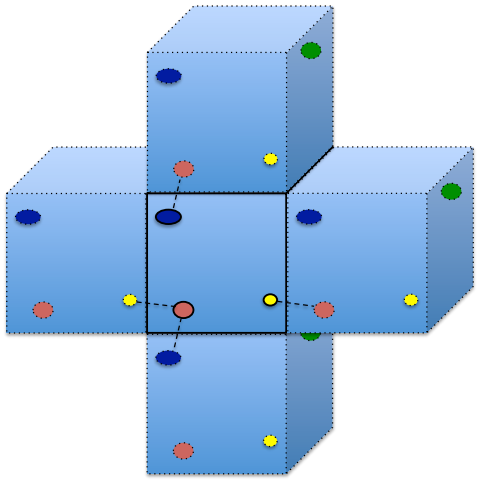

Figure 2.22. Representation of 3-Dimensional Periodic Boundary Conditions.

MD simulations that use molecular representations of every atom in the system as a ball make use of all-atom (AA) models (Figure 2.23a), an example of this type of approach is the CHARMM force field.[211-212] However, a simplified coarse-grained (CG) model (Figure 2.23c) can be used, allowing simulations to be run on length and time scales 2-3 orders of magnitude larger than atomistic simulations. The coarse-grained MARTINI force field is

developed by the groups of Marrink and Tieleman for this representation.[213-214] The MARTINI model follows a four-to-one mapping, where a single bead represents four heavy atoms. One example is CG water bead, composed of 4 water molecules, which allows an acceptable trade-off between computational efficiency and chemical representability. The ring-like molecules need a higher resolution and thus they are represented in a two-to-one mapping.[214] The MARTINI model presents 4 main types of interaction sites: polar (P), non-polar (N), apolar (C) and charged (Q). Within a main type, subtypes according to the hydrogen-bonding capabilities (d = donor, a = acceptor, da = both, 0 = none) and to its degree of polarity (from 1 = lower polarity to 5 = higher polarity) are specified for each bead.

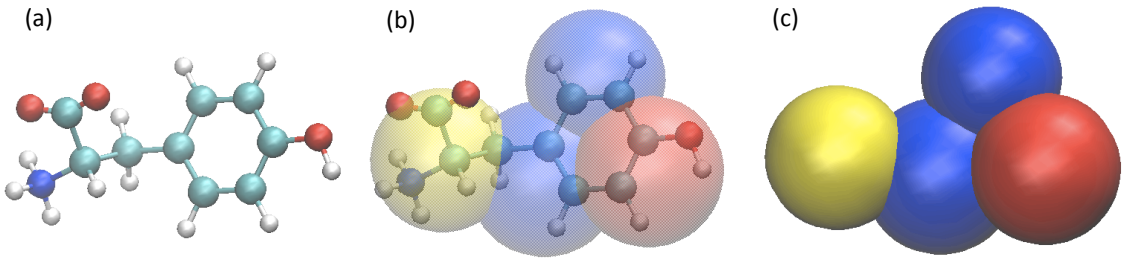

Figure 2.23. Tyrosine MD representations using (a) atomistic; (b) atomistic and coarse-grained; (c) coarse-grained representations.

The total energy is also determined by the sum of nonbonded energy and bonded terms in the MARTINI force field, following the general force field (Equation 2.4).[214] However, the non-bonded interactions between the particles i and j at distance r_{ij} are described by the shifted Lennard-Jones 12-6 potential (Equation 2.5):

$$V_{LJ} = 4\varepsilon_{ij}\left[\left(\frac{\sigma_{ij}}{r_{ij}}\right)^{12} - \left(\frac{\sigma_{ij}}{r_{ij}}\right)^{6}\right] \qquad \text{(Equation 2.5)}$$

with the strength of the interaction, given by the LJ well-depth ε_{ij}, ranging from 5.6 kJ.mol^{-1}, for interactions between strongly polar groups, and 2.0 kJ.mol^{-1}, for interactions between polar and apolar groups. In turn, σ_{ij} represents the closest distance (the collision diameter) between two particles i and j (at zero energy), the effective size of σ = 0.47 nm for each

interaction pair is assumed, except for the cases of ring-ring interactions (σ = 0.43 nm), antifreeze particles and interactions between charged and the most apolar types. In addition to the LJ interaction, charged groups (type Q with charge magnitude q) are modelled by a shifted Coulombic potential energy function (Equation 2.6):

$$V_{el} = \frac{q_i q_j}{4\pi\varepsilon_0\varepsilon_r r_{ij}} \qquad \text{(Equation 2.6)}$$

with a relative dielectric constant ε_r = 15 or 2.5 for explicit screening when combined with standard or polarizable water, respectively, and ε_0 the vacuum dielectric constant. The global screening constant of 15 is used due to the absence of partial charges in the standard Martini water model. Bonded interactions between chemically connected coarse-grained particles are also described by weak harmonic functions (Equations 2.7 to 2.10):

$$V_{bond} = \frac{1}{2}k_b\left(l_{ij} - l_0\right)^2 \qquad \text{(Equation 2.7)}$$

$$V_{angle} = \frac{1}{2}k_a\left\{\cos\left(\theta_{ijk}\right) - \cos(\theta_0)\right\}^2 \qquad \text{(Equation 2.8)}$$

$$V_{dihedral} = k_d\left[1 - \cos\left(\phi_{ijkl} - \phi_0\right)\right] \qquad \text{(Equation 2.9)}$$

$$V_{imp\ dihedral} = k_{id}\left(\phi_{ijkl} - \phi_0\right)^2 \qquad \text{(Equation 2.10)}$$

In the MARTINI force field developed for proteins (version v2.1),[215] the force constants k are normally weak, allowing for the molecule to be flexible. The term l_{ij} refers to the bond length between particles i and j in comparison to the reference bond length l_0, θ_{ijk} the angle between i, j and k in comparison to the reference angle θ_{ijk}, ϕ_{ijkl} the dihedral angle between i, j, k and l in comparison to the reference dihedral angle ϕ_0. For the dihedrals, a proper dihedral potential is used to impose secondary structure of the peptide backbone, even though they are not accurately modelled, and improper dihedrals to prevent out-of-plane distortions of planar groups.[215]

This model is able to provide information about molecules' self-assembled interactions and properties, even though atomistic detail is lost.[216] Although this loss of atomistic detail when using coarse-graining precludes the analysis of, *e.g.*, hydrogen bonds between

peptides, many parameters such as polarity, charge and non-bonded interaction tendencies are considered in the parameterisation of the beads. The non-bonded interactions have been parameterised based on thermodynamic data such as the free energy of hydration, of vaporisation and, most importantly, partitioning free energies between water and several different organic solvents for each amino acid. Bonded interactions were taken from the distributions of bond lengths, angles and dihedrals from the respective atomistic geometry or from comparison to atomistic simulations. These are essential for the stabilisation of the secondary structure of a peptide or protein,[217] especially angle and dihedral potential energy functions. The secondary structure needs to be defined and established *a priori* since their transformations are not modelled in the current Martini force field parameterisation. The assigned parameters were validated by different tests such as the partitioning of all amino acid side chains and comparison with atomistic simulations.[215]

Based on the already mentioned differences between atomistic and coarse-graining methods, a compromise between the level of detail and the extension of the simulations must be taken for each system depending on the desired objectives. The election of the starting structures, system size and length of the simulations is also critical for the achievement of the required information in each case. The environment in which biological and self-assembly processes normally occur is an aqueous solution, which is the reason why water is usually added to the calculations. However, the water molecules significantly increase the terms to be calculated, making the calculation more time-consuming and thus computationally more expensive. However, the significant contribution that the environment makes to the behaviour of the biological systems means that the water can not be simply neglected and as such the development of water models for use in molecular dynamics simulations is an active and on-going area of research.

A “simple” and accurate water model, TIP3, uses three partial charged sites and is overall neutral in order to reproduce the electrostatic interactions in each atom. A Lennard-Jones function is used to compute the van der Waals interaction between two water molecules with a single point centred on the oxygen atom, having no contribution from the hydrogen atoms. A modification to this model, the so-called TIP3P, is used by CHARMM force field,[211] calculating van der Waals interactions that involve hydrogen atoms, differing

slightly in the geometry of each water molecule, in the hydrogen charges and in the parameters. By using a fixed water geometry, the model avoids the calculation of the bonded terms for the solvent, which reduces the time of the overall simulation. For coarse-grained Martini force fields, a P4 bead is used to represent water.[214] Alternatively, polarisable water can be used, which consists of three water particles (a central, a positively and a negatively charged) instead of the standard four waters per bead in the standard Martini force field.[218]

2.4.2 MD simulations of self-assembled structures

Since MD simulations allow for studies of conformational changes over time, these methods are adequate for dynamic macromolecular systems where functionality depends on structure. Following the increasing interest in self-assembled systems, MD has appeared as a potential application to attain more information about the supramolecular interactions that give rise to the final structures of biomolecules and peptides. In fact, it is thought that detailed information on the self-assembly process and final structures can be obtained, which is not easily accessible by any other technique or experiment.[219] Therefore, further understanding on both the supramolecular detail and the mechanism of formation of different peptide nanostructures has been made possible through the use of MD simulations of these systems.[220-221]

Atomistic MD simulations have been used to study the preferred conformations of peptides and aromatic peptide amphiphiles in the assembled structure.[80, 207, 216, 222-225] Details on the molecular level such as the non-covalent interactions responsible for the self-assembly process and consequent conformation can be obtained from these types of simulations. Using this approach of a pre-defined structure, followed by a short simulation or minimisation, several researchers have proposed a model of self-assembled Fmoc-(short) peptide amphiphiles to correlate the distances between functional moieties observed in the experimental data with the model structure. Smith *et al.* has used minimisations to gain further insight over the Fmoc-FF tubular structure,[68] Hughes *et al.* to conclude about sequence dependent assembly of Fmoc-dipeptide methyl esters,[77] and Xu *et al.* of Fmoc-LLL nanotubes.[226] All of these showed an agreement of the distances for π-stacked fluorene

rings and H-bond spacing between experimental and computational methods. However, MD simulations can provide more insight than simple energy minimisations since these account for the conformational changes of the self-assembled structures throughout the simulation time. Mu *et al.* have shown that Fmoc-AA molecules assemble into fibril structures independently of the initial model used. They also showed the typical dimensions for fibril diameter and π-stacking are in agreement with Wide Angle X-ray Scattering (WAXS) experiments.[207] Computational methods can then be used in combination with experimental spectroscopic and analytical methods that do not provide explicit results on their own in order to gain further insights into the supramolecular structure. In addition, free energy profile studies have been carried out using all-atom MD simulations for the understanding of the peptide amphiphiles self-assembly mechanism.[227]

However, the self-assembly of biomolecules such as amphiphilic peptides normally occurs on a time scale greater than the microsecond region. Atomistic methods are computationally too expensive (time-consuming) for large systems over this simulation time. For this reason, coarse-grained models have been adopted for many systems,[228-232] to allow the evaluation of the aggregation of aromatic peptide amphiphiles, peptide amphiphiles and also pure peptides.

The self-assembly of Fmoc-dialanine peptides into hydrogels is simulated when using a coarse-grained model with MARTINI force field and the self-assembly properties are obtained, including details on the distribution of Fmoc planes.[216] The main conclusion that aromatic interactions between fluorene rings are the main driving force of assembly is in reasonable agreement with Mu *et al*., who ran atomistic MD simulations on the same system, as mentioned earlier. The diphenylalanine dipeptide has also been shown to self-assemble into a varied range of nanostructures when an extended CG study is carried out, which demonstrated the concentration-dependent nature of the nanostructures obtained.[228] Schatz's group also studied free-energy profiles of peptide amphiphiles when using CG simulations,[233] and were able to achieve more thermodynamic and kinetic information, relative to the atomistic simulations.

In addition to their application between specific systems, CG methods have also been applied to differentiate between possible outcomes of competitive design experiments. Based on dynamic peptide libraries and spectroscopic tools, different atomistic models of Fmoc-dipeptides were built and then validated by analysing the stability of the structures through MD simulations, which aided in the understanding of the supramolecular arrangements.[234] In addition, and due to the wide variety of possible building blocks tailored for the design of new architectures, computational screening has been demonstrated to be extremely useful to discover new promising candidates for self-assembly. Frederix *et al.* performed a complete CG screening study of the aggregation ability of all possible dipeptides and tripeptides,[84-85] predicting the self-assembly propensity of all possible combinations of amino acids, which was then proven experimentally.

The analysis of computational results is significantly more applicable when correlated with experimental data, which is why the combination of theory and experiment is essential. As already explored in Section 2.2.2.1, the understanding of the preferred interactions and mode of assembly becomes possible by using MD in combination with experimental evidence.

3 Enzymatically-triggered emulsions stabilised by interfacial nanofibre networks

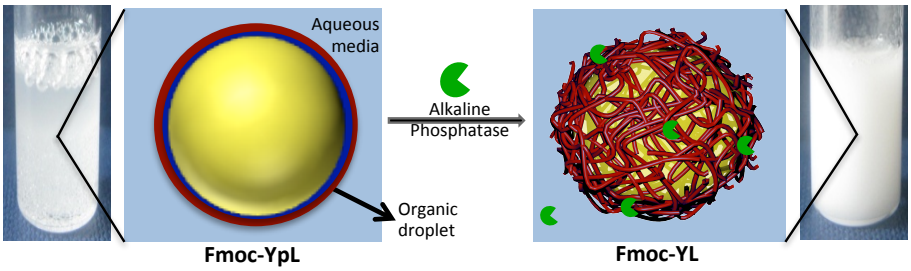

3.1 Introduction

Surfactants are commonly used in the cosmetics, food, coating and pharmaceutical industries to stabilise emulsions by decreasing the interfacial tension between two immiscible phases, avoiding droplet coalescence.[127, 131] Over the last decades, alternatives to common surfactants have been developed, as reviewed in Chapter 2.[131] Approaches include Pickering emulsions based on solid particles,[145-146, 235] bolaamphiphiles,[236] microcapsules,[151, 237] and surfactant-like peptides,[169] for water-in-oil, oil-in-water or even water-in-oil-in-water emulsions.[150]

The ability to stabilise emulsions on-demand adds control over formulation and processing of emulsions, which may have benefits to industrial applications,[131, 184] *e.g.*, when using ingredients with limited shelf-lives or by facilitating mixing by preventing instantaneous stabilisation. Pepfactants (long chain (21-mer) peptide surfactants) have been demonstrated to (de)stabilise foams and emulsions at fluid-fluid interfaces in an environmentally-responsive manner by changing the solution pH or by adding metal ions.[5, 198] However, certain ingredients, such as proteins, can be sensitive to changes in pH or temperature due to denaturation. In addition, these methods are not scalable since pH changes based on acid/base switching can damage industrial equipment and temperature drops require time and high-energy consumption in a large-scale production process.[147, 238]

As discussed in the Literature Review (Chapter 2), self-assembly of small molecules into organised and stable structures is a topic of significant interest.[239] Polymers[240] and low molecular weight gelators have been studied and designed to produce gels throughout non-covalent interactions.[171, 241] As one particularly versatile class of gelators, aromatic peptide amphiphiles, consisting of a short (di- or tri-) peptide sequences capped at the N-terminus with an aromatic hydrophobic functional group such as Fmoc, have been studied extensively in relation to their ability to form self-supporting hydrogels.[43-44, 53, 242] A number of chemicals and physical triggers have been used for Fmoc-peptides and more generally for other self-assembling systems to initiate self-assembly and to influence the produced nanostructures.[2, 51, 68, 91, 93, 172] In particular, biocatalytic self-assembly of aromatic peptide amphiphiles enables control of the self-assembly process under constant and

physiological conditions.[104] After Bing Xu's group exploited enzymatic self-assembly of Fmoc-amino acid using an alkaline phosphatase to form a Fmoc-Y hydrogel under basic conditions,[61] many others followed.[3, 55, 107, 118, 243]

Fmoc- (and pyrene-) dipeptide amphiphiles were demonstrated to self-assemble into nanofibrous networks at the aqueous/organic interface when mixed in a biphasic system upon brief shaking by hand and had the ability to stabilise emulsions.[79] These emulsifiers undergo micelle-to-fibre reconfiguration based on changes in non-covalent interactions. Whilst the ability of an emulsion to withstand a range of environmental conditions is attractive, it is beneficial to have control over the formation process (*i.e.*, triggered emulsification). Therefore, the innovative aspects of this work are focused on the possibility of combining the advantages of aromatic peptide amphiphile network formation at interfaces (stability) with biocatalytic triggering of self-assembly to enable the control of the on-demand stabilisation of emulsions.

In combining these features, fundamental questions about the ability to enzymatically initiate a self-assembly process at the water/solvent interface are also addressed, which has not been demonstrated to date. Some alkaline phosphatases are membrane-bound and integral membrane proteins (others are secreted into the cytosol), suggesting that they are able to operate at interfaces.[244] More generally, many studies have shown the stability and activity of enzymes in non-aqueous (including biphasic) media.[245-247]

Thus, we describe the phosphatase-mediated conversion of a phosphorylated peptide amphiphile with modest emulsion stabilisation capability to the corresponding dephosphorylated gelator, which forms a stable interfacial network (Figure 3.1a). The first part of this study details the enzymatic conversion, using alkaline phosphatase, of the precursor Fmoc-tyrosyl-phosphate-leucine-OH (Fmoc-Y*p*L, Figure 3.1b) into Fmoc-tyrosyl-leucine-OH (Fmoc-YL, Figure 3.1b) in aqueous buffer. The resulting hydrogel is characterised and the non-covalent interactions that dictate the nanostructure formation are analysed experimentally and correlated with simulations. Having established the ability of the enzyme to trigger the self-assembly process, the second part of the study is to investigate the on-demand formation of amphiphilic Fmoc-YL fibres at the chloroform/water interface, converting the surfactant-adsorbed biphasic mixture into a

network-stabilised emulsion (Figure 3.1a). Finally, we demonstrate delayed activation by storage of the solvent mixtures with phosphorylated peptides for periods of up to one month with stabilisation of the emulsion upon enzyme addition and shaking.

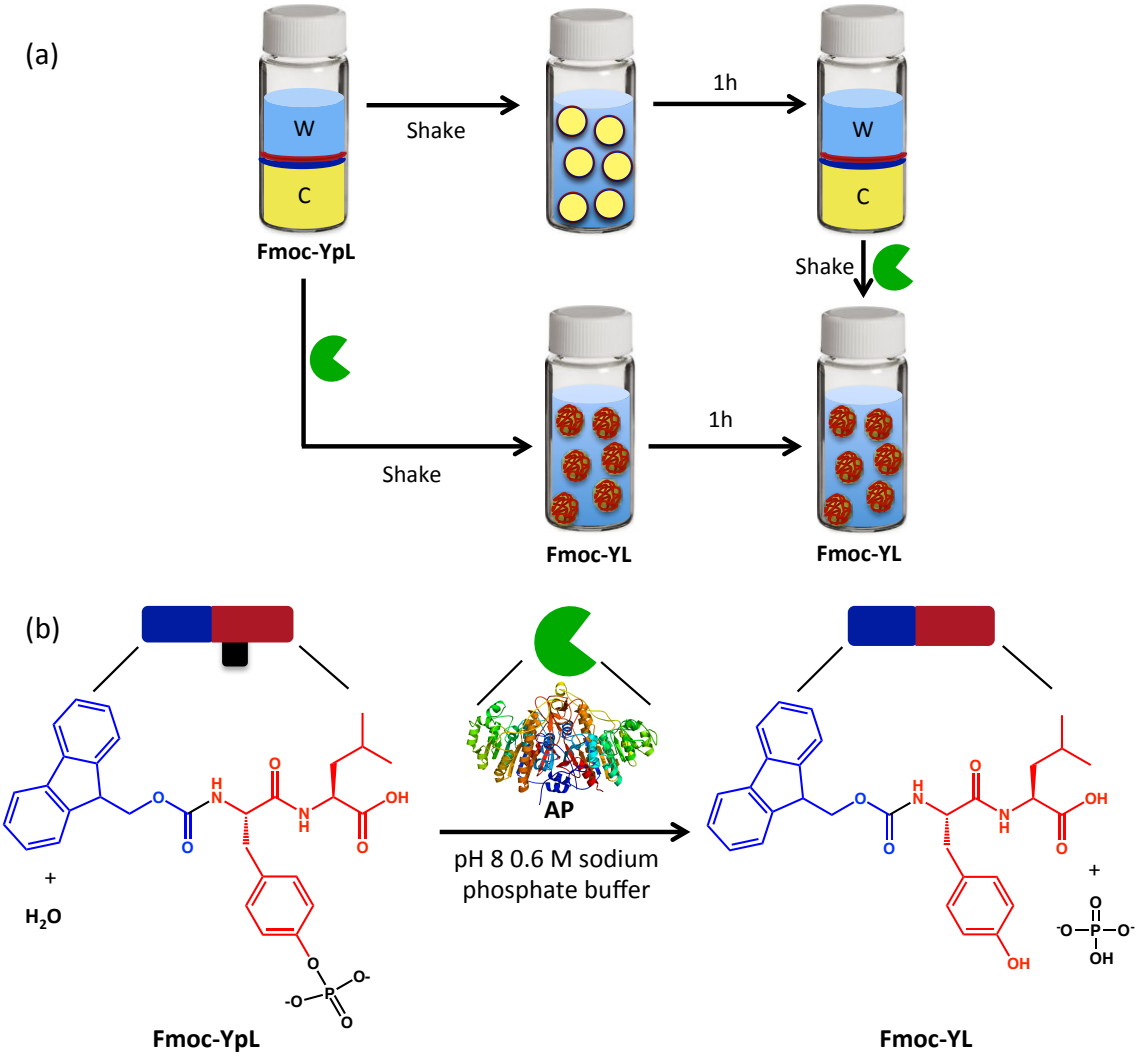

Figure 3.1. (a) Schematic representation of the behaviour of Fmoc-Y*p*L before and after alkaline phosphatase dephosphorylation in a chloroform/water biphasic system, showing the ability of Fmoc-YL to stabilise emulsions, contrary to Fmoc-Y*p*L which follows a surfactant-type behaviour and relaxes back to two-phases after 1 hour. Cyan blue represents water, yellow chloroform and green the alkaline phosphatase; (b) Cartoon and schematic representation of the enzymatic conversion from Fmoc-Y*p*L to Fmoc-YL when using the enzyme alkaline phosphatase (structure from Protein Data Bank).

3.2 Enzyme-triggered self-assembly of Fmoc-YL in aqueous buffer

3.2.1 Conversion: Macro/Microscopic characterisation

The precursor solution, 10 mM Fmoc-Y*p*L in 0.6 M sodium phosphate buffer pH 8, remains a solution after 24 h from preparation (inset of Figure 3.2a) and does not show any evidence of fibre formation. Instead, aggregates are visible by TEM (Figure 3.2a) and AFM imaging (Figure 3.2b), which is believed to be due to the electrostatic repulsion between anionic phosphate groups. Upon addition of alkaline phosphatase, the hydrophobic/hydrophilic balance is changed as expected,[109] and the soluble non-assembling precursor Fmoc-Y*p*L is converted into the more hydrophobic Fmoc-YL hydrogelator. A nanofibrous network is thus produced (Figure 3.2c and Figure 3.2d), which results in transformation of a clear solution to a self-supporting hydrogel. Similar observations have been reported using Fmoc-Y*p*,[61-62] Fmoc-FY*p*,[107, 242, 243] Fmoc-Y*p*S and Fmoc-Y*p*N.[55]

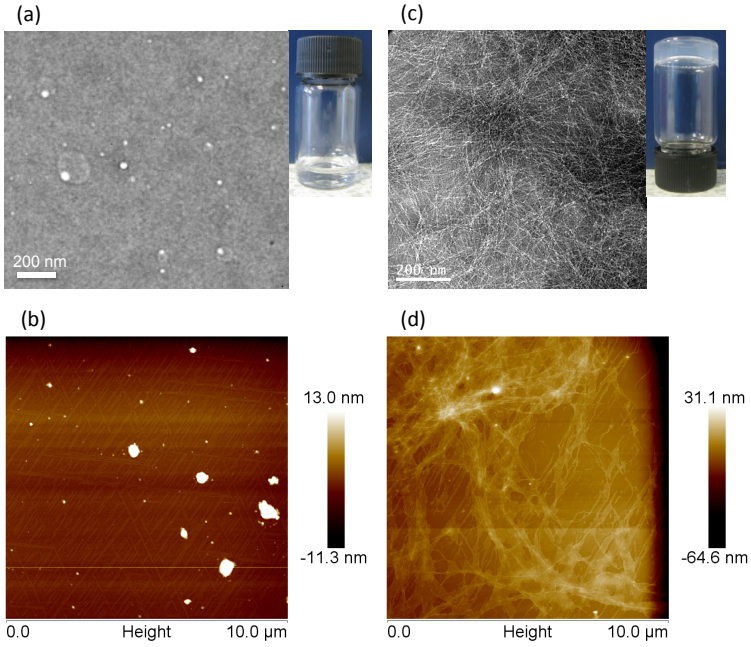

Figure 3.2. (a) TEM image (Ammonium molybdate 2% stain) and macroscopic appearance of Fmoc-Y*p*L; (b) AFM image of Fmoc-Y*p*L; (c) TEM image (Ammonium molybdate 2% stain) and macroscopic appearance of

Fmoc-YL, produced after 24 h from enzyme addition to Fmoc-Y*p*L; (d) AFM image of Fmoc-YL, produced after 24 h from enzyme addition to Fmoc-Y*p*L.

Monitoring of the dephosphorylation reaction by reverse-phase HPLC (Figure 3.3) revealed that approximately 63% of Fmoc-Y*p*L is converted into Fmoc-YL after 1 hour, with complete conversion to Fmoc-YL achieved within 24 hours.

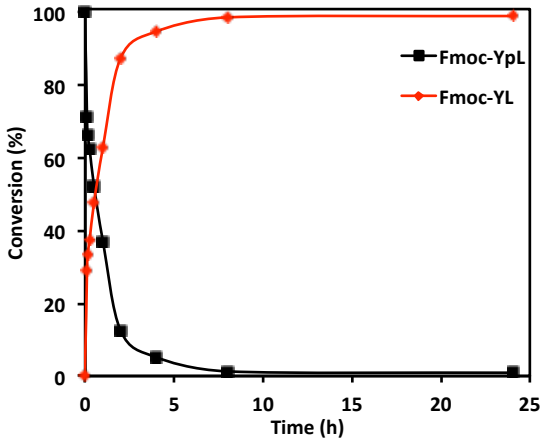

Figure 3.3. Conversion % from Fmoc-Y*p*L to reaction product Fmoc-YL monitored by reverse-phase HPLC from the time alkaline phosphatase is added.

Fmoc-YL is known to also form a hydrogel when environmental changes, such as pH, are used to initiate self-assembly.[63] In order to compare the different ways of triggering self-assembly, Fmoc-YL gel was produced by heating the 10 mM Fmoc-YL in 0.6 M sodium phosphate buffer, pH 8, to 80 °C and subsequently cooling down the sample. After 24 h, a hydrogel composed of less entangled nanofibres was observed (Appendix 1, Figure I.1a), when in comparison with the enzymatically formed Fmoc-YL. This might be explained by formed metastable states upon *in situ* catalysis through kinetic control, affecting the gelation rate and the morphology properties,[120] as previously discussed in Chapter 2.

The mechanical properties of the Fmoc-YL hydrogel formed 24 h after alkaline phosphatase was added to the precursor Fmoc-Y*p*L were evaluated by oscillatory rheology. The Fmoc-Y*p*L was not measured since it remains a solution and characterising its viscosity was not part of the main objectives of this study. From a previous dynamic strain

sweep (Figure 3.4a), the sample showed a weak dependence from 0.1 to 10% of strain, proving it is a hydrogel. In fact, the crossover point, when the loss modulus G'' becomes higher than the storage modulus G', is only reached at around 10% strain, when the hydrogel breaks down into a solution. The dynamic frequency sweep (Figure 3.4b) was then performed after setting the strain amplitude within the linear viscoelastic regime.

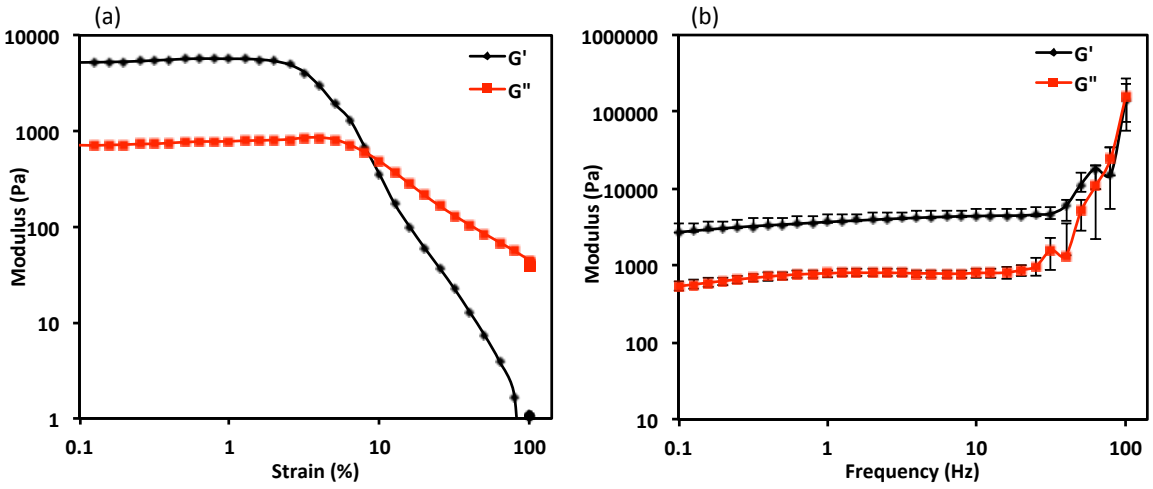

Figure 3.4. Rheology behaviour of Fmoc-YL 24 h after enzyme addition to the precursor Fmoc-Y*p*L: (a) Strain sweep; (b) dynamic frequency sweep (1% strain used).

The G' value ($3.7x10^3$ Pa) was found to be one order of magnitude larger than the G'' ($7.4x10^2$ Pa), taken from the moduli average between 0.1-10 Hz. Based on the definition of Yan and Pochan,[248] this indicates a viscoelastic material is produced. However, they are not frequency independent, where the upturn at high frequencies might be due to a thickening instability, as previously mentioned.[59, 249] When Fmoc-YL was formed following environmental changes (more specifically through a heating/cooling cycle instead of an enzyme that initiates self-assembly), a less rigid hydrogel is formed, which is observed by the inverted vial test (Appendix 1, Inset of Figure I.1a). In fact, it presents lower G' and G'' values of $7.9x10^1$ Pa and $2.3x10^1$ Pa, respectively (Appendix 1, Figure I.1b), which indicates its less viscoelastic nature. Even though Fmoc-YL self-assembles into a hydrogel when a temperature trigger is used, a more stable hydrogel is formed when it is enzymatically produced, which occurs due to the more entangled nanofibrous network seen

previously (Figure 3.2c). Catalytic control has previously been shown to promote mechanical strength using nucleophilic aniline catalysis.[120]

3.2.2 Supramolecular interactions: Nanostructure characterisation

As mentioned in Chapter 2, the self-assembly process of aromatic peptide amphiphiles is known to be controlled by the hydrophobic effect and weak non-covalent interactions such as π-stacking between fluorenyl groups and hydrogen bonding between amino acids.[2, 68, 250]

3.2.2.1 Fluorescence spectroscopy

Fluorescence spectra can provide evidence of aromatic interactions, since the aromatic groups may interact to form excimers, which emit at lower energy and cause shifts to higher wavelengths (resulting in red-shifted emission spectra) relative to the non-interacting aromatic group.[2] From the non-normalised emission curves (Figure 3.5a), a significant reduction of fluorescence signal intensity over time (especially at 24 hours) is most likely, at least in part, due to scattering as the gel is more turbid compared to the precursor solutions. When comparing the normalised emission curves throughout time, it is possible to observe a red-shift on the fluorenyl peak (approximately 320 nm) after dephosphorylation and gelation, in agreement with what has been reported for Fmoc-Y*p*[78] and Fmoc-F*p*Y.[118] The emergence of this red-shift over time upon the addition of alkaline phosphatase is represented in Figure 3.5b. The initial blue-shift occurs due to the disruption of stacking interactions when phosphate groups are initially cleaved, followed by a red-shift that points to a gradually formed fluorenyl stacking arrangement, which gives rise to fibres as previously observed for the dephosphorylation of Fmoc-Y*p*.[78] The shoulder (peak at 375 nm), associated with an organisation of fluorenyl groups in micellar aggregates,[61, 78, 106] is only visible before the addition of alkaline phosphatase, which supports a micelle to fibre transition, by rearrangement of the peptide chains and aromatic moieties upon dephosphorylation. The disappearance of this peak is also visible for the environmentally-triggered Fmoc-YL, even though a smaller 1 nm red-shift is observed for this 24 h after preparation (Appendix 1, Figure I.1c).

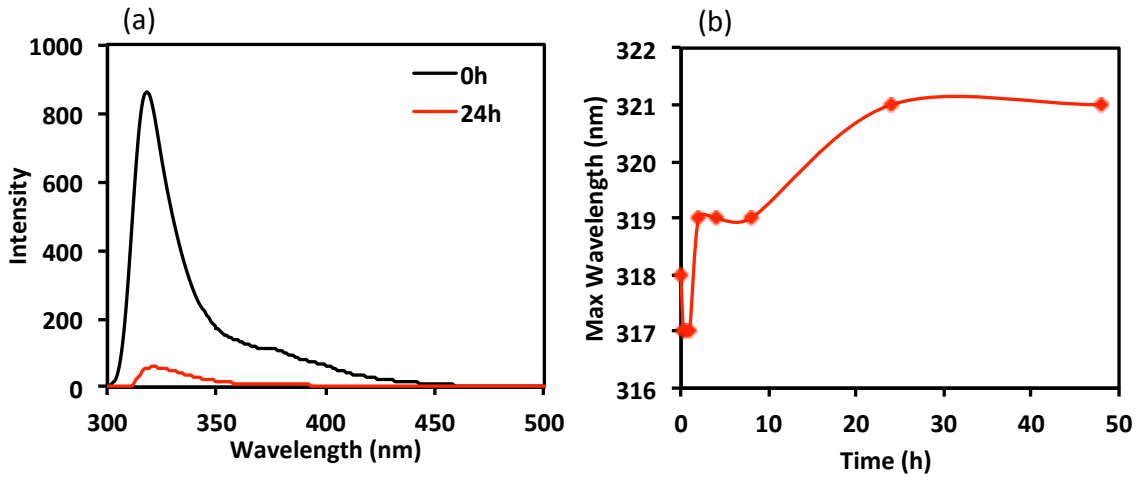

Figure 3.5. (a) Non-normalised fluorescence emission spectra of Fmoc-Y*p*L (0 h) and Fmoc-YL achieved 24 h after enzyme addition (excitation 280 nm); (b) Representation of the λ_{max} wavelength at which fluorenyl peaks were observed from the time of enzyme addition, showing a gradual red-shift.

3.2.2.2 FTIR spectroscopy

Fourier transform infrared (FTIR) absorbance can be used to analyse the H-bonding environment of the self-assembled peptide structure.[2] A comparison of the peaks in the amide I region of the spectra (Figure 3.6) indicates the nature of H-bonding interactions for the carbonyl moieties in both the precursor Fmoc-Y*p*L and the hydrogelator Fmoc-YL, after 24 h of alkaline phosphatase addition to Fmoc-Y*p*L. The prominent band for Fmoc-YL at ~1625 cm^{-1} is indicative of a β-sheet-like arrangement of the monomers, while the intensity of the band at ~1680 cm^{-1} is related to the formation of H-bonds with the carbonyl group of the carbamate moiety in Fmoc.[74] The absence of these peaks in the precursor solution confirms that there is no such persistent H-bonded structure present in Fmoc-Y*p*L. For both Fmoc-Y*p*L and Fmoc-YL, the FTIR spectra reveal a broad peak at approximately 1580 cm^{-1}, which indicates a deprotonated fraction of terminal carboxylates.[251]

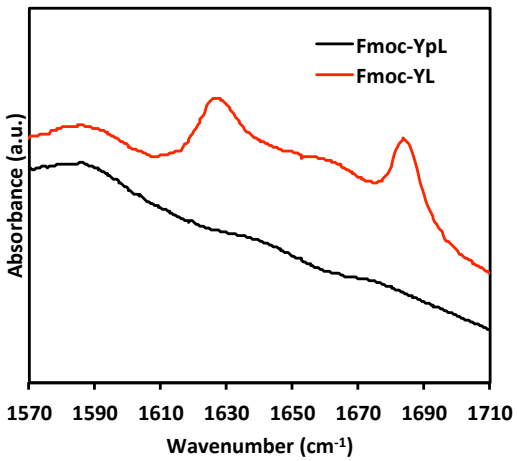

Figure 3.6. Amide I region of FTIR absorbance of Fmoc-Y*p*L and Fmoc-YL produced from dephosphorylation of its precursor (24 h after).

The formation of stable, persistent, intermolecular interactions is critical for the transition from micellar aggregates, observed for Fmoc-Y*p*L, and one-dimensional nanostructures formed by Fmoc-YL. However, and since no direct extrapolation from proteins can be made to short peptide systems, it is not possible to conclude about the nanostructure conformation based on the peaks given by the IR spectrum.[74] The temperature-triggered self-assembled Fmoc-YL results in hydrogels with slightly broader peaks at the bands related to the β-sheet-like arrangement (Appendix 1, Figure I.1d), which indicates a less well-ordered H-bonding network and explains the less entangled nanofibres that give rise to a weaker hydrogel.

3.2.2.3 Molecular Dynamics simulations

In order to gain further insight into the difference in supramolecular interactions upon dephosphorylation, but not focusing on the kinetics of this process, we performed molecular dynamics simulations of the aqueous systems, with an initial random arrangement of 60 molecules of either Fmoc-Y*p*L or Fmoc-YL. Due to the computational demands of atomistic MD simulations, the size and length of the MD simulations used in this work are not sufficient to predict the final structure of the self-assembled systems. Rather, we use the atomistic MD simulations to demonstrate the tendency for the types of

structures that can be formed and the interactions that are dominant during their formation with an emphasis on the effects of supramolecular organisation in the absence or presence of the phosphate group.

Snapshots taken throughout the simulation time reveal that the 60 molecules of Fmoc-Y*p*L tend to form an aggregate (Figure 3.7a), with a clustering of the fluorenyl groups (represented in blue) and solvent exposure of phosphate groups (represented in black). In turn, Fmoc-YL tends to form a more well-established structure already before 50 ns, preferably assembling into a more extended, fibre-like structure (Figure 3.7b).

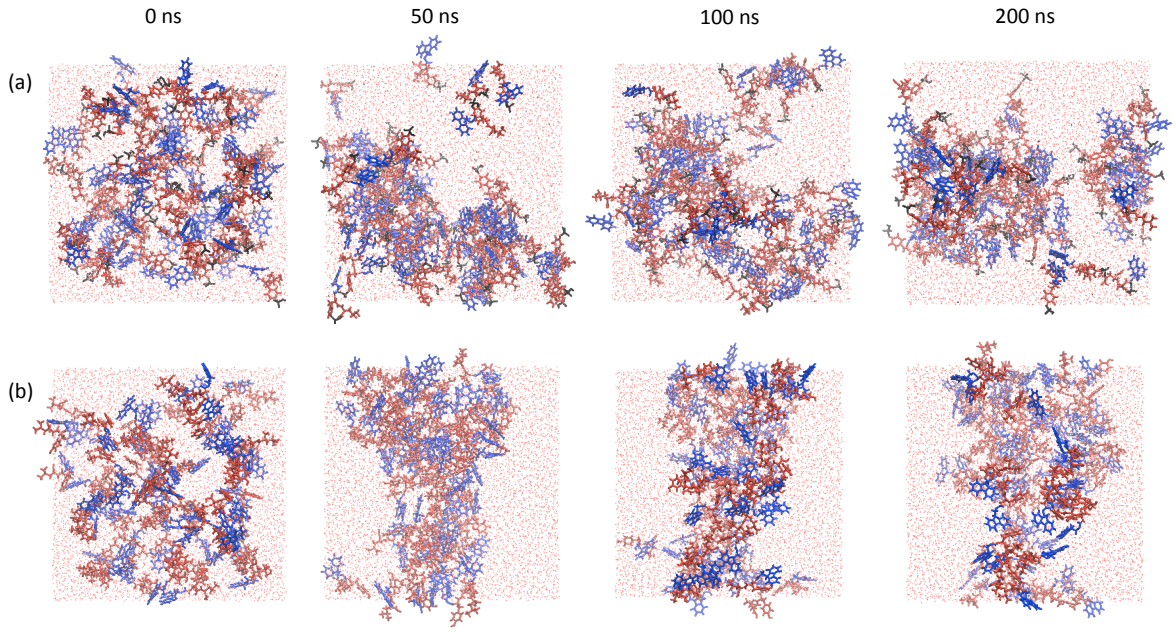

Figure 3.7. Snapshots of both systems in aqueous medium throughout the simulation time (0, 50, 100 and 200 ns): (a) Fmoc-Y*p*L; (b) Fmoc-YL. Fmoc is represented in blue, Tyrosine and Leucine in red, phosphate group in black, sodium ions in grey and water in red points.

It is clear that no equilibrated structure would be reached after 200 ns simulation time and the course of this aggregation/fibre formation cannot be compared to the experimental gelation time. Nevertheless, these observations are in agreement with the imaging obtained from AFM and TEM, since Fmoc-Y*p*L is shown to form aggregates whereas Fmoc-YL formed nanofibrous networks (Figure 3.2). We can see the Fmoc-YL fibre-type structure tending to be formed by 200 ns as a detailed small part of the whole concentrated

nanofibrous entangled network observed experimentally. In addition to the qualitative data provided by the final snapshots, which allows for an overall view of the behaviour of the molecules in the simulation, the analysis of the possible supramolecular interactions between the residues was also performed. The further understanding of the non-covalent interactions responsible for each self-assembly process can be achieved by correlating evidence from MD simulations with FTIR and fluorescence spectroscopy for H-bonding arrangement and π-stacking, respectively, as previously demonstrated for Fmoc-dipeptide amphiphiles.[234]

The first 50 ns of the simulation involve the aggregation of the monomers and the formation of H-bond networks for both Fmoc-Y*p*L (Figure 3.8a) and Fmoc-YL systems (Figure 3.8b). However, after 50 ns the H-bonding networks show distinctly different characteristics.

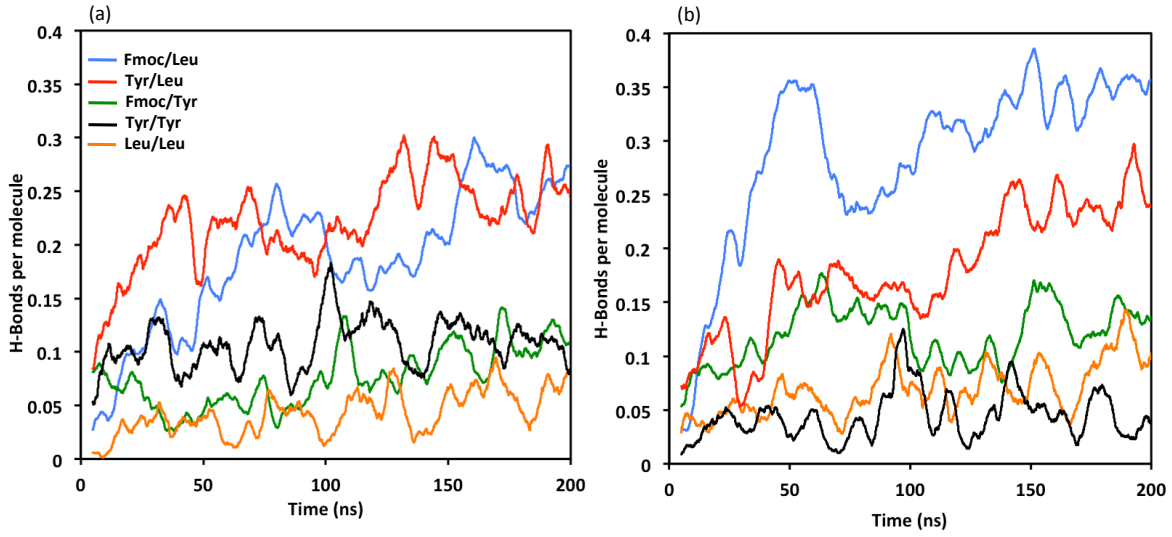

Figure 3.8. Hydrogen bonds per Fmoc-Y*p*L (a) and Fmoc-YL (b) molecules throughout the aqueous simulation.

The MD simulation of Fmoc-Y*p*L shows no persistent H-bonds forming between the residues of the monomers of Fmoc-Y*p*L. However, there is a slight preference for the formation of H-bonds between the Fmoc and Leu residues of monomers and between the Tyr and Leu residues (Figure 3.8a). Within the final stage of the simulation, the only H-bond interactions between Fmoc and Leu involved the carbamate carbonyl and the

protonated C-terminus of Leu, as seen in the snapshot of the interaction between two molecules in the inset of Figure 3.9a. Nonetheless, the relative ordering of these interactions changes throughout the lifetime of the simulation. This variability in the H-bond network is indicative of a lack of structure in the aggregate.

In contrast, the MD simulation of Fmoc-YL shows a clear preference for the formation of Fmoc/Leu H-bonds, followed by the persistent formation of Tyr/Leu H-bonds (Figure 3.8b). These trends suggest that a final H-bonding stabilised structure is formed for Fmoc-YL (Figure 3.9b). The stability of the Fmoc/Leu interaction is consistent with the FTIR band at ~1680 cm^{-1} (Figure 3.6), which is indicative of H-bonding of the carbonyl group in the carbamate of Fmoc. This main H-bond interaction between the carbonyl group in the Fmoc moiety and the carboxylic acid of leucine in the C-terminus is presented in the snapshot of two Fmoc-YL molecules (Inset of Figure 3.9b).

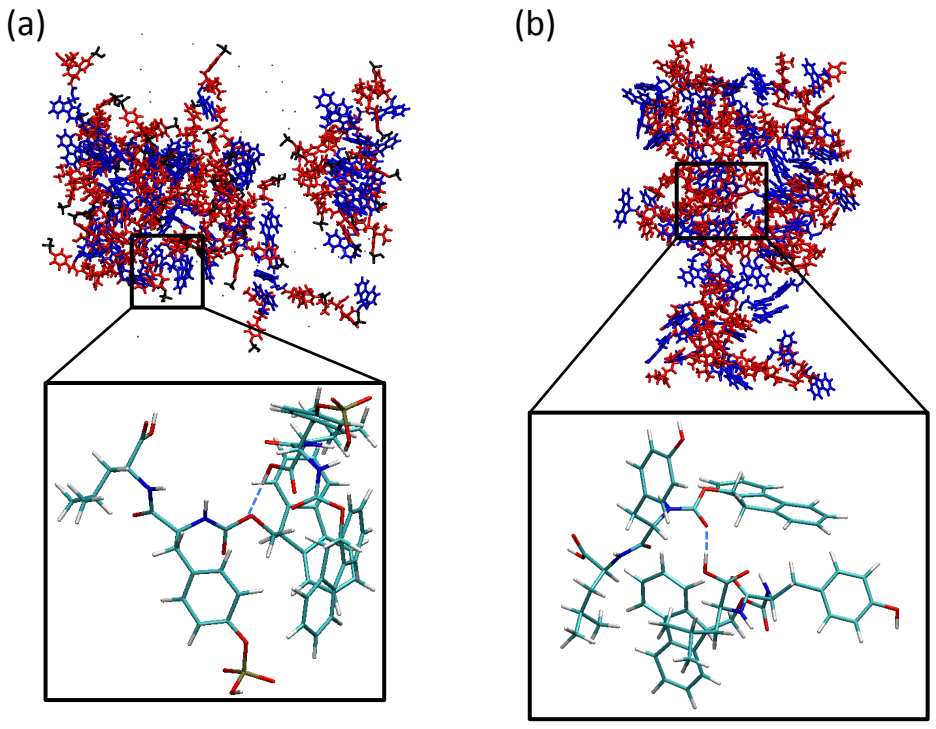

Figure 3.9. (a) Snapshot of the system of Fmoc-Y*p*L after 200 ns throughout the aqueous simulation (Fmoc is represented in blue, Tyrosine and Leucine in red, phosphate group in black, ions in grey and water is ommited for clarity). Inset presents, in dashed line, one Fmoc/Leu H-bonding (between oxygen in carbamate group and terminal leucine OH) between 2 molecules, and the Fmoc group clustering, coloured by atom type; (b) Snapshot of the system of Fmoc-YL after 200 ns throughout the aqueous simulation. Inset presents, in dashed

line, one Fmoc/Leu H-bonding (between carbonyl oxygen on the Fmoc carbamate and terminal leucine OH) between 2 molecules, coloured by atom type.

Moreover, the Tyr/Leu H-bonding interactions are also present and increasing throughout the simulation, which is consistent with the ~1625 cm^{-1} band in the FTIR (Figure 3.6). The less frequent H-bonding interaction is between Tyr and Tyr residues for Fmoc-YL, whereas for Fmoc-Y*p*L this was higher due to the interactions with the phosphate group, counted as part of the Tyr residue. In addition, the presence of the hydrophilic phosphate group raises the H-bonds between tyrosine and water (Figure 3.10a). In fact, the majority of the Tyr/water H-bonds (red line) is given by the contribution of the phosphate group with water (blue line). This is additional evidence for the hydration effect of the phosphate groups, which forces the Fmoc-Y*p*L molecules to assemble into aggregates, where Fmoc stacks inside and the phosphate groups interact with water. For the simulation of Fmoc-YL, the Tyr/water H-bonds are decreased and, in general, all the possible interactions with water decrease as the ordered structure starts to be formed and peptide-peptide interactions increase (Figure 3.10b).

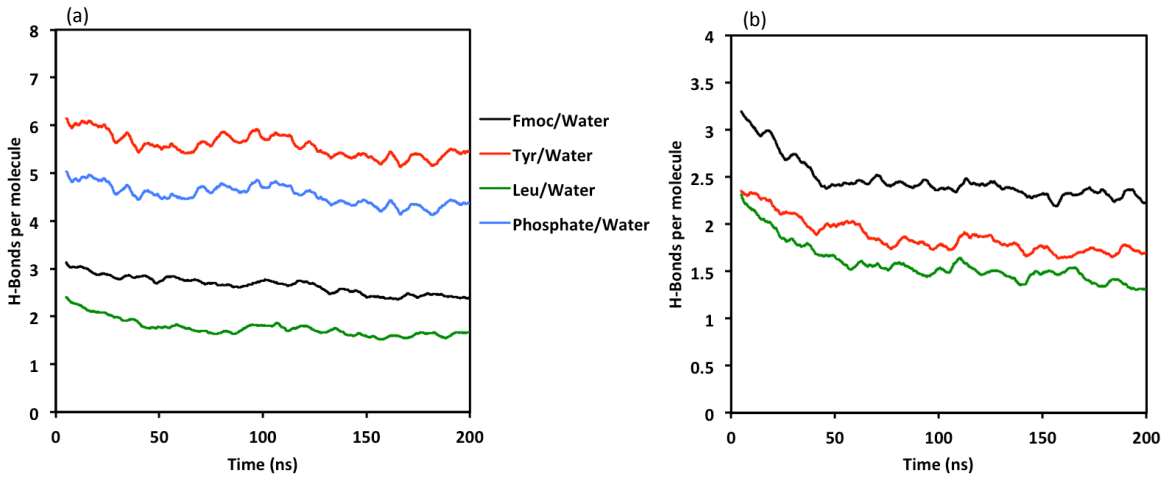

Figure 3.10. H-Bonds per molecule between each residue and water for (a) Fmoc-Y*p*L and (b) Fmoc-YL throughout the aqueous simulations.

The ability to identify the main H-bonding pairs from MD simulations and correlate them with the bands in the FTIR amide I spectra indicate a preferred H-bonded organised network of the Fmoc-YL monomers.

In addition to the H-bond descriptor, we also performed an analysis that does not consider specific interactions, such as H-bonds, which is termed the *proximity* analysis. In this case, the number of residues closer than 5.5 Å to a defined chemical moiety is investigated throughout the simulations. This diagnostic indicates the aggregation/interaction tendency of different chemical moieties without considering what physical processes drive these tendencies. Subsequent analysis of this diagnostic can reveal trends that can then be associated with physical processes, for example a close persistent proximity between aromatic residues can suggest the number of π-stacking interactions per molecule.

For Fmoc-Y*p*L (Figure 3.11a), Fmoc and Leucine are the residues that are more frequently close to each other, which can be due to a CH-π interaction between the L sidechain and Fmoc group (< 5.5 Å). Given the evidence from the H-bond analysis (Figure 3.8a), it would be more likely that this was a reflection of the H-bonds between the Fmoc carbonyl and the Leu C-terminus. However, there is an average of ~ 1.6 leucines closer than 5.5 Å to an Fmoc monomer per molecule (excluding the one from the own molecule) and only ~ 0.3 of them account for H-bonds. This suggests that the preferred formed conformation has Fmoc and leucine close to each other, which can be due to other interaction types as CH-π interaction. Fmoc/Tyr and Fmoc/Fmoc are also very frequently close to each other throughout the simulation, with the green and purple curves fluctuating between each other (Figure 3.11a). From the H-bonding data, there are very few interactions between Fmoc/Tyr (Figure 3.8a) and no H-bonds can be formed between Fmoc and Fmoc moieties. In this case, everything points to possible π-stacking occurring between the residues.

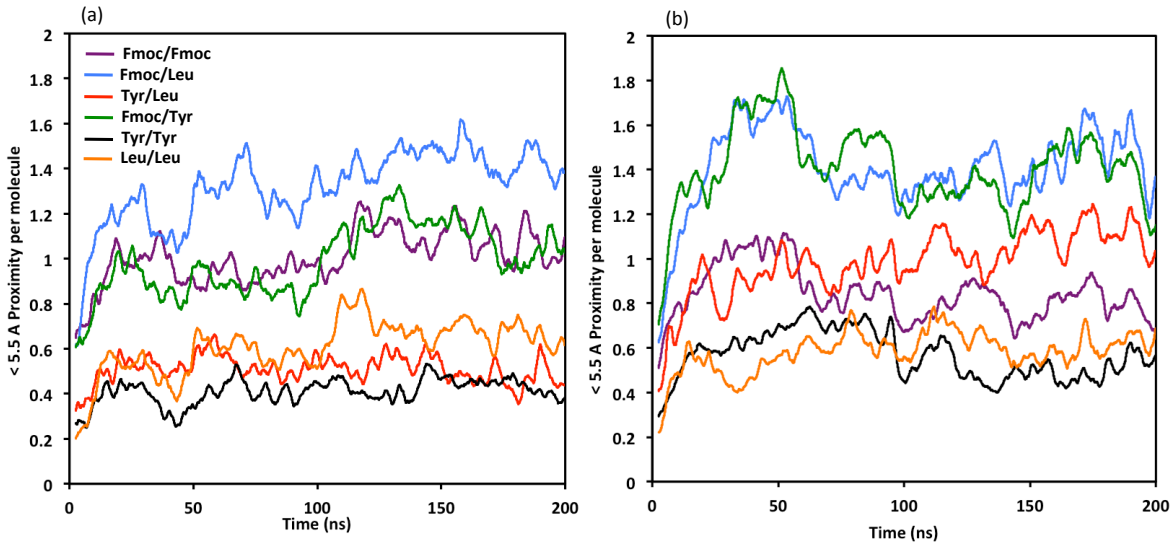

Figure 3.11. Proximity per molecule between residues for (a) Fmoc-Y*p*L and (b) Fmoc-YL throughout the aqueous simulation.

Fmoc/Leu and Fmoc/Tyr are the closest residues for the Fmoc-YL system (Figure 3.11b), in a higher range than the phosphorylated precursor. However, their proximity throughout the simulation time is similar, not showing a clear preference for either one or the other. The 50 ns time point is determinant, as it was shown before through the H-bonds analysis (Figure 3.8b). When analysing the proximity between Fmoc-Fmoc groups (purple curve), *e.g.*, a separation is observed after 50 ns, whereas an increased closeness tendency between these is seen for the Fmoc-Y*p*L molecules (Figure 3.11a). Bearing in mind this Fmoc-Fmoc proximity has been previously assigned to π-stacking interactions for Fmoc-Y*p*L, which predominantly aggregates with fluorenyl moieties stacking in the centre, there is enough evidence showing the same does not occur for the Fmoc-YL gelator. The only curve that keeps increasing after the 50 ns throughout the Fmoc-YL aqueous simulation is the one corresponding to the Tyr/Leu proximity, which can be due to CH-π interaction between the Leu sidechain and Tyr ring. From the combination of this proximity and H-bond analysis (Figure 3.8b), there is enough evidence to conclude that H-bonds are the most predominant interactions between Tyr/Leu, which is also given from the FTIR spectra, as previously discussed. Correlating back with the tendencies presented in Figure 3.8b, Fmoc groups from Fmoc-YL are shown to be involved in the H-bondings established with Leu and Tyr

from other molecules to form more well-ordered fibre-type structures (Figure 3.9b). The combination of different sources of information from experimental and computational techniques is critical for the understanding of which interactions are responsible for the preferred nanostructures formed. From experimental techniques as fluorescence spectroscopy (Figure 3.5) and FTIR (Figure 3.6), together with the H-bonds (Figure 3.8) and proximity (Figure 3.11) analysis, it can be concluded that H-bonds are not as important for the Fmoc-Y*p*L final structure as π-stacking or hydrophobic effect, while Fmoc-YL depends more on the H-bonds for the formation of fibrous-type structures.

3.3 Enzyme-triggered emulsion stabilisation

3.3.1 Conversion in non-aqueous systems: Macroscopic characterisation

When chloroform is added in a 1:1 volume ratio to the 5 mM Fmoc-Y*p*L buffer solution followed by hand-shaking for 5 seconds, an emulsion is formed due to its surfactant-like behaviour, where the amphiphile adsorbs at the chloroform/buffer interface. However, Fmoc-Y*p*L is unable to effectively stabilise the interface and de-emulsification occurs after one hour (Figure 3.12a). By contrast, when alkaline phosphatase is added to the biphasic system containing Fmoc-Y*p*L and only then hand-shaken, an emulsion is created, which remains for weeks (Figure 3.12b). This is observed when using two different formation approaches, where the addition of chloroform and emulsification only after 24 h from AP addition and fibre formation shows a similar behaviour (seen from the imaging techniques).

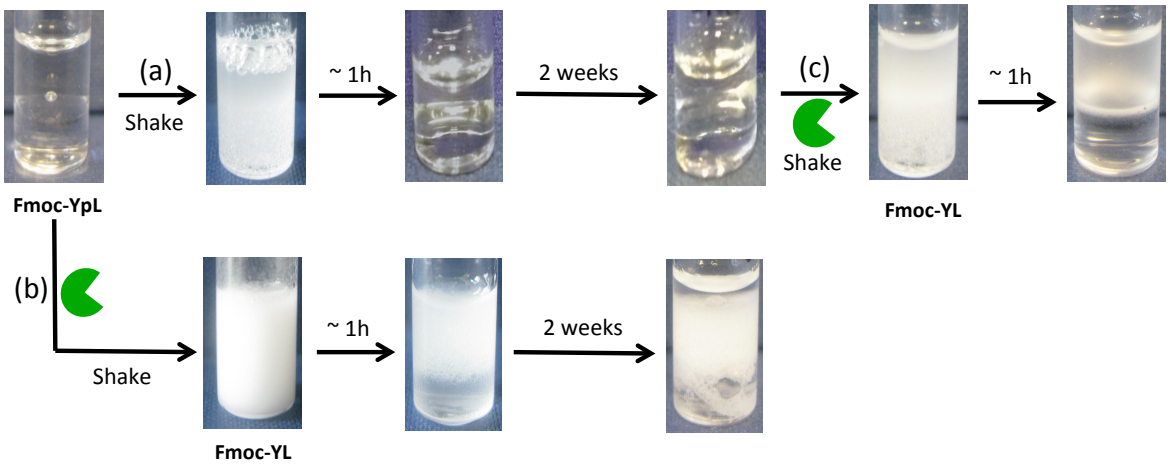

Figure 3.12 Optical photographs of glass vials showing the behaviour of the different aromatic peptide amphiphiles in a chloroform/buffer biphasic system, immediately after hand shaking for 5 seconds and after 1 hour/2 weeks: (a) Fmoc-Y*p*L forms a temporary emulsion that de-emulsifies after 1 h; (b) Fmoc-Y*p*L is converted into Fmoc-YL when alkaline phosphatase (green) is added to Fmoc-Y*p*L upon preparation, forming a more stable emulsion, still stable after 2 weeks; (c) Fmoc-YL is formed when AP is added to the completely de-emulsified Fmoc-Y*p*L after 2 weeks storage, forming a stable emulsion and proving on-demand emulsification.

This change in the emulsification behaviour suggests that there is a rapid enzymatic conversion from Fmoc-Y*p*L into Fmoc-YL, even when alkaline phosphatase is used in a non-aqueous medium. The activity of this enzyme in the biphasic system was verified by the full conversion from Fmoc-Y*p*L into Fmoc-YL when in a 1:1 chloroform:aqueous buffer system, comparable to when in the aqueous buffer, while it only dephosphorylates 20% of Fmoc-Y*p*L when in pure chloroform (Figure 3.13a). In turn, when alkaline phosphatase is added to the de-emulsified Fmoc-Y*p*L after storage for 2 weeks, a stable emulsion is also achieved (Figure 3.12c), showing that on-demand emulsification is possible. This on-demand conversion was shown with similar conversion rates when alkaline phosphatase was added to biphasic Fmoc-Y*p*L mixtures at 1 week, 2 weeks and 1 month after the chloroform-in-water emulsion has been prepared (Figure 3.13b).

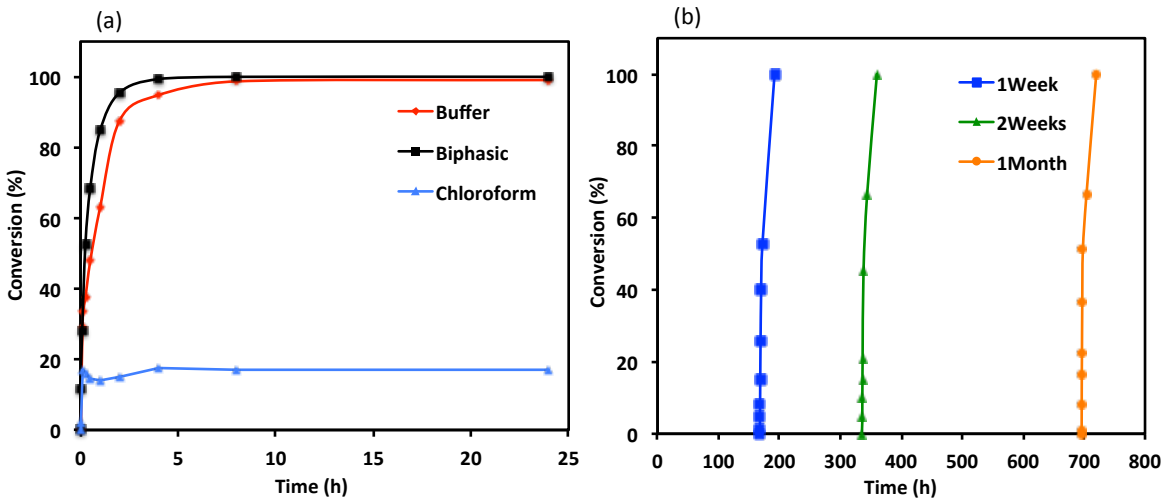

Figure 3.13. (a) Dephosphorylation monitored by reverse-phase HPLC in buffer, buffer/chloroform biphasic system and chloroform; (b) Dephosphorylation in biphasic systems when alkaline phosphatase is added at different time points.

Although complete conversion from Fmoc-Y*p*L to Fmoc-YL is observed after different storage times, we note that the kinetics are slower when the precursor emulsion has been allowed to stabilise for a longer period of time prior to enzyme addition – 8 h for complete conversion after immediate addition (Figure 3.13a, black line) and 24 h for complete conversion after storage for one month (Figure 3.13b, orange line).

A dephosphorylation assay of a p-nitrophenyl phosphate (pNPP) substrate for phosphatase can also be used to assess alkaline phosphatase activity.[252] In addition to the 1:1 buffer:chloroform volume ratio used before, the enzyme activity was also measured when aqueous buffer is present in higher volume ratios. The enzyme was shown to present the same activity as in a 100% aqueous buffer medium when chloroform was added up to a 7:3 buffer:chloroform volume ratio (Figure 3.14). It has been previously shown that, upon the addition of a small volume of organic solvent, different enzymes' activity can increase or even go beyond their activity in a pure aqueous medium, which is explained by the better resemblance of aqueous-organic solvent mixtures to the cellular microenvironments when compared to pure water.[253] However, in a 1:1 buffer:chloroform ratio, alkaline phosphatase decreased its activity by approximately 45% (Figure 3.14, blue curve) and AP was shown not to be active in a pure chloroform system, which is also in agreement with what was

shown previously for acid phosphatase[254] and alkaline phosphatase in the presence of methanol and acetonitrile, among other solvents.[255] Simopoulos and Jencks also reported a slight or no effect on the k_{cat}/K_m rate of alkaline phosphatase when co-solvents are present at low concentrations, but from ≥15 % (volume of co-solvent) a rapid decrease in the catalytic activity occurs, as the enzyme's structure is disrupted.[255]

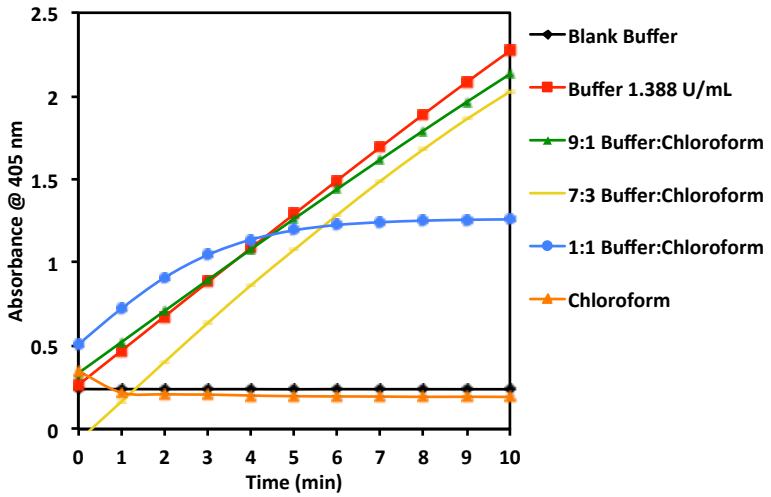

Figure 3.14. Alkaline phosphatase activity in different (non-)aqueous systems, where the dephosphorylation reaction of the substrate p-nitrophenyl phosphate (pNPP) is monitored by the UV-Vis absorbance at 405 nm through 10 min.

3.3.2 Microscopic characterisation of interfacial structures

It is believed that emulsions are stabilised by the formation of nanostructures that self-assemble at the interface between aqueous buffer and chloroform, as demonstrated previously for non-enzyme triggered systems.[79] We investigated the structure of the chloroform-in-water droplets stabilised by the amphiphiles 24 hours after preparation by using different microscopic methods. The Fmoc-Y*p*L biphasic mixture is a thermodynamically very unstable emulsion. As already mentioned in Chapter 2, when there is a large interfacial area, excess Gibbs energy is high and thus the droplets tend to coalesce and two phases are again formed. From TEM imaging, the observed are not believed to be droplets (Figure 3.15a) but a drying effect artefact. In fact, drying the samples may have changed the morphologies as the chloroform gets evaporated. When alkaline phosphatase is

added to the 5 mM Fmoc-Y*p*L and left to dephosphorylate it for 24 h, a gel is formed, to which chloroform was then added. After this, the mixture was hand-shaken and emulsification occurs, where nanofibres were already present (Figure 3.15b), differently from what was shown in the macroscopic image (Figure 3.12b). The concentration of Fmoc-YpL was decreased to 2.5 mM, to avoid the formation of a hydrogel before chloroform addition, and the images are presented in Appendix 2, Figure I.2b. Nanofibres are observed to form in the environment of small droplets and/or at the interface of the droplets, which stabilises the emulsion for longer periods of time. In turn, when AP is added to Fmoc-Y*p*L de-emulsified biphasic mixture after being stored for 1 month (Figure 3.15c), nanofibres are again formed at the interface and surroundings of the chloroform droplets.

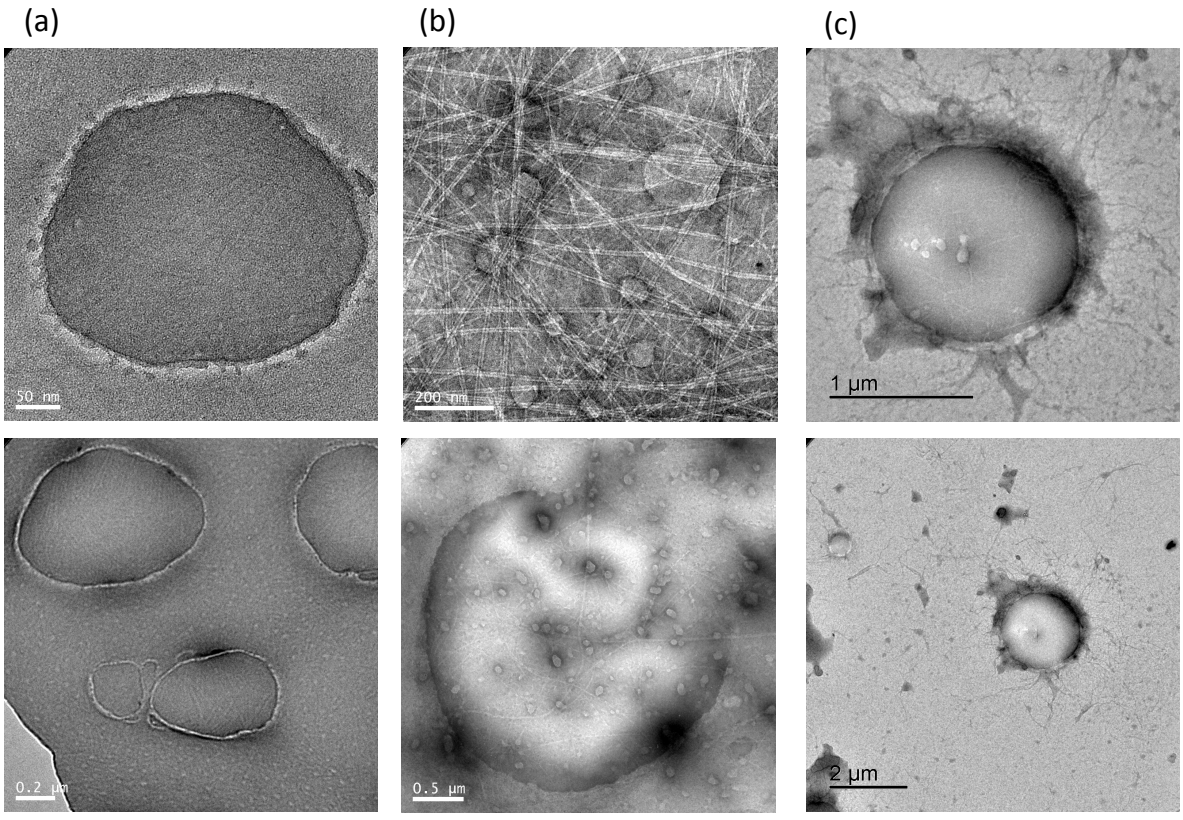

Figure 3.15. TEM images of chloroform-in-buffer emulsion stabilised by (a) Fmoc-Y*p*L; (b) Fmoc-YL, when enzyme is added upon preparation and (c) Fmoc-YL, when enzyme is added to Fmoc-Y*p*L two-phases mixture after 1 month storage. (More TEM images are presented in Appendix 2).

For the immediate addition of alkaline phosphatase to Fmoc-Y*p*L mixture, it was possible to observe by SEM, upon air-drying, the presence of many spherical structures (Figure 3.16a). One example of the Fmoc-YL stabilised chloroform-in-water droplets is shown in Figure 3.16b, which is larger than the others but presents some structures at the interface. The fluorescence microscopy images were obtained using Thioflavin T to report on the supramolecular self-assembly and gelation as reported previously.[256] Figure 3.16c shows fluorescence at the interface of chloroform-in-water droplets, which indicates they are stabilised by interfacial Fmoc-YL nanofibrous networks when alkaline phosphatase is added upon preparation. Some other fluorescence microscopy images are presented in Appendix 3, showing fluorescence especially at the interface but also as spheres inside the droplets. Non-enzymatically formed Fmoc-YL has been shown to self-assemble into interfacial nanofibres, stabilising emulsions,[79] as already mentioned. This control was also performed within this study in order to directly correlate with the enzymatically-triggered emulsifying ability (Appendix 4, Figure I.4). The different microscopy images (Appendix 4, Figure I.4a, b and c) corroborate the theory of nanofibrous-stabilised chloroform-in-water droplets.

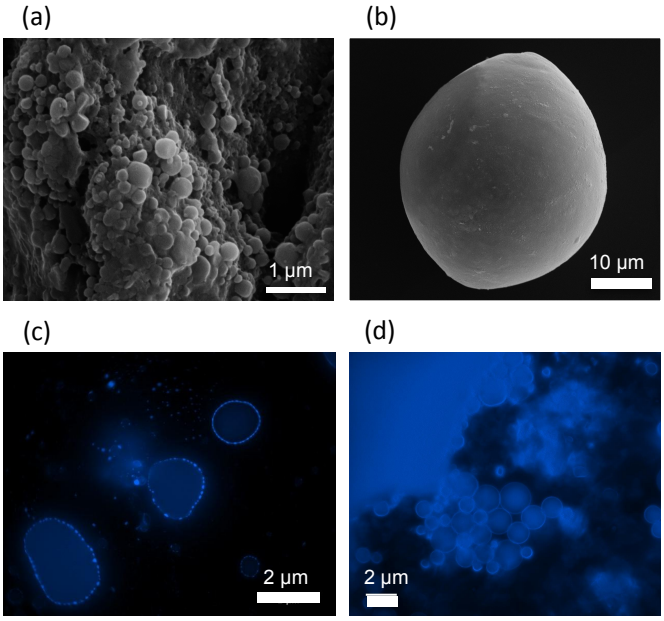

Figure 3.16. (a) and (b) SEM images of chloroform-in-water emulsion droplets stabilised by Fmoc-YL when enzyme is added upon preparation; (c) Fluorescence microscopy image of chloroform-in-water emulsion stabilised by Fmoc-YL nanofibrous networks, when enzyme is added upon preparation, labelled by ThT.

More images of this sample are presented in Appendix 3; (d) Fluorescence microscopy image of chloroform-in-water droplets stabilised by Fmoc-YL when enzyme is added to Fmoc-Y*p*L two-phases mixture after 1 month storage.

In turn, on-demand stabilised emulsions by Fmoc-YL at the chloroform/buffer interface when AP is added to the Fmoc-Y*p*L de-emulsified mixture after 1 month storage was also observed (Figure 3.16d). TEM (Figure 3.15c) and fluorescence microscopy (Figure 3.16d) images show the formation of chloroform-in-water droplets stabilised by Fmoc-YL when alkaline phosphatase is added 1 month after preparation, showing the possibility of enzymatically triggering the stabilisation of the emulsions. The fluorescence emission in a changed wavelength range is attributed to the intercalation of ThT with self-assembled fibres, with the control alkaline phosphatase in buffer with ThT showing almost the same emission as ThT only in buffer (Appendix 5, Figure I.5a). The presence of chloroform in the system can increase the fluorescence as in Appendix 5, Figure I.5c. However, it should be noted that we observe a different emulsification when the enzyme is added immediately or after some time of storage. Somewhat less stable emulsions are apparent upon activation after storage, as there is more fluorescence inside the droplets for the on-demand stabilised emulsion (Figure 3.16d). Other fluorescence microscopy images (more representative of the samples) were used to characterise the droplet size of the emulsions obtained when phosphatase was immediately added (Figure 3.17a) and after 1 month of storage (Figure 3.17b). Upon enzyme immediate addition, smaller droplets are formed (0.39 ± 0.18 μm) when compared to addition after Fmoc-Y*p*L biphasic mixture after 1-month storage (1.62 ± 0.54 μm). However, the droplet size is more homogeneous when the enzyme is added after the biphasic system has had time to stabilise for longer, as it fits better a normal distribution. The slightly slower conversion for the on-demand formed emulsion, observed from Figure 3.13b, can possibly impact upon the supramolecular order of the interfacial layers formed.

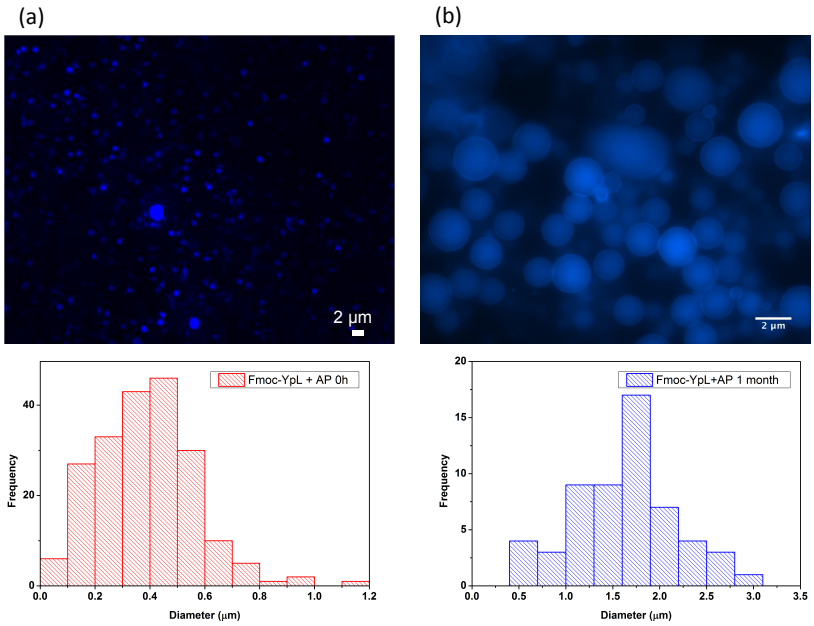

Figure 3.17. (a) Fluorescence microscopy and histogram of droplet size distribution of chloroform-in-water emulsions stabilised by nanofibrous networks of Fmoc-YL when alkaline phosphatase is added upon preparation. Bin width of 0.1 µm, defined as the 1/10 maximum drop size; (b) Fluorescence microscopy and histogram of droplet size distribution of chloroform-in-water emulsions stabilised by nanofibrous networks of Fmoc-YL when alkaline phosphatase is added to Fmoc-Y*p*L two-phases mixture after being stored for 1 month. Bin width of 0.3 µm, defined as the 1/10 maximum drop size.

3.3.3 Interfacial partitioning study

The tendency of both aromatic peptide amphiphiles (Fmoc-Y*p*L and Fmoc-YL) to transfer into chloroform, remain in aqueous buffer (labelled as water in figures) or adsorb at the interface was investigated by UV-Vis spectroscopy, measuring the absorbance in each phase (Figure 3.18a and Figure 3.18b). 31% of Fmoc-Y*p*L remains in the aqueous buffer phase (Table 3.1), while for Fmoc-YL 14% is still in buffer, with the remainder transferred to the interface. The higher tendency of Fmoc-Y*p*L to remain in water, when compared to Fmoc-YL, is due to its preference to interact with water.

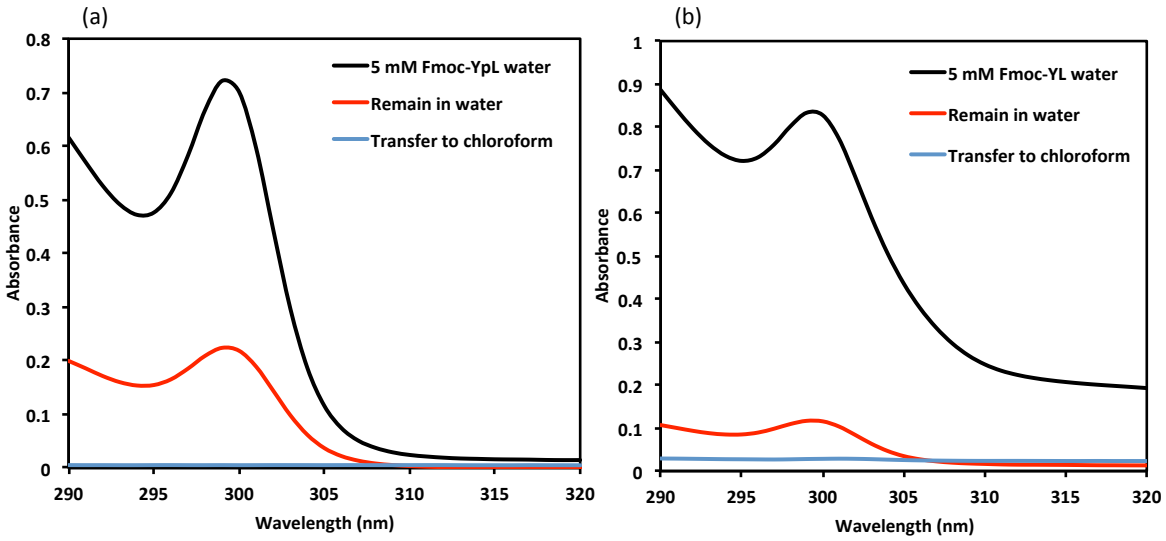

Figure 3.18 (a) Absorption spectra of Fmoc-Y*p*L in 5 mM buffer solution, amount remained in buffer and transferred to chloroform; (b) Absorption spectra of Fmoc-YL in 5 mM buffer solution, remained in buffer and transferred to chloroform.

Table 3.1. Partitioning of peptides (Fmoc-Y*p*L and Fmoc-YL) between water, chloroform and remaining at the water/chloroform interface, along with logP values of each calculated in ChemDraw version 14.0 from PerkinElmer.

	Remained in water (%)	**Transferred to chloroform (%)**	**Transferred to interface (%)**	**LogP**
Fmoc-Y*p*L	31.03	0.74	68.23	5.67
Fmoc-YL	14.01	3.45	82.53	4.73

From these results, we can conclude that both amphiphiles tend to partition at the chloroform/water interface. However, Fmoc-YL is able to remain at the interface to a greater extent as nanofibrous networks are formed at the interface (shown by imaging the emulsion droplets in Figure 3.15b and Figure 3.16c).

A degree of fibre formation may occur in the aqueous phase when Fmoc-Y*p*L is converted into Fmoc-YL as its concentration in the aqueous component narrowly exceeds the critical aggregation concentration of ~0.5 mM*.

3.3.4 Supramolecular interactions: Nanostructure characterisation

FTIR spectroscopy is also used for the biphasic mixtures to assess whether self-assembling H-bonding conformations are formed. Ordered hydrogen bond networks are present in the emulsions formed upon the addition of alkaline phosphatase to Fmoc-Y*p*L both immediately and 1 month after storage (Figure 3.19). However, an additional absorbance peak at around 1640 cm^{-1} suggests a less ordered H-bonding network for both, when in comparison to the pure aqueous systems (Figure 3.6). In contrast, no peaks indicative of secondary structure formation in the amide I region were observed in the Fmoc-Y*p*L system.

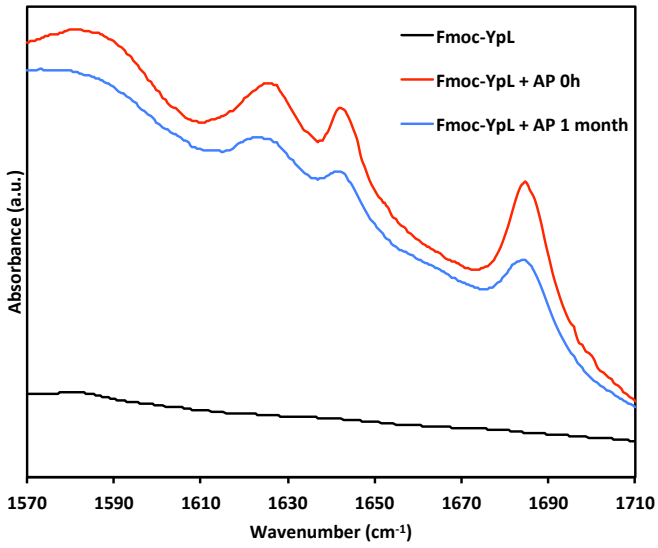

Figure 3.19 Amide I region of FTIR absorbance of Fmoc-Y*p*L (black line) and Fmoc-YL emulsions, the latter formed when alkaline phosphatase is added immediately (red) or after one month of Fmoc-Y*p*L two-phase system storage (blue).

* This value was taken by using a drop weight surface tension method for different known concentrations during an internship in LOF, Solvay.

The less sharp peaks for the on-demand emulsification curves observed by FTIR upon enzyme addition after 1 month (blue spectrum, Figure 3.19) suggest an overall less organised H-bonded conformation after delayed emulsification. This observation is in agreement with the previously discussed lower emulsification ability after the Fmoc-Y*p*L biphasic system has been prepared and stored for longer times. Moreover, the lower degree of ordering in the system is also similar to the Fmoc-YL stabilised emulsions when environmental changes are used to initiate the nanofibrous network formation (Appendix 4, Figure I.2d). This hints at a better emulsion stabilisation when Fmoc-YL interfacial nanofibres are triggered by dephosphorylation from Fmoc-Y*p*L. This, together with the increased time control over the emulsifying ability when the enzyme is added, is highly attractive for different applications.

3.3.4.1 Molecular Dynamics simulations of partitioning behaviour

MD simulations were carried out to investigate the ability of Fmoc-Y*p*L and Fmoc-YL to form ordered structures in a biphasic environment. To this end, 60 molecules of Fmoc-Y*p*L or Fmoc-YL were randomly distributed in the water phase of a large box, which contained a TIP3P water model besides octanol [1:1 ratio by volume]. The tendency of both Fmoc-Y*p*L and Fmoc-YL to aggregate towards the interface of the solvents was observed in the simulations (see snapshots throughout both simulations in Figure 3.20a and Figure 3.20b).

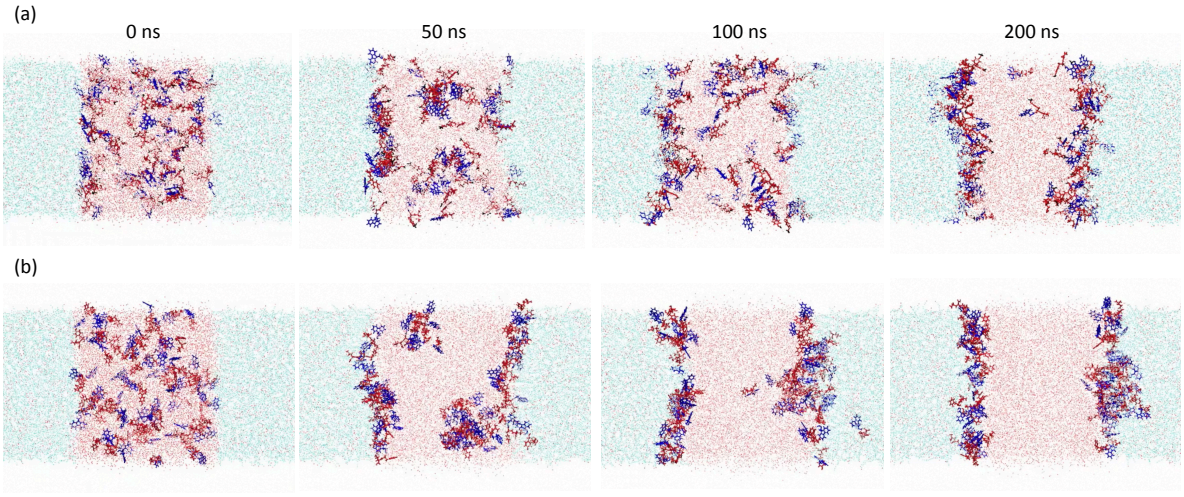

Figure 3.20. Snapshots of both systems in a water/octanol medium throughout the simulation time (0, 50, 100 and 200 ns): (a) Fmoc-Y*p*L; (b) Fmoc-YL. Fmoc is represented in blue, Tyrosine and Leucine in red, phosphate group in black, sodium ions in grey, water in red points and octanol in cyan points.

From the final snapshots of the system it is clear that although both systems are able to assemble at the interface of the solvents, Fmoc-Y*p*L is evenly distributed along the length of the box, with minimal penetration into the octanol solvent (occurring predominantly for the Fmoc residues and the Leu residues) and with the phosphate groups of the tyrosine facing the water phase (Figure 3.20a). In contrast, Fmoc-YL is able to form a more ordered aggregate which allows partitioning of the resulting fibre-like structure into the octanol phase (Figure 3.20b), which is qualitatively consistent with the results from partitioning experiments (Figure 3.18a and Table 3.1). The arrangement of Fmoc-Y*p*L at the interface suggests a surfactant-type adsorption of the amphiphile at the interface, with the hydrophilic monomers facing the water and the hydrophobic the octanol. On the other hand, Fmoc-YL is able to form a nanofibrous network at the interface, which is consistent with the partitioning data (Table 3.1) and the ability of the dephosphorylated peptide to stabilise the chloroform-in-water emulsion over an extended period.

The quantitative analysis for the further understanding of non-covalent interactions was also carried out for the biphasic systems. As observed in the aqueous simulations, Fmoc-Y*p*L has no strong H-bonding preference since the curves fluctuate throughout the simulation (Figure 3.21a). Even though Fmoc/Leu are almost always the most frequent, H-

bonds formed between the phosphate groups also play an important role, as seen in the example of two stacked molecules in the inset of Figure 3.22a.

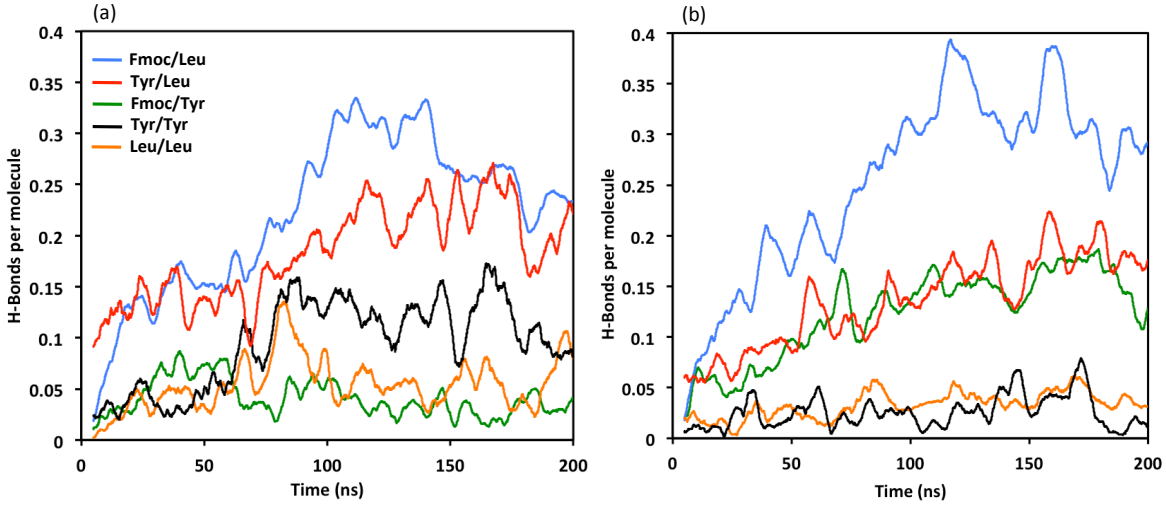

Figure 3.21. (a) Hydrogen bonds per molecule between Fmoc-Y*p*L molecules throughout the biphasic system simulation; (b) Hydrogen bonds per molecule between Fmoc-YL molecules throughout the biphasic system simulation.

In contrast, the formation of a nanostructure in the case of Fmoc-YL is again evident by the persistence of the Fmoc/Leu H-bonds (Figure 3.21b). The Fmoc/Leu interaction is predominantly given by the H-bonded carbonyl oxygen of the Fmoc carbamate and leucine's C-terminus OH (Figure 3.22b), which is in agreement with the FTIR amide I bands (Figure 3.19). Also Tyr/Leu and Fmoc/Tyr H-bonds increase, to a lesser extent, during the lifetime of the MD simulation (Figure 3.21b). The similarity between these results and the ones for Fmoc-YL in aqueous medium (Figure 3.9b) indicates the same fibre-like structure is formed regardless of the presence of octanol.

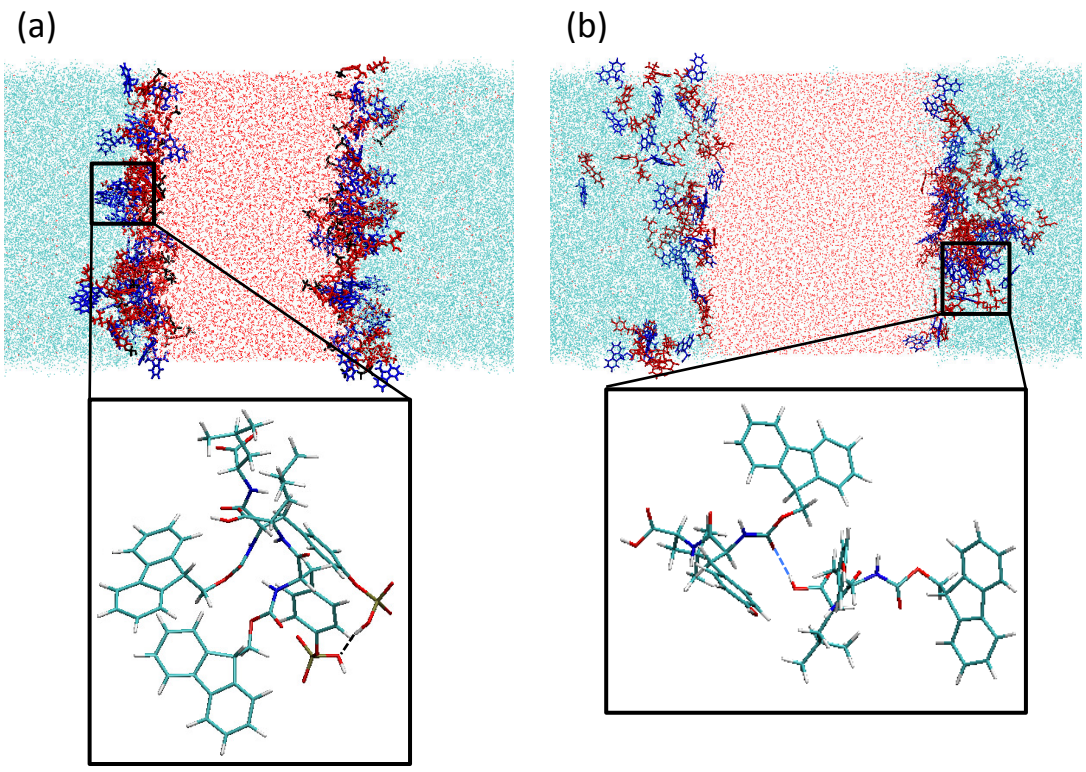

Figure 3.22. (a) Snapshot of Fmoc-Y*p*L system after 200 ns of biphasic simulation. Fmoc is represented in blue, Tyrosine and Leucine in red, phosphate group in black, ions in grey, water in red and octanol in cyan. Inset presents one Tyr/Tyr H-bonding (between OH and O of the phosphate groups) between 2 molecules, coloured by atom type; (b) Snapshot of Fmoc-YL system after 200 ns of biphasic simulation. Fmoc is represented in blue, Tyrosine and Leucine in red, water in red and octanol in cyan. Inset presents Fmoc/Leu H-bond established between 2 molecules (between carbonyl oxygen on the Fmoc carbamate and terminal leucine OH), coloured by atom type.

The H-bonds between each residue and water were shown to be slightly less when Fmoc-Y*p*L is in a biphasic system (Figure 3.23a), when compared to a water medium (Figure 3.10a), where the small difference is due to the H-bonds established with octanol instead (in dashed lines). The main interactions between the aromatic peptide and water are again due to the presence of the phosphate group capped to the tyrosine. The curves are fairly stable throughout the simulation time, indicating there is no tendency for the interaction between Fmoc-Y*p*L molecules in order to form a more well-ordered structure. This corroborates the theory that the molecules tend to stack at the octanol/water interface in a traditional

surfactant manner where the phosphate groups are hydrated and the peptide/peptide interactions are not critical as there is no formation of preferred nanostructure.

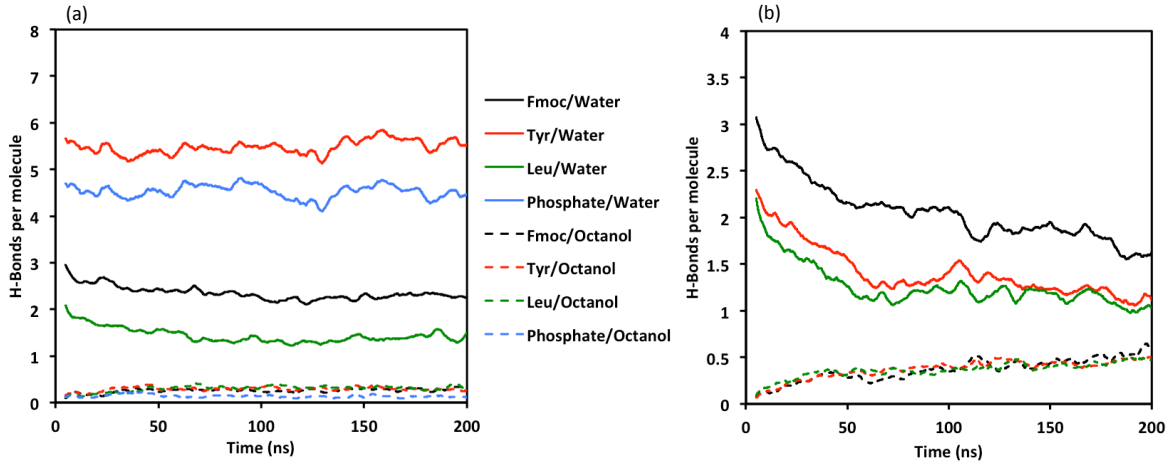

Figure 3.23. H-Bonds per molecule between each residue and water and octanol for (a) Fmoc-Y*p*L and (b) Fmoc-YL throughout the biphasic simulations.

On the other hand, the Fmoc-YL undergoes a completely different behaviour (Figure 3.23b), where the number of H-bonds with water decreases throughout the lifetime of the simulation. In addition to the H-bonds established between different residues within Fmoc-YL molecules (Figure 3.21b), the established H-bondings with octanol also contribute for this, which is in agreement with the snapshots in Figure 3.20b and with the partitioning study (Figure 3.18b). The H-bonds number range is approximately the same as for Fmoc-Y*p*L except for the Tyr/Water interactions, which is higher for the latter due to the phosphorylated Tyr. The system tends to an equilibrated stabilised structure after approximately 50 ns, when the number of H-bonds does not vary much more. Altogether, these results show that Fmoc-YL tends to form a stabilised nanofibre, in both an aqueous medium and in a water/octanol system.

Fmoc and leucine were the residues more frequently close to each other during the whole Fmoc-Y*p*L simulation (Figure 3.24a), followed by Fmoc and tyrosine, which again indicates π-stacking occurring between these latter residues. However, the purple curve for Fmoc-Fmoc is reduced, when compared with the aqueous simulation (Figure 3.11a), which suggests a lower stacking of the Fmoc groups and the production of a different preferred

structure rather than aggregates, as only stacked molecules adsorb at the octanol/water interface.

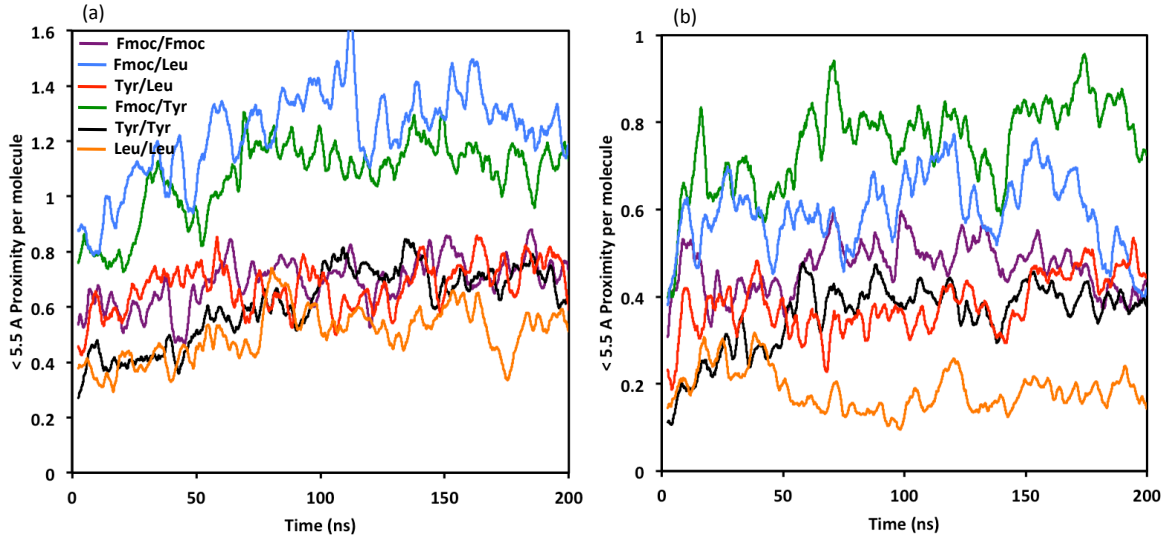

Figure 3.24. Proximity per molecule between residues for (a) Fmoc-Y*p*L and (b) Fmoc-YL throughout a biphasic simulation.

For the Fmoc-YL system, the proximity between Fmoc and tyrosine exceeds the Fmoc/Leu proximity throughout the time course of the simulation (Figure 3.24b). In general, the Fmoc-YL molecules are more distant from each other when compared to the Fmoc-Y*p*L (note the y-axis scale difference). Since this has not been observed for the aqueous MD simulations (Figure 3.11), a less ordered nanofibrous structure is probably formed when Fmoc-YL self-assembles at the interface, which is consistent with the analysis of the structure based on the FTIR spectrum (Figure 3.19).

3.4 Conclusions

In this study, we have demonstrated the use of aromatic dipeptide amphiphiles that enzymatically self-assemble at organic/aqueous interfaces to stabilise chloroform-in-water emulsions. We have demonstrated that Fmoc-YL is able to self-assemble in aqueous buffer following its enzymatic generation from the non-gelator precursor Fmoc-Y*p*L, which was a

solution, comprised of aggregates. The self-assembled Fmoc-YL was shown to form nanofibres through non-covalent interactions, including π-stacking and H-bonding. These supramolecular interactions responsible for the self-assembly were shown by fluorescence and FTIR spectroscopy, and correlated with all-atom molecular dynamics simulations.

There is some evidence pointing to the enzymatically-triggered Fmoc-YL self-assembly into nanofibrous networks at the chloroform/water interface when in a biphasic system, stabilising the chloroform-in-water droplets and generating emulsions that remain for months. The alkaline phosphatase was shown to be active in an aqueous-organic solvent medium, which was, to our knowledge, not demonstrated before.

The stability of the emulsions and the achievement of an on-demand emulsifier by adding the enzyme at different time points provide a promising tool for mixing applications in chemical processes that involve ingredients that do not tolerate changes in pH and temperature. Thus, we propose that the concept of enzymatically-triggered emulsions may find applications in, *e.g.*, certain food or cosmetics ingredients.[257-258] Our recent discovery of emulsifiers made of unmodified tripeptides also suggests applications in food science and cosmetics may be possible with an extension of this work to those systems.[182]

3.5 Materials and Methods

3.5.1 Materials

All reagents were purchased at the highest purity available (≥ 98%) and used as supplied, unless stated otherwise. Fmoc-Tyr($PO(NMe_2)_2$-OH (537.55 $g.mol^{-1}$) was purchased from Novabiochem. Fmoc-Tyr(tBu)-OH (459.53 $g.mol^{-1}$), L-Leucine tert-butyl ester hydrochloride (223.74 $g.mol^{-1}$) and alkaline phosphatase from bovine, expressed in *Pichia pastoris* (5000 $U.mg^{-1}$ protein, 20 mg $protein.mL^{-1}$, 0.049 mL, Apparent molar weight 160 kDa) were supplied by Sigma Aldrich. One enzyme unit corresponds to the quantity of alkaline phosphatase hydrolysing 1 μmol of 4-nitrophenyl phosphate per minute at pH 9.8 and 37°C.

3.5.2 Fmoc-YL Synthesis and analysis

Fmoc-Tyr-OH (1 g), L-Leucine tert-butyl HCl (0.666 g) and HBTU (1.13 g) were dissolved in approximately 15 mL of dimethylformamide (DMF). 1.08 mL (0.742 $g.cm^{-3}$ density) of DIPEA was added and the solution was stirred for 24 hours. The product was precipitated out by adding 1 M sodium bicarbonate solution (~ 50 mL) and extracted into ethyl acetate (~ 50 mL). The ethyl acetate extract was then washed in duplicate with equal volumes of saturated brine, 1 M HCl and brine again. The resulting organic layer was then dried using magnesium sulphate, filtered and the ethyl acetate removed by vacuum evaporation. The solid was then purified by column chromatography using 1.5 - 5% methanol in dichloromethane (DCM) as eluent. Fractions were tested using Thin Layer Chromatography (TLC) under UV (254 nm) light to visualise the compound spots, and the ones containing the compound were combined and evaporated in vacuum. The compound was dissolved in the minimum volume of DCM and added 10 mL of pure trifluoroacetic acid (TFA) to remove the tert-butyl groups. The reaction mixture was stirred overnight and the solvents removed by evaporation in vacuum. Excess TFA was removed by azeotropic distillation with toluene. The resulting solid is dispersed by ultrasonication and toluene was removed by evaporation in vacuum (procedure carried out in triplicate). The resulting solid was washed with cold diethyl ether for 6 times and the product dried under vacuum to obtain a white powder (Purity 88.25% assessed by reverse-phase HPLC, 0.604 g). The compound was further purified by preparative HPLC using acetonitrile/water and only collecting the compound at its retention time. The collected samples were combined and freeze-dried, resulting in a final purity of > 99.9%.

^{1}H δ (400 MHz, DMSO): 12.53 (1H, s, OH), 9.12 (1H, s, Tyr OH), 8.15 (1H, d, J = 7.9 Hz, NH), 7.88 (2H, d, J = 7.5 Hz, 2 Ar CH), 7.67 - 7.62 (2H, m, 2 Ar CH), 7.47 (1H, d, J = 8.9 Hz, NH), 7.42 - 7.38 (2H, m, 2 Ar CH), 7.33 – 7.23 (2H, m, 2 Ar CH), 7.10 (2H, d, H = 8.4 Hz, 2 Ar CH), 6.64 (2H, d, J = 8.4 Hz, 2 Ar CH), 4.23 - 4.11 (5H, m, Fmoc CH, Fmoc CH_2, 2 $C_{\alpha}H$), 3.37 - 3.32 (1H, m, Tyr CH), 2.88 - 2.69 (1H, m, Tyr CH), 2.66 - 2.51 (1H, m, Leu CH), 1.56 - 1.32 (2H, m, Leu CH_2), 0.88 (3H, d, J = 6.5 Hz, Leu CH_3), 0.84 (3H, d, J = 6.5 Hz, Leu CH_3). Spectrum can be found in Appendix 6, Figure I.6.

^{13}C δ (100 MHz, DMSO): 174.9 (C=O, Leu), 172.7 (C=O, Tyr), 156.6 (C=O, Fmoc), 144.6 (Ar C, Tyr), 141.5 (Ar C), 131.1 (Ar C), 129.8 (Ar C), 129.1 (Ar C), 128.5 (Ar C), 127.9 (Ar C), 126.2 (Ar C), 121,0 (Ar C), 115.7 (Ar C), 66.5 (CH_2, Fmoc), 57.1 (C_α, Tyr), 51.2 (C_α, Leu), 47.5 (CH, Fmoc), 37.5 (CH_2, Tyr), 25.2 (CH, Leu), 23.7 (CH_3, Leu), 22.3 (CH_3, Leu). 40.3 (CH_2, Leu) predicted by Chemdraw, undermasked by solvent. Spectrum can be found in Appendix 6, Figure I.7.

^{19}F δ (400 MHz, DMSO): No TFA peak at ~ 73 ppm.

MM: 516.59 $g.mol^{-1}$, MS (ES+): 517.0 $[M + H]^+$, 539.2 $[M + Na]^+$.

Elemental analysis – Found: C, 69.50%; H, 6.41%; N, 5.15%; Expected for $C_{30}H_{32}N_2O_6$: C, 69.75%; H, 6.24%; N, 5.42%; O, 18.58%; F, 0%.

3.5.3 Fmoc-Y*p*L Synthesis and analysis

Fmoc-Tyr($PO(NMe_2)_2$-OH (1 g) was dissolved instead of Fmoc-Tyr(tBu)-OH with L-Leucine tert-butyl HCl (0.499 g) and HBTU (0.847g) in approximately 15 mL of dimethylformamide (DMF). 0.810 mL (0.742 $g.cm^{-3}$ density) of DIPEA was added and the solution was stirred for 24 hours. The same procedure was followed but after stirring the reaction mixture with 10 mL of trifluoroacetic acid (TFA) to remove the tert-butyl groups, 1 mL of water was added and the mixture stirred for 24 hours to remove the dimethylamine groups. The following steps were maintained as for Fmoc-YL synthesis and a white powder was obtained (Purity 75.73% assessed by reverse-phase HPLC, 0.585 g). The compound was further purified by preparative HPLC using acetonitrile/water and only collecting the compound at its retention time. The collected samples were combined and freeze-dried, resulting in a final purity of 97.96%.

^1H δ (400 MHz, DMSO): 8.56 (2H, Broad s, NH&OH), 7.89 - 7.87 (2H, m, 2 Ar CH), 7.73 - 7.67 (2H, m, 2 Ar CH), 7.54 (1H, d, J = 8.16 Hz, NH), 7.44 - 7.39 (2H, m, 2 Ar CH), 7.35 - 7.29 (2H, m, 2 Ar CH), 7.18 – 6.95 (4H, m, 4 Ar CH), 4.24 - 4.13 (5H, m, Fmoc CH, Fmoc CH_2, Tyr $C_\alpha H$, Leu $C_\alpha H$), 3.58 (2 OH, Broad s, phosphate), 2.91 - 2.68 (2H, m, Tyr CH_2), 1.58 - 1.46 (2H, m, Leu CH_2), 1.40 - 1.36 (1H, m, Leu CH), 0.86 - 0.81 (6H, m, Leu $2CH_3$). Spectrum can be found in Appendix 6, Figure I.8.

^{13}C δ (100 MHz, DMSO): 174.21 (C=O, Leu), 171.73 (C=O, Tyr), 155.47 (C=O, Fmoc), 144.71 (Ar C), 142.61 (Ar C), 141.56 (Ar C), 130.54 (Ar C), 128.52 (Ar C), 127.98 (Ar C), 126.26 (Ar C), 121.49 (Ar C), 120.96 (Ar C), 118.97 (Ar C), 73.40 (CH_2, Fmoc), 63.98 (C_α, Tyr), 51.35 (C_α, Leu), 47.49 (CH, Fmoc), 39.12 (CH_2, Tyr), 34.78 (CH, Tyr), 25.10 (CH, Tyr), 23.59 (CH_3, Tyr), 22.55 (CH_3, Tyr). Spectrum can be found in Appendix 6, Figure I.9.

^{19}F δ (400 MHz, DMSO): No TFA peak at ~ 73 ppm.

MM: 596.57 $g.mol^{-1}$, MS (ES+): 597.0 $[M + H]^+$, 619.2 $[M + Na]^+$.

Elemental analysis – Found: C, 58.40%; H, 5.21%; N, 4.04%; Expected for $C_{30}H_{33}N_2O_9P$: C, 60.40%; H, 5.58%; N, 4.70%; O, 24.14%; P, 5.19; F, 0%.

3.5.4 Preparation of aqueous and biphasic samples

10 mM of synthesised and purified Fmoc-Y*p*L was prepared in 1 mL pH 8 0.6 M sodium phosphate buffer by vortexing and immediately added 50 μL of alkaline phosphatase (0.0555 $U.\mu L^{-1}$, or 55.5 $U.mL^{-1}$ enzyme concentration) and vortexed during approximately 0.5 minutes. All characterisation was done after 24 h except when stated otherwise. For the Fmoc-Y*p*L precursor, the preparation was the same except no enzyme was added.

Biphasic mixtures were prepared in the same way but in a 5 mM concentration to avoid formation of hydrogels. For the imaging techniques, 24 hours after the preparation of 500 μL Fmoc-Y*p*L in buffer and alkaline phosphatase addition (to assure full dephosphorylation), 500 μL chloroform were added to Fmoc-YL in aqueous buffer and hand-shaken for 5 seconds to make a 50:50 chloroform-in-water emulsion. For the HPLC dephosphorylation monitored in a biphasic system and time-course experiments, including macroscopic photographs, the chloroform was added to the Fmoc-Y*p*L in buffer, added the enzyme, hand-shaken immediately (maximum 10 seconds after) and measured time zero. To check if the system may be stabilised on-demand, besides an immediate addition of alkaline phosphatase to the Fmoc-Y*p*L samples, the enzyme was added into the de-emulsified biphasic system of Fmoc-Y*p*L 1 week, 2 weeks and 1 month after preparation and immediately hand-shaken. Neutral and negative controls have been carried out by using

no emulsifier, just using alkaline phosphatase or a traditional surfactant such as SDS in different concentrations. The macroscopic photographs of 1 min, 1 h and 1 day after are presented in Appendix 7.

3.5.5 HPLC

3.5.5.1 Enzymatic conversion monitoring by reverse-phase HPLC

To monitor the dephosphorylation by alkaline phosphatase, samples of 50 µL were taken at different times after the addition of alkaline phosphatase (t = 0 h) and diluted in 500 µL of 50% acetonitrile solution containing 0.1% TFA. 50 µL of each sample was injected on a Dionex P680 system with a Macherrey-Nagel 250 mm x 4.6 mm C18 column for reverse-phase HPLC. The mobile phase comprised of water and acetonitrile at a flow rate of 1 $mL.min^{-1}$. The gradient was kept constant at 20% (v/v) acetonitrile in water until 4 minutes, then gradually rised to 80% (v/v) acetonitrile in water at 35 minutes and decreasing it to 20% acetonitrile in water at 42 min. The intensity of the peptide peaks was analysed using a UVD170U UV-Vis detector at a 300 nm wavelength and Chromeleon software was used to analyse the spectra and calculate the conversion throughout the time based on the peptide integrated peak areas at specific retention times.

3.5.5.2 Purification of peptides by preparative HPLC

For the synthesised purity check, a certain amount of powder was dissolved in 500 µL of 50% acetonitrile solution containing 0.1% TFA, being injected and ran through the column as mentioned before. As the peptides showed some presence of impurities (by the appearance of peaks in addition to the known 27.5 min and 23 min retention times for Fmoc-YL and Fmoc-Y*p*L, respectively), preparative HPLC was used to purify them. 1 mL of the dissolved compound in 1:1 water:acetonitrile + 0.1% TFA was injected at different times, in a Phenomenex Luna 5 µm C18(2) 100 Å Axia preparative column (100 mm length, 21.2 mm internal diameter, 5 µm fused silica particles). Water and acetonitrile was used as the mobile phase at a flow rate of 9 $mL.min^{-1}$. The gradient was linear to 20% (v/v) acetonitrile in water, gradually rising to 80% (v/v) acetonitrile in water at 40 minutes and decreasing it to 20% acetonitrile in water at 46 min. By analysing the intensity of the

peptide peaks at a 300 nm wavelength, only the peptide peak was collected, assuring the freeze-dried resulting liquid reaches a at least 99% purity, when measured again by reverse-phase HPLC.

3.5.6 Transmission Electron Microscopy

Carbon-coated copper grids (300 mesh) were glow discharged in vacuum for 10-15 seconds. Then, the support films were touched onto the mixture surface, blotted with filter paper and settled for 30 seconds. For the aqueous samples, ammonium molybdate 2% was used as a negative stain, while for the water/chloroform mixtures another negative stain was used (1% aqueous methylamine vanadate obtained from Nanovan, Nanoprobes). The samples were then dried for 10 minutes and imaged using a FEI TECNAI TEO microscope operating at 200 kV (Physics Department, University of Glasgow). The software Digital Micrograph from Gatan was used to see the images.

3.5.7 Atomic Force Microscopy

Aliquots of 10 μL of the aqueous phase samples were deposited onto a freshly cleaved mica surface (1.5 cm x 1.5 cm; G250-2 Mica sheets 1" x 1" x 0.006"; Agar Scientific Ltd, Essex, UK) and left to air-dry on the mica for ~30 min. The images were obtained by scanning the mica surface in air under-ambient conditions using a Multimode 8 scanning probe microscope (Digital Instruments, Santa Barbara, CA, USA), operating using the new mode PeakForce QNM (SIPBS, EPSRC Centre for Innovative Manufacturing in Continuous Manufacturing and Crystallisation (CMAC), University of Strathclyde). The AFM measurements were obtained using ScanAsyst-air probes, for which the spring constant (0.32 N/m; nominal 0.4 N/m) and deflection sensitivity had been calibrated, but not the tip radius (the nominal value used was 2 nm). AFM images were collected at random spot surface sampling and the images analysed using NanoScope Analysis software version 1.40.

3.5.8 Rheology

The mechanical properties of Fmoc-YL hydrogels were assessed using a Malvern Kinexus rheometer with temperature controlled at 20°C and a 20 mm parallel plate geometry with a 0.9 mm gap. Before any measurement, amplitude sweeps were performed at constant frequency of 1 Hz from shear strain 0.01 – 100% to ensure work at the linear viscoelastic regime. Oscillatory rheology was performed in the 0.1-100 Hz frequency range 24 h after sample preparation by carefully loading the gels on to the rheometer with a spatula with no dilution. Triplicates were carried out for all the samples and the average data is shown.

3.5.9 Fluorescence Spectroscopy

Fluorescence emission spectra were recorded between 300 and 600 nm with an excitation light at wavelength 280 nm (for fluorenyl groups in Fmoc) at medium response, 3 nm bandwidth and 1 nm data pitch. Fluorescence emission spectra were measured on a Jasco FP-6500 spectrofluorometer with light measured orthogonally to the excitation light with a scanning speed of 500 $nm.min^{-1}$. The samples were immediately placed in a UV cuvette and measured, with no dilution, at different times after the addition of alkaline phosphatase (which was set as t = 0 h).

3.5.10 FTIR Spectroscopy

Fourier Transform Infrared spectroscopy spectra were recorded on a Bruker Optics Vertex 70 spectrophotometer (Physics Department, University of Strathclyde). Measurements were performed in a standard IR cell holder (Harrick Scientific), in which the sample was placed between two CaF_2 windows separated by a 50 μm PTFE spacer. The spectra were taken in the region 1570 and 1710 cm^{-1} over 25 scans at a resolution of 1 cm^{-1}. pH 8 0.1 M deuterated oxide phosphate buffer was used to prepare the samples, they were measured with no dilution and the curves background corrected.

3.5.11 UV-Visible Spectroscopy

3.5.11.1 Enzymatic activity assay

For the enzymatic activity assay, 850 μL of pH 8 0.6 M sodium phosphate buffer (or mixture of buffer and organic solvent according to each volume ratio), 100 μL of 100 mM pNPP phosphatase substrate and 50 μL of enzyme, were placed into a cuvette, giving a final phosphatase concentration of 1.4 $U.mL^{-1}$. The dephosphorylation reaction was then monitored by UV-Vis by recording the absorbance at 405 nm every 1 min for 10 min, since p-nitrophenol is a chromogenic product that absorbs at 405 nm. Spectra were recorded between 250 and 400 nm on a Jasco UV-660 spectrophotometer.

3.5.11.2 Partition coefficient and interface study

From the 1:1 chloroform-water mixture, without mixing, 20 μL of the aqueous buffer or the chloroform layers were taken and diluted in 2 mL of buffer and chloroform, respectively, in a cuvette, and the absorbance measured. The percentage of the peptide that remained in water, transferred to chloroform or to the interface was calculated, using the 5 mM peptide in water absorbance as a reference. LogP values for each compound were calculated in ChemDraw version 14.0 from PerkinElmer by following Crippen's method,[259] Viswanadhan's fragmentation[251] and Broto's method.[260]

3.5.12 Fluorescence Microscopy

The chloroform-in-water droplets were imaged on an Upright Epifluorescent Microscope (Nikon, Eclipse E600) (Centre for Biophotonics, SIPBS, University of Strathclyde) after being transferred from the emulsion layer onto a glass slide, which was covered with a coverslip and mounted. 1 $mg.mL^{-1}$ Thioflavin T (ThT) in 0.6 M pH 8 phosphate buffer was used to prepare the 5 mM samples, to label the aqueous phase in the emulsion layers and the self-assembled peptides. Images were acquired using Zeiss x10, x20 dry objectives and x40, x60, x100 oil objectives. An appropriate DAPI filter was used for the ThT labeled samples (365 nm excitation WL, 435-485 nm emission WL).

3.5.13 Scanning Electron Microscopy

The emulsion phase was deposited onto a double-sided carbon conductive tape and subject to air-drying and under vacuum in an exicator. As soon as the samples were dried, they were sputter coated under vacuum in a Polaron SEM coating system SC515 with a gold/palladium target. The samples were then imaged using a JEOL6400 Scanning microscope at 10 kV (Department of Chemistry, University of Glasgow) and Olympus Scandium use for image collection.

3.5.14 AA-MD Simulations

3.5.14.1 Water and biphasic simulations

All-atomistic Molecular Dynamic (AA-MD) simulations were carried out in NAMD (NAnoscale Molecular Dynamics) program[261] using the CHARMM force field,[211-212] with Fmoc parameterisation developed in the group.[262] Each system was minimised, at 300 K, with the steepest descent technique to minimise the forces that would otherwise pull and push the atoms apart (Typical input file is presented in Appendix 8). After the system was minimised, it was gradually heated from 0 to 300 K for 55 ps, followed by 445 ps equilibration at 300 K, to ensure system stabilisation (Typical input file is presented in Appendix 9). Finally, the systems were run within an NPT ensemble at 1 atm and 300 K for 200 ns. Langevin Dynamics (LD) was used to keep temperature constant[263] and Langevin piston Nose-Hoover algorithm to keep pressure at 1 atm.[264] A 2.0 fs time step was used to integrate Newton's motion equation along with a 12 Å cut-off for the non-bonded interactions (Typical input file is presented in Appendix 10). Periodic boundary conditions in the three-dimensional coordinates have been used. 60 molecules of Fmoc-Y*p*L or Fmoc-YL were randomly placed in a box by using genbox, incorporated in the Gromacs package.[265] TIP3P water model was chosen for the solvation of the box, with sodium ions added to compensate the phosphate negative charges and produce an overall neutral system.

For the biphasic MD simulations, the molecules in water were put close to an octanol box, which is not a model and so Newton's laws of motion are computed at every instance, turning the simulation computationally more expensive.

3.5.14.2 Simulation analysis

Visual Molecular Dynamics (VMD) program[266] was used to visualise the formed structures throughout the simulation time, using snapshots from this interface. Hydrogen bonds have been analysed using VMD H-bonds analysis tool. Only polar atoms (N, O, S, F) have been taken into account, a donor-acceptor distance of 3.5 Å was used with a 30° angle cut-off. H-bonds between each pair (except Fmoc-Fmoc, that are unable to form H-bonds) have been counted every 5 frames till the end of the simulation, which corresponds to saving the number of H-bonds each 50 ps. Since it accounts for all possible H-bonds independently of the donor/acceptor, Leu/Tyr, *e.g.*, is counted as Tyr/Leu. The proximity between each pair of residues in less than 5.5 Å is also analysed, which can account for π-stacking interactions. A script that counts the number of close residues to each other every 10 ps, excluding within the same molecule, was developed for this (Appendix 11).

4 Biocatalytic control over emulsion stabilisation by tripeptide nanofibrous networks

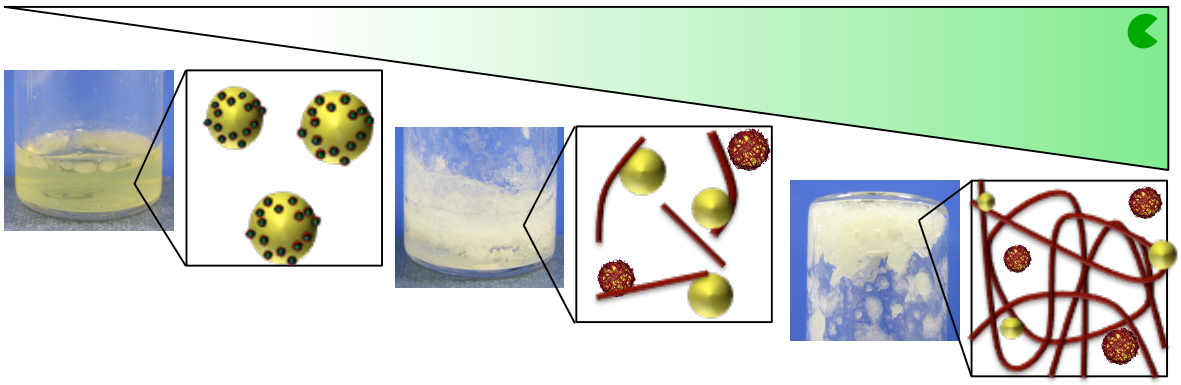

4.1 Introduction

As mentioned before, the creation of temporarily stabilised emulsions is critical in a variety of industrial processes such as equipment cleaning, enhanced oil recovery, cosmetic emulsion formulations and biological applications, when emulsions or foams are desired only during a specific stage.[131, 184, 196] The ability to control the stabilisation/destabilisation of emulsions has been widely studied over the past years, as previously mentioned. Among the stimuli-responsive emulsifiers designed are those that respond upon changing pH,[5, 198, 267] temperature,[268] light irradiation[190] or exchange of gases (CO_2/N_2).[131, 184]

Peptides are attractive building blocks for self-assembled stimuli-responsive materials[12, 269-270] (including emulsions) since they are chemically versatile, biocompatible and biodegradable. This is desirable for various medical, pharmaceutical or nanotechnological applications, as explained in Chapter 2. Several peptide amphiphiles have been shown to self-assemble into different nanostructures through the hydrophobic effect, aromatic interactions and H-bonding, forming self-supporting gels.[2, 271-273] The responsiveness in these systems is achievable because these structures are assembled through weak non-covalent interactions that easily rearrange upon environmental or chemical changes.

In addition to environmental changes such as temperature and pH,[172, 274] (bio-) catalytic reactions have been extensively used to control self-assembly (or dis-assembly),[61, 107, 109, 120, 275] allowing for a stimulus to be applied at constant, physiological conditions. Hirst *et al.* have shown that the amount of biocatalyst used can direct the self-assembly pathway resulting in (kinetic) control of the supramolecular organisation of the final supramolecular structure.[3] They also demonstrated that these kinetically locked gels may be 'unlocked' to access a minimum energy state by performing a heat/cool cycle.[3] The kinetics of self-assembly and subsequent gelation control have been studied by varying different parameters,[276] such as ionic strength of the peptide solution,[277] peptide concentration[278] or change in the peptide sequence.[279] The balance between kinetic and thermodynamic aspects of peptide assembly and gelation are still far from fully understood and are difficult to precisely control, despite continued investigation.[117, 280-281]

In the previous chapter, it was demonstrated that emulsions can be stabilised on-demand, by making use of a biocatalytically-triggered self-assembly of nanofibrous networks of aromatic peptide amphiphiles (9-fluorenylmethoxycarbonyl (Fmoc)-peptides) at the aqueous/organic interface. However, Fmoc-peptide amphiphiles contain a non-biological component (Fmoc), which may not be acceptable for specific applications (cosmetics, food, *etc.*). As a biocompatible alternative to Fmoc-peptides, it has been demonstrated that a number of tripeptides are suitable self-assembly motifs which show nanofibrous gelation. In particular, the tripeptides containing two adjacent aromatic amino acids flanked by an acidic or basic amino acid, such as H-lysyl-tyrosyl-phenylalanine-OH (KYF)[85] or by incorporation of both L and D enantiomers, as reported by Marchesan *et al.*.[81] Interface-stabilising peptides may act as either traditional surfactants which form a stabilising monolayer at the interface (H-aspartyl-diphenylalanine-OH, DFF and FFD) or emulsifiers that self-assemble into interfacial nanofibre networks, stabilising oil-in-water droplets (KYF, KFF and KYW (where W is tryptophan)).[182]

We now combine the advantages of using unprotected tripeptides with the biocatalytic self-assembly of nanofibres in both aqueous and biphasic systems, creating the first reported examples of biocatalytically assembled tripeptide gels and emulsions. This may be achieved by simply phosphorylating the tyrosine residues to reduce the self-assembly tendency in tripeptides, which is subsequently restored upon enzymatic dephosphorylation. The first objective is therefore (i) to demonstrate that an alkaline phosphatase can be used to dephosphorylate a non-gelator H-Lys-Tyr(PO_3H_2)-Phe-OH (KY*p*F) (Figure 4.1a) and trigger the self-assembly into nanofibres in a bulk aqueous system. In addition, (ii) we interrogate the enzymatic pathway to assess whether varying the biocatalyst amount can kinetically control the fibre network properties (Figure 4.1b, 2 and 3). The third aim is (iii) to investigate the entanglement of these nanofibres at the oil droplets' interface and/or within the aqueous environment to stabilise oil-in-water emulsions upon enzyme addition. Finally (iv), to investigate whether the emulsion stabilisation and consequent properties of these emulsions can be tuned by varying enzyme concentration (Figure 4.1c, 2 and 3).

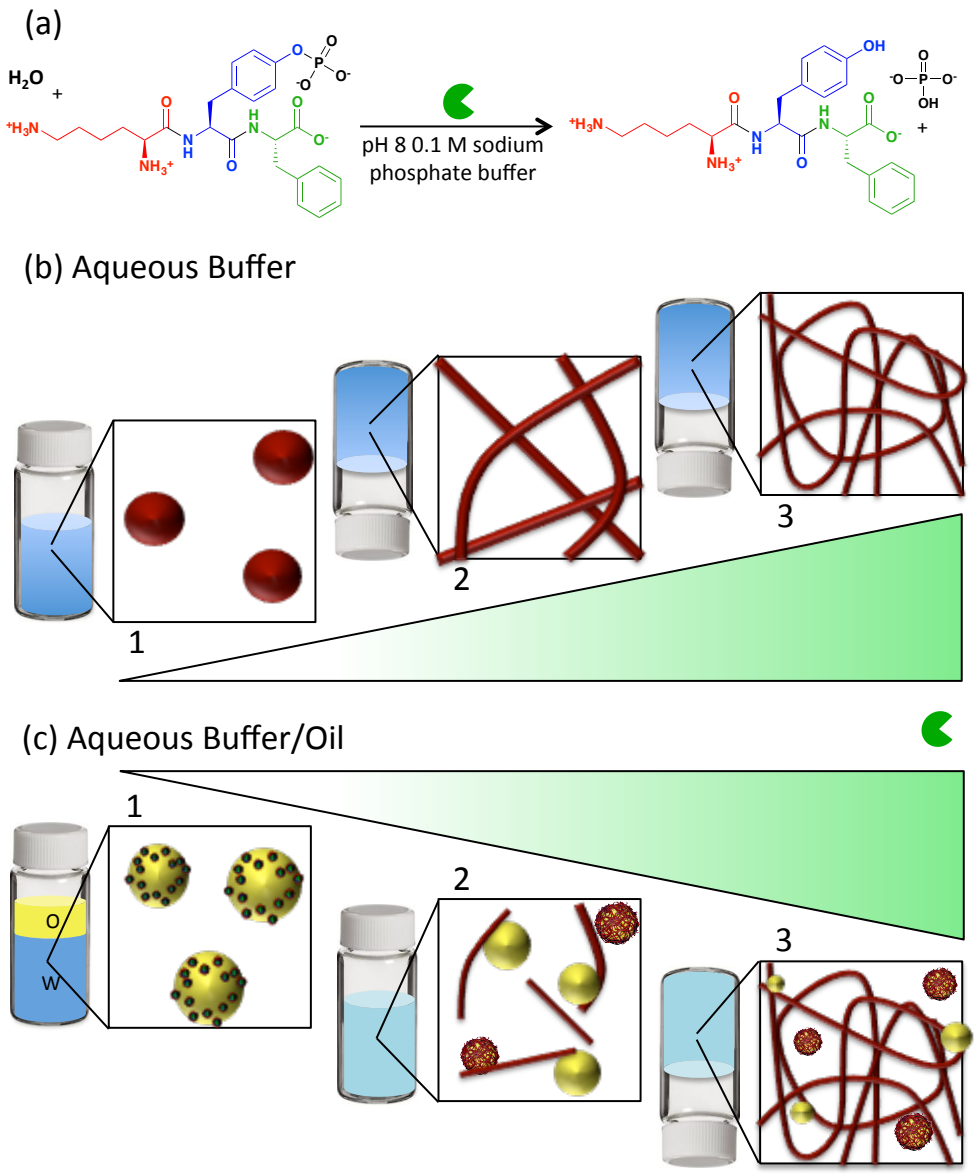

Figure 4.1. (a) Schematic representation of the enzymatic conversion from KY*p*F into KYF upon exposure to alkaline phosphatase (Green); (b) In aqueous buffer, alkaline phosphatase addition converts a precursor solution composed of KY*p*F spherical aggregates (b1) into a hydrogel composed of a KYF nanofibrous network, with the morphology and subsequent hydrogel stiffness controlled by the amount of catalyst which determines the kinetics of dephosphorylation (b2 versus b3); (c) In a biphasic system, alkaline phosphatase addition converts a two-phase system with some KY*p*F micelles at the interface of oil droplets (c1) into a more established oil-in-water emulsion by the formation of nanofibres at the interface and surrounding oil droplets, with the emulsifying ability controlled by the specific amount of enzyme used (c2 versus c3).

4.2 Biocatalytic control over self-assembly into hydrogelators

4.2.1 Enzyme concentration effect over conversion rate in aqueous buffer

The dephosphorylation from the precursor KY*p*F at 40 mM in 0.1 M phosphate buffer to the tripeptide KYF is followed by reverse-phase HPLC (Figure 4.2a). In order to study the biocatalytic self-assembly of tripeptides, samples with a final alkaline phosphatase (AP) concentration of 6.6, 3.3, 1.3 and 0.07 μM were prepared (which corresponds to 55.2, 27.6, 11.0 and 0.55 $U.mL^{-1}$, respectively (See Section 4.6.2 for *Preparation of aqueous and biphasic samples*). For the control sample, when no AP is added, KY*p*F remains unchanged after 24 h, while tyrosine dephosphorylation is observed from the moment AP is added in the other samples (Figure 4.2a). As expected,[282] a faster dephosphorylation occurs when more catalyst is present. The formation of reaction product follows a rate profile which is linear at the start (see Figure 4.2b for detailed conversion in the first hour), and then gradually decreases until full conversion is achieved.[283] For all enzyme concentrations tested except 0.07 μM AP, >90% of KYF is formed after 24 hours, which is in line with the previously reported full dephosphorylation from Fmoc-Y*p*-OH into Fmoc-Y-OH within 24 h, reported by Thornton and co-workers.[62] The highlighted circles in Figure 4.2a represent the gelation time for each sample as determined by vial inversion.

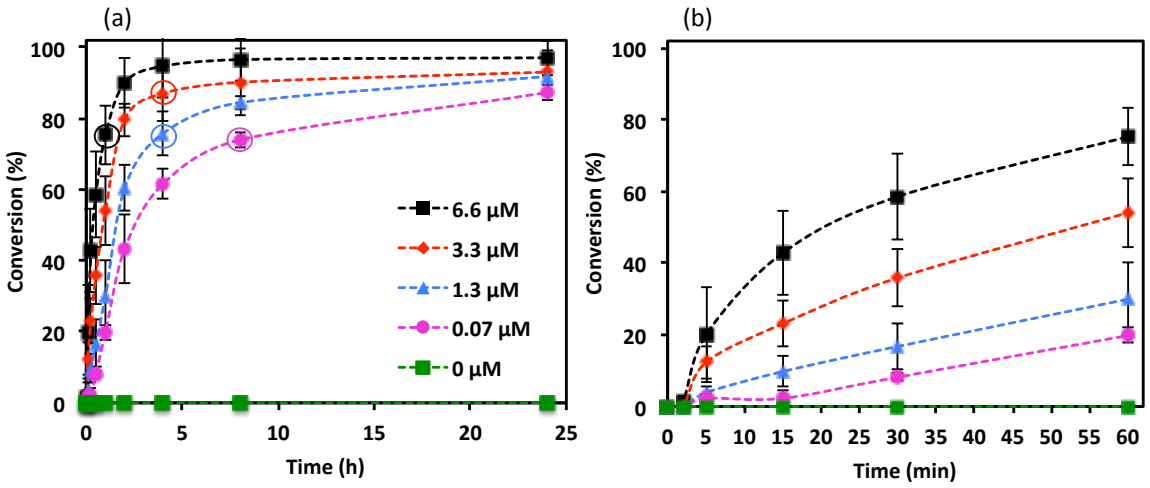

Figure 4.2. (a) HPLC conversion from KY*p*F into KYF in buffer when using different concentrations of alkaline phosphatase. Circles represent the first point where gelation was observed for each concentration as determined by vial inversion; (b) Detailed conversion at the first 60 min from the moment alkaline phosphatase is added, at different concentrations.

4.2.2 Enzyme concentration effect over morphology

The morphology of the gels formed by biocatalytic gelation was studied using TEM. This imaging was performed 24 h after the addition of alkaline phosphatase, when all samples were hydrogels (except the no enzyme control), although the gelation time was different for each one, as mentioned. The precursor KY*p*F gives rise to a clear solution with only some aggregates observed (Figure 4.3a), which is due to the greater affinity of the phosphate groups of the tyrosine with water. Upon enzymatic cleavage of the solubilising phosphate group, the amphiphilicity of the molecules is changed and self-assembly occurs creating nanofibrous networks.

The morphology of the nanofibres observed by TEM after 24 h differs markedly when varying the enzyme concentration (Figure 4.3). The samples where low catalyst concentration (0.07 µM) was used presents fibres of approximately 14 nm diameter (Figure 4.3b), while the sample where the highest catalyst amount was used (6.6 µM) forms much thinner fibres (approximately 3 nm diameter). The latter presents a dense and entangled nanofibrous network (Figure 4.3e), in contrast to the less entangled fibre bundles observed

for the other hydrogels. The differences in fibre size (Figure 4.3f) and network type observed suggest that the growth pathways, gelator formation rate and gelation time (governed by the catalyst amount) can influence the final materials' structure.[120] It is worth noting that when KYF gel is formed non-enzymatically by direct dissolution into a pH 8 0.1 M phosphate buffer, the nanofibres formed are thicker than when using 6.6 μM AP (4.6±2.1 nm *versus* 2.8±1.7 for 6.6 μM AP sample) and less entangled (See Appendix 12). This difference might be explained by the disordered nucleation and less organised gelation in comparison to the spatio-temporal controlled enzymatic dephosphorylation that leads to more uniform fibre formation.

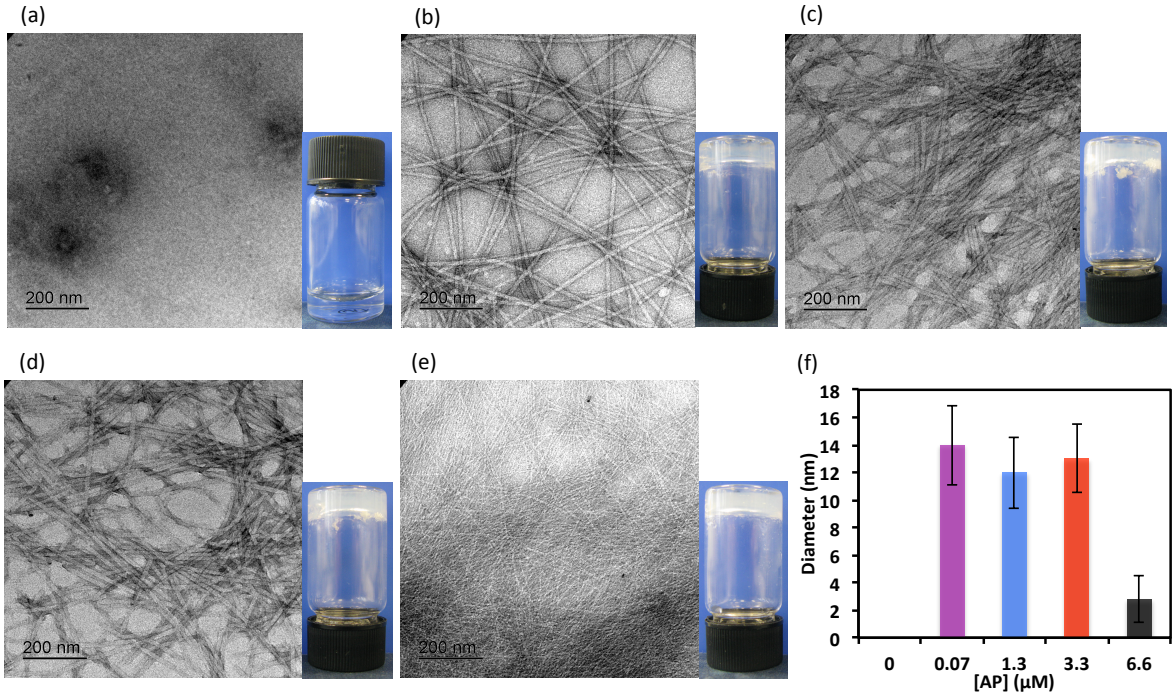

Figure 4.3. TEM images and macroscopic photographs (insets) taken 24 h after preparation of the aqueous samples: (a) KY*p*F precursor; (b) KY*p*F added 0.07 μM alkaline phosphatase; (c) 1.3 μM AP; (d) 3.3 μM AP; (e) 6.6 μM AP (more TEM images are presented in Appendix 12); (f) Nanofibre diameter analysis [obtained by image analysis] for each concentration, showing much thinner fibres for the highest enzyme concentration tested.

4.2.3 Enzyme concentration effect over mechanical properties

In order to evaluate and compare the mechanical properties of the hydrogels when using different enzyme concentrations, dynamic frequency sweep measurements were carried out (see Figure 4.4), after first performing the strain sweep to ensure the correct range and conditions were used (Appendix 13).

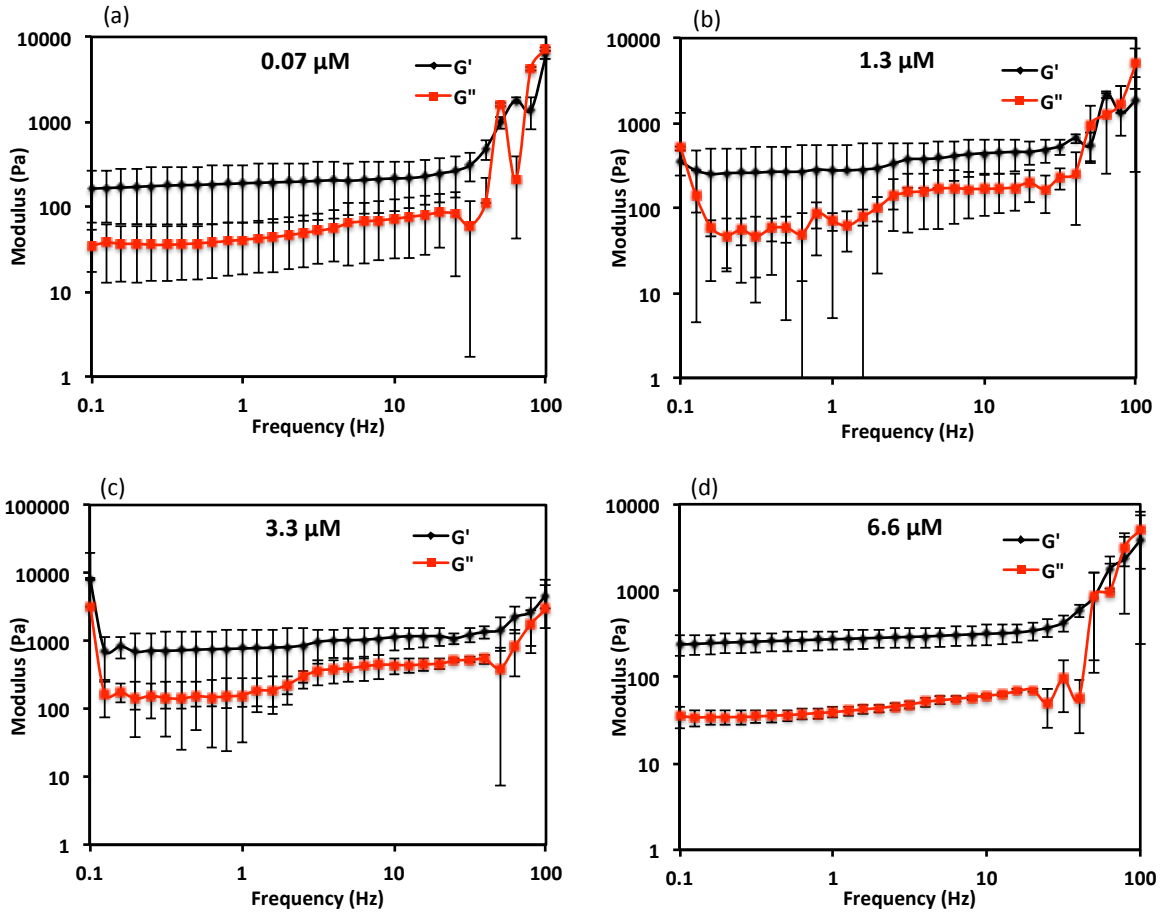

Figure 4.4. Frequency sweep measurements showing viscoelastic behaviour of the different produced hydrogels: (a) KY*p*F + 0.07 µM AP; (b) KY*p*F + 1.3 µM AP; (c) KY*p*F + 3.3 µM AP; (d) KY*p*F + 6.6 µM AP (1% strain used).

In Figure 4.5, the storage (G') and loss (G'') moduli are plotted *versus* enzyme concentration. Based on the definition of Yan and Pochan,[248] all samples except that obtained at 1.3 µM AP present viscoelastic behavior and can be considered viscoelastic materials as G' is more than one order of magnitude greater than G'' (Table 4.1). This is in agreement with the macroscopic observation by vial inversion (Figure 4.3). However, there

is an upturn in G' and G'' moduli at higher frequencies, which is possibly explained by a thickening instability, as previously mentioned.[59, 249] The highest hydrogel elasticity would be expected for the hydrogel with the highest level of entanglement of fibres (Figure 4.3e), as observed for an enzyme-triggered self-assembly of octapeptides.[119] Even though the error bars for the 3.3 μM alkaline phosphatase sample are larger than for the other enzyme concentration used, which suggests higher variability in the properties of this material, it presents the highest G' and G'' values, decreasing again for the 6.6 μM AP sample.

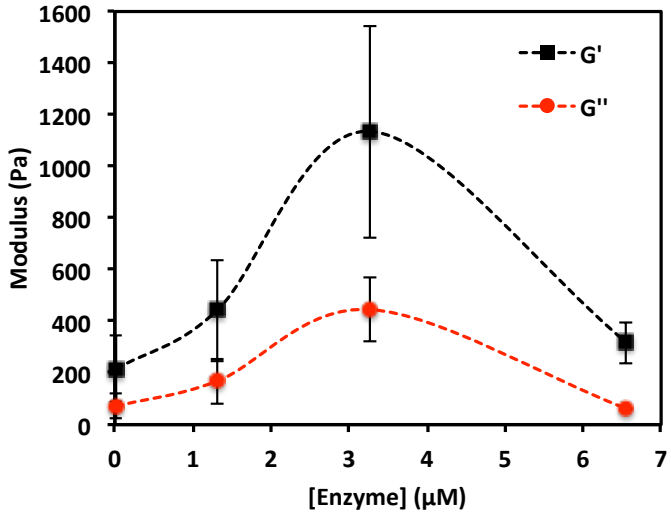

Figure 4.5. Rheology behaviour of the hydrogels produced when using different enzyme concentrations, measured at 24 h (modulus at 10 Hz plotted).

Table 4.1. Storage (G') and Loss (G'') modulus of each hydrogel at 10 Hz

[AP] (μM)	G' (Pa)	G'' (Pa)
0.07	2.2×10^2	7.2×10^1
1.3	4.4×10^2	1.7×10^2
3.3	1.1×10^3	4.5×10^2
6.6	3.2×10^2	6.1×10^1

Boekhoven and co-workers have also reported a maximum storage modulus obtained for a certain concentration of catalyst aniline, with higher concentrations leading to the decrease of this G' value.[120] We propose that the presence of alkaline phosphatase in excess can be detrimental for the nanofibrous network and hydrogel production due to the fast dephosphorylation which outpaces the self-assembly rates, giving rise to formation of kinetically trapped disorganised regions. As previously shown for esterase catalysed assembly of a range of Fmoc-dipeptides,[3] different metastable states of the same self-assembling tripeptide can be produced by simply varying the catalyst amount, which affects the conversion rate, non-covalent interactions, network morphologies and subsequent mechanical properties.

4.2.4 Enzyme concentration effect over supramolecular interactions

In order to investigate the supramolecular structures formed when using different enzyme amounts, spectroscopic techniques (fluorescence, FTIR and MD simulations) were used to further characterise the non-covalent interactions involved in the self-assembly process for all samples where different enzyme amounts were used.

4.2.4.1 Fluorescence spectroscopy

From fluorescence spectroscopy, all the samples, including the precursor solution KY*p*F, present a tyrosine emission peak at approximately 300 nm. However, upon the addition of alkaline phosphatase, a gradual red-shift is observed, as seen in the time-course for the maximum wavelength of the different samples (Figure 4.6a). This shift indicates the formation of more favorable π-π stacking interactions upon assembly and gelation, which occurs gradually after the AP is added. For each enzyme concentration, similar red-shifts are observed (to 311 nm), but they appear at different rates (see Figure 4.6b for further details regarding the red-shift of each sample at different timings). As may be expected, higher enzyme concentrations show more rapid emergence of red-shifts over time, proving self-assembly occurs more rapidly for the 6.6 μM AP sample and slower when 0.07 μM of enzyme is used.

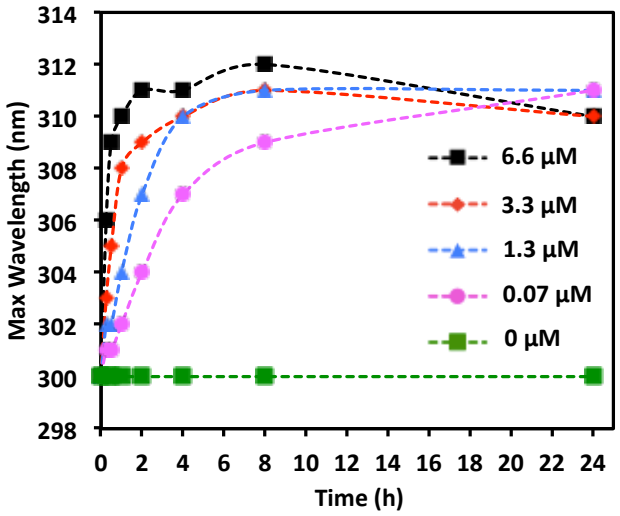

Figure 4.6. (a) Maximum wavelength (normalised intensity) throughout the time from enzyme addition showing the red-shift occurring for the samples where 6.6 µM, 3.3 µM, 1.3 µM or 0.07 µM alkaline phosphatase is used. The precursor where no enzyme is added showed no red-shift.

The full spectra (non-normalised) at 1 h, 2 h and 24 h (Figure 4.7), reveal a gradual intensity drop for the peak at around 300 nm, which is due to the increase in opacity when a solution is transformed into a hydrogel and it may also relate to quenching of signal due to enhanced aromatic-aromatic interactions.

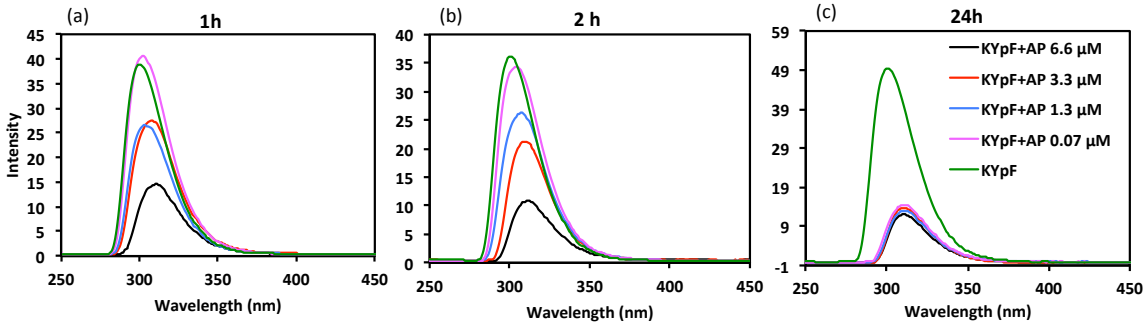

Figure 4.7. Fluorescence emission spectra of the different samples 1 h after the addition of alkaline phosphatase in different amounts (a); 2 h after (b); and after 24 h of enzyme addition (c), showing the red-shift and intensity decrease for all except KY*p*F precursor (green curve).

This intensity decrease, together with the red-shift, provides evidence that the kinetics of the self-assembly process and hydrogel formation are dictated by the enzyme concentration. For the lowest enzyme concentration used in this study, a gel is formed between 4 and 8 h, occurring later due to the slower dephosphorylation, which was already apparent from the HPLC time-course (Figure 4.2a). Altogether, these observations provide evidence that the kinetics of the self-assembly process and hydrogel formation influence the nature of the nanostructures formed, which was observed by microscopy techniques (Figure 4.3) and is further investigated by FTIR spectroscopy.

4.2.4.2 FTIR spectroscopy

The amide I region of the spectra obtained by Fourier transform infrared (FTIR) was analysed to observe H-bonded networks between the amide backbones for the samples where different enzyme concentrations were used (Figure 4.8a). The precursor KY*p*F (Green curve - when no alkaline phosphatase is added) does not present evident peaks in this region, except a low intensity broad peak at around 1590 cm^{-1}, characteristic of the deprotonated fraction of C-terminus carboxyl groups.[74] However, the appearance of intense peaks at the amide region proves that H-bonded networks are formed during biocatalytic assembly. Comparably to what was mentioned in Chapter 3 for capped short peptides, the analysis of FTIR peaks for tripeptide assemblies cannot be simply extrapolated from the secondary structure of proteins either.[74] Nevertheless, the peaks around 1620 and 1650 cm^{-1} indicate the formation of organised hydrogen bond networks between the amide groups of the tripeptides. The shift from the carboxylate peak to approximately 1560 cm^{-1} in the amide II region for the hydrogels formed upon addition of enzyme is related to changes in the NH bending vibration. This change is explained by the formation of salt bridges between the C-terminus and the N-terminus of the peptide chain or that terminal carboxyl group and lysine's side chain. This is consistent with the interpretation reported previously for non-enzymatically assembled KYF.[85, 182]

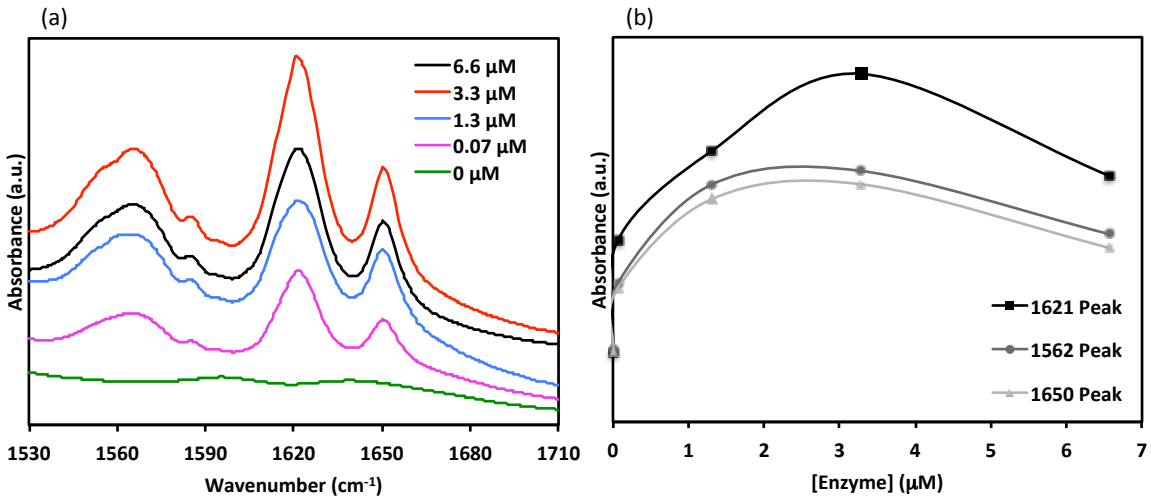

Figure 4.8. (a) FTIR spectra for all samples when different AP amounts are used, measured 24 h after; (b) Absorbance maximum at specific wavenumbers from FTIR spectra *versus* alkaline phosphatase concentration used.

It is notable that a more well-ordered H-bonded structure is formed when the KYF is biocatalytically produced compared to non-enzymatic (for comparison, see Appendix 14). Since 87% KYF had already been produced and a gel was formed by the time that the FTIR was performed (24 h), the broader peaks observed for the lower enzyme concentration (0.07 µM) confirm that a slower conversion gives rise to less well-ordered H-bonded network. The formation of more ordered structures has been reported before when increasing the enzyme amount and may be related to the localised and early-stage nucleation and fibre growth.[3] It should be noted that sharper peaks are observed for the 3.3 µM hydrogel, and these are broader again at higher enzyme concentration (See Figure 4.8b for trend), which suggests that there is an optimum enzyme concentration (*ca.* 3.3 µM AP) for the formation of more well-ordered H-bonded networks. This is in agreement with the rheology results (Figure 4.5) and thus corroborates that there is an optimum enzyme concentration that gives rise to a stiffer hydrogel. We propose that, at a higher enzyme concentration than the optimum, the formation of KYF peptides outpaces the kinetics of the self-assembly process, giving rise to less ordered assemblies. However, the effect is related to the kinetics of the self-assembly process, and not just enzyme concentration, as the

presence of the enzyme was shown not to be disruptive to the H-bonded networks when present together with the non-enzymatically produced KYF hydrogel (Appendix 14).

4.2.4.3 Molecular Dynamics simulations

In order to further assess the differences in supramolecular interactions between KYF and KY*p*F, that is unable to form fibres, computer simulations were used. Coarse-grained molecular dynamics simulations were used rather than all-atom simulations, where larger systems could be simulated for longer and more closely represent the experimentally-observed behaviour. Detail is lost and it is not possible to precisely analyse the non-covalent interactions through which preferred nanostructures are formed. Instead, these coarse-grained MD simulations are useful to compare assembling tendencies. For the comparison between KYF and the phosphorylated KYF (KY*p*F), the parameterisation of phosphorylated tyrosine was necessary, since no topology was available for this. The parameterisation of the mentioned phosphorylated tyrosine for KY*p*F is fully described in Section 4.6.11.2 of Materials and Methods.

Coarse-grained molecular dynamics simulations of KY*p*F (Figure 4.9a), when using the parameterised Q2a bead, or of KYF (Figure 4.9b) showed different assembly tendencies after being run for 10 μs in a water box. KY*p*F assembles into aggregates, while KYF forms more ordered nanofibres, as already reported.[182] This result is consistent with observed experimental behaviour (Figure 4.3).

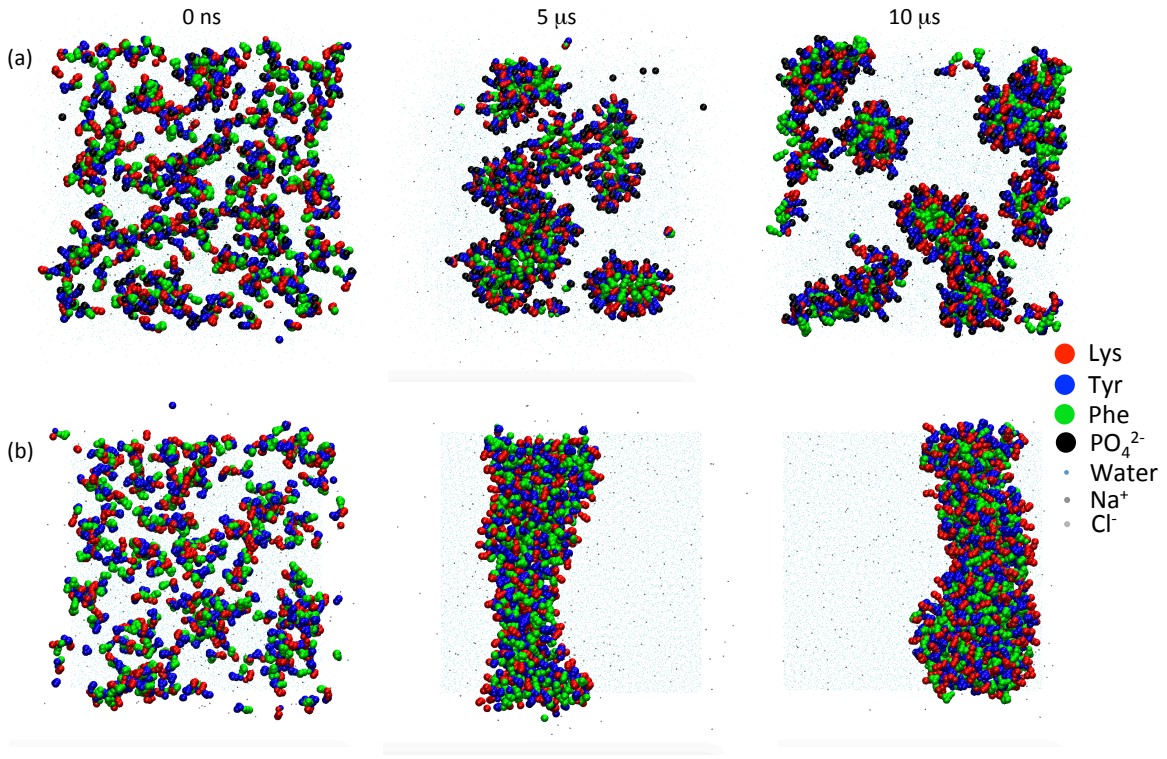

Figure 4.9. Snapshots of CG-MD simulation of KY*p*F when using Q2a bead (a) and KYF (b). Colour labelling used as in inset.

However, the initial KY*p*F system using the Qa bead (with the standard P4-Qa interaction potential) resulted in fibre formation when 300 molecules were randomly put in a water box and ran for 10 μs (Figure 4.10), which is not consistent with the experimental results.

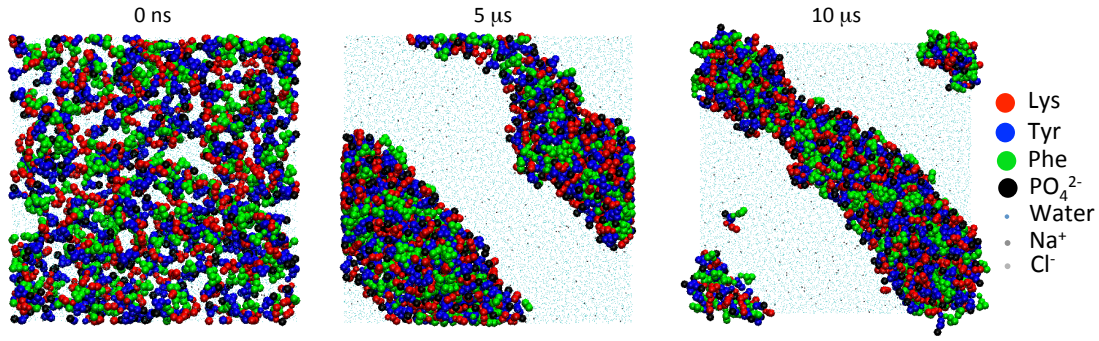

Figure 4.10. Snapshots of CG-MD simulation of KY*p*F when Qa bead is used, in the beginning of the simulation, 5 μs and 10 μs after, showing fibre formation. Colour labelling used as in inset.

Surprisingly, these results indicate that the lack of fibre formation in the case of KY*p*F is not due to increased repulsion between the phosphate anions, as initially expected from related systems with phosphorylated tyrosine.[61, 284] Rather, through the parameterisation of the phosphate group it is evident that the lack of fibre formation in the case of KY*p*F is due to the greater hydration of the phosphate group in the modified tripeptide, given by the stronger non-bonded interaction between phosphate groups from tyrosine and water molecules. The fact that the subtle change in the hydrophilicity of the modified tripeptide is the critical factor in determining the self-assembly ability of the compound, rather than specific interactions in the self-assembled state has important implications for the future development of related systems.

4.3 Biocatalytic control over emulsion stabilisation

Following an optimisation from the emulsion studies presented in Chapter 3, a different preparation was followed in order to make the process more reproducible: a 1:9 oil:buffer volume ratio was used, the enzyme was added after the oil and a top-bench homogeniser was used instead of hand-shaking to mix the two phases. A food-grade rapeseed oil was chosen as the water immiscible solvent in order to achieve a completely biocompatible emulsion stabilisation system that can have different applications in the food or cosmetic industries.

4.3.1 Enzyme concentration effect over conversion rate in non-aqueous systems

The system was also investigated in aqueous/organic biphasic systems in order to assess the capability of kinetically controlled fibrous networks to stabilise emulsions to different extents depending on the catalyst amount in use. It is shown, using HPLC, that KY*p*F is transformed into KYF when AP is added to the biphasic mixture (Figure 4.11a). Following the finding that enzyme concentration dictates the conversion rate and subsequent formation of nanofibrous entangled networks in the aqueous system, different alkaline

phosphatase amounts were also used for the biphasic mixtures. From reverse-phase HPLC (Figure 4.11), the conversion from KY*p*F into KYF were observed to be dependent on the phosphatase concentration, which is in agreement with what has been observed for the aqueous systems (Figure 4.2a).

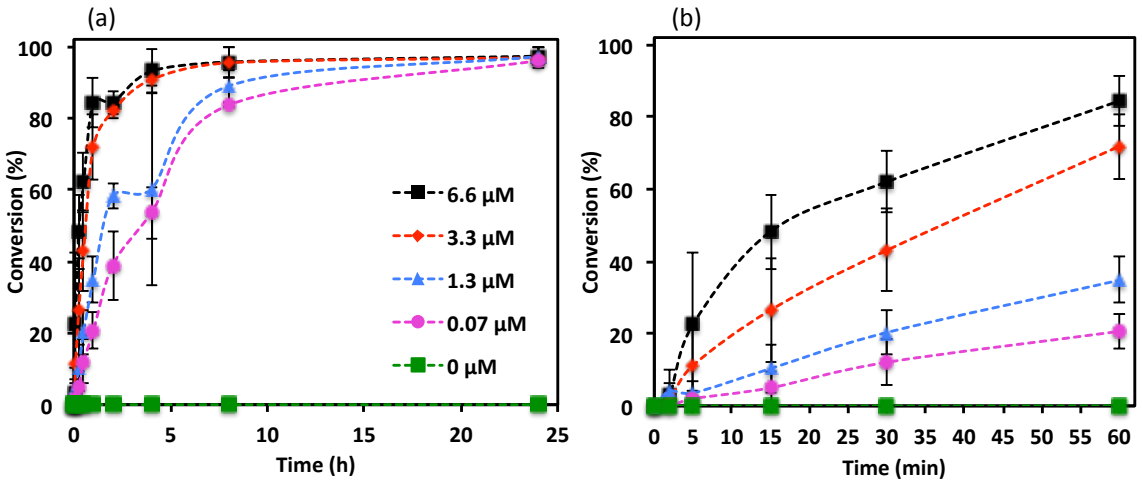

Figure 4.11. (a) HPLC conversion from KY*p*F into KYF in the biphasic system when using different concentrations of alkaline phosphatase; (b) Detailed conversion at the first 60 min from the moment alkaline phosphatase is added, at different concentrations.

The results show that the enzyme is still active when rapeseed oil is added to the aqueous system, which was also proven by an enzymatic pNPP assay (Figure 4.12). For the alkaline phosphatase in rapeseed oil only, the absorbance does not increase throughout the 10 min of experiment, which suggests no conversion happens and thus the phosphatase is not active in this oil. However, its activity gradually increases when increasing the aqueous buffer volume ratio in the system (1:1, 7:3 and, in a higher extent, 9:1), showing the enzyme is capable of displacing to the aqueous medium and remain active. The alkaline phosphatase is shown to have its activity decreased to a lesser extent when in a 9:1 buffer:rapeseed oil mixture, when comparing to a 100% aqueous buffer medium (Figure 4.12).

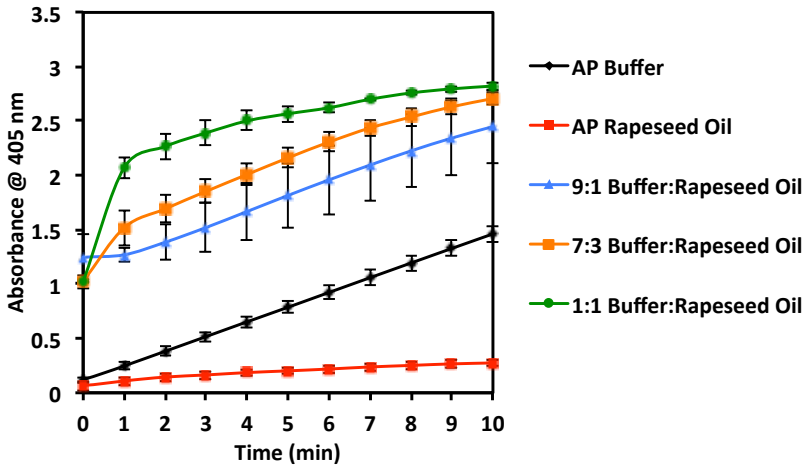

Figure 4.12. Enzyme activity in different (non-)aqueous systems, where the dephosphorylation reaction of 4-nitrophenyl phosphate (pNPP) is monitored by the UV-Vis absorbance at 405 nm through 10 min. Curves shown represent the subtraction of each measurement by the corresponding blank (Appendix 15).

Higher absorbance values are observed at time zero when rapeseed oil is present in the samples due to the stabilisation time after phase mixing. Due to this measurement artefact, each measurement was subtracted by the blank of the respective ratio with pNPP and no enzyme.

4.3.2 Enzyme concentration effect over morphology

When rapeseed oil is added to the 40 mM KY*p*F in 0.1 M sodium phosphate buffer (1:9 v/v) and homogenised using a top-bench homogeniser (See *Preparation of aqueous and biphasic samples* subsection of Materials and Methods), a temporary and unstable emulsion is formed, which separates into two phases in less than 1 hour. Phosphorylated KYF is not able to stabilise emulsions, which is shown by its de-emulsified appearance 24 h after preparation (inset of Figure 4.13a). However, when alkaline phosphatase is added immediately after the oil addition and the mixture is homogenised for 10 seconds, a stable emulsion is created (Figure 4.13), which remains for more than 1 week (Figure 4.15d).

From the TEM images and macroscopic photographs taken after 24 h from enzyme addition and emulsion formation (Figure 4.13 and Appendix 16), a significant difference is observable when varying the amount of catalyst used. All emulsions have the appearance of

gel-like samples, except the KY*p*F + 0.07 μM AP sample and the no enzyme control. However, they are not considered to be self-supporting gels because they flow when the vial is inverted.

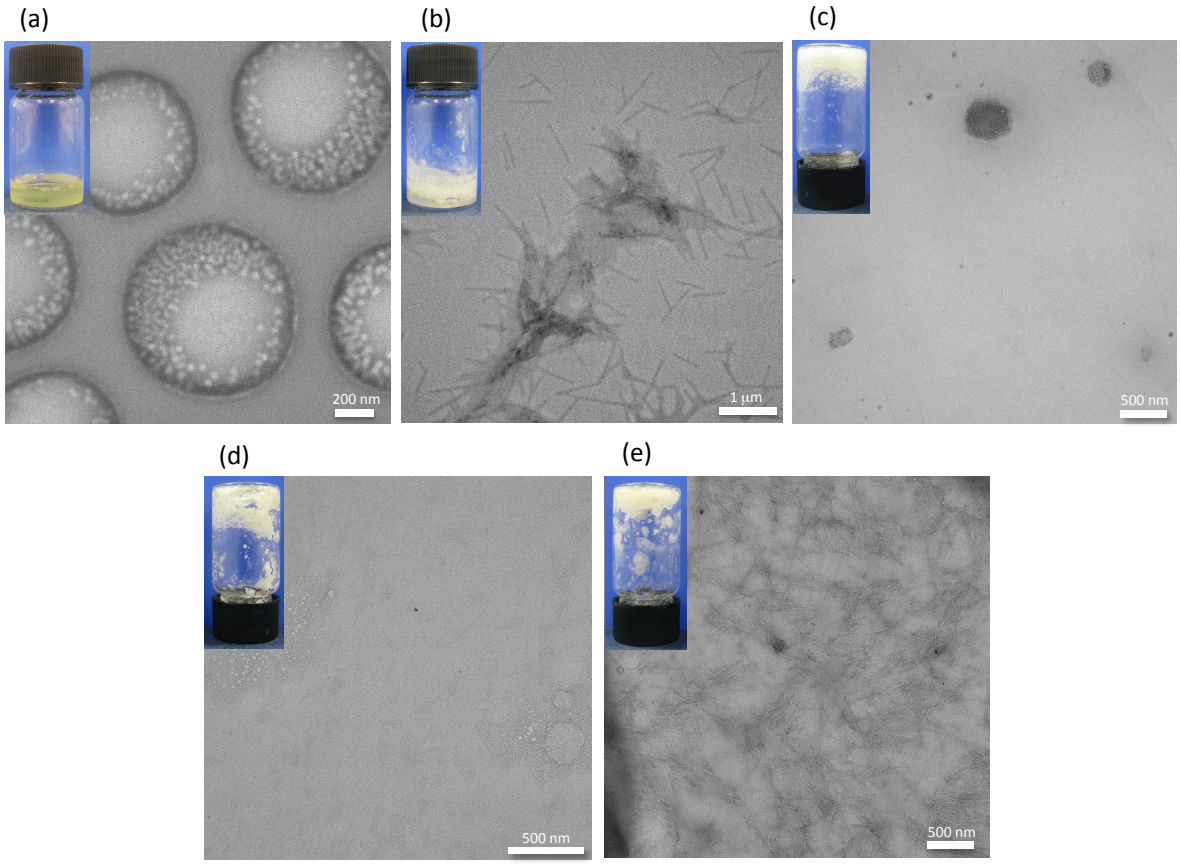

Figure 4.13 Photographs of macroscopic aspect and TEM images obtained 24 hours after preparation of the different 9:1 buffer:rapeseed oil samples: (a) KY*p*F precursor showing micelles at the interface of the oil droplets; (b) KY*p*F added 0.066 μM alkaline phosphatase; (c) 1.3 μM AP; (d) 3.3 μM AP; (e) 6.6 μM AP (More TEM images are presented in Appendix 16).

While the emulsions with the lowest enzyme concentration are stabilised by the formation of some un-entangled short fibres in the environment of the droplets, the 6.6 μM AP concentration emulsion is constituted by an entangled network of nanofibres that is able to stabilise small oil-in-water droplets.

Fluorescence microscopy obtained after 24 h from homogenising the mixture showed no fluorescence for the control KY*p*F (Figure 4.14a), which proves that there is no β-sheet H-

bonded arrangement when phosphatase is not added. By contrast, all the biocatalytically produced KYF-stabilised emulsions show the fluorescent probe Thioflavin T (used to label the tripeptide aqueous solution before the oil addition) at the oil/buffer interface and at the aqueous phase. The fluorescence microscopy images indicate denser fibrous networks at the droplets' interface in addition to stained material throughout the samples. This occurs especially for the emulsion where, *e.g.*, 6.6 μM phosphatase is added (Figure 4.14e), which is in agreement with the TEM images (Figure 4.13e) where an entangled nanofibrous network is observed in the environment. Since evidence from TEM and fluorescence microscopy point to the two ways to decrease the coalescence rate, it is believed that both routes play a role in the emulsification, in particular at high enzyme concentrations. In addition to the droplet stabilisation by interfacial nanofibrous networks as previously reported,[79, 284] where an amphiphilic structure delays droplet coalescence, another mechanism by which emulsions are stabilised is by the viscosity increase of the continuous phase. As mentioned in Chapter 2, gelled emulsions or high internal phase emulsions (HIPEs) have been shown to delay or prevent coalescence or creaming through the formation of a gel matrix where droplets are embedded,[157, 285-286] reducing their mobility. It is believed that the emulsification occurs by these two main mechanisms, whereby the nanofibres introduce some kind of Pickering stabilisation and also increase the viscosity of the continuous medium.

A droplet size distribution study (using fluorescence microscopy image analysis) was carried out in order to compare the different emulsion stabilities when using different enzyme amounts. Three different fluorescence microscopy images were used to characterise the droplet size of each emulsion - with the results presented as histograms (see Figure 4.14). When 0.07 μM alkaline phosphatase is added to KY*p*F (Figure 4.14b) there is a lower number of droplet counts and high polydispersity due to the presence of some bigger droplets. The emulsion where 1.3 μM AP was used also presents droplets with inconsistent sizes (Figure 4.14c), while the one with 3.3 μM AP follows a more normal distribution (Figure 4.14d). The emulsion with the highest enzyme concentration tested is more uniform, with smaller droplets observed (Figure 4.14e). A smaller average droplet diameter is noted when more catalyst is used (Table 4.2), which corroborates the theory of

higher emulsion stabilisation when higher enzyme concentration is used and more entangled nanofibres are formed.

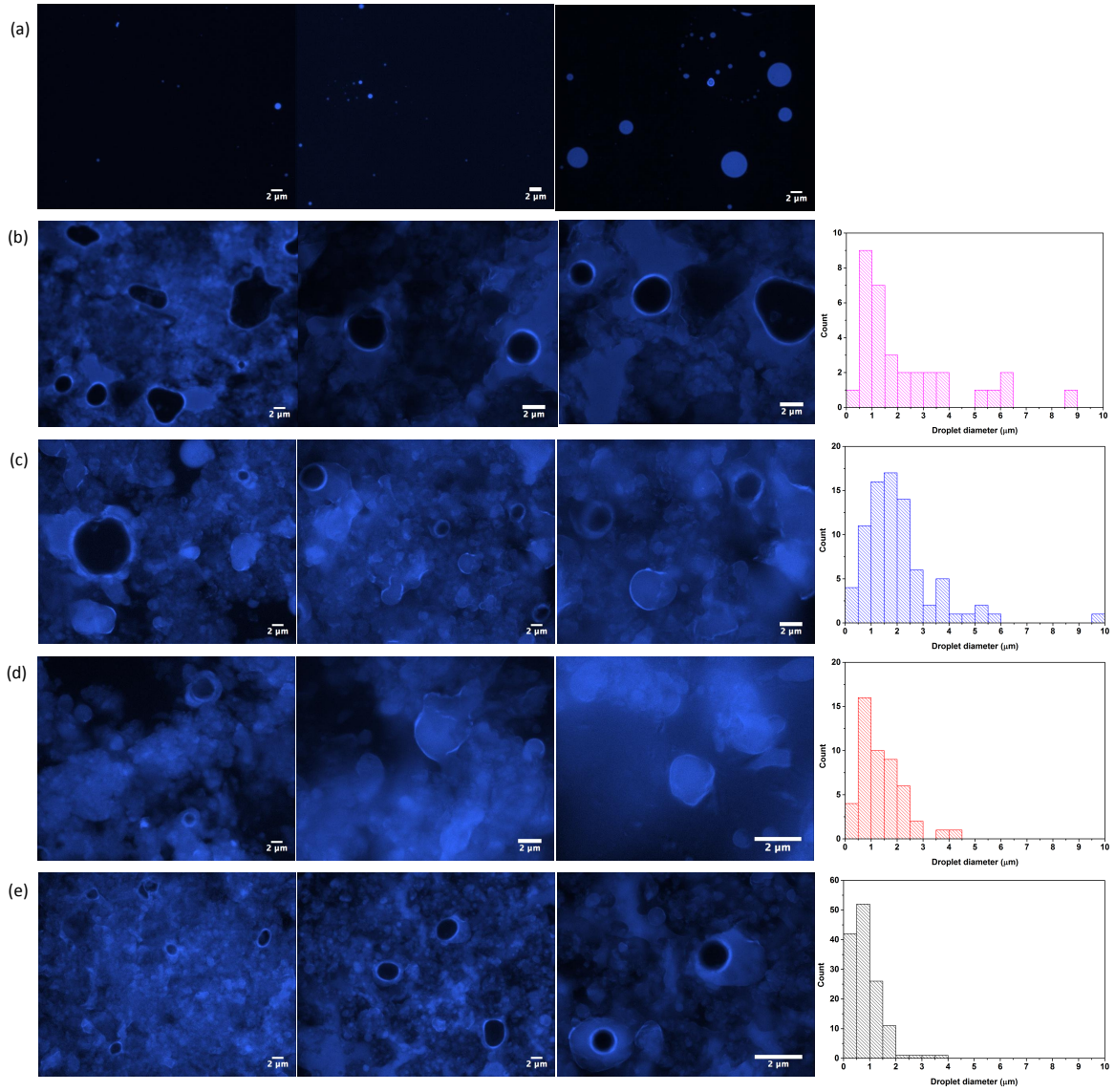

Figure 4.14. Fluorescence microscopy images obtained 24 hours after preparation of the different 9:1 buffer:rapeseed oil samples, labelled by ThT, and droplet size distribution histogram with a bin width of 0.5 µm, based on the analysis of 3 different areas: (a) KY*p*F control without the addition of alkaline phosphatase; (b) KY*p*F added 0.07 µM alkaline phosphatase; (c) 1.3 µM AP; (d) 3.3 µM AP and (e) 6.6 µM AP.

In addition, the emulsions were also characterised after 1 week of storage at room temperature to study their relative stabilities over time (Figure 4.15).

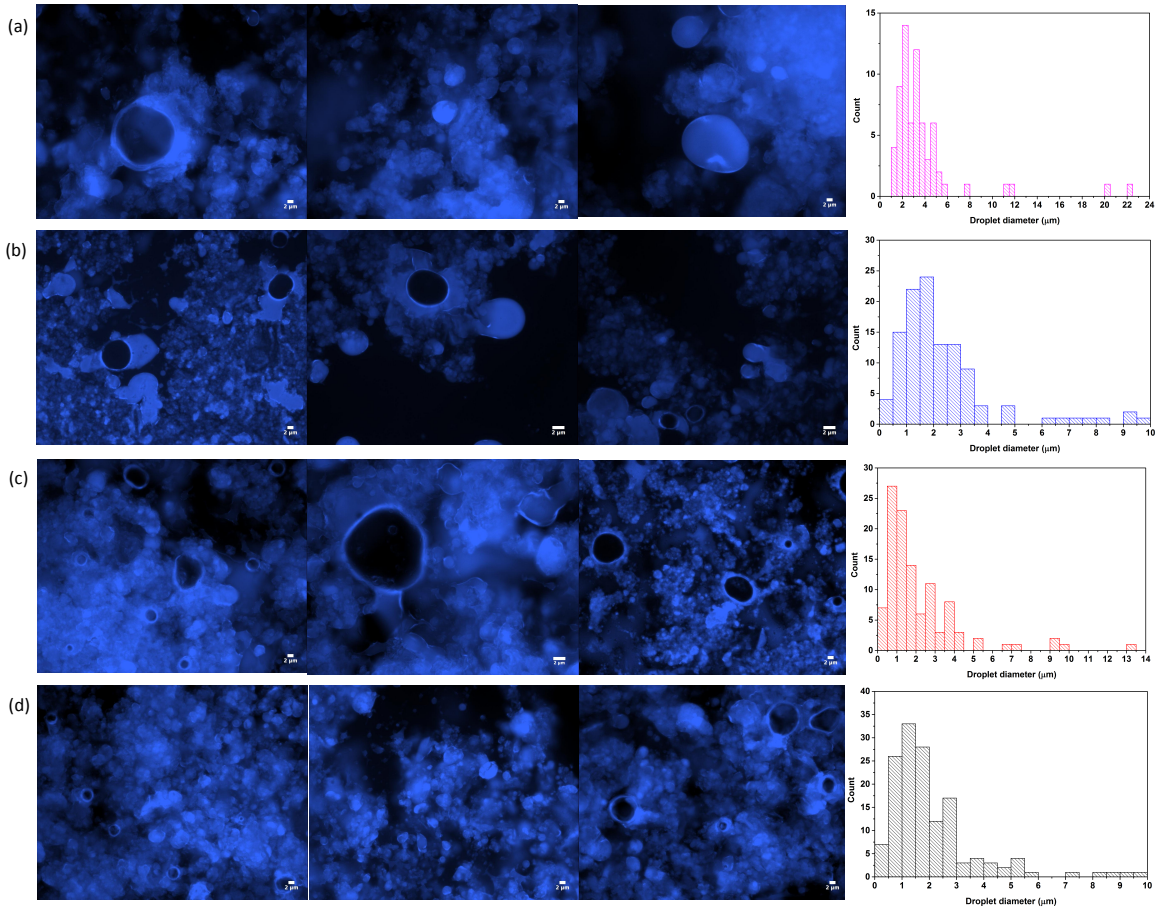

Figure 4.15. Fluorescence microscopy images obtained 1 week after preparation of the different 9:1 buffer:rapeseed oil samples, labelled by ThT, and droplet size distribution histogram with a bin width of 0.5 μm, based on the analysis of 3 different areas: (a) KY*p*F added 0.07 μM alkaline phosphatase; (b) 1.3 μM AP; (c) 3.3 μM AP and (d) 6.6 μM AP.

The droplet size average increases for all samples after 1 week (Table 4.2), although they retain a similar relative distribution. It is observed that coalescence is retarded when nanofibrous networks are formed, which occurs predominantly for the highest enzyme amount used (Figure 4.15d). The number of droplet counts is larger upon increasing the enzyme amount, which is observed from the fluorescence microscopy images and histograms (Figure 4.15) (note the difference in the y-axis scale).

Table 4.2. Droplet diameters observed for the different samples when using varying enzyme concentrations 24 h after preparation and 1 week after preparation

[AP] (μM)	Droplet diameter (μm)	
	24 h	**1 week**
0	No fluorescence	No fluorescence
0.07	2.3±2.0	3.9±3.6
1.3	2.1±1.5	2.3±1.9
3.3	1.4±0.8	2.2±2.1
6.6	0.9±0.6	2.1±1.7

4.3.3 Enzyme concentration effect over supramolecular interactions

4.3.3.1 FTIR spectroscopy

To investigate the formation of self-assembled structures in the biphasic mixtures, FTIR spectroscopy was performed on the different samples (Figure 4.16a) after 24 h from preparation. Since the spectra are similar to those of the aqueous samples (Figure 4.8a), we conclude that there is the formation of self-assembled nanofibrous networks is achieved through the same key interactions. This similarity in the FTIR spectra between aqueous and non-aqueous systems has been shown previously for the Fmoc-dipeptide system in Chapter 3.

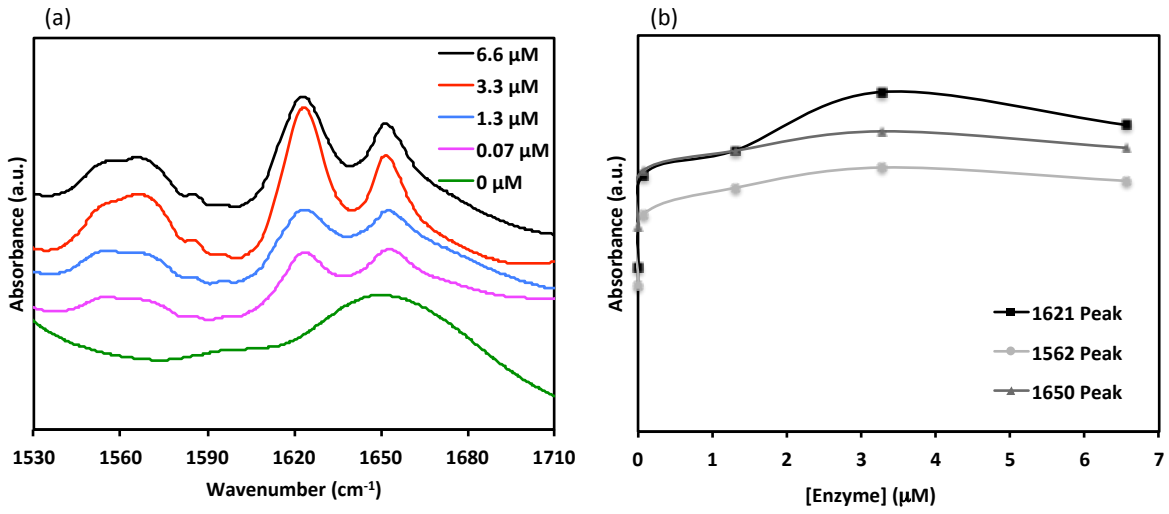

Figure 4.16. (a) FTIR spectra of the oil-in-water emulsions when different enzyme concentrations are used, measured 24 h after; (b) Absorbance maximum at specific wavenumbers from FTIR spectra *versus* alkaline phosphatase concentration used.

Comparing the FTIR spectrum for KY*p*F in aqueous solution (Figure 4.8a – green curve) and in biphasic mixture (Figure 4.16 – green curve) reveals the appearance of a peak at around 1650 cm^{-1} for the biphasic state. This could possibly be associated with the presence of rapeseed oil, which contains a carboxylic acid (see curve for the 100% rapeseed oil in Appendix 17). This could also explain the more similar relative intensity of the 1650 cm^{-1} and 1620 cm^{-1} peaks, in comparison to the aqueous samples (Figure 4.8).

Comparison of the spectra for the different emulsions reveals broader peaks for the samples where lower concentration of catalyst is added (and slower conversions occur), which indicates less well-ordered H-bonded networks. Once again, there is an exception for the 3.3 µM AP sample, which presents sharper peaks than the highest enzyme concentration (See detailed trend in Figure 4.16b). This again suggests the existence of an enzyme optimum concentration, in agreement with the previous results from FTIR (Figure 4.8b) and rheology (Figure 4.5) of the hydrogels. Not accounting for this exception, the emulsion stability increases when increasing the enzyme concentration added to the aqueous/organic mixture.

4.3.3.2 Molecular Dynamics simulations in biphasic system

In order to further investigate and compare the behaviour of both KY*p*F and KYF when in a biphasic system and assess their emulsifying ability, CG-MD simulations in a water/octane system (See Section 4.6.11.1 from Materials & Methods) were run. As visible from the snapshots in the beginning, mid-term and final stage of both the simulations (Figure 4.17), the organic solvent tends to aggregate as droplets, with both the tripeptides assembling at the interface between water and octane.

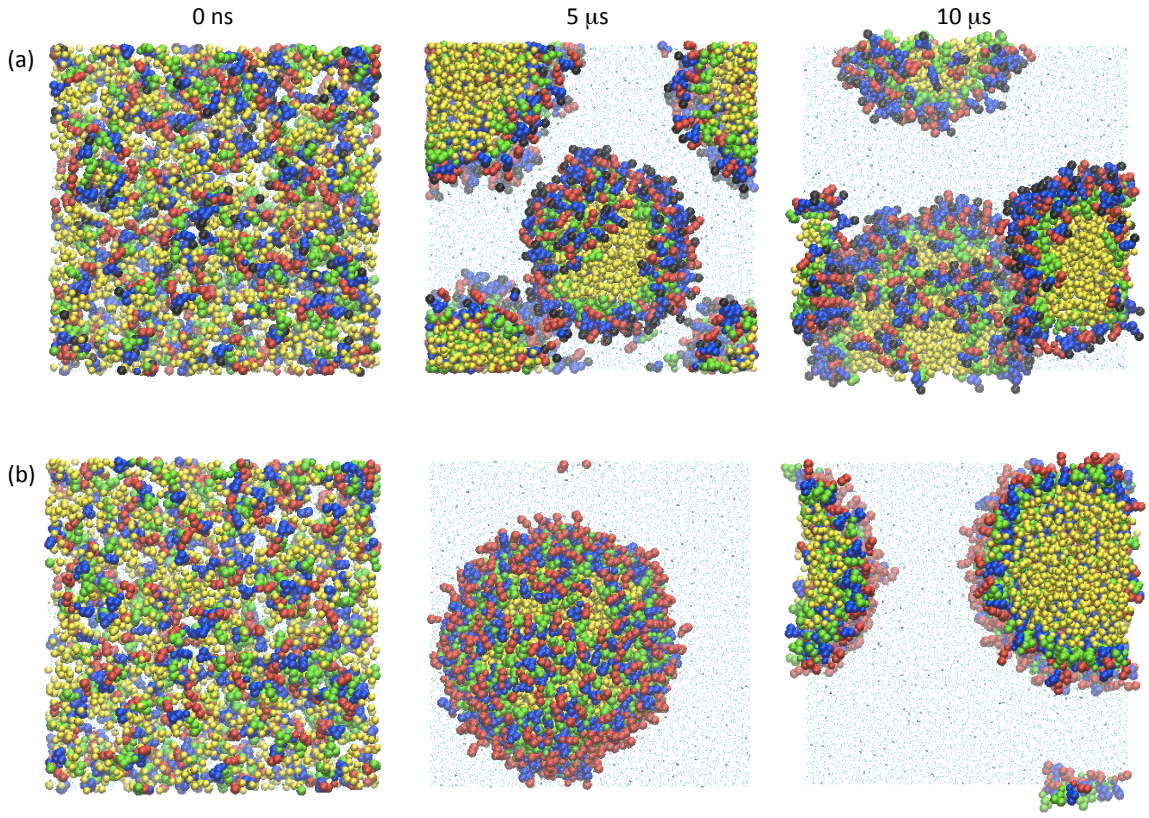

Figure 4.17. Snapshots of CG-MD simulations in a water/octane system for: (a) KY*p*F when using Q2a bead; (b) KYF. Color labelling used as in inset from Figure 4.10 plus the octane beads in yellow.

As expected, the phosphate groups of KY*p*F (black beads) tend to face the water phase, while hydrophobic phenylalanine residues (green beads) face the core of the droplets (Figure 4.17a). Even though micelles are not visible, the droplets tend to merge together

throughout the simulation time, in contrast with the KYF-stabilised emulsions (Figure 4.17b). Due to detail limitations when using a CG model, it is not clear if interfacial nanofibres are formed for the KYF system. Nevertheless, a more well-ordered amphiphilic structure is evident at the interface (Figure 4.17b). This proves that KY*p*F and KYF are both amphiphilic but assemble at the interface in a distinct manner. The KY*p*F follows a more traditional surfactant stabilisation, as observed previously for, *e.g.*, DFF.[182] Upon dephosphorylation, interfacial fibres are formed, which stabilises the emulsions for longer, as reported for non-enzymatically formed KYF.[182]

4.3.4 On-demand emulsion stabilisation

Having demonstrated that the kinetics of assembly can influence emulsion stabilisation in a tunable manner, we then investigate if enzymatic conversion provides temporal control - in that the emulsion can be formed when required after storage of the pre-emulsion solutions. The activation of the emulsifying ability by adding an enzyme at different time points was shown previously for an Fmoc-capped dipeptide at a 1:1 water:chloroform system in Chapter 3. In the current system, when alkaline phosphatase is added upon preparation of the emulsion and right before emulsifying it, the emulsion is still stable after 1 week (Figure 4.18b), as already mentioned. In turn, when alkaline phosphatase is added to the 1-week old totally de-emulsified KY*p*F biphasic mixture (using a 6.6 μM AP) (Figure 4.18a) and homogenised again (Figure 4.18c), a similar gel-like milky emulsion is produced.

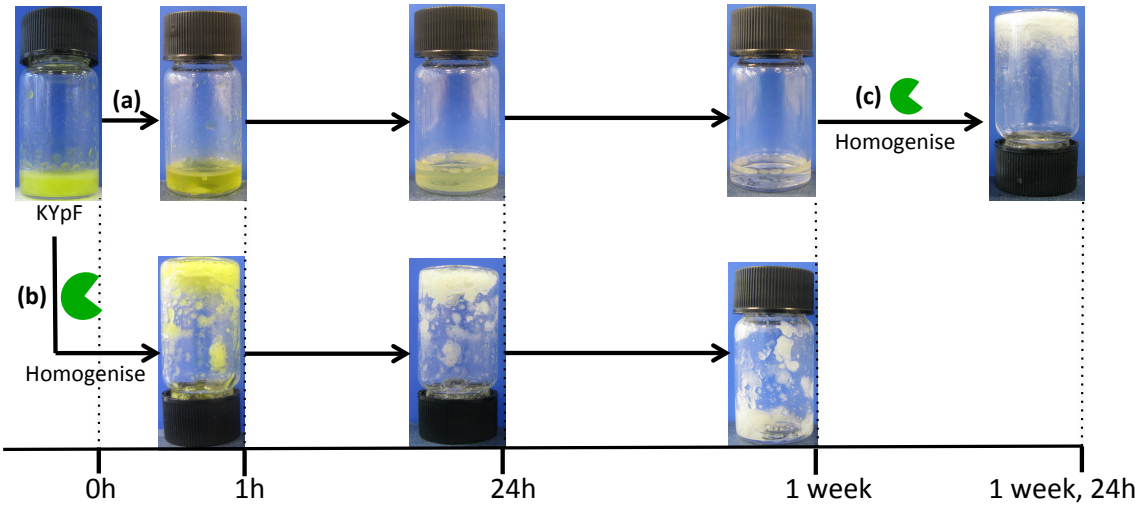

Figure 4.18. Optical photographs of glass vials showing the behaviour of the different tripeptides in a rapeseed oil/buffer biphasic system over time: (a) KY*p*F forms a temporary emulsion that de-emulsifies after 1 h; (b) KY*p*F is converted into KYF when alkaline phosphatase (green) is added at 6.6 µM to KY*p*F and homogenised, forming a more stable gel-type emulsion, still stable after 1 week; (c) KYF is formed when 6.6 µM AP is added to the completely de-emulsified KY*p*F after 1 week storage, forming a stable gel-like emulsion and proving on-demand emulsification.

When the alkaline phosphatase is added after 1 week, KY*p*F is dephosphorylated into KYF at the same conversion rate, as followed by reverse-phase HPLC (Figure 4.19). It is expected that all the enzyme concentrations would follow the same conversion rates as when added upon preparation and thus the proof-of-concept was carried out with just the highest phosphatase concentration.

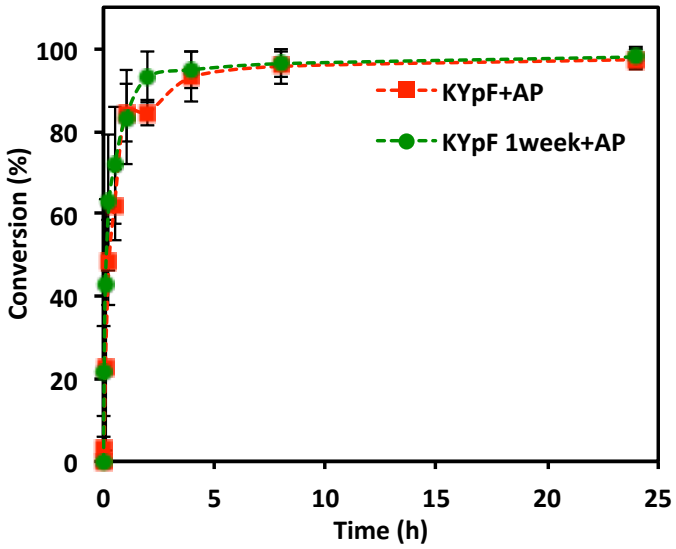

Figure 4.19. HPLC conversion from KY*p*F into KYF in buffer/rapeseed oil system when enzyme is added upon preparation and after 1 week storage.

The on-demand formation of nanofibrous-stabilising emulsions is also shown by microscopy. From the TEM images (Figure 4.20), nanofibrous networks are shown to be mainly in the aqueous surroundings of the droplets, stabilising the rapeseed oil-in-water emulsion.

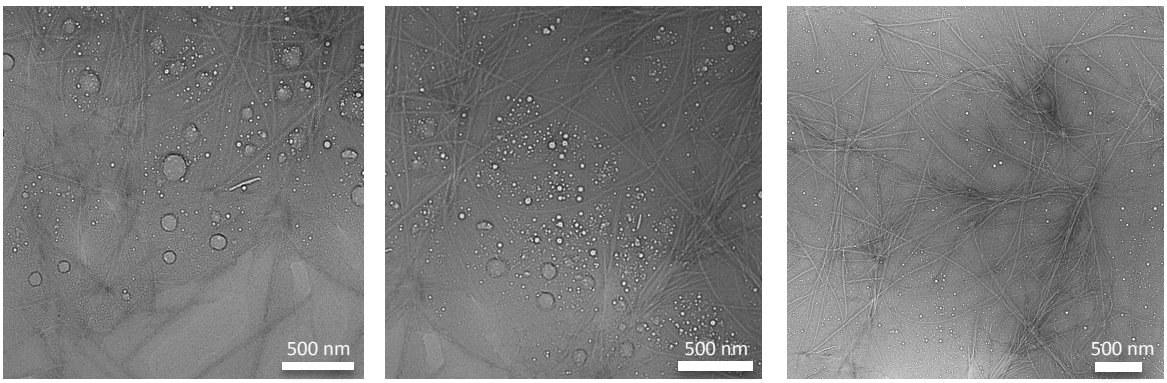

Figure 4.20. TEM images of the emulsion formed upon the addition of 6.6 μM AP to the 1 week-old KY*p*F two-phase system.

From fluorescence microscopy images (Figure 4.21), the presence of fluorescent probe ThT (used to label the tripeptide aqueous solution before the oil addition) is mainly evident at

the oil/water interface and less at the aqueous phase, which suggests there are nanofibrous networks stabilising the oil-in-water droplets as we reported previously.[79, 182, 284] This indicates that both routes play a role in the stabilisation of the emulsion upon delayed emulsification.

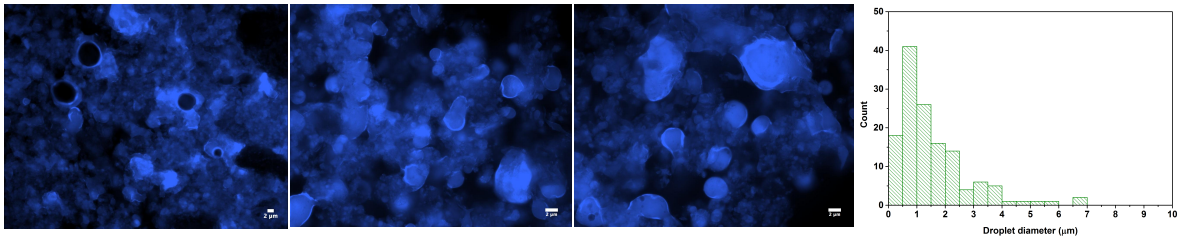

Figure 4.21. Fluorescence microscopy images, labelled by ThT, of the rapeseed oil-in-water droplets stabilised by KYF fibres when AP is added to KY*p*F in fully de-emulsified form after stored for one week; and droplet size distribution histogram with a bin width of 0.5 μm, based on the analysis of 3 different areas.

The droplet size distribution for the emulsion formed when 6.6 μM phosphatase is added to the de-emulsified KY*p*F mixture after 1 week of storage was also carried out (Figure 4.21). The average droplet diameter was of 1.6±1.3 μm for this sample, which is larger than when the same concentration of AP is added upon preparation (0.9±0.6 μm) (Table 4.2). However, it followed a normal distribution, comparable to when the enzyme was added immediately upon preparation (Figure 4.14e).

From FTIR spectra (Figure 4.22), the peaks in the amide I region for the KY*p*F biphasic system when adding alkaline phosphatase after one week of storage are the same as the ones for the sample where the enzyme is added upon preparation. These results corroborate the presence of nanofibrous networks, formed through H-bonded structures, even when the biocatalytic self-assembly and emulsion stabilisation is triggered after one week of storage.

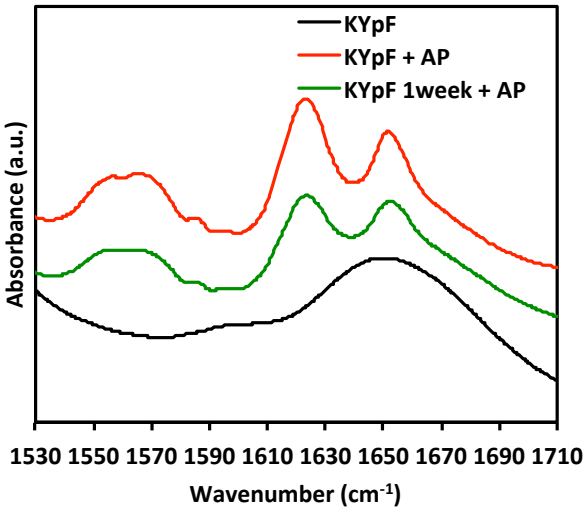

Figure 4.22. FTIR spectra of aqueous/organic systems of KY*p*F, when enzyme is added upon preparation and after 1 week storage.

4.4 Thermal unlocking of kinetic emulsions

The thermal stability of the emulsions was studied for the different samples in order to verify the impact of the kinetics of their formation on their stability. Upon heating, all samples were shown to coalesce and phase separate after being kept for 30 min at 50 °C (Table 4.3), which is observed by the appearance of a transparent liquid portion or disruption of the milky gel-like consistency. There is the notable exception of 6.6 μM AP, which de-emulsified only at 60 °C, implying increased stability of this emulsion. This suggests the possibility to tune the emulsion stability by varying the enzyme concentration used to enable emulsifying ability.

Table 4.3. Thermal stability study for the emulsions when various concentrations of alkaline phosphatase are used. Based on macroscopic analysis of the emulsion vials when left at increasing temperatures from 35 until 60 °C for 30 min

	[AP] (μM)			
Temperature (°C)	**0.07**	**1.3**	**3.3**	**6.6**
35		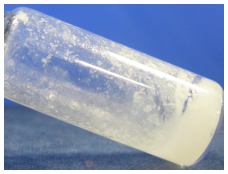		
40				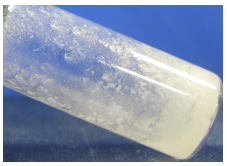
45				
50				
55		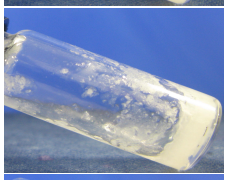		
60				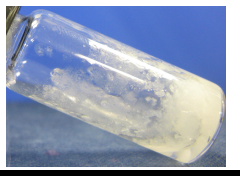

This shows the highest enzyme concentration produces the most stable emulsions, even though FTIR analysis of the 3.3 μM AP sample indicates that the latter presents the most well-ordered H-bonded networks (Figure 4.16). This can be explained by the more entangled nanofibrous networks at the aqueous medium for the highest enzyme concentration used (Figure 4.3 and Figure 4.13), which can delay droplet coalescence.[287-288]

The 3.3 and 6.6 μM enzyme concentration samples were then used for a more detailed study on the possibility of de-emulsification and subsequent re-emulsification by performing a heat/cool cycle. The biocatalytic self-assembly of fibres in the water/rapeseed oil system was followed by light microscopy (Figure 4.23).

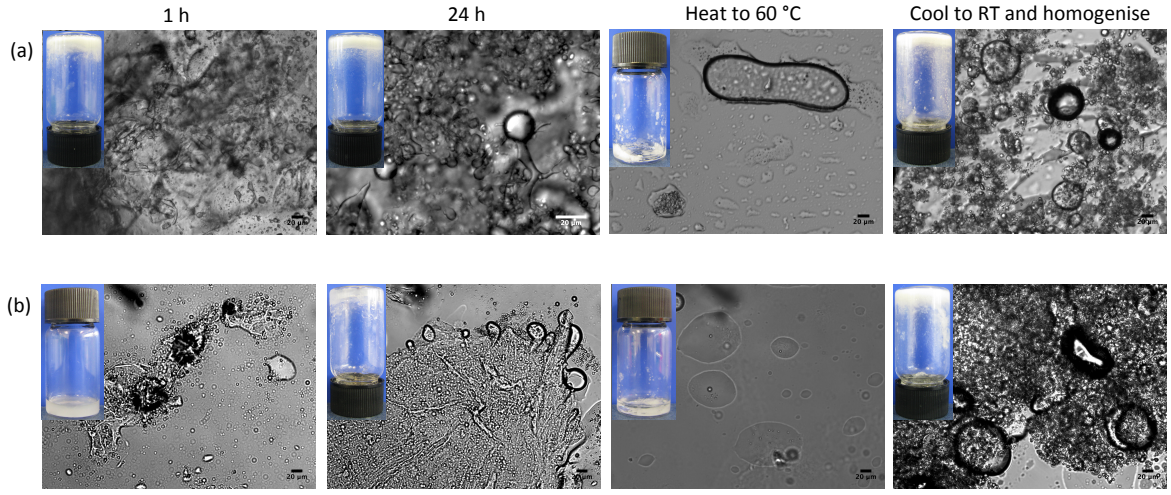

Figure 4.23. Photograph of the macroscopic aspect and light microscopy image of the two oil-in-water emulsions after 1 h, after 24 h, after increasing temperature to 60 °C for 1 hour and after cooling it down to room temperature (RT) overnight and homogenising again. These are presented for the emulsions formed when: (a) 6.6 μM alkaline phosphatase is added upon preparation; (b) 3.3 μM alkaline phosphatase is added upon preparation.

The KY*p*F + 6.6 μM AP sample shows fibre formation and gelation 1 h after phosphatase addition and fibres stabilising droplets 24 h after (Figure 4.23a), where kinetically trapped structures were possibly formed. In comparison, when 3.3 μM enzyme was added to the KY*p*F in a 9:1 aqueous buffer:rapeseed oil mixture upon preparation, there is no gel-like emulsion formed after 1 h as it takes longer to form (approximately 2 h), but it is visible after 24 h (Figure 4.23b). When these two stable emulsions were incubated at 60 °C for 1 h, they underwent total disruption of the fibres, which led to droplet coalescence and phase separation (Seen from the photographs of the macroscopic aspect, droplet deformation and size increase present in Figure 4.23a and b). However, after gradually cooling them down (overnight) to room temperature and then homogenising for 10 seconds again, stable gel-like emulsions were again formed for both enzyme concentrations used (Figure 4.23).

In order to assess the re-establishment of the H-bonded structures responsible for the fibre formation, FTIR spectroscopy was recorded for the emulsions where 6.6 and 3.3 μM AP was used at the key time points (Figure 4.24a and Figure 4.24b, respectively). The spectra show disorganisation of the H-bonded network when the emulsions were heated up for 1 h to 60 °C (red curves), mainly for the sample with 6.6 μM AP, for which all the peaks broadened, especially the one at 1550 cm^{-1}, which is characteristic of salt bridges. However, the peaks sharpen again after the system is cooled-down to room temperature and homogenised (grey curves), indicating formation of the nanofibres that are able to stabilise O/W emulsions again.

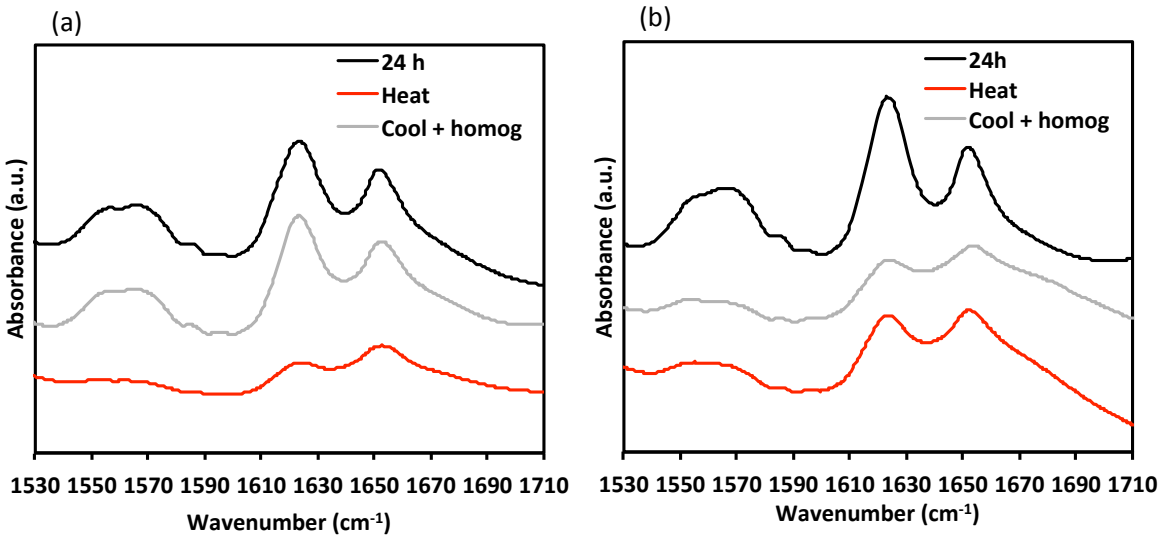

Figure 4.24. (a) FTIR spectra of the emulsion after 24h from the addition of 6.6 μM AP, after heated to 60 °C and after cooled down to room temperature and re-homogenised; (B) FTIR spectra of the emulsion after 24h from the addition of 3.3 μM AP, after heated to 60 °C and after cooled down to room temperature and re-homogenised.

In order to further understand the impact of the kinetic control over the structures formed and their effect on emulsion stability after heating and then cooling down the samples, the de-emulsifying temperature was checked again. Both emulsions were disrupted when heated to 40 °C (Figure 4.25a for the 6.6 μM and Figure 4.25b for the 3.3 μM AP samples), observed by the disruption of the gel-like emulsion and formation of two phases.

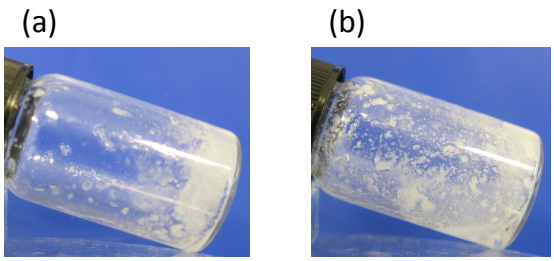

Figure 4.25. Photograph of the macroscopic aspect of the biphasic systems after being heated for 30 min at 40 °C, consequently to having been de-emulsified and re-homogenised again, showing the samples where 6.6 μM (a) and 3.3 μM AP (b) were used present the same de-emulsifying ability after the kinetically trapped structures are produced.

That is, the de-emulsifying temperature was found to be the same for both samples, independently of the original enzyme concentration used, after the initial heat/cool cycle. Since, before the heat/cool cycle, they presented different de-emulsifying temperatures (60 vs. 50 °C, respectively, as seen in Table 4.3), given that these equilibrate after the heat/cool cycle this indicates the rearrangement of the systems to a common state.

4.5 Conclusions

In summary, the biocatalytic self-assembly of phosphorylated tripeptide precursors in aqueous buffer into nanofibres was demonstrated, where the biocatalyst amount used is a critical parameter dictating the self-assembly process, which gives rise to the formation of pathway-dependent nanofibrous networks. When in biphasic mixtures, amphiphilic entangled nanofibrous networks are formed at the aqueous/organic interface and surrounding aqueous phase of the droplets, stabilising oil-in-water emulsions *via* interfacial tension decrease and also increased medium viscosity. The tuning of the enzyme concentration used to trigger the self-assembly process of fibres can also be carried out to control emulsion stability by increasing the nanofibrous entangled network that prevents droplet coalescence.

We showed that simple tripeptides can be used as responsive emulsifiers under physiological and unchanged environmental conditions since it is possible to stabilise emulsions on-demand by adding an enzyme. The tunability achieved by using the desired catalyst amount combined with the temporal stimulus given by the possibility of adding the enzymatic stimulus when desired without having to change the conditions is potentially attractive for different cosmetic or food applications.

4.6 Materials and Methods

4.6.1 Materials

All reagents were purchased at the highest purity available (≥ 98%) and used as supplied, unless stated otherwise. H-Lys-Tyr(PO_3H_2)-Phe-OH acetate salt (KY*p*F) (536.16 $g.mol^{-1}$) was purchased from Bachem at the highest > 97% purity available and used as supplied. Alkaline phosphatase from bovine, expressed in *Pichia pastoris* (5379 $U.mg^{-1}$ protein, 21 mg $protein.mL^{-1}$, 0.044 mL, apparent molar weight 160 kDa) was supplied by Sigma Aldrich. One enzyme unit corresponds to the quantity of alkaline phosphatase hydrolysing 1 μmol of 4-nitrophenyl phosphate (pNPP) per minute at pH 9.8 and 37 °C.

4.6.2 Preparation of aqueous and biphasic samples

40 mM KY*p*F was dissolved in 1 mL pH 8 0.1 M sodium phosphate buffer, a constant volume of 50 μL was added from different dilutions of alkaline phosphatase buffered solution to achieve a final AP concentration between 0 $U.mL^{-1}$ (for the precursor control) and 55.2 $U.mL^{-1}$ (see corresponding concentrations used in Table 4.4) and vortexed for 1 min. All samples were left for 24 h before characterisation was carried out except otherwise stated.

Table 4.4. Conversion between alkaline phosphatase concentrations used

	Dilution	U.mL^{-1}	mg.mL^{-1}	µM
Flask	Reference	1104.5	21	131.3
1	20x	55.2	1.1	6.6
2	40x	27.6	0.5	3.3
3	100x	11.0	0.2	1.3
4	2000x	0.6	0.01	0.07

For the biphasic systems, 100 µL rapeseed oil was added to 900 µL 40 mM KY*p*F in aqueous buffer. After the same volume of different enzyme dilutions was added to each sample, they were homogenised in a VWR VDI 12 S2 top-bench homogeniser at speed 6 for 10 seconds. All samples were left for 24 h before characterisation was carried out except otherwise stated. For the thermal unlocking of kinetic emulsions, emulsions were heated at the temperature specified in each case and let to cool down overnight at room temperature.

4.6.3 HPLC conversion

To monitor the dephosphorylation by alkaline phosphatase, aliquots of 25 µL were taken at different times after the addition of alkaline phosphatase (t = 0 h) and diluted in 500 µL of 50% acetonitrile solution containing 0.1% TFA. An aliquot of 50 µL from each diluted sample was injected on a Dionex P680 system with a Macherrey-Nagel 250 mm 4.6 mm C18 column for reverse-phase HPLC. The mobile phase comprised of water and acetonitrile at a flow rate of 1 mL.min^{-1}. The gradient was linear to 20% (v/v) acetonitrile in water at 4 minutes, gradually rising to 80% (v/v) acetonitrile in water at 35 minutes and decreasing it to 20% acetonitrile in water at 42 min. The area of the peptide peaks was

analysed using a UVD170U UV-Vis detector at a 265 nm wavelength to calculate the conversion and the average of triplicates is shown.

4.6.4 Transmission Electron Microscopy

For the aqueous samples, carbon-coated copper grids (300 mesh) were glow discharged in vacuum for 10–15 seconds, the support films were touched onto them, blotted with filter paper and settled for 30 seconds. 1% aqueous methylamine vanadate obtained from Nanovan, Nanoprobes was used as a negative stain, the samples dried for 10 minutes and imaged using a FEI TECNAI TEO microscope operating at 200 kV (Physics Department, University of Glasgow). For the biphasic systems, carbon-coated copper grids (400 mesh) were used and also glow discharged. Then each sample was dropped into the grid, blotted, dropped Nanovan and blotted till dry. They were then imaged using a FEI Titan Halo microscope at 300 kV (ASRC, City University of New York).

4.6.5 Rheology

Rheological properties of the different hydrogels were assessed using a Malvern Kinexus rheometer with temperature controlled at 20°C and a 20 mm parallel plate geometry with a gap of 0.9 mm. Before any measurement, amplitude sweeps were performed at constant frequency of 1 Hz from shear strain 0.01 – 100% to ensure work at the linear viscoelastic regime. Oscillatory rheology was performed 24 h after sample preparation by carefully loading the gels on to the rheometer with a spatula and no dilution. Triplicates were carried out for all the samples and the average data is shown.

4.6.6 Fluorescence Spectroscopy

Fluorescence emission spectra were recorded between 250 and 600 nm with an excitation wavelength of 274 nm (for tyrosine) at medium response, 3 nm bandwidth and 1 nm data pitch. Fluorescence emission spectra were measured on a Jasco FP-6500 spectrofluorometer with light measured orthogonally to the excitation light with a scanning speed of 500 $nm.min^{-1}$. The samples were immediately placed in a cuvette and measured,

with no dilution, at different times after the addition of alkaline phosphatase (which was set as t = 0 h).

4.6.7 FTIR Spectroscopy

FT-IR spectra were recorded on a Bruker Optics Vertex 70 spectrophotometer (Physics Department, University of Strathclyde). Measurements were performed in a standard IR cell holder (Harrick Scientific), in which the sample was placed between two CaF_2 windows separated by a 50 mm PTFE spacer. The spectra were acquired in the region 1530 and 1710 cm^{-1} over 25 scans at a resolution of 1 cm^{-1}. pH 8 0.1 M D_2O phosphate buffer was used to prepare the samples and the curves background corrected.

4.6.8 UV-Visible Spectroscopy

4.6.8.1 Enzymatic activity assay

For the enzymatic activity assay, 850 μL of buffer (or mixture of buffer and organic solvent according to each volume ratio), 100 μL of 100 mM pNPP phosphatase substrate and 50 μL of enzyme were placed into a cuvette, giving a final phosphatase concentration of 1.4 $U.mL^{-1}$. The dephosphorylation reaction was then monitored by UV-Vis by recording the absorbance at 405 nm every 1 min for 10 min, since p-nitrophenol is a chromogenic product that absorbs at 405 nm. Spectra were recorded between 250 and 400 nm on a Jasco UV-660 spectrophotometer and the average of triplicates by the subtraction of each corresponding blank shown.

4.6.9 Fluorescence Microscopy

The oil-in-water droplets were imaged on an Upright Epifluorescent Microscope (Nikon, Eclipse E600) (SIPBS, University of Strathclyde) after being transferred from the emulsion layer onto a glass slide, which was covered with a coverslip and mounted. 1 $mg.mL^{-1}$ Thioflavin T (ThT) in 0.1 M pH 8 phosphate buffer was used to prepare the samples, to label the aqueous phase in the emulsion layers and the self-assembled peptides. Images

were acquired using Zeiss 10x, 20x dry objectives and 40x, 60x, 100x oil objectives. An appropriate DAPI filter was used for the ThT labeled samples (365 nm excitation WL, 435-485 nm emission WL).

4.6.10 Light Microscopy

The emulsions were pipetted into a glass slide, covered with a coverslip and mounted in a fluorescence microscope (Eclipse LV 100 Nikon, Vienna, Austria) (TIC, University of Strathclyde) with an optical filter of 438/22 nm, a dichromatic mirror 458nm and a filter for detection of the fluorescence at 483/32nm. The images were recorded with a black and white Photometric Coolsnap HQ camera (Photometrics, Tucson, USA). 20x and 50x objectives were used.

4.6.11 CG-MD Simulations

4.6.11.1 Water and biphasic simulations

Molecular dynamics simulations were carried out in GROMACS 4.5.3[289] using MARTINI force field (version 2.2)[214]. The model used for KYF is identical to the KYF modelled previously,[182] while the phosphorylated KYF calculations involved the addition of a new bead to the Martini force field. The parameterisation of the mentioned phosphorylated tyrosine for KY*p*F is fully described below. A cubic box of 12.5 x 12.5 x 12.5 nm^3 containing 300 zwitterionic tripeptides, randomly placed, was created, neutralised and filled with standard CG water. This box was minimised for 5000 steps and equilibrated for 500 million steps of 20 fs timestep, giving 10 μs simulation time, which equates to an effective 40 μs of atomistic simulation time because of the smoothness of the CG potentials.[214] The Berendsen algorithms[290] were to keep temperature and pressure around 303 K and 1 bar, respectively. See examples of minimisation and equilibration input files in Appendix 18 and 19. For the biphasic simulations, the same procedure was followed with the addition of 1000 molecules of octane, to ensure a water density approximated to the experimental value. Visual Molecular Dynamics (VMD) program[266] was used to visualise the formed structures throughout the simulation time, using snapshots from this interface.

4.6.11.2 Parameterisation of phosphorylated tyrosine

Parameterising phosphorylated tyrosine (TYP) was carried out by initially adding a Qa bead (charged bead with H-acceptor capacity) to tyrosine (TYR), followed by an iterative process. A -2 charge was used for the initial Qa bead since the phosphate group is present in its HPO_4^{2-} form when at pH 8. To determine the bonded parameters to assign to it, atomistic simulations of one molecule of TYR and TYP were run in water for 20 ns and mapped into coarse-grained representation by defining the centre of mass of the atoms corresponding to each mapped coarse-grained bead, as represented in Figure 4.26.

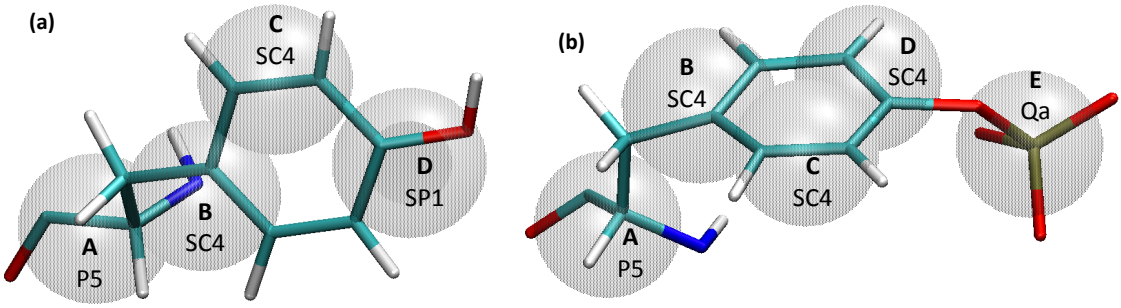

Figure 4.26. Schematic representation of atomistic to coarse-grained molecules of: (a) tyrosine, TYR; (b) phospho-tyrosine, TYP.

The distribution functions for bond lengths, bond angles and dihedral angles were calculated by using the scripts in Appendix 20, 21 and 22, respectively, for the phosphorylated tyrosine residue in KY*p*F (Figure 4.27a) and the standard tyrosine in KYF (Figure 4.27b). They were thus compared, since the bonded parameters for standard tyrosine were previously assigned by Marrink et al.[215] There were some differences, for instance the B-D bond length became smaller within phosphorylated tyrosine, when the centre of mass is moved due to the oxygen no longer being part of that bead. The mass of the bead is set to be the same as any other CG bead (72 amu), the backbone-side chain (and side chain-side chain) bonded parameters were kept from TYR parameters, such as *e.g.*, the constraints for the ring beads to ensure a perfect ring distribution. The bond length and angle including the E (Qa) bead were taken from the average between the two appearing peaks, following the methodology followed by the creators of Martini. These parameters

were added to the martinize.py script[215, 218, 291] (Appendix 23) to create a Gromacs topology file for phosphorylated tyrosine (TYP) (Appendix 24) as opposed to standard tyrosine (TYR) (Appendix 25).

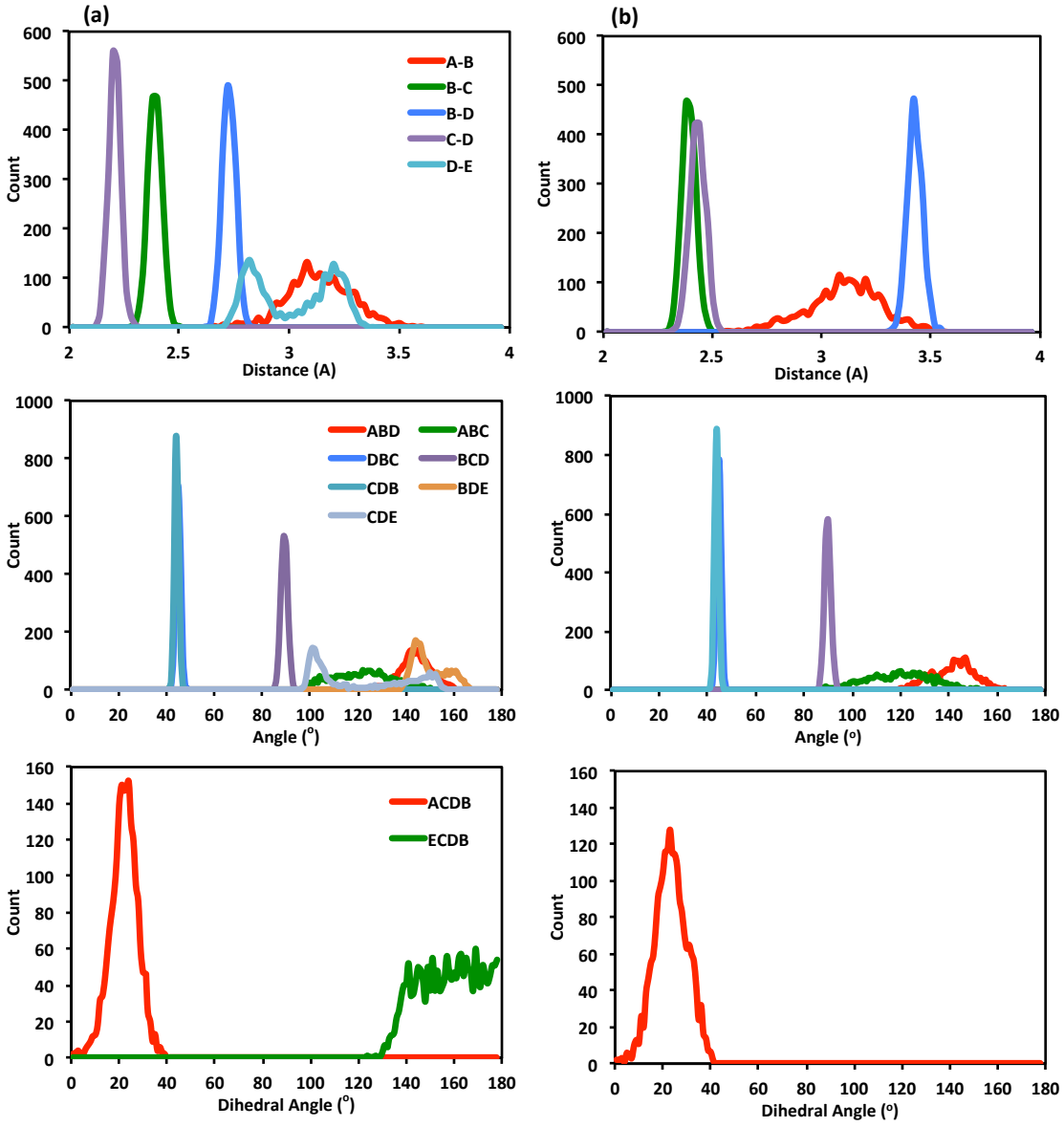

Figure 4.27. Distribution functions of bonds, angles and dihedral angles for: (a) TYP in KY*p*F; (b) TYR in KYF, based on atomistic simulations of one KY*p*F and one KYF molecule, respectively.

In order to initially validate this parameterisation, the partition coefficient between octanol and water was determined using a computational method, which can be compared to the experimentally determined value.

The partition coefficient K_{ow} is obtained by the Equation 4.1:

$$K_{ow} = \frac{[solute]_{octanol}}{[solute]_{water}} \quad \text{(Equation 4.1)}$$

The partition free energy ΔG_{ow} and the partition coefficient K_{ow} are related by the Equation 4.2:

$$\Delta G_{ow} = -2.303RT \log K_{ow} \quad \text{(Equation 4.2)}$$

where the log K_{ow} is calculated from the free energy of solvation between octanol and water at equilibrium, using the gas constant R=8.314 J.mol^{-1} and temperature T=293.15 K.

Each amino acid was placed, separately, in a water/octanol box of 15 x 5 x 5 nm^3, centred in the water phase and neutralised. It was minimised with the steepest descent technique for 5000 steps, gradually heated from 0 to 300 K for 60 ps under a NVT ensemble and equilibrated at 300 K and 1 bar for 60 ps under NPT conditions. It was then pulled through the longest x-axis (0.002 nm/ps pull rate) from water to octanol for 4.5 ns using umbrella sampling.[292-293] When the solute is pulled from the centre of the water on the right-hand side of the box (in red points) to the octanol on the left-hand side of the box (in cyan points), it reaches the point shown in Figure 4.28. The trajectory was saved every 30 ps and each frame was sampled and equilibrated under NPT ensemble for 150 ps and ran for 9 ns. The energies at each time point are then obtained by using a weighted histogram analysis method (WHAM) incorporated in Gromacs package.[265]

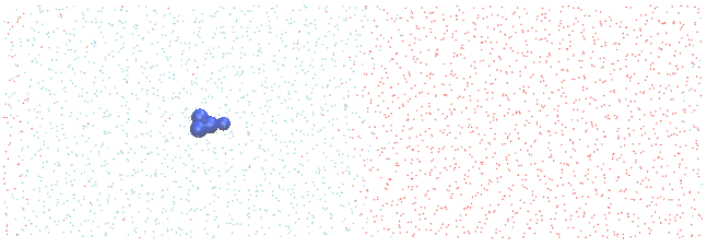

Figure 4.28. Snapshot of the final frame considered for umbrella sampling of Tyrosine, when it is already in the centre of the octanol phase.

When analysing the free energy graphs obtained when pulling the molecule from water to octanol (Figure 4.29), all molecules tested have shown to have relatively amphiphilic properties since they present lower free energies at the interface between water and oil. In particular, this amphiphilicity is observed for KYF and KY*p*F, which also present a hydrophilic (K) and hydrophobic bead (F) in addition to the tyrosine.

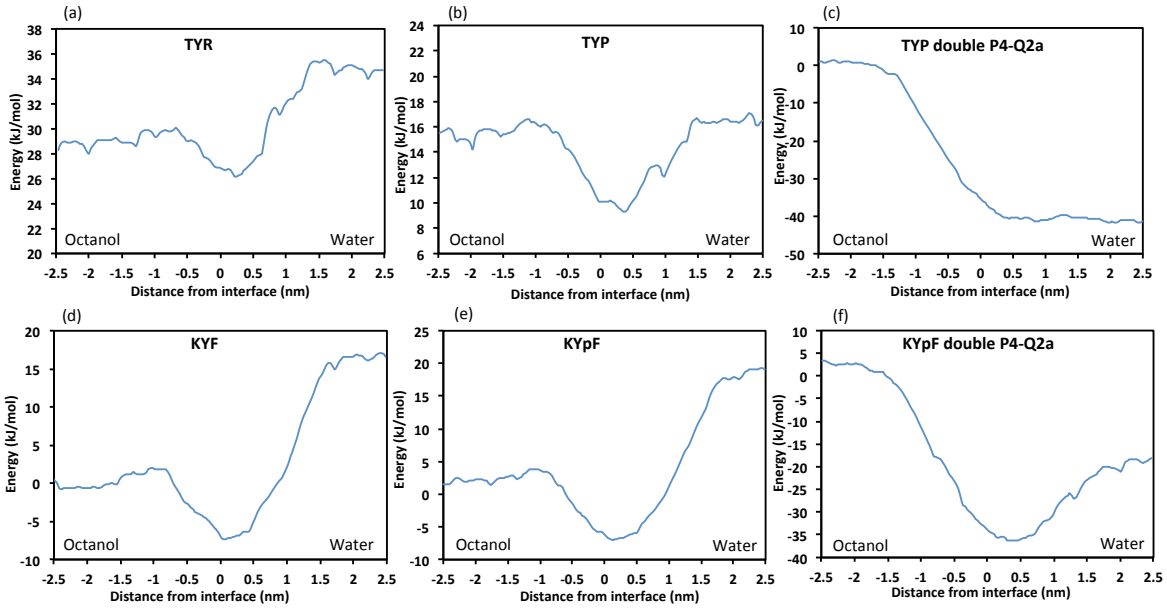

Figure 4.29. Free Energy landscapes when pulling each molecule from water to octanol phase using umbrella sampling: (a) Tyrosine; (b) Phosphorylated tyrosine; (c) Phosphorylated tyrosine using Q2a bead; (d) KYF; (e) KY*p*F using phosphorylated tyrosine; (f) KY*p*F using phosphorylates tyrosine with Q2a bead.

However, the validation needs first to be carried out for the simple phosphorylated tyrosine, in comparison to standard tyrosine, and thus the logP values are presented for the amino acids (Table 4.5).

Table 4.5. Free energy difference and calculated *versus* experimental logP values for each amino acid

	ΔG_{ow}	logP	
	(kJ/mol)	Calculated	Experimental
TYR	-5.6	1	2.3[294]
TYP	-0.50	0	-2.2 ± 0.6
TYP double P4-Q2a	41	-7	

Although phosphorylated tyrosine presents a lower tendency to move to the octanol when in comparison to tyrosine (Figure 4.29b compared to Figure 4.29a), hydrophilicity is not completely achieved since the reverse migration to octanol is still favorable. The developers of Martini warn of the possible need to increase the solvation free energy for Ca^{2+} ions to achieve a realistic description of these.[214] Since they also report on improved behaviour by increasing the hydration strength of phosphate moieties[214] and this is an iterative process, we increased the Lennard-Jones well-depth for water-phosphate interactions (P4-Q2a). To achieve this, we created a new bead, called Q2a, and increased by a factor of two the C_6 and C_{12} values for P4-Q2a present in martini_v2.2.itp file, when in comparison with P4-Qa, keeping the other interactions unchanged from Qa. Consequently, the migration from water to octanol was very unfavourable (Figure 4.29c), with a logP value of -7.3. Thus, while the standard tyrosine parameterisation underestimates the hydrophobicity of tyrosine (calculated logP = 1 vs. experimental logP = 2; Table 4.5), the hydrophilicity of the phosphorylated tyrosine is overestimated (calculated logP = -7 vs. experimental logP = -2; Table 4.5). While the difference between the calculated and experimental logP values (Table 4.6) is relatively large, we believe that it is acceptable

given the deviations seen across the parameterised amino acids within the Martini description (MUE(logP) = 1.5; MAXE(logP) = 4, MINE(logP) = -3).[215]

The shake-flask method was used to determine the partition coefficient experimentally.[295] The emission of phosphorylated tyrosine samples of known concentrations in water and octanol was measured using the same spectrofluorometer mentioned in Materials and Methods to obtain a calibration curve in each of the solvents (Figure 4.30). The same parameters were used, including the excitation wavelength for Tyrosine (274 nm). The shake-flask method was then used to determine the partition coefficient experimentally by adding 2 mL of octanol to samples of 2 mL of phospho-tyrosine (1 nM) in pH 8 0.1 M phosphate buffer and vigorously shaking them for 30 sec. After leaving the samples to stand for 4 h at room temperature, 1 mL of each phase was taken to a cuvette and the fluorescence spectroscopy emission measured. Averaged results of 7 different samples were taken to determine the partition coefficient and logP value (Table 4.6).

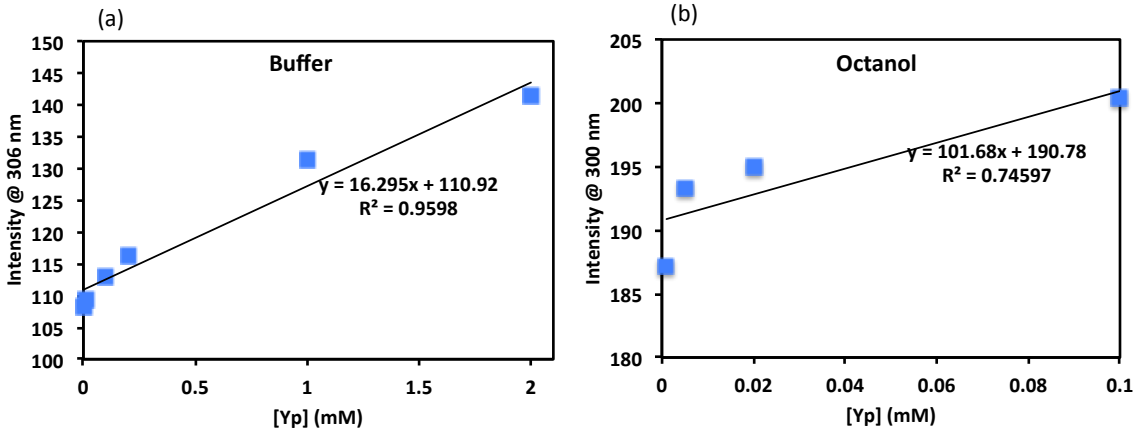

Figure 4.30. Calibration of the emission fluorescence intensity for phospho-tyrosine in different concentrations in (a) aqueous phosphate buffer and (b) 1-octanol.

Table 4.6. Experimental results for partition coefficient (K_{ow}) and logP determination of Y*p*

	K_{ow}	logP
1	0.029	-1.53
2	0.022	-1.67
3	0.009	-2.03

4	0.002	-2.76
5	0.003	-2.60
6	0.004	-2.37
7	0.007	-2.14
Average	0.011	-2.16
St Dev	0.010	0.454

At each stage, CG distributions are analysed and the bonded interactions corrected accordingly, in an ad-hoc manner. The last ECDB dihedral angle information, *e.g.*, was removed since the ACDB dihedral is enough to ensure planarity, having indeed reached more similar curves to the atomistic simulations on its absence. The modified LJ parameters were used for the KY*p*F simulations, where Q2a was used to represent the phosphate group. The distributions of the bonded interactions for these simulations when using 1 molecule of KY*p*F are presented in Figure 4.31a, where they can be compared to KYF (Figure 4.31b) or even to the information taken from atomistic simulations of one molecule (Figure 4.27).

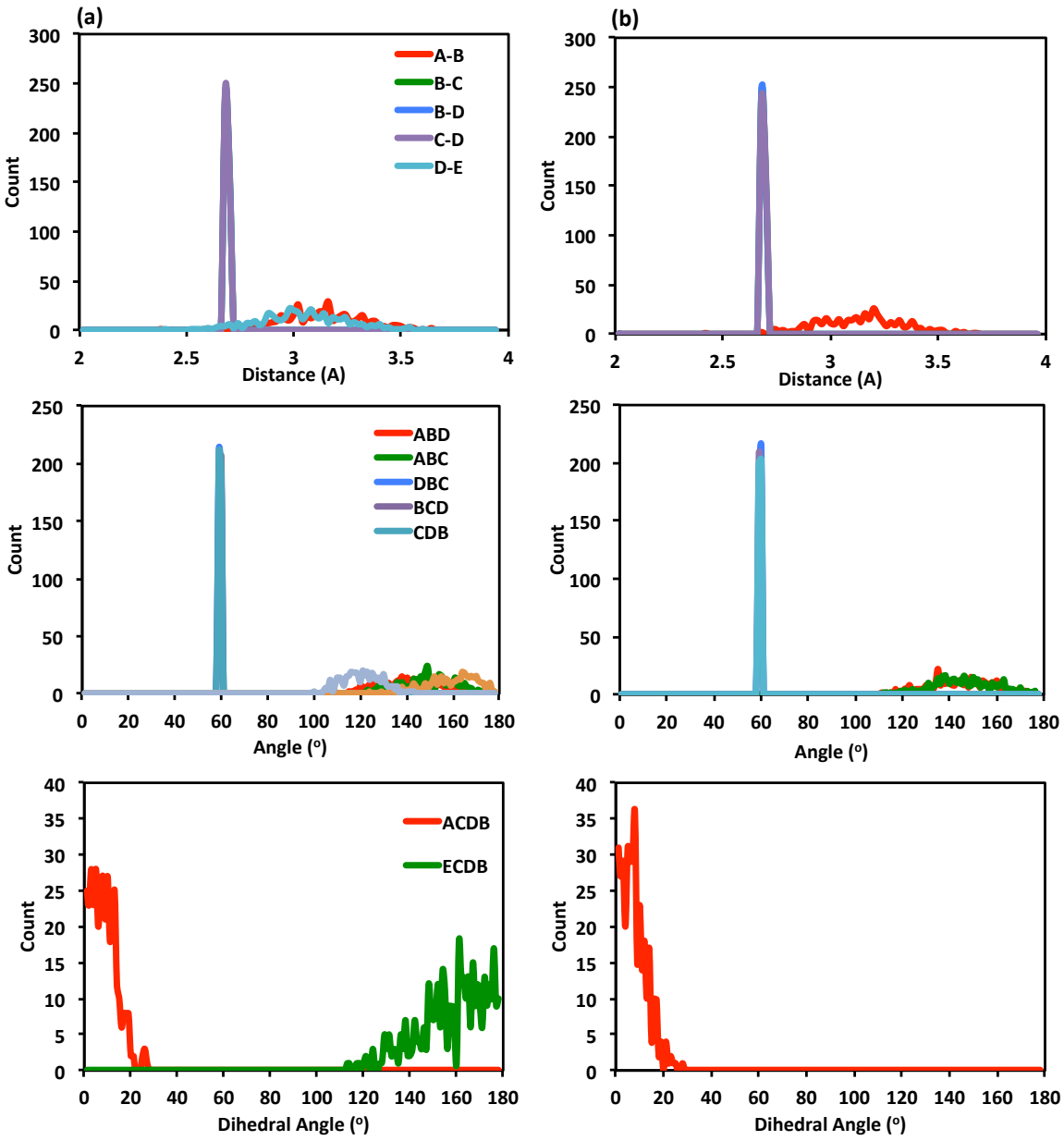

Figure 4.31. Distribution functions of bonds, angles and dihedral angles for: (a) TYP in KY*p*F; (b) TYR in KYF, based on coarse-grained simulations of one KY*p*F and one KYF molecule, respectively.

5 Computational prediction of DFF-dipeptide co-assembly

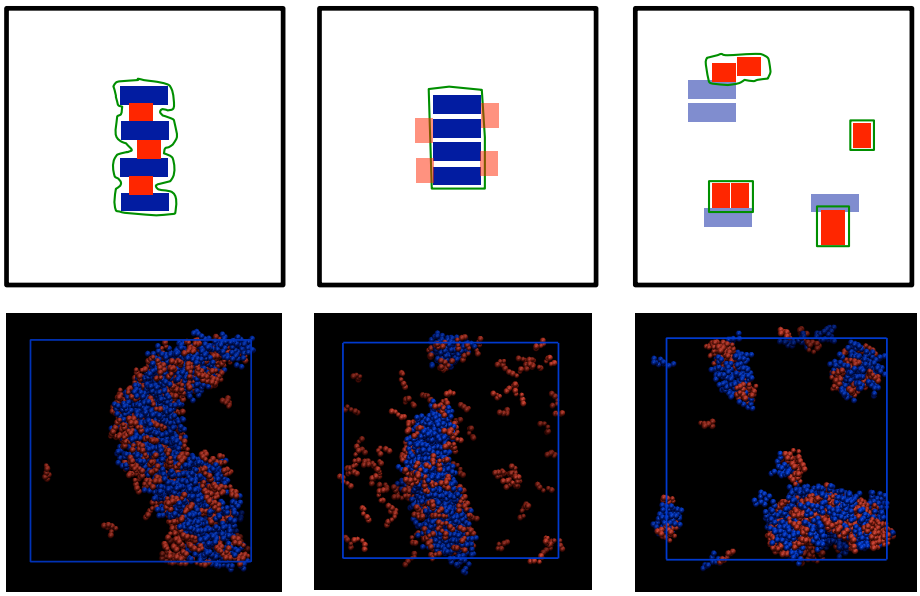

5.1 Introduction

Stimulus-responsive peptide self-assembly has been exploited throughout the last years due to the enhanced control achieved over nanostructure formation as a function of environmental conditions,[269] as mentioned in Chapter 2. A simpler, non-covalent trigger for the formation of supramolecular structures would offer further advantages by avoiding the need to chemically modify the peptides or change the environmental conditions.

Co-assembly of two or more different initial units is of great interest as to produce unique complex supramolecular structures, whose physical and mechanical properties can be modulated. Fmoc-peptide based gelators/surfactants have been shown to co-assemble into nanofibres, with varying functionality at the surface depending on the chemical nature of the building blocks.[106] The achievement of more complex structures and control of the physical properties have also been demonstrated through the co-assembly of diphenylalanine dipeptide nanotubes.[296] The self-assembly/co-assembly of different Fmoc-phenylalanine derivatives has been carefully studied and insight into the nature of the competing π-π interactions obtained.[297] In addition, co-assembly allows for an extra control over assembly: it has indeed been reported as a trigger, where gelation critically depends on the interconnection of two components (*e.g.*, oppositely charged amino acids Fmoc-E and K).[298]

Fleming *et al.* carried out a design study to elucidate different co-assembly models: orthogonal, cooperative and disruptive (Figure 5.1).[58] They hypothesised and showed that orthogonal co-assembly occurs when the hydrogelator and surfactant molecules establish their preferred interactions, however not compromising the preferred supramolecular structure of the gelator (Figure 5.1a).[58] This happens when the constituents are sufficiently different, avoiding for partial incorporation or disruption of the structures. On the other hand, cooperative co-assembly was observed when the building blocks cooperatively assemble into their shared preferred mode of self-assembly (Figure 5.1b). In that case study, it occurred when the molecules shared the preference to assemble into β-sheet H-bonded networks, reinforcing the final structure.[58] When the molecules only have the same aromatic moieties, intercalation of groups can occur that compromise the otherwise formed

β-sheet fibrous structure.[58] Fleming *et al*. name this disruptive co-assembly (Figure 5.1c) as it compromises the integrity of the desired supramolecular arrangements. However, we prefer to see this as a perturbed co-assembly, since the nanofibrous networks are changed but can lead to the formation of other equally interesting structures.

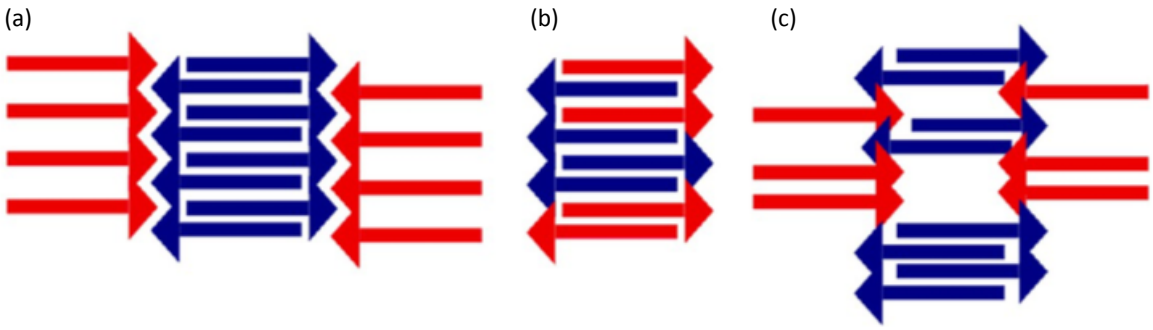

Figure 5.1. Schematic drawing showing the different types of co-assembly: (a) Orthogonal; (b) Cooperative; (c) Disruptive/Perturbed. Figure adapted with permission from Fleming, S. *et al.*, *Biomacromolecules* 2014, *15* (4), 1171-1184.[58] Copyright (2014) American Chemical Society.

A similar nomenclature was also used by Adams' group, who studied the combination of two varying low molecular weight (LMW) gelators and their mode of assembly to control the mechanical properties of gels.[299] They have shown that, apart from co-assembly, self-sorting can occur, by which there is independent assembly of each constituent into different fibre networks.[300-301] Orthogonal self-assembly (different from orthogonal co-assembly), which is the independent but simultaneous assembly of different supramolecular structures within the same system, has recently received increased attention. Different constituents, such as gelators and surfactants, are able to self-assemble independently into, *e.g.*, fibrillar networks with micelles, and coexist, each with their own characteristics.[154, 302] This approach has been utilised since such systems can potentially create novel and more complex architectures that neither system could achieve individually.[302]

To date, the discovery of co-assembled systems has either been through serendipity or on the basis of simple (*e.g.*, charge complementarity) rules. Computational screening methods can be helpful to provide insight into the design parameters of different materials.[84-85] An example class of LMW gelators and surfactants are unprotected tripeptides, which have

been predicted computationally[85] and shown to assemble in aqueous medium and stabilise oil-in-water emulsions through different mechanisms.

Tripeptides, such as H-aspartyl-phenylalanyl-phenylalanine-OH (DFF), have been shown to create bilayers in aqueous medium that form a weakly stabilising monolayer at the interface between water and oil. On the other hand, tripeptides, such as H-lysyl-tyrosyl-phenylalanine-OH (KYF), are able to self-assemble into fibres in water, that subsequently create strong interfacial networks capable of stabilising oil-in-water droplets for extended periods.[182] Tripeptide co-assembly can be attractive and, to our knowledge, no computational approaches exist to predict this.

In particular, the possibility to tune the assembly of a tripeptide (*e.g.*, DFF, Figure 5.2a – blue and white rectangle) into other specific structures through co-assembly with dipeptides (Figure 5.2a – red rectangle) would allow for time control while using a biocompatible LMW surfactant. A dipeptide would be the trigger to convert bilayer-type arrangements of DFF (Figure 5.2b) into nanofibres (Figure 5.2c) in an aqueous medium and possibly of monolayer-type adsorption at the water/oil interface into nanofibrous networks that create more stable emulsions.

The aim of this study is thus to investigate whether coarse-grained molecular dynamics screening methods can be used to evaluate the co-assembly of DFF and dipeptides to give desired structures. The objective is not to predict or select the best option for a specific application, but to explore the molecular search space from the 400 possible combinations of dipeptides with DFF, to determine the design rules for modulating the assembly of DFF. In this work, a screening of all possible dipeptides in combination with a tripeptide aqueous solution of DFF is carried out to assess the ability of nanofibre formation. The behaviour of these co-assembled systems is also analysed in a water/octane biphasic system to test if interfacial nanofibrous networks could give rise to more stable emulsions.

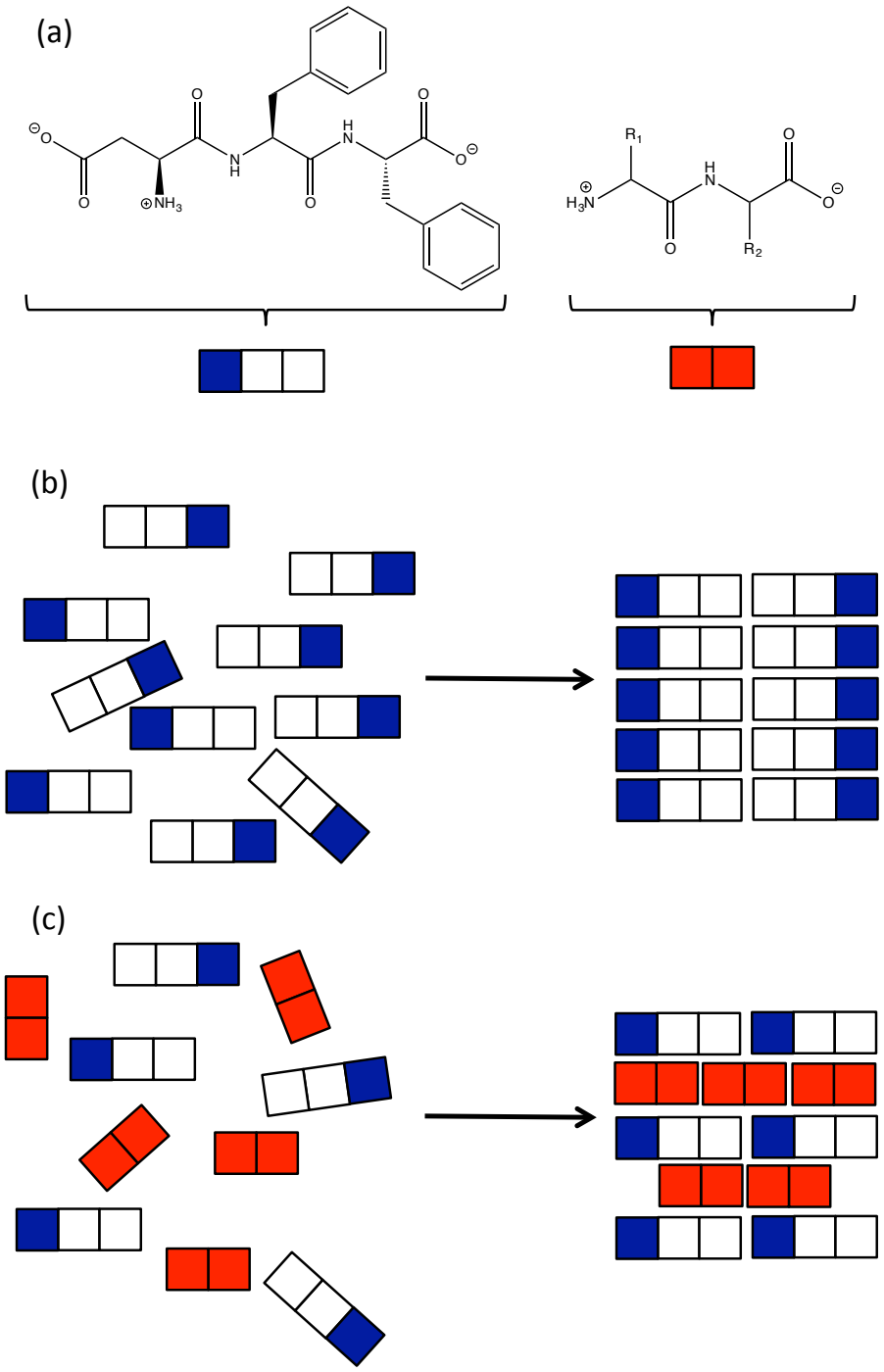

Figure 5.2. Schematic representation of: (a) Chemical structures of DFF and generic dipeptide and respective drawings using blue for Asp and white for Phe within the DFF rectangle and red rectangle for any dipeptide, independently of its sequence; (b) Assembly of DFF into bilayers in an aqueous system, with the Asp facing the water and Phe the interior; (c) Organisation of DFF/dipeptide into fibres in an aqueous system, when cooperative co-assembly of DFF with a specific dipeptide occurs.

5.2 Methods

A full screening of all the possible dipeptides in combination with DFF was carried out using GROMACS molecular dynamics package, version 4.5.3[289] and MARTINI force field (version 2.2).[214] Peptide structures were converted to the CG representation by using martinize.py script.[291]

To start with, 300 molecules of DFF (in its zwitterionic form) were randomly placed in a 12.5 x 12.5 x 12.5 nm^3 box with a minimum distance of 3 Å between them and the box was solvated with MARTINI CG standard water. The system was then neutralised, by adding 300 sodium ions to compensate for the negative aspartic acid charges, and energy minimised using the steepest descent integrator. Berendsen algorithms are used to keep temperature at 303 K and pressure at 1 bar.[290] All the simulations were equilibrated for 100 ns using a 25 fs time step, which equates to an effective 400 ns of atomistic simulation time because of the smoothness of the CG potentials.[214]

For the screening of all dipeptides with DFF in water, 150 molecules of each dipeptide (in their zwitterionic form) were added to the same size cubic box with 150 molecules of DFF, separately. The boxes were then solvated, neutralized (depending on the side chains of each dipeptide), minimised in the same way and also equilibrated for 100 ns.

For the screening of all dipeptides with DFF in biphasic systems, the same protocol as when it is in water was used but 1000 molecules of octane added before solvation in order to achieve a density of water approximate to the experimental value (999 $kg.m^{-3}$). Octane was used to represent a very apolar phase, in order to simulate a highly unfavourable water/oil mixture.

The conformations obtained for each of the simulated systems were analysed based on their aggregation propensity (AP). The calculation of the solvent-accessible surface area (SASA) in $Å^2$ after assembly and its comparison to the initial SASA is a way to quantify the level of aggregation of the different peptides.[84] The AP score is defined as the ratio between the SASA in the randomised initial state of the simulation and the SASA in the final configuration of the simulation, according to Equation 5.1:

$$\text{AP score} = \frac{\text{SASA}_{\text{initial}}}{\text{SASA}_{\text{final}}} \qquad \text{(Equation 5.1)}$$

The SASA values were calculated using the VMD scripting tools.[266] The typical rolling sphere radius of 1.4 Å was used, as it approximates the radius of a water molecule. The AP score is calculated for the whole system (AP_{total}), for only DFF molecules (AP_{DFF}), for only dipeptide molecules (AP_{dip}) or for octane (AP_{oct}). This is achieved by using a specific selection of atoms/beads for the SASA determination, as presented in Appendix 26.

The hydrophilicity-corrected AP_{total} score (AP_H) is used to generate design rules for hydrogelators as hydrophobic peptides can be insoluble and a positive bias is needed for hydrophilic peptides. This is done by introducing a measure of the hydrophilicity, by using the change in free energy when the dipeptide (the DFF is not taken into consideration as it remains for all the systems) is transferred from water to n-octanol $\Delta G_{w,o}$. This is obtained from Equation 5.2:

$$AP_H = (AP_{total})^{\alpha}.(\Delta G_{w,o})'_{dip} \qquad \text{(Equation 5.2)}$$

The $AP_{total,}$ score is calculated from Equation 5.1 accounting for all the atoms in the system except solvent and ions. When $AP_H{}'$ is calculated, AP_{total} is normalised between 0 and 1 by following Equation 5.3:

$$AP_{total}{}' = \frac{AP_{total} - (AP_{total})_{min}}{(AP_{total})_{max} - (AP_{total})_{min}} \qquad \text{(Equation 5.3)}$$

In turn, α is a coefficient that can be varied according to the desired weight of the normalised AP score to the AP_H score, where α = 2 is used in this case to obtain a good compromise between the hydrophilicity of each dipeptide and the AP score. The normalised $(\Delta G_{w,o})_{dip}$ value is obtained by Equation 5.4:

$$(\Delta G_{w,o})'_{dip} = \frac{(\Delta G_{w,o})_{dip} - (\Delta G_{w,o})_{min}}{(\Delta G_{w,o})_{max} - (\Delta G_{w,o})_{min}} \qquad \text{(Equation 5.4)}$$

where $(\Delta G_{w,o})_{dip}$ is calculated by the sum of the free energies of transfer of the two constituent amino acids from water to n-octanol (kcal.mol^{-1}). The $\Delta G_{w,o}$ values used were

those reported by Wimley and White.[303] The values for the charged side chain amino acids as used in this work are taken, except for histidine, where the value corresponding to the neutral amino acid was used. $\left(\Delta G_{w,o}\right)_{min}$ represents the most hydrophobic dipeptide (-2.09 x 2 = -4.18 for WW) and $\left(\Delta G_{w,o}\right)_{max}$ the most hydrophilic dipeptide (3.64 x 2 = 7.28 for DD), normalising each dipeptide in a 0-1 scale.

5.3 Design of co-assembled DFF with dipeptides in aqueous systems

5.3.1 DFF self-assembly in aqueous systems

DFF has previously been shown to form bilayers in aqueous medium after 9.6 μs of a CG-MD simulation.[182] In this work, DFF started to self-assemble into bilayer-type structures in aqueous medium by the end of the 100 ns simulation (Figure 5.3b). Even though equilibrated structures are clearly not reached after 100 ns, this simulation time was shown to be enough for an initial screening and for calculating and extracting conclusions regarding the aggregation propensity.[84]

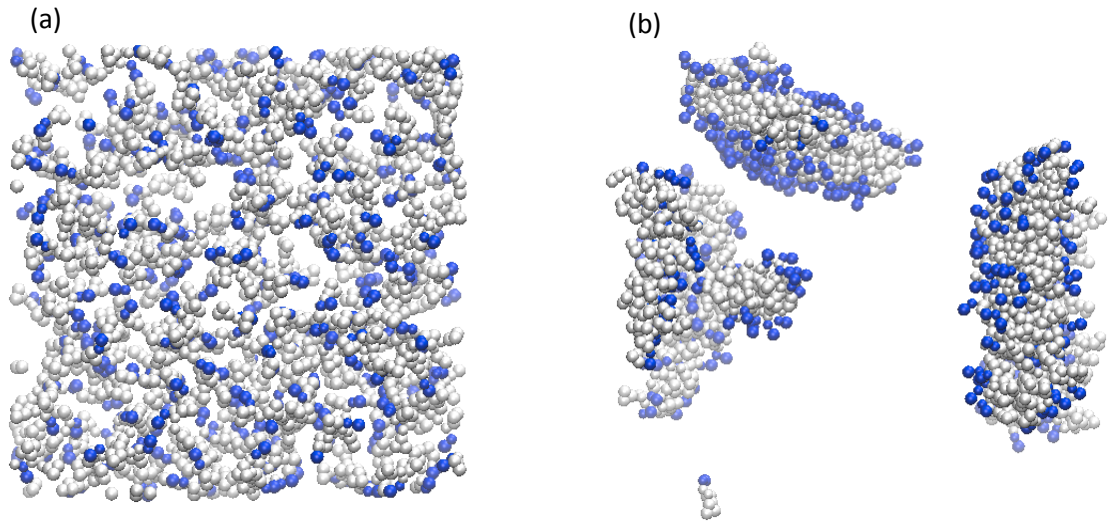

Figure 5.3. Snapshots of the DFF control system in the beginning (a) and end of the simulation (100 ns) (b) in a water box. Phenylalanine is represented in white and aspartic acid in blue VDW particles. Water beads are omitted for clarity.

The AP score for DFF alone in aqueous medium was found to be 2.25, which is explained by the decrease of the solvent-accessible surface area throughout the course of the simulation. This suggests that there is aggregation of the molecules, when comparing the initial random state and the final moment, and is in line with the previous findings.

5.3.2 Screening of co-assembled dipeptides and DFF in water

The 400 dipeptides based on the 20 canonical amino acids, when combined with DFF in a water box in a 1:1 ratio, show different behaviours over the CG-MD simulation, which is reflected in the analysed total aggregation propensity score (AP_{total}) (Figure 5.4a).

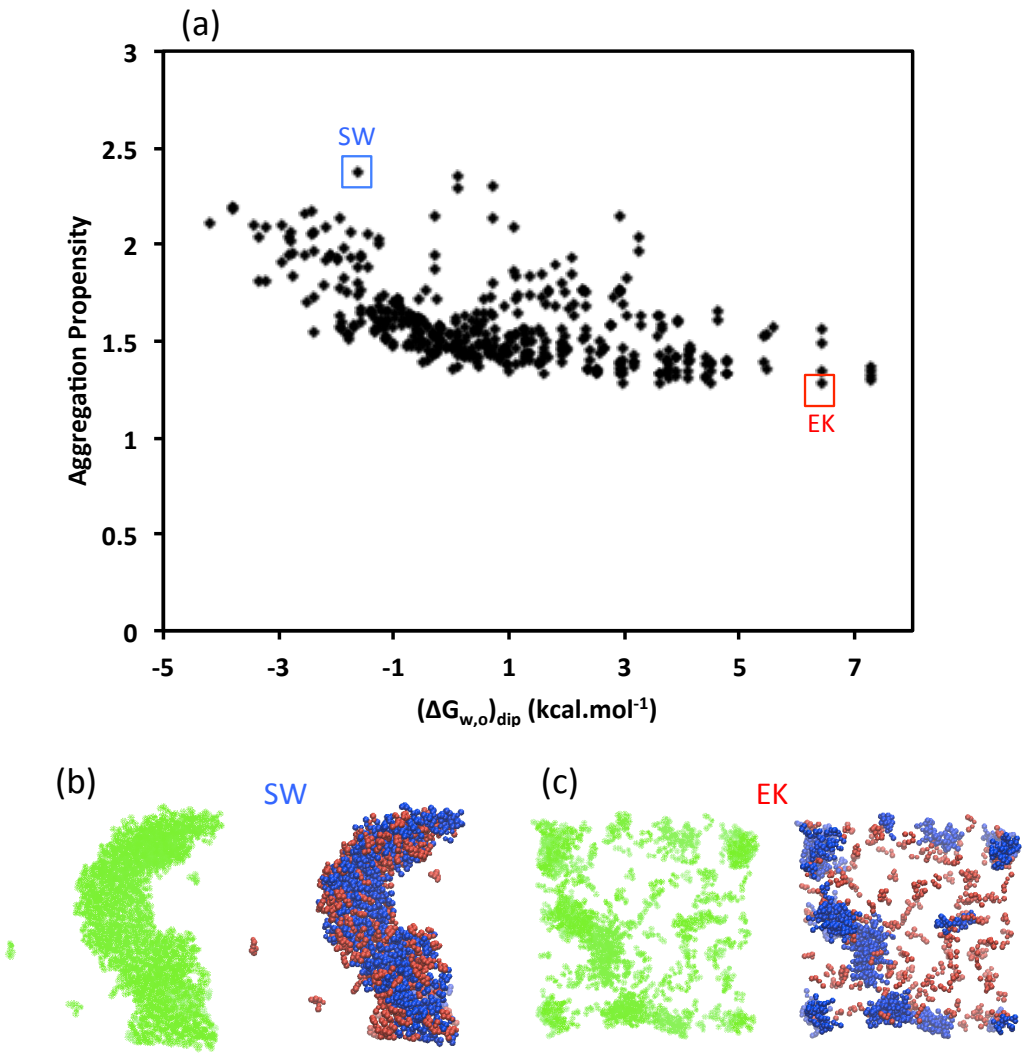

Figure 5.4. (a) Total aggregation propensities of the different DFF/dipeptide systems in a water box, plotted as a function of the dipeptide hydrophilicity ($\Delta G_{w,o}$). Highlight for the highest and lowest values achieved; (b) Final (100 ns) snapshots for the highest DFF/SW system: the green dotted region represents the final total solvent-accessible surface area, while the blue beads represent the DFF molecules and the red beads the SW; (c) Final (100 ns) snapshots for the lowest DFF/EK: the green dotted region represents the final total solvent-accessible surface area, while the blue beads represent the DFF molecules and the red beads the EK.

The AP_{total} values are plotted against the dipeptides' hydrophilicity (see details in Methods) and range from 2.4 to 1.3 (for SW and EK, respectively, as highlighted in Figure 5.4a – see full table of results in Appendix 27). The highest AP score is observed for DFF/SW, for which a fibre structure is formed, where the final surface area is small (Figure 5.4b) in comparison to the initial state and thus gives a higher aggregation score. The lowest AP

score is achieved for the non-assembling DFF/EK, where the SASA is large (Figure 5.4c). The highest total aggregation propensity values are reached by the most hydrophobic dipeptides, that more favourably get transferred from water to n-octanol phase ($\Delta G_{w,o} < 0$). In addition to the AP_{total}, the AP_{DFF} and AP_{dip} scores are also analysed, when accounting only for DFF or dipeptide molecules, respectively. These present different ranges of values and different tendencies as a function of the dipeptide hydrophilicity (Figure 5.5a). The dipeptide that reached the highest AP_{total} when combined with DFF was SW (represented in green), while SK reached the maximum AP_{DFF} (cyan marks) and FF the maximum AP_{dip} score (orange).

The positioning of these systems within all the AP_{total}, AP_{DFF} and AP_{dip} range is presented in Figure 5.5a, allowing for the detailed analysis of each system. A schematic drawing of the different co-assembly behaviours believed to occur for the systems reaching the maximum AP scores is also presented in Figure 5.5. The final snapshots (after 100 ns) of the simulations that achieved the highest and lowest AP scores, accounting for the total system (AP_{total}), for only DFF molecules (AP_{DFF}) or for only the dipeptides (AP_{dip}) are presented in Figure 5.6. In fact, the maximum and minimum of the different AP scores result in very different combinations of dipeptide and DFF as the scores vary according to what they account for.

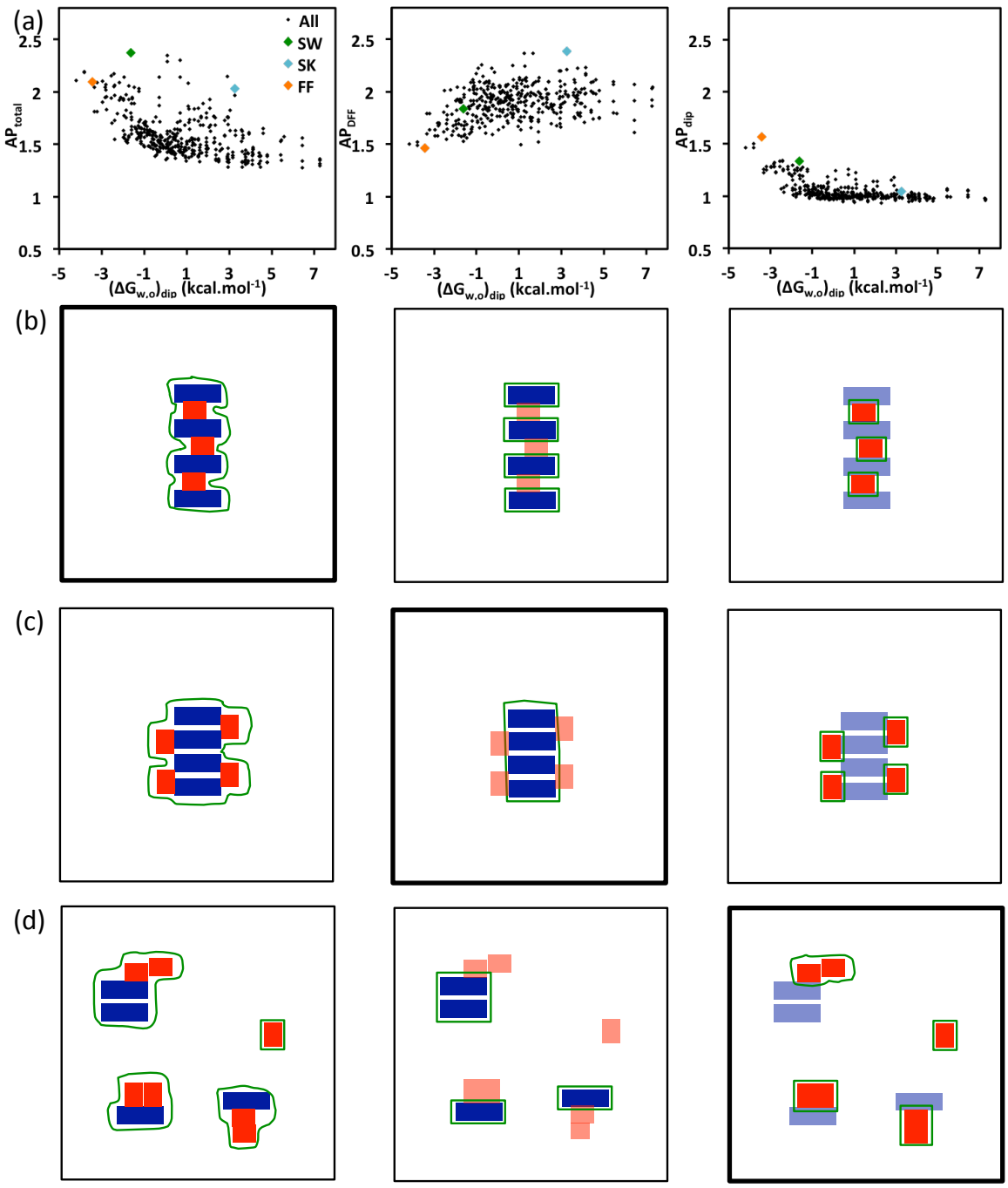

Figure 5.5. (a) Positioning of the DFF in combination with SW, SK and FF amongst the whole range of AP_{total}, AP_{DFF} and AP_{dip} for all the systems, plotted as a function of the dipeptide hydrophilicity ($\Delta G_{w,o}$); (b) Schematic representation of the cooperative co-assembly, where dipeptides cooperate with the DFF to form fibres (representing *e.g.*, DFF/SW); (c) Schematic representation of the orthogonal co-assembly, where dipeptides coat the DFF fibres (representing *e.g.*, DFF/SK); (d) Schematic representation of the perturbing co-assembly, where dipeptides tend to aggregate between themselves independently from the DFF (representing *e.g.*, DFF/FF). DFF is represented in blue (including Asp and Phe) and dipeptides in red, while water beads

are omitted for clarity. The green line represents the solvent accessible surface area in each case and the highlighted squares represent the maximum of each of the scoring systems (AP_{total}, AP_{DFF} or AP_{dip}).

For Figure 5.5b, the type of aggregation as observed for DFF/SW (maximum AP_{total}) is represented. The AP_{total} scores are high due to the decreased solvent accessible area of the whole system when DFF and dipeptides interact together to form a fibre (Figure 5.6). However, the AP_{DFF} and AP_{dip} scores are independently not as high due to the intercalated nature of the DFF tripeptide and the dipeptide, *e.g.,* SW. We see this type of assembly as property strengthening, related back to the previously stated nomenclature as cooperative co-assembly (Figure 5.1b).

The highest AP_{DFF} is achieved for SK (AP = 2.38, Appendix 27), higher than AP_{DFF} for DFF on its own (Figure 5.3b). This suggests the formation of a bilayer-type structure (observed from the final snapshot in Figure 5.6), with the aspartic acids from the DFF (in blue) facing the outside to interact with some SK dipeptides. As represented in Figure 5.5c, the dipeptides coat the fibre/bilayer in arrangements such as the one observed for SK, which increases the whole surface accessible area and thus do not present the highest AP_{total} scores. Since there are two independent modes of assembly, this is considered to follow orthogonal assembly (Figure 5.1a).

In turn, dipeptides that have high AP_{dip} scores such as diphenylalanine (FF) self-assemble independently (*perturbing self-assembly*), as shown before for dipeptides only in aqueous medium.[84] FF also interacts with the phenylalanines from DFF but does not improve the independent assembly of DFF (Figure 5.5d), actually accounting for one of the lowest AP_{DFF} scores (AP_{DFF} = 1.47, Appendix 27), showing it can be prejudicial to the tripeptide structure (*i.e.*, perturbing co-assembly).

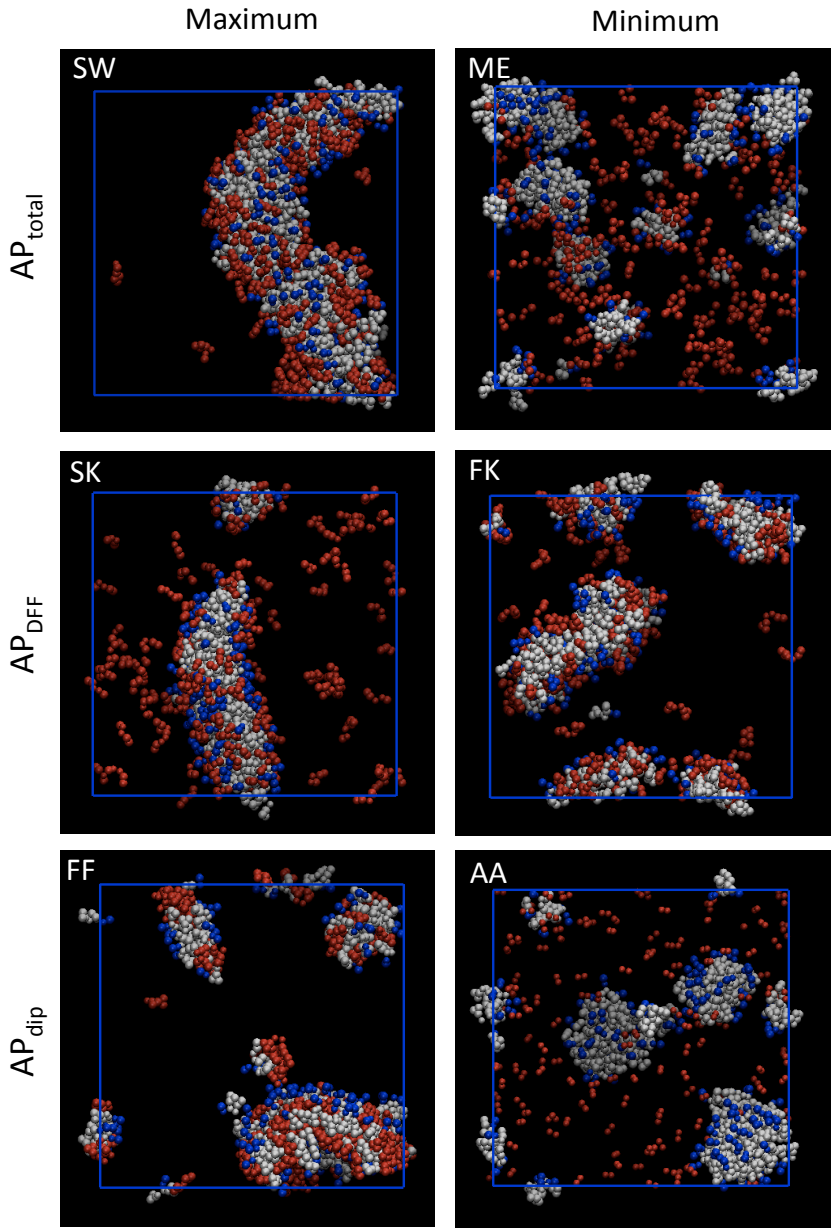

Figure 5.6. Final snapshots (100 ns) of different dipeptides in combination with DFF. These 6 are presented since they reached the maximum and minimum AP scores, as labelled. Phenylalanine from DFF is represented in white and aspartic acid from DFF in blue VDW particles, all dipeptides are represented in red, while water beads are omitted for clarity.

The lowest AP_{total} score, achieved by ME (Figure 5.6), suggests a totally non-interacting structure, as both DFF and ME are more attracted to water than to interact between them. The presence of the ME makes DFF behave in a different way (AP_{DFF} = 1.66, Appendix

27), when in comparison to DFF on its own (AP_{DFF} = 2.25), which is probably due to the negative charge of glutamic acid, creating repulsion between D and E. This is thus seen as perturbing co-assembly (Figure 5.1d).

As observed from Table 5.1 for the top 10 AP_{total} but also from Appendix 27, almost all dipeptides have an effect over the individual DFF assembly, since the AP_{DFF} is decreased when compared to the DFF alone in water (AP = 2.25).

Table 5.1. List of the top 10 dipeptides as ranked by AP_{total} score, also presenting their AP_{DFF} and AP_{dip} scores, together with the observed structure from the simulation final snapshot

No.	dip	AP_{total}	AP_{DFF}	AP_{dip}	Observed structure	Final snapshot
1	SW	2.37	1.84	1.34	Interconnecting fibres	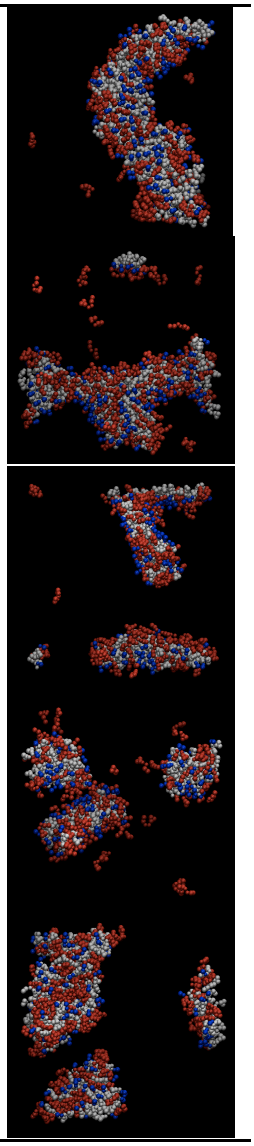
2	RF	2.35	1.82	1.25	Interconnecting branched fibres	
3	KW	2.30	1.76	1.25	Interconnecting branched fibres	
4	FR	2.29	1.83	1.16	Aggregates	
5	FW	2.19	1.49	1.47	Aggregates	

6	WF	2.18	1.52	1.50	Aggregates	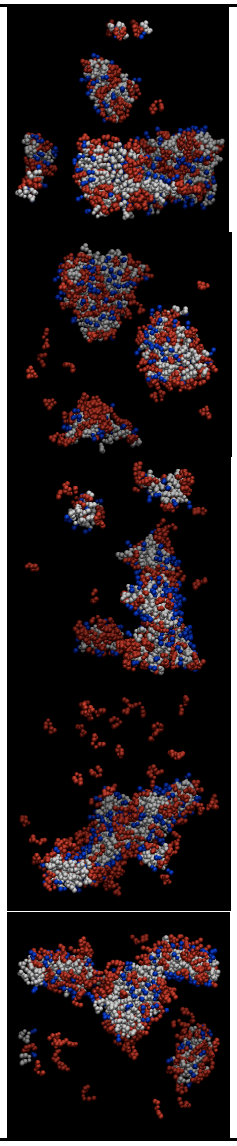
7	YF	2.17	1.70	1.34	Aggregates	
8	VW	2.15	1.80	1.33	Coating fibre-type	
9	KH	2.15	2.20	1.18	Coating fibre-type	
10	RW	2.14	1.78	1.19	Coating fibre-type	

As observed from Table 5.1, dipeptides that present the highest AP_{total} scores have at least one aromatic amino acid. This presents no surprise as the hydrophobic effect is known to dominate self-assembly in water, while hydrophilic dipeptides show a low tendency to aggregate with DFF (such as DE, with one of the lowest AP_{total} values and highest $\Delta G_{w,o}$). In turn, a wide range of AP scores is noticed for dipeptides with intermediate hydrophilicity values. This happens even for dipeptides with similar H values, such as for the previously presented ME (AP_{total} = 1.28) and KH (AP_{total} = 2.15), with a $\Delta G_{w,o}$ value of around 3.15 kcal.mol^{-1} each. This shows that MD simulations need to be carefully analysed, since the hydrophilicity is not a unique factor that determines the self-assembly propensity.

5.3.3 Generation of design rules for co-assembled tri/dipeptide hydrogelators

Highly hydrophobic dipeptides with both aromatic amino acids can be insoluble in water and prevent the formation of networks in water, which restricts potential applications. The formation of big aggregates observed for *e.g.*, FW or YF (Table 5.1) might suggest that there are solubility issues, however the AP score used here cannot distinguish between assembled and precipitated aggregates.

Based on these reasons, it has been proposed before that the hydrophobicity cannot be the only factor determining the aggregation propensity and especially hydrogelation ability of a peptide. Hydrogel formation requires favourable interactions between nanofibres formed and the solvent, thus requiring inclusion of hydrophilic groups, which has been shown by Ramos Sasselli *et al*.[281] The design of the peptide sequence, and thus hydrophilicity and interactions, have been shown to play a key role in the control of the gelation mechanism and self-assembling hydrogel properties.[304] Thus, a corrected AP score system that favours hydrophilic residues was developed for tripeptides.[85] We use the AP_H score for the total system as explained in Section 5.2. When correcting this indicator by adding a positive bias towards hydrophilic peptides, the highest scoring dipeptides are not the most hydrophobic ones (Figure 5.7). The more hydrophilic dipeptides are now ranked higher than more hydrophobic dipeptides with the same AP_{total} score.

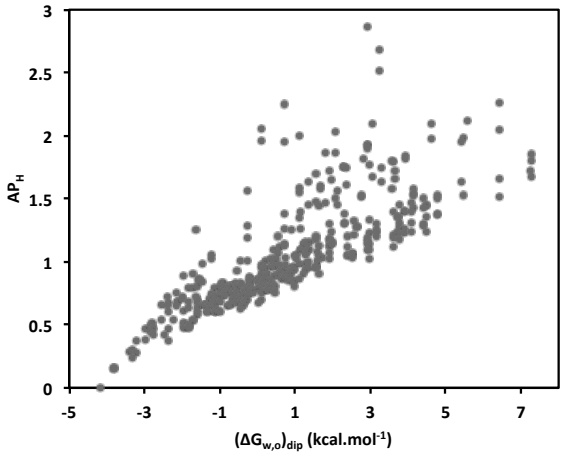

Figure 5.7. Hydrophilicity-corrected aggregation propensities (AP_H) of the different DFF/dipeptide systems in a water box, plotted as a function of the dipeptide hydrophilicity ($\Delta G_{w,o}$).

It is possible to analyse and compare the different AP scoring systems when plotting both AP_{total} and AP_H together (Figure 5.8). There were only 29 systems, out of 400, for which the AP_{total} was higher than 2 (red diamonds). This cut-off value has been shown to be a reasonable indicator for the selection of the best dipeptides for self-assembly.[84] However, the presence of DFF significantly increases the surface area in the beginning of the simulation when in comparison to the dipeptide alone. Therefore, there is an increased possibility to decrease the SASA upon assembly/aggregation, depending on the mode of assembly, and thus increase the AP scores. In this way, it is not possible to directly compare with the system of dipeptides only and one should consider a higher AP score in order to appoint the system as a good candidate. When comparing the two scoring systems, there are seven dipeptides (KH, SK, KW, RF, KF, FR and WK) that fall into both categories of $AP_{total} > 2$ and AP_H top 30 (blue squares) and these all have intermediate hydrophilicity values.

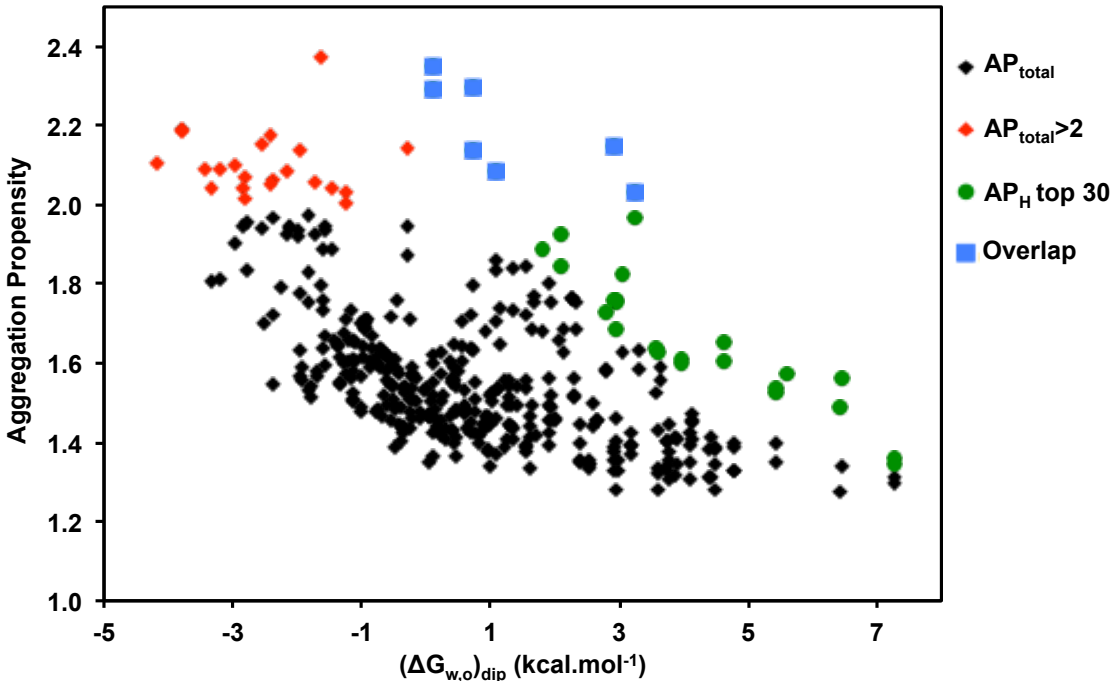

Figure 5.8. Aggregation propensity plotted as a function of the dipeptide hydrophilicity ($\Delta G_{w,o}$). Black diamonds represent the AP_{total}, which also includes the red triangles, that represent the dipeptides for which $AP_{total} > 2$. The green circles represent the top 30 hydrophilicity-corrected AP_H and the blue squares the overlap between the highest from the two methods.

We then analysed the average contribution of each amino acid to the AP_H scores obtained after 100 ns, by comparing the aggregation propensities when a certain amino acid is placed in position 1 or 2 (N-terminus or C-terminus, respectively) of the peptide chain. Previously, we have shown the sequence dependence for the aggregation propensity in the case of tripeptides, where it was possible to generate design rules and take conclusions about the relative positioning of the amino acids in the tripeptide to encourage hydrogelation.[85] Therefore, we applied the same process to determine which dipeptide should be used for the production of the best interconnection between dipeptide and DFF, which produces nanofibres and, consequently, hydrogels.

As observed from Figure 5.9, aromatic (Figure 5.9a) and cationic (Figure 5.9c) amino acids are the ones that more strongly promote aggregation, contributing to higher AP_H' values.

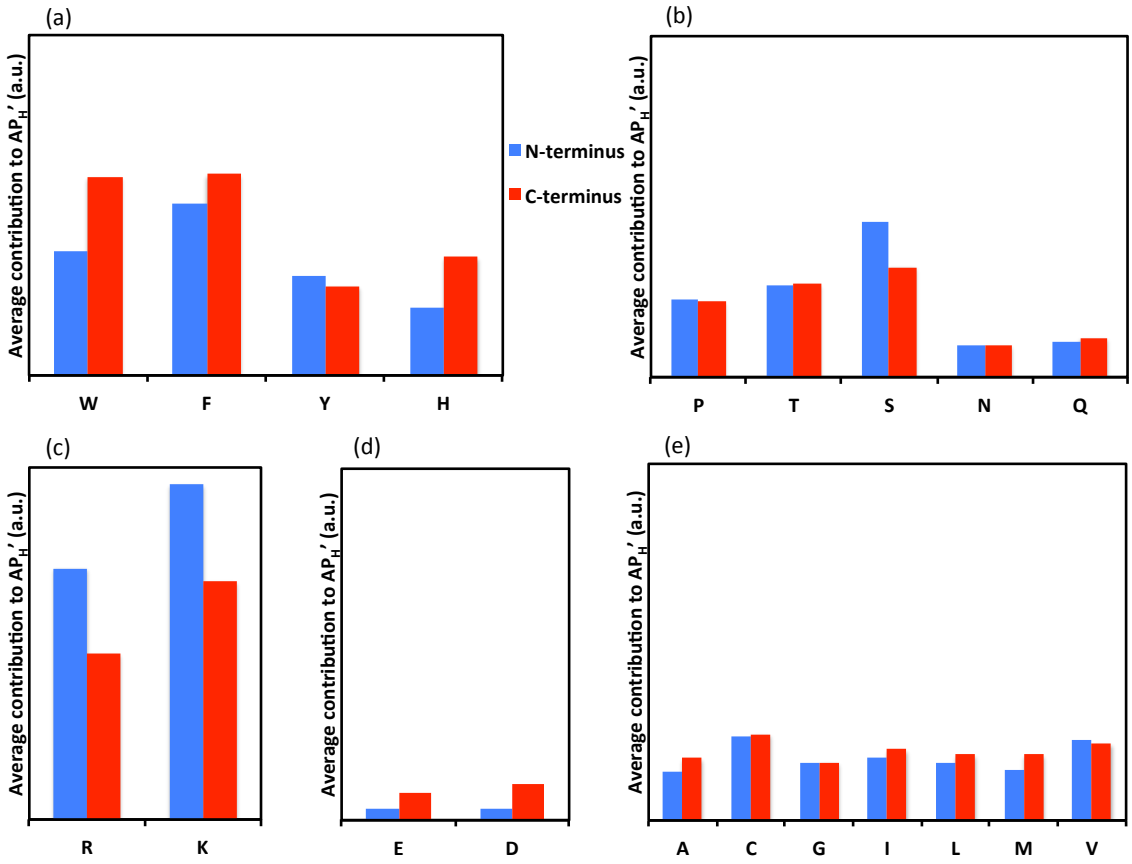

Figure 5.9. Average AP_H' scores of the dipeptides, when in combination with DFF, in a water medium, with the corresponding amino acid on the x-axis in the N-terminus or C-terminus. Amino acids are grouped per: (a) Aromatic; (b) Hydrophilic; (c) Cationic; (d) Anionic; (e) Small/hydrophobic side chains.

Aromatic amino acids are more favourable in the C-terminus position than at the N-terminus, except for tyrosine, where the difference is not significant. In contrast, higher AP_H scores are reached when cationic amino acids are placed in the N-terminus. A similar behaviour was observed for tripeptides,[85] where the cationic and H-bonding donor amino acids K, R, S and T are advantageous in position 1 of the chain. In this case, the relative positioning of hydrophilic amino acids (Figure 5.9b), including T, is irrelevant, except for S, which has a preference for the N-terminus. There is a slight preference for negatively charged amino acids (E and D) to be positioned at the C-terminus (Figure 5.9d), while there is no sequence dependence for small hydrophobic side chains (Figure 5.9e).

In general, there was no particular preference for the position of uncharged hydrophilic/hydrophobic amino acids within the dipeptide. Even though the positioning of the two amino acids within a dipeptide was not expected to have as strong a dependence on the ability to aggregate as for tripeptides or larger peptides/proteins, the relative position in some of the cases was shown to be an important factor. It is possible to conclude that the most favourable formulation for the interaction between DFF and a dipeptide is possibly when the dipeptide is composed by a cationic amino acid at the N-terminus and an aromatic amino acid at the C-terminus.

The positioning of the amino acids can indeed determine the mode of interaction between each dipeptide and the tripeptide DFF and, consequently, the type of structure formed. This is proved by the distinct behaviour of similar dipeptides presented in Table 5.1, when analysed more closely. RF and FR are amongst the overlapped dipeptides that belong to the $AP_{total} > 2$ and top 30 AP_H. Even though they present similar AP values (AP_{total} but also AP_{DFF}, AP_{dip} and AP_H), RF forms branched fibres while FR creates aggregates. The indication that the cationic arginine is more favourable to aggregation when in the N-terminus position (Figure 5.9c) and the aromatic phenylalanine in the second position (Figure 5.9a) is then corroborated. This can be explained by the positively charged H-bond donating amino acid R, which increases the opportunity for self-assembly when at the N-terminus. In turn, the phenylalanine is preferred at the C-terminus, allowing for aromatic interactions with the Phe moieties from DFF. The difference between SW and WS is also in agreement with the rules, but this is apparent from the scoring system, where SW presents the highest AP_{total} score and WS only ranks no. 63 in the AP_{total} score (Appendix 27). It has been previously noted that SF presented an AP score (non-corrected) 0.6 times higher than FS,[84] which is due to the possibility of H-bond formation when the hydrophilic serine is at the N-terminus.

All together, these rules were shown to be critical for guiding the selection of specific dipeptides in order to achieve the aggregation and self-assembly properties required. In this particular case, a number of dipeptides are shown to assemble in combination with DFF, forming fibres instead of bilayers. The combination of a cationic hydrophilic amino acid at

the N-terminus and an aromatic amino acid such as F or W in the C-terminal position of the dipeptide would promote cooperative co-assembly with the amphiphilic DFF.

5.3.4 Generation of design rules for co-assembled tri/dipeptide better emulsifiers

Following the interfacial nanofibrous-stabilised emulsions reported in the previous chapters of this thesis, this co-assembly behaviour is also extrapolated to the biphasic systems, following the belief that co-assembled fibres could be formed at the interface between two immiscible liquids. The rationale used for the selection of the best dipeptide that, in combination with DFF, could become a good emulsifier was thus based on the water simulations and on the ability of DFF and dipeptide to undergo cooperative co-assembly into interconnected nanofibrous networks.

When AP_{DFF} is very high ($AP_{DFF} > 2.2$), nanofibres or bilayers are formed with the dipeptide coating their interface in an orthogonal manner, such as in the case of KH or SK (Table 5.1 and Figure 5.6, respectively). These types of structures are not considered to be stable enough to protect octane droplets' interface once used in a biphasic system. The systems where both DFF and dipeptides cooperate to reach a collaborative fibrous structure in water would be of interest to stabilise a biphasic medium. These nanofibres would assemble at the interface between water and oil, reducing the attraction between droplets, but also at the aqueous environment to increase the viscosity of the medium and delay droplet coalescence, as previously reported in Chapter 4. We next investigated whether dipeptides that show this type of co-assembly behaviour could be identified.

As previously presented, the highest overall AP_{total} score was reached when H-seryl-tryptophan-OH (SW) is added to DFF in aqueous medium and this system formed the desired stable nanofibres. However, it has been shown before that this does not occur for all the following systems scoring the highest AP_{total} (Table 5.1), and so the use of the empirical cut-off $AP_{total} > 2$ does not work for the selection of the best emulsifiers either. In addition, SW only ranks no. 108 when using the hydrophilicity-corrected scoring system and the highest AP_H is achieved for KH, shown previously to form coated fibres (orthogonal co-

assembly) (Table 5.1). These two quick tests immediately excluded the AP_H scoring system for the selection of the cooperative co-assembly system capable of forming an interconnecting fibrous-type emulsifier. The respective AP scores were analysed in order to select the parameters that define the appropriate systems.

The selection of the systems that possibly undergo a cooperative assembly between DFF and the dipeptide at the interface involves the study of the compromise between the AP_{DFF} and AP_{dip} values. In order to avoid taking into account too hydrophobic dipeptides that tend to aggregate by themselves and undergo perturbed assembly, the absolute value of the difference between the AP scores for DFF in the presence of the dipeptide (AP_{DFF}) and the DFF alone in water $(AP_{DFF})_0$ should be lower than 0.7. On the other hand, to discard the previously described orthogonal co-assembly systems and account only for interconnecting fibre formation through cooperative co-assembly, the absolute value of the difference between the AP scores for dipeptide with DFF (AP_{dip}) and dipeptide alone (using as $(AP_{dip})_0$ the reported AP values from dipeptide screening)[84] should be higher than 1, as below:

$$\begin{cases} |(AP_{DFF}) - (AP_{DFF})_0| < 0.7 \\ \left|(AP_{dip}) - (AP_{dip})_0\right| > 1. \end{cases}$$

The combination of these conditions filters the systems where co-assembly between the tripeptide and the dipeptide molecules occurs in an interactive way to achieve nanofibrous networks. The dipeptides that satisfy these conditions are analysed through CG simulations of a water/octane system in the Section 5.4.2.

5.4 Design of co-assembled DFF with dipeptides in biphasic systems

5.4.1 DFF self-assembly in biphasic systems

When in a biphasic system of water and octane, DFF was seen to adsorb at the interface, with the hydrophilic anionic aspartic acid preferentially exposed to the water and phenylalanine residues facing the organic solvent in the interior of the droplet.[182] The same tendency was observed in this work, where octane droplets are formed and DFF tends to assemble at the interface as a monolayer by the end of 100 ns, following a traditional surfactant behaviour (Figure 5.10b).

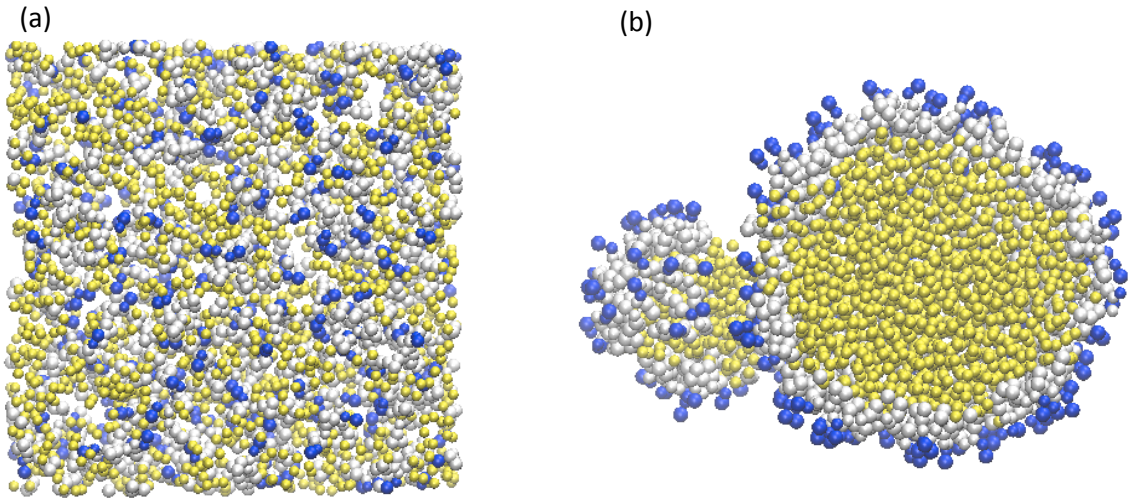

Figure 5.10. Snapshots of the DFF control system in the beginning (a) and end of the simulation (100 ns) (b) in a water/octane box. Phenylalanine is represented in white and aspartic acid in blue VDW particles. Octane is in yellow, while water beads are omitted for clarity.

In a water/octane system, AP_{total} only scored 1.63, as opposed to the 2.25 reported before for the aqueous system. This is due to the formation of DFF interfacial monolayers at the dispersed octane droplets in water, which increases the area, in contrast with aggregation of DFF molecules into a bilayer (Figure 5.3b). Since the initial randomised state mimics an ephemeral moment where water and octane are mixed without the dispersion of one into the other, which occurs immediately after homogenisation, the octane accessible area is lowered throughout the simulation due to the formation of droplets. The octane AP score (AP_{oct}), calculated following the same Equation 5.1 but only taking into account octane molecules, is 1.30. Since the presence of peptides at the interface is not detected by the probe, this scoring system provides information only about the shape and size of octane

droplets. In fact, a control system with water/octane and no addition of surfactant or peptide also undergoes the same behaviour and presents a similar value of AP_{oct} (1.24), which proves this value is only dependent on the association of octane in droplets. However, and as explained in Chapter 2, emulsions are metastable systems where water and octane tend to decrease their interfacial free energy by minimising the interfacial area in the absence of a surfactant. If the surfactant is not effective enough, the droplets coalesce and two phases are again formed. Even though these processes are not captured in a short simulation of 100 ns, extended simulations would allow for the assessment of the long-term stability of emulsions, but this is not within the scope of this study.

5.4.2 Screening of co-assembled dipeptides and DFF in biphasic systems

When in a water/octane system, the AP_{total} for the DFF with dipeptides ranges from 1.85 for KW and 1.19 for EH, as presented in Figure 5.11a (see Appendix 28 for the full data).

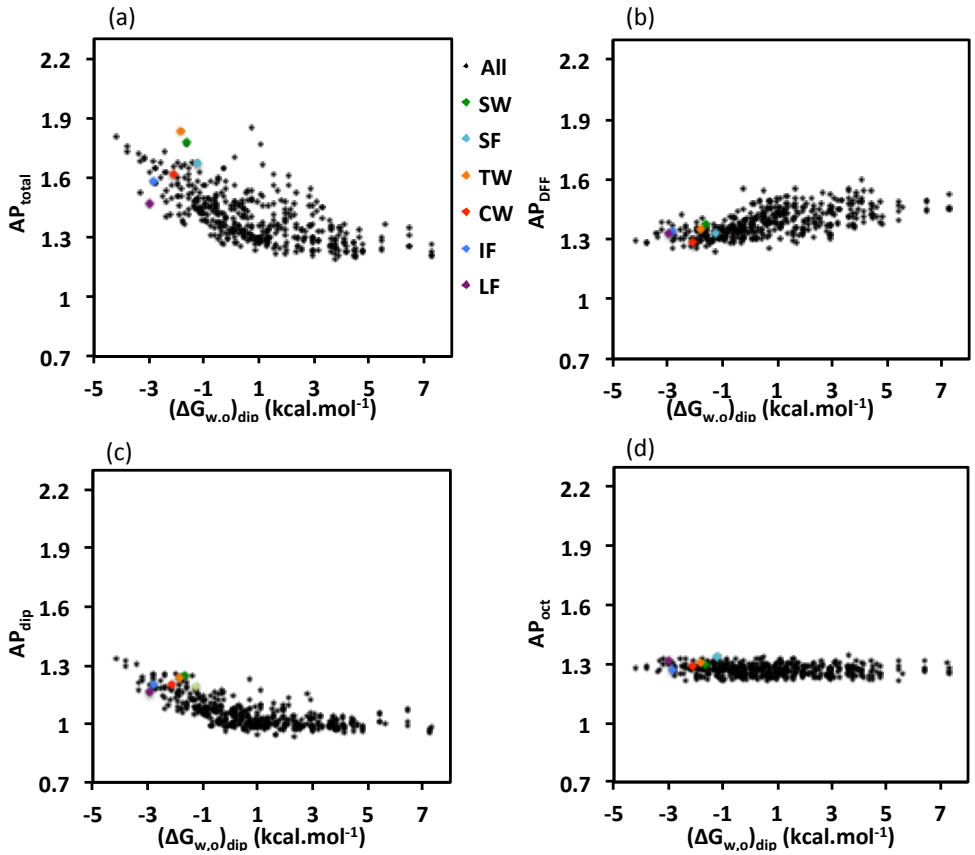

Figure 5.11. Positioning of the DFF in combination with each one of the six filtered dipeptides according to the criteria presented above for emulsifiers (SW, SF, TW, CW, IF and LF) amongst the whole range of: (a) AP_{total}; (b) AP_{DFF}; (c) AP_{dip}; (d) AP_{oct} for all the systems.

The distinct range observed for the AP_{total} score of the molecules in biphasic systems when compared to the aqueous systems (Figure 5.4a) is due to their tendency to assemble at the octane droplets' interface. The AP_{DFF} score range (Figure 5.11b) also decreases when compared to the same systems in a water box (Figure 5.5a). This can be explained by the increased SASA when interfacial networks are formed, instead of fibres or aggregates, which had been already observed and discussed for DFF on its own (Figure 5.10b).

The AP_{oct} score only varies in 9.9% from the minimum to the maximum value achieved (Figure 5.11d), which is not considered to be significant when in comparison to the difference in AP_{total} of 46.2% in water or 35.8% in biphasic systems. This indicates that the

type of co-assembly between DFF and each dipeptide, and inherently the relative positioning of the amino acids, do not highly influence the shape of the octane droplets.

The selected systems from the aqueous simulations that meet the criteria defined previously in Section 5.3.4 are positioned in a similar place within the whole range of AP values for the biphasic simulations. These systems are moderately hydrophobic and score high for the AP_{total} (Figure 5.11a), but do not achieve the highest values. Regarding the AP_{dip} value, these filtered systems are also within the highest scoring systems, with the highest occurring for the most hydrophobic dipeptides, that tend to aggregate between them.

5.4.3 Investigating rules for better emulsifiers

The biphasic CG simulations of DFF with those six dipeptides that meet the previously defined criteria for better emulsifiers are visually analysed to conclude whether nanofibres are formed that can stabilise droplets in a different way (Figure 5.12).

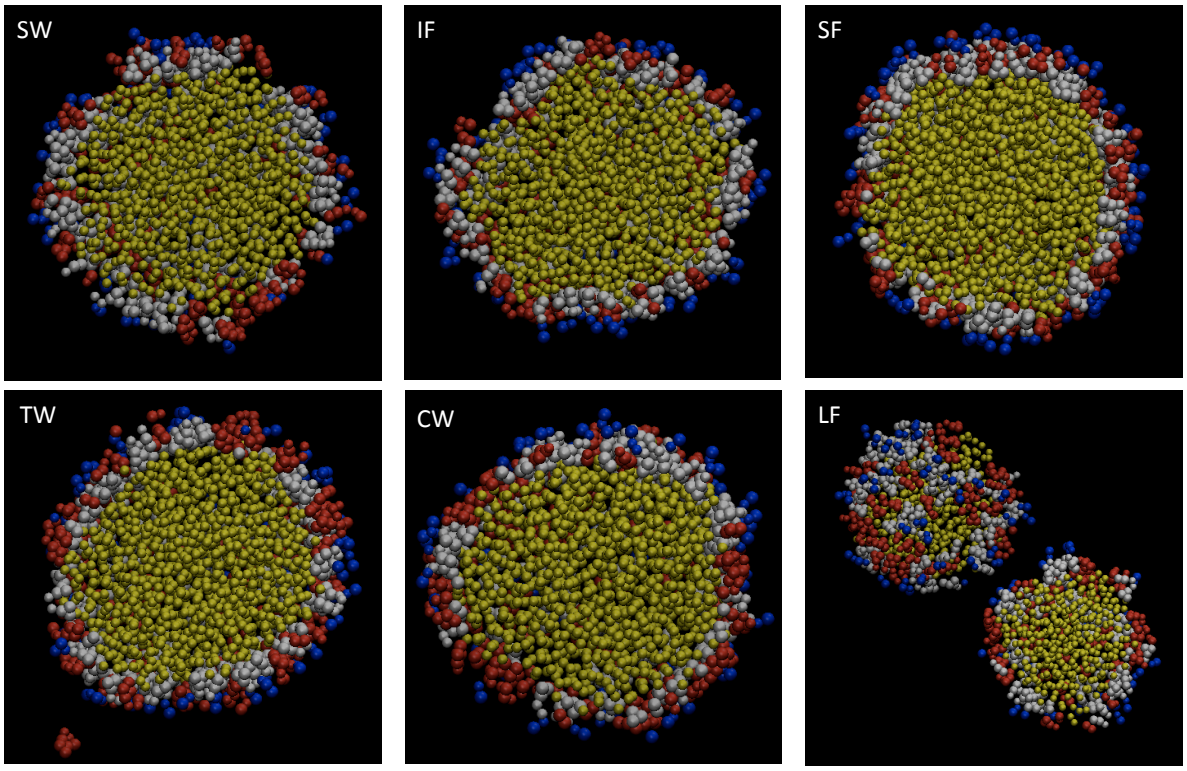

Figure 5.12. Final snapshots (100 ns) of different dipeptides in combination with DFF in a water/octane system. These 6 were the filtered dipeptides according to the criteria presented above for emulsifiers.

Phenylalanine from DFF is represented in white and aspartic acid from DFF in blue VDW particles, all dipeptides are represented in red, octane in yellow and water beads are omitted for clarity.

The system that reached the highest AP_{total} in the aqueous simulations, when SW is used in combination with DFF, presents a very well-covered stable water/octane interface. Even though it is not possible to clearly observe nanofibres at the interface due to the low detail of a CG model, it is clear that the interactions between the peptides are affecting the arrangement of the peptides at the interface, rather than simply responding to the environment of the octane and water as in the pure surfactant-type adsorption observed for DFF (Figure 5.10b). This implies that a more efficient emulsification may be achieved. The other selected systems present a similar behaviour, which validates the previously established rules for better emulsifiers. The LF forms two droplets by the end of 100 ns and less coverage of the droplets is apparent, which might be associated with the higher interfacial area obtained by the droplet split, while the number of peptidic molecules (total of 300) for the coverage remains the same. The predicted behaviour from different criteria is merely indicative and there can be exceptions, only suggesting which systems should be further analysed throughout the simulation time.

As previously explained and observed from Figure 5.11, the highest AP score is not necessarily indicative of the most effective emulsifier, since a cooperative co-assembly between DFF and the dipeptide is believed to be necessary for a proper fibrous coverage of the emulsion droplets. Nevertheless, the total AP score (AP_{total}) was more closely analysed for all the biphasic systems in order to study the tendencies for the co-assembly and investigate any trends in the data. By calculating the average contribution of each amino acid to the AP_{total} values when placed in the N-terminus or C-terminus of the peptide chain (Figure 5.13), it is possible to observe aromatic amino acids are again the ones more prone to assemble when in a water/octane system. However, there is no significant preference for either the N-terminal or C-terminal position within the dipeptide (Figure 5.13a).

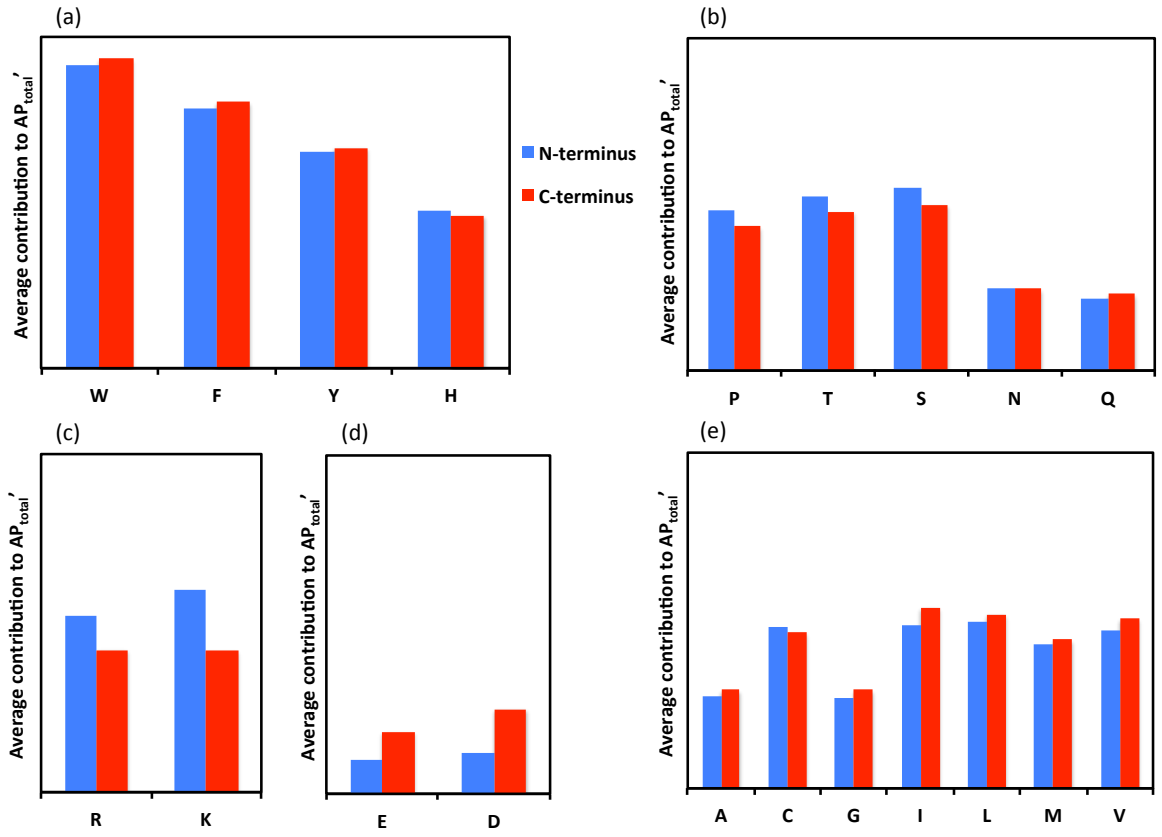

Figure 5.13. Average AP_{total} scores of the dipeptides, when in combination with DFF, in a water/octane medium, with the corresponding amino acid on the x-axis in the N-terminus and C-terminus. Amino acids are grouped per: (a) Aromatic; (b) Hydrophilic; (c) Cationic; (d) Anionic; (e) Small/hydrophobic side chains.

The dipeptides contributing less for assembly are the anionic ones (Figure 5.13d), these perturb the DFF mode of assembly, which was already visible from the whole picture (Figure 5.11a).

Especially the co-assembly of SW, SF, TW and CW with DFF in a water/octane system were able to convert a surfactant-type emulsification of the tripeptide DFF into a more stabilising interfacial network (Figure 5.12). This choice validates the design rules for hydrogelators and also the tendencies studied for biphasic systems (Figure 5.13), as the selected dipeptides are formed by a hydrophilic and an aromatic amino acid, more specifically at the N-terminus and C-terminus, respectively.

5.5 Conclusions

In this chapter we have developed a coarse-grained molecular dynamics screening method to investigate the creation of desired materials through the co-assembly of tripeptides with dipeptides. The addition of specific dipeptides as a non-covalent on-demand trigger for the formation of different desired structures was studied, using the tripeptide DFF as a case study.

A screening of the 400 possible dipeptides combined with the tripeptide DFF allowed for the aggregation propensity analysis and further understanding of the dependence of the peptidic sequence over the co-assembly behaviour. The co-assembly in water of some dipeptides with DFF was shown to convert its bilayer into nanofibres and other structures. From the analysis of the average contribution to the hydrophilicity-corrected AP_H score, the positioning of the different amino acids within the dipeptide was shown to be not so crucial as for tripeptides.[85] However, the combination of a hydrophilic (in particular cationic) and an aromatic amino acid in the N-terminal and C-terminal position of the dipeptide, respectively, was concluded to be the best sequence for the production of hydrogelators. The analysis of the behaviour of these systems in water also allowed for the extrapolation to the biphasic system and to create rules for the formation of interfacial nanofibrous networks, leading to better emulsifiers. CG simulations of the promising dipeptides with DFF in a water/octane medium, which on its own follows a surfactant-type behaviour, were shown to form droplet-stabilising interfacial structures.

The identification of promising systems that can potentially co-assemble into hydrogels while in water and into more effective emulsifiers while in a biphasic system can then trigger further investigation due to their responsive nature. Even though the prediction of the best hydrogelator or emulsifier was not the aim of this work, there is evidence that co-assembled systems can be designed through MD simulations to achieve desired structures for specific applications. Different design methods and filters can also be developed regarding the desired properties of the assembled peptides.

6 Conclusions and Further Work

6.1 Conclusions

In this work, we have shown the possibility of creating responsive and more effective emulsifiers based on peptides, as alternatives to traditional surfactants. Different peptide sequences were studied, in order to conclude on structure/function relationships.

Alkaline phosphatase was used to initiate self-assembly by converting solutions composed of spherical aggregates of phosphorylated precursors into aromatic peptide amphiphiles (Fmoc-tyrosyl-leucine-OH, Fmoc-YL) that form nanofibrous networks and subsequently hydrogels. By using a combination of experimental (fluorescence, FTIR spectroscopy) and computational techniques (atomistic molecular dynamics simulations), further insight on the non-covalent interactions responsible for the self-assembly process was achieved. Hydrogen bonding arrangements and π-stacking interactions were shown to occur upon dephosphorylation into Fmoc-YL, giving rise to nanofibres. In biphasic organic/aqueous systems, enzymatically-triggered Fmoc-YL fibrous networks are believed to assemble at the interface of chloroform droplets, thus providing a means of droplet emulsion stabilisation. Alkaline phosphatase was shown to be active in non-aqueous media, which was, to our knowledge, not demonstrated before. We demonstrated that this enables the on-demand emulsification by enzyme addition, even after storage of the biphasic mixture for several weeks, by converting a de-emulsified mixture into a more stable emulsion. Fluorescence microscopy, electron microscopy and UV-Vis spectroscopy techniques were used to prove the formation of interfacial networks and characterise the emulsion droplets. MD simulations also supported the distinct interfacial assembly of the amphiphiles. Fmoc-YL tended to form an organised fibre-like structure, mainly based on the H-bonded network and π-stacking, as opposed to Fmoc-Y*p*L, which follows a traditional monolayer surfactant-type behaviour, with preferred interactions with water and minimum contact with octanol.

After showing it is possible to stabilise oil-in-water emulsions on-demand, a biocompatible unprotected self-assembling tripeptide KYF was assessed as for responsive emulsification ability. While following the same enzymatic mechanism to trigger the self-assembly into nanofibres in a bulk aqueous system, the biocatalyst amount and subsequent dephosphorylation rate were shown to kinetically control the fibre network properties.

More entangled fibrous networks and stiffer gels were formed when higher enzyme concentration was used, with an exception for an optimum concentration, which produced the most organised H-bonded structure. Coarse-grained molecular dynamics simulations do not provide evidence on the established interactions but suggest which is the preferred behaviour of each tripeptide state. KY*p*F forms spherical aggregates, mainly due to the increased hydration level given by the phosphate group, while KYF tends to form fibre-type structures. When in biphasic mixtures, KYF nanofibres are shown to self-assemble at the aqueous/organic interface but also throughout the surrounding buffer when used in a 9:1 aqueous buffer:rapeseed oil system, stabilising the oil-in-water droplet emulsions. From MD simulations in a biphasic mixture, octane droplets were formed with the tripeptides at the aqueous/organic interface and a more well-ordered structure is evident at the interface for the KYF, in contrast to KY*p*F. In addition to the time control over emulsification ability upon enzyme addition, the emulsion stabilisation and consequent properties were tuned by varying the enzyme concentration, which affects on the stabilising nanofibrous networks at the interface and/or at the aqueous environment. This approach can be attractive for various cosmetics, food or biomedical applications since tunability of tripeptide emulsion stability and on-demand stabilisation of emulsions can be achieved.

A computational coarse-grained molecular dynamics screening study was used to evaluate the formation of co-assembled structures between a tripeptide DFF and each possible dipeptide, which would act as a non-covalent trigger. Different types of co-operative, orthogonal or perturbed co-assembly have been proposed, depending on the amino acid sequence within the dipeptide in the presence of DFF. Based on different scoring systems, the combination of DFF with a dipeptide composed by a cationic and an aromatic amino acid at the N- and C-termini, respectively, was shown to undergo co-operative assembly. This type of co-assembly was shown to form nanofibrous networks, which give rise to hydrogels in aqueous systems and more effective emulsifiers in biphasic systems. The identification of these promising systems can trigger further investigation due to the ability of achieving desired structures for specific applications and to their responsive nature, which is further discussed in the Future Work section.

In summary, the development of biocompatible responsive peptide-based emulsifiers is innovative and presents direct applications in the food and cosmetics industries.

6.2 Further Work

Following the main conclusions drawn from this work, there are numerous opportunities for further development and future work within this area. After the discovery that droplet emulsions can be stabilised on-demand by assembled interfacial nanofibres, the change in some conditions can be interesting to gain further understanding of their role in the assembly and consequent emulsification process.

The study of different peptide sequences could further elucidate the sequence/structure relationship, whereas the role of the supramolecular interactions would also be assessed. Since it has been shown that different tripeptides follow distinct interfacial assembly behaviours depending on their sequence, a complete set of design rules to predict the interfacial entanglement of fibres to stabilise emulsions would be beneficial for future emulsifier design. This would be achievable through a coarse-grained screening method of the different Fmoc-dipeptides or, more interestingly, of uncapped tripeptides in a water/octane system.

pH and temperature were shown to be determinant for the formed nanostructures, which endows these as environmental stimuli that can be used in addition to the enzymatic trigger. It would also be interesting to assess whether the same mechanism is effective in other different solvents apart from chloroform or rapeseed oil. The concentration dependence, not only of the enzyme but also of the peptides, could be investigated as for the extent of the reported alternative emulsion stabilisation. Further studies on the possibility of viscosity increase and gelation of the aqueous continuous phase to stabilise emulsions can also be carried out. This would be helpful to obtain a picture of the concentration dependence over the emulsifying ability.

Since the proposed mechanism is different from a traditional surfactant-adsorbed emulsion stabilisation, it is more meaningful to characterise the emulsifier and the emulsion stability by imaging the droplets and measure their size over the time, as it has been carried out. Nevertheless, further emulsion characterisation could be achieved by calculating the interfacial tension when using the different emulsifying systems.

The development of an on/off switchable system could attract further interest within the cosmetics/food/pharmaceutical industries due to the control of formation of emulsions or foams at a specific stage of process. This could possibly be achieved by using a second enzyme to control the disassembly of nanofibrous networks and consequent de-emulsification. Furthermore, the micelles or emulsion droplets observed in Chapter 3 and 4 may be used to encapsulate drugs or active species. In fact, a de-emulsification mechanism by adding a second enzyme could be used for the controlled drug delivery, endowing these as promising drug carriers for targeted drug delivery within biomedical applications. Bolaamphiphiles or capsules could also be developed for the encapsulation of hydrophilic drugs, if necessary. Enzyme immobilisation after the biocatalytic-triggered emulsion stabilisation could additionally be attractive, whereby the enzyme could then be removed from the system and possibly reused.

As both all-atom and coarse-grained molecular dynamics simulations use a non-reactive force field, it was not possible to model the enzymatic conversion or the effect of enzyme amount on the reaction, only to analyse the initial and final stages. As this would be a considerable undertaking, it could be exploited in a future work, whereby the reaction kinetics of nanostructure formation would be computationally studied.

Regarding Chapter 5, extended simulations of the systems would allow for the achievement of the preferred structure and for the evaluation of the stability over time for the different emulsions. After a computational screening and design method has been developed, which indicates promising candidates for co-assembly, the obvious following step is to test its accuracy on selected combinations.

Some preliminary tests were carried out experimentally, with the available dipeptides in the laboratory. Unfortunately there were no examples of cationic/aromatic dipeptides available.

Therefore, we tested the anionic/aromatic dipeptide DF in aqueous medium. This aims to validate the computational design as a proof of concept only – *i.e.*, can the design rules be used to predict whether a combination of tripeptide and dipeptide will elicit the formation of a hydrogel. For complete characterisation of the nanostructures formed through the co-assembly of the system, further characterisation and analysis is required.

The control DFF (purchased at > 98% purity from Chinapeptides), at 40 mM concentration in water, remains a free flowing solution after 24 h (Figure 6.1a), as reported previously.[182] The turbid aspect can be explained by the pH adjustment to a slightly lower value of 7.4 rather than 7.5, by using 0.5 M NaOH. This is in agreement with the creation of a bilayer as seen from the initial simulation of DFF in water. When 40 mM was prepared in 1 mL water and neutralized the pH, a control of the dipeptide DF (purchased at > 98% purity from Sigma-Aldrich) was a clear solution after 24 h (Figure 6.1b), which agrees with the dipeptide AP score reported by Frederix *et al.* as 1.1, suggesting no particular aggregation or fibres are formed.[84] The samples were vortexed and sonicated to ensure dissolution. For the co-assembly test, the dipeptide DF powder corresponding to a final 40 mM was added to the 40 mM DFF. After 24 h, a hydrogel is formed (Figure 6.1c).

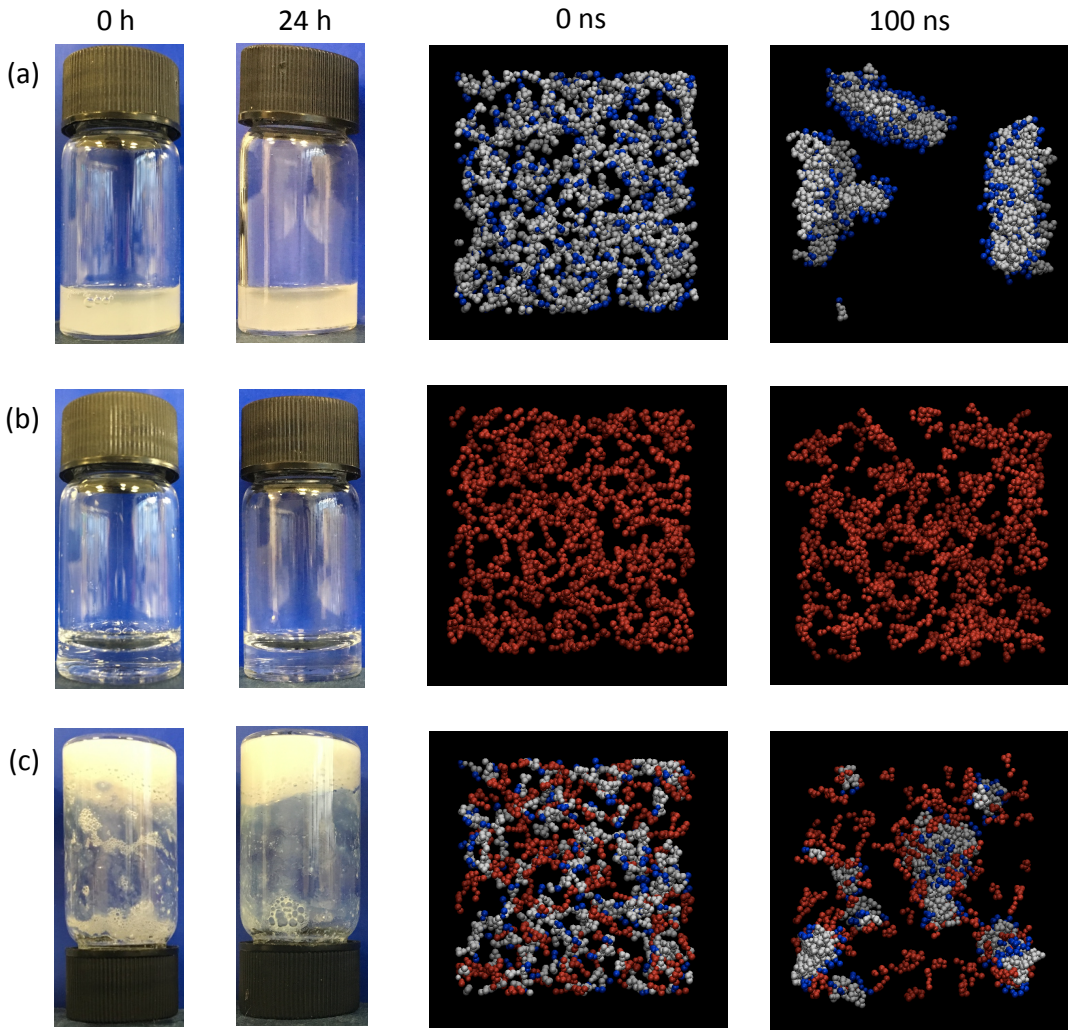

Figure 6.1. Photographs of the macroscopic aspect of the water samples at time zero, immediately after vortexing, and after 24 h, and initial (0 ns) and final snapshots (100 ns) of the CG-MD simulation for: (a) DFF only; (b) DF only; (c) DFF co-assembled with DF in aqueous system. Phenylalanine from DFF is represented in white and aspartic acid from DFF in blue VDW particles, all dipeptide molecules (DF) are represented in red, while water beads are omitted for clarity.

Even though DF only scores 1.45 for the overall system (AP_{total} in position 286 out of 400, Appendix 27), it shifts to position 251 upon the hydrophilicity correction (AP_H' = 0.014). Although DF did not appear as a preferred dipeptide based on the individual scores or the design rules based on the AP_H' values, it formed a hydrogel. In fact, it presents a hydrophilic amino acid at the N-terminus and an aromatic amino acid at the C-terminal position. The snapshot taken after the 100 ns CG-MD simulation of DFF+DF shows no

nanofibre formation but rather the appearance of some aggregates with the dipeptide interacting in some areas with DFF and coating it in other areas (Figure 6.1c). The simulation length is possibly not enough to achieve the preferred structure, but it is believed that the extended CG-MD simulation would show nanofibrous-type structures.

For the preliminary tests in biphasic systems, when 100 μL rapeseed oil are added to 900 μL 40 mM DFF in water and homogenised by 10 seconds, a temporary emulsion was produced (Figure 6.2a – 0h) which de-emulsified into two phases before 4 h. This is in agreement with what has been previously reported[182] and also with the observed traditional surfactant-type emulsification ability in Chapter 5. The study of the dipeptide, SF, in isolation also demonstrated the same behaviour (Figure 6.2b), most likely adsorbing at the interface between oil and water as a monolayer. When 40 mM SF is added to the DFF in a 9:1 water:rapeseed oil system, a more stable emulsion is formed, since it is a stable emulsion by 8 h and it was not completely de-emulsified after 24 h (Figure 6.2c). The co-assembly between DFF and the dipeptide SF is possibly responsible for the formation of nanofibres that delay the coalescence of the oil-in-water droplets. This corroborates the generated rules that pointed at SF as a promising dipeptide for the co-assembly with DFF, converting its traditional monolayer-type into a fibrous-type emulsifier. From the simulation of this system in water/octane (see Section 5.4.3), the interconnection between SF and DFF, that creates a protective layer at the interface, is clear and can explain the greater droplet stabilisation. In addition, SF presents one of the highest AP_{total} scores when in a biphasic system (position 19 in Appendix 27), which is in agreement with the high cooperation between tripeptides and dipeptides and complete coverage of the droplets, which prevents de-emulsification.

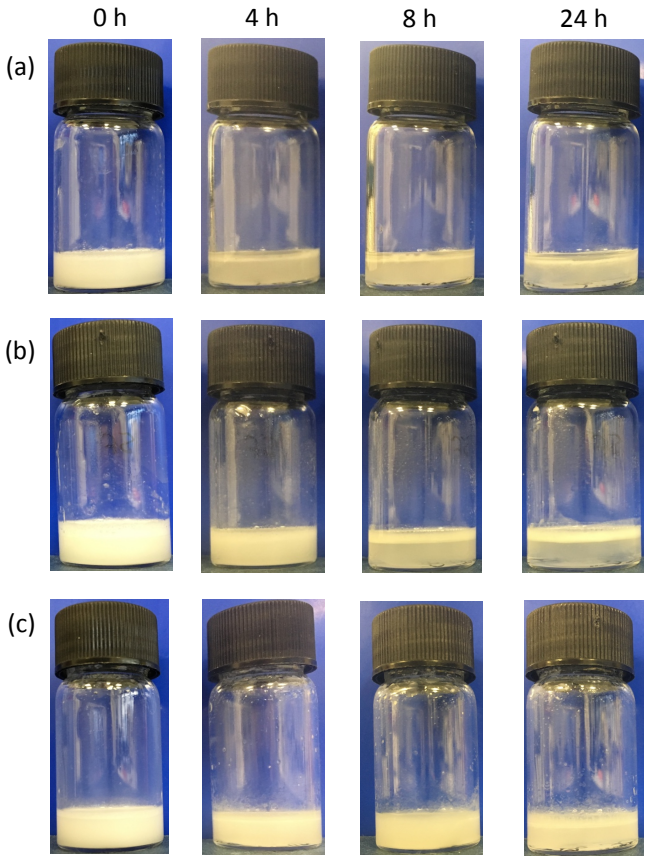

Figure 6.2. Photographs of the macroscopic aspect of the emulsions at time zero (immediately after homogenisation), 4 h, 8 h and 24 h after to check the stability of the emulsions throughout the time: (a) DFF only; (b) SF only; (c) DFF co-assembled with SF in a biphasic system.

A preliminary experimental test confirms the previously established rules for hydrogelators, where DFF forms a hydrogel upon the addition of DF, suggesting the formation of nanofibres. In turn, when SF is added to a biphasic mixture of DFF and homogenised, a more stable emulsion is reached when in comparison to the tripeptide or the dipeptide on their own. A computational screening was thus proven to be helpful for the design of unique functional soft materials through co-assembly. However, further characterisation through microscopic and spectroscopic techniques is required in order to reveal whether nanofibres are present in both aqueous and biphasic systems and to understand the non-covalent interactions responsible for the assembly process. Additionally, different design methods can be used in the future as for the creation of innovative desired nanostructures.

7 References

1. Whitesides, G.; Mathias, J.; Seto, C., Molecular self-assembly and nanochemistry: a chemical strategy for the synthesis of nanostructures. *Science* **1991,** *254* (5036), 1312-1319.
2. Fleming, S.; Ulijn, R. V., Design of nanostructures based on aromatic peptide amphiphiles. *Chemical Society Reviews* **2014,** *43* (23), 8150-8177.
3. Hirst, A. R.; Roy, S.; Arora, M.; Das, A. K.; Hodson, N.; Murray, P.; Marshall, S.; Javid, N.; Sefcik, J.; Boekhoven, J.; van Esch, J. H.; Santabarbara, S.; Hunt, N. T.; Ulijn, R. V., Biocatalytic induction of supramolecular order. *Nature chemistry* **2010,** *2* (12), 1089-94.
4. Santoso, S.; Hwang, W.; Hartman, H.; Zhang, S., Self-assembly of surfactant-like peptides with variable glycine tails to form nanotubes and nanovesicles. *Nano Letters* **2002,** *2* (7), 687-691.
5. Malcolm, A. S.; Dexter, A. F.; Middelberg, A. P., Peptide surfactants (Pepfactants) for switchable foams and emulsions. *Asia - Pacific Journal of Chemical Engineering* **2007,** *2* (5), 362-367.
6. Zelzer, M.; Ulijn, R. V., Next-generation peptide nanomaterials: molecular networks, interfaces and supramolecular functionality. *Chemical Society Reviews* **2010,** *39* (9), 3351-3357.
7. Adler-Abramovich, L.; Gazit, E., The physical properties of supramolecular peptide assemblies: from building block association to technological applications. *Chemical Society Reviews* **2014,** *43* (20), 6881-6893.
8. Zhang, S.; Holmes, T.; Lockshin, C.; Rich, A., Spontaneous assembly of a self-complementary oligopeptide to form a stable macroscopic membrane. *Proceedings of the National Academy of Sciences* **1993,** *90* (8), 3334-3338.
9. Ghadiri, M. R.; Granja, J. R.; Milligan, R. A.; McRee, D. E.; Khazanovich, N., Self-assembling organic nanotubes based on a cyclic peptide architecture. *Nature* **1993,** *366* (6453), 324-327.
10. Gazit, E., The "correctly folded" state of proteins: is it a metastable state? *Angewandte Chemie International Edition* **2002,** *41* (2), 257-259.
11. Hamley, I., Self-assembly of amphiphilic peptides. *Soft Matter* **2011,** *7* (9), 4122-4138.
12. Fairman, R.; Åkerfeldt, K. S., Peptides as novel smart materials. *Current Opinion in Structural Biology* **2005,** *15* (4), 453-463.
13. Lim, H. L.; Hwang, Y.; Kar, M.; Varghese, S., Smart hydrogels as functional biomimetic systems. *Biomaterials Science* **2014,** *2* (5), 603-618.
14. Lowik, D. W. P. M.; Leunissen, E. H. P.; van den Heuvel, M.; Hansen, M. B.; van Hest, J. C. M., Stimulus responsive peptide based materials. *Chemical Society Reviews* **2010,** *39* (9), 3394-3412.
15. Ulijn, R. V.; Smith, A. M., Designing peptide based nanomaterials. *Chemical Society Reviews* **2008,** *37* (4), 664-675.
16. Montalbetti, C. A. G. N.; Falque, V., Amide bond formation and peptide coupling. *Tetrahedron* **2005,** *61* (46), 10827-10852.
17. Rodnina, M. V.; Beringer, M.; Wintermeyer, W., How ribosomes make peptide bonds. *Trends in biochemical sciences* **2007,** *32* (1), 20-26.
18. Merrifield, R. B., Solid-phase peptide synthesis. *Adv Enzymol Relat Areas Mol Biol* **1969,** *32*, 221-296.

19. Escuder, B.; Miravet, J. F., *Functional Molecular Gels*. Royal Society of Chemistry: Cambridge, England, 2013; Vol. 1.
20. Williams, R. J.; Smith, A. M.; Collins, R.; Hodson, N.; Das, A. K.; Ulijn, R. V., Enzyme-assisted self-assembly under thermodynamic control. *Nat Nanotechnol* **2009,** *4* (1), 19-24.
21. Whitesides, G. M.; Grzybowski, B., Self-assembly at all scales. *Science* **2002,** *295* (5564), 2418-2421.
22. Gazit, E., Self-assembled peptide nanostructures: the design of molecular building blocks and their technological utilization. *Chemical Society Reviews* **2007,** *36* (8), 1263-1269.
23. Ozin, G. A.; Arsenault, A. C.; Cademartiri, L., *Nanochemistry: a chemical approach to nanomaterials*. Royal Society of Chemistry: Cambridge, England, 2009.
24. van Esch, J. H., We Can Design Molecular Gelators, But Do We Understand Them?†. *Langmuir* **2009,** *25* (15), 8392-8394.
25. Birchall, L. S.; Roy, S.; Jayawarna, V.; Hughes, M.; Irvine, E.; Okorogheye, G. T.; Saudi, N.; De Santis, E.; Tuttle, T.; Edwards, A. A.; Ulijn, R. V., Exploiting CH-[small pi] interactions in supramolecular hydrogels of aromatic carbohydrate amphiphiles. *Chemical Science* **2011,** *2* (7), 1349-1355.
26. Weiss, R. G.; Terech, P., *Molecular gels: materials with self-assembled fibrillar networks*. Springer Science & Business Media: Dordrecht, The Netherlands, 2006.
27. Johnson, E. K.; Adams, D. J.; Cameron, P. J., Peptide based low molecular weight gelators. *Journal of Materials Chemistry* **2011,** *21* (7), 2024-2027.
28. Estroff, L. A.; Hamilton, A. D., Water gelation by small organic molecules. *Chem Rev* **2004,** *104* (3), 1201-1218.
29. Yu, G.; Yan, X.; Han, C.; Huang, F., Characterization of supramolecular gels. *Chemical Society Reviews* **2013,** *42* (16), 6697-6722.
30. Cardoso, A. Z.; Alvarez Alvarez, A. E.; Cattoz, B. N.; Griffiths, P. C.; King, S. M.; Frith, W. J.; Adams, D. J., The influence of the kinetics of self-assembly on the properties of dipeptide hydrogels. *Faraday Discussions* **2013,** *166* (0), 101-116.
31. Orbach, R.; Mironi-Harpaz, I.; Adler-Abramovich, L.; Mossou, E.; Mitchell, E. P.; Forsyth, V. T.; Gazit, E.; Seliktar, D., The Rheological and Structural Properties of Fmoc-Peptide-Based Hydrogels: The Effect of Aromatic Molecular Architecture on Self-Assembly and Physical Characteristics. *Langmuir* **2012,** *28* (4), 2015-2022.
32. Nelson, D. L.; Lehninger, A. L.; Cox, M. M., *Lehninger principles of biochemistry*. 4th ed.; Macmillan: Gordonsville, U.S.A., 2005.
33. Steed, J. W.; Atwood, J. L., Concepts. In *Supramolecular Chemistry*, John Wiley & Sons, Ltd: West Sussex, England, 2000; pp 1-48.
34. Atkins, P., *Physical chemistry : quanta, matter, and change*. 10th ed.; W. H. Freeman and Co.: Oxford, England, 2014.
35. Jeffrey, G. A., *An introduction to hydrogen bonding*. Oxford university press: New York, 1997; Vol. 32.
36. Gao, J.; Kelly, J. W., Toward quantification of protein backbone–backbone hydrogen bonding energies: An energetic analysis of an amide - to - ester mutation in an α - helix within a protein. *Protein Science* **2008,** *17* (6), 1096-1101.
37. McGaughey, G. B.; Gagné, M.; Rappé, A. K., π -Stacking interactions alive and well in proteins. *Journal of Biological Chemistry* **1998,** *273* (25), 15458-15463.

38. Martinez, C. R.; Iverson, B. L., Rethinking the term "pi-stacking". *Chemical Science* **2012,** *3* (7), 2191-2201.
39. Moore, D. S., Amino acid and peptide net charges: a simple calculational procedure. *Biochemical Education* **1985,** *13* (1), 10-11.
40. Tang, C.; Smith, A. M.; Collins, R. F.; Ulijn, R. V.; Saiani, A., Fmoc-Diphenylalanine Self-Assembly Mechanism Induces Apparent p K a Shifts. *Langmuir* **2009,** *25* (16), 9447-9453.
41. Kumar, S.; Nussinov, R., Salt bridge stability in monomeric proteins1. *Journal of Molecular Biology* **1999,** *293* (5), 1241-1255.
42. Kumar, S.; Nussinov, R., Close ‐ range electrostatic interactions in proteins. *ChemBioChem* **2002,** *3* (7), 604-617.
43. Vegners, R.; Shestakova, I.; Kalvinsh, I.; Ezzell, R. M.; Janmey, P. A., Use of a gel ‐ forming dipeptide derivative as a carrier for antigen presentation. *Journal of Peptide Science* **1995,** *1* (6), 371-378.
44. Yang, Z.; Gu, H.; Zhang, Y.; Wang, L.; Xu, B., Small molecule hydrogels based on a class of antiinflammatory agents. *Chemical communications* **2004,** (2), 208-209.
45. Zhang, Y.; Gu, H.; Yang, Z.; Xu, B., Supramolecular hydrogels respond to ligand-receptor interaction. *Journal of the American Chemical Society* **2003,** *125* (45), 13680-13681.
46. Reches, M.; Gazit, E., Casting Metal Nanowires Within Discrete Self-Assembled Peptide Nanotubes. *Science* **2003,** *300* (5619), 625-627.
47. Mahler, A.; Reches, M.; Rechter, M.; Cohen, S.; Gazit, E., Rigid, Self-Assembled Hydrogel Composed of a Modified Aromatic Dipeptide. *Advanced Materials* **2006,** *18* (11), 1365-1370.
48. Reches, M.; Gazit, E., Self-assembly of peptide nanotubes and amyloid-like structures by charged-termini-capped diphenylalanine peptide analogues. *Israel Journal of Chemistry* **2005,** *45* (3), 363-371.
49. Reches, M.; Gazit, E., Formation of closed-cage nanostructures by self-assembly of aromatic dipeptides. *Nano letters* **2004,** *4* (4), 581-585.
50. Gazit, E., A possible role for π -stacking in the self-assembly of amyloid fibrils. *The FASEB Journal* **2002,** *16* (1), 77-83.
51. Jayawarna, V.; Ali, M.; Jowitt, T. A.; Miller, A. F.; Saiani, A.; Gough, J. E.; Ulijn, R. V., Nanostructured Hydrogels for Three ‐ Dimensional Cell Culture Through Self ‐ Assembly of Fluorenylmethoxycarbonyl‐Dipeptides. *Advanced Materials* **2006,** *18* (5), 611-614.
52. Braun, H.-G.; Cardoso, A. Z., Self-assembly of Fmoc-diphenylalanine inside liquid marbles. *Colloids and Surfaces B: Biointerfaces* **2012,** *97*, 43-50.
53. Orbach, R.; Adler-Abramovich, L.; Zigerson, S.; Mironi-Harpaz, I.; Seliktar, D.; Gazit, E., Self-assembled Fmoc-peptides as a platform for the formation of nanostructures and hydrogels. *Biomacromolecules* **2009,** *10* (9), 2646-2651.
54. Debnath, S.; Shome, A.; Das, D.; Das, P. K., Hydrogelation through self-assembly of Fmoc-peptide functionalized cationic amphiphiles: potent antibacterial agent. *The Journal of Physical Chemistry B* **2010,** *114* (13), 4407-4415.
55. Hughes, M.; Debnath, S.; Knapp, C. W.; Ulijn, R. V., Antimicrobial properties of enzymatically triggered self-assembling aromatic peptide amphiphiles. *Biomaterials Science* **2013,** *1* (11), 1138-1142.

56. Yang, Z.; Liang, G.; Wang, L.; Xu, B., Using a kinase/phosphatase switch to regulate a supramolecular hydrogel and forming the supramolecular hydrogel in vivo. *Journal of the American Chemical Society* **2006,** *128* (9), 3038-3043.
57. Wang, H.; Yang, C.; Tan, M.; Wang, L.; Kong, D.; Yang, Z., A structure–gelation ability study in a short peptide-based 'Super Hydrogelator'system. *Soft Matter* **2011,** *7* (8), 3897-3905.
58. Fleming, S.; Debnath, S.; Frederix, P. W. J. M.; Hunt, N. T.; Ulijn, R. V., Insights into the Coassembly of Hydrogelators and Surfactants Based on Aromatic Peptide Amphiphiles. *Biomacromolecules* **2014,** *15* (4), 1171-1184.
59. Hughes, M.; Birchall, L. S.; Zuberi, K.; Aitken, L. A.; Debnath, S.; Javid, N.; Ulijn, R. V., Differential supramolecular organisation of Fmoc-dipeptides with hydrophilic terminal amino acid residues by biocatalytic self-assembly. *Soft Matter* **2012,** *8* (45), 11565-11574.
60. Hughes, M.; Xu, H.; Frederix, P. W. J. M.; Smith, A. M.; Hunt, N. T.; Tuttle, T.; Kinloch, I. A.; Ulijn, R. V., Biocatalytic self-assembly of 2D peptide-based nanostructures. *Soft Matter* **2011,** *7* (21), 10032-10038.
61. Yang, Z.; Gu, H.; Fu, D.; Gao, P.; Lam, J. K.; Xu, B., Enzymatic Formation of Supramolecular Hydrogels. *Advanced Materials* **2004,** *16* (16), 1440-1444.
62. Thornton, K.; Smith, A.; Merry, C. R.; Ulijn, R., Controlling stiffness in nanostructured hydrogels produced by enzymatic dephosphorylation. *Biochemical society transactions* **2009,** *37* (4), 660.
63. Fleming, S.; Debnath, S.; Frederix, P. W. J. M.; Tuttle, T.; Ulijn, R. V., Aromatic peptide amphiphiles: significance of the Fmoc moiety. *Chemical Communications* **2013,** *49* (90), 10587-10589.
64. Ryan, D. M.; Anderson, S. B.; Nilsson, B. L., The influence of side-chain halogenation on the self-assembly and hydrogelation of Fmoc-phenylalanine derivatives. *Soft Matter* **2010,** *6* (14), 3220-3231.
65. Hartgerink, J. D.; Beniash, E.; Stupp, S. I., Peptide-amphiphile nanofibers: a versatile scaffold for the preparation of self-assembling materials. *Proceedings of the National Academy of Sciences* **2002,** *99* (8), 5133-5138.
66. Beniash, E.; Hartgerink, J. D.; Storrie, H.; Stendahl, J. C.; Stupp, S. I., Self-assembling peptide amphiphile nanofiber matrices for cell entrapment. *Acta Biomater* **2005,** *1* (4), 387-397.
67. Yang, Z.; Ho, P.-L.; Liang, G.; Chow, K. H.; Wang, Q.; Cao, Y.; Guo, Z.; Xu, B., Using β-Lactamase to Trigger Supramolecular Hydrogelation. *Journal of the American Chemical Society* **2006,** *129* (2), 266-267.
68. Smith, A. M.; Williams, R. J.; Tang, C.; Coppo, P.; Collins, R. F.; Turner, M. L.; Saiani, A.; Ulijn, R. V., Fmoc-Diphenylalanine Self Assembles to a Hydrogel via a Novel Architecture Based on π-π Interlocked β-Sheets. *Advanced Materials* **2008,** *20* (1), 37-41.
69. Silva, G. A.; Czeisler, C.; Niece, K. L.; Beniash, E.; Harrington, D. A.; Kessler, J. A.; Stupp, S. I., Selective differentiation of neural progenitor cells by high-epitope density nanofibers. *Science* **2004,** *303* (5662), 1352-1355.
70. Zhou, M.; Smith, A. M.; Das, A. K.; Hodson, N. W.; Collins, R. F.; Ulijn, R. V.; Gough, J. E., Self-assembled peptide-based hydrogels as scaffolds for anchorage-dependent cells. *Biomaterials* **2009,** *30* (13), 2523-2530.

71. Wang, H.; Wang, Z.; Song, D.; Wang, J.; Gao, J.; Wang, L.; Kong, D.; Yang, Z., Enzyme-assisted formation of nanosphere: a potential carrier for hydrophobic compounds. *Nanotechnology* **2010,** *21* (15), 155602.
72. Wang, H.; Ren, C.; Song, Z.; Wang, L.; Chen, X.; Yang, Z., Enzyme-triggered self-assembly of a small molecule: a supramolecular hydrogel with leaf-like structures and an ultra-low minimum gelation concentration. *Nanotechnology* **2010,** *21* (22), 225606.
73. Shao, H.; Parquette, J. R., A π-conjugated hydrogel based on an Fmoc-dipeptide naphthalene diimide semiconductor. *Chemical Communications* **2010,** *46* (24), 4285-4287.
74. Fleming, S.; Frederix, P. W. J. M.; Ramos Sasselli, I.; Hunt, N. T.; Ulijn, R. V.; Tuttle, T., Assessing the Utility of Infrared Spectroscopy as a Structural Diagnostic Tool for β-Sheets in Self-Assembling Aromatic Peptide Amphiphiles. *Langmuir* **2013,** *29* (30), 9510-9515.
75. Xu, H. X.; Das, A. K.; Horie, M.; Shaik, M. S.; Smith, A. M.; Luo, Y.; Lu, X. F.; Collins, R.; Liem, S. Y.; Song, A. M., A.; Turner, ML; Xiao, P.; Kinloch, IA; Ulijn, RV. *Nanoscale* **2010,** *2* (6), 960-966.
76. Yang, Z.; Liang, G.; Xu, B., Supramolecular hydrogels based on [small beta]-amino acid derivatives. *Chemical Communications* **2006,** (7), 738-740.
77. Hughes, M.; Frederix, P. W.; Raeburn, J.; Birchall, L. S.; Sadownik, J.; Coomer, F. C.; Lin, I.-H.; Cussen, E. J.; Hunt, N. T.; Tuttle, T., Sequence/structure relationships in aromatic dipeptide hydrogels formed under thermodynamic control by enzyme-assisted self-assembly. *Soft Matter* **2012,** *8* (20), 5595-5602.
78. Thornton, K.; Abul-Haija, Y. M.; Hodson, N.; Ulijn, R. V., Mechanistic insights into phosphatase triggered self-assembly including enhancement of biocatalytic conversion rate. *Soft Matter* **2013,** *9* (39), 9430-9439.
79. Bai, S.; Pappas, C.; Debnath, S.; Frederix, P. W. J. M.; Leckie, J.; Fleming, S.; Ulijn, R. V., Stable Emulsions Formed by Self-Assembly of Interfacial Networks of Dipeptide Derivatives. *ACS nano* **2014,** *8* (7), 7005-7013.
80. Eckes, K. M.; Mu, X.; Ruehle, M. A.; Ren, P.; Suggs, L. J., β Sheets Not Required: Combined Experimental and Computational Studies of Self-Assembly and Gelation of the Ester-Containing Analogue of an Fmoc-Dipeptide Hydrogelator. *Langmuir* **2014,** *30* (18), 5287-5296.
81. Marchesan, S.; Easton, C. D.; Kushkaki, F.; Waddington, L.; Hartley, P. G., Tripeptide self-assembled hydrogels: unexpected twists of chirality. *Chemical Communications* **2012,** *48* (16), 2195-2197.
82. Moitra, P.; Kumar, K.; Kondaiah, P.; Bhattacharya, S., Efficacious Anticancer Drug Delivery Mediated by a pH‐Sensitive Self‐Assembly of a Conserved Tripeptide Derived from Tyrosine Kinase NGF Receptor. *Angewandte Chemie International Edition* **2014,** *53* (4), 1113-1117.
83. Marchesan, S.; Easton, C. D.; Styan, K. E.; Waddington, L. J.; Kushkaki, F.; Goodall, L.; McLean, K. M.; Forsythe, J. S.; Hartley, P. G., Chirality effects at each amino acid position on tripeptide self-assembly into hydrogel biomaterials. *Nanoscale* **2014,** *6* (10), 5172-5180.
84. Frederix, P. W. J. M.; Ulijn, R. V.; Hunt, N. T.; Tuttle, T., Virtual Screening for Dipeptide Aggregation: Toward Predictive Tools for Peptide Self-Assembly. *J Phys Chem Lett* **2011,** *2* (19), 2380-2384.

85. Frederix, P. W.; Scott, G. G.; Abul-Haija, Y. M.; Kalafatovic, D.; Pappas, C. G.; Javid, N.; Hunt, N. T.; Ulijn, R. V.; Tuttle, T., Exploring the sequence space for (tri-) peptide self-assembly to design and discover new hydrogels. *Nature chemistry* **2014**.
86. Tamamis, P.; Adler-Abramovich, L.; Reches, M.; Marshall, K.; Sikorski, P.; Serpell, L.; Gazit, E.; Archontis, G., Self-assembly of phenylalanine oligopeptides: insights from experiments and simulations. *Biophysical journal* **2009,** *96* (12), 5020-5029.
87. Adams, J. A., Kinetic and catalytic mechanisms of protein kinases. *Chem Rev* **2001,** *101* (8), 2271-2290.
88. Castelletto, V.; Cheng, G.; Greenland, B. W.; Hamley, I. W.; Harris, P. J. F., Tuning the self-assembly of the bioactive dipeptide l-carnosine by incorporation of a bulky aromatic substituent. *Langmuir* **2011,** *27* (6), 2980-2988.
89. Adams, D. J.; Butler, M. F.; Frith, W. J.; Kirkland, M.; Mullen, L.; Sanderson, P., A new method for maintaining homogeneity during liquid–hydrogel transitions using low molecular weight hydrogelators. *Soft Matter* **2009,** *5* (9), 1856-1862.
90. Stryer, L., Biochemistry, 1995. *Chapter* **1995,** *14*, 385.
91. Tang, C.; Ulijn, R. V.; Saiani, A., Effect of Glycine Substitution on Fmoc–Diphenylalanine Self-Assembly and Gelation Properties. *Langmuir* **2011,** *27* (23), 14438-14449.
92. Roy, S.; Javid, N.; Frederix, P. W. J. M.; Lamprou, D. A.; Urquhart, A. J.; Hunt, N. T.; Halling, P. J.; Ulijn, R. V., Dramatic Specific-Ion Effect in Supramolecular Hydrogels. *Chemistry – A European Journal* **2012,** *18* (37), 11723-11731.
93. Lin, Y.; Qiao, Y.; Tang, P.; Li, Z.; Huang, J., Controllable self-assembled laminated nanoribbons from dipeptide-amphiphile bearing azobenzene moiety. *Soft Matter* **2011,** *7* (6), 2762-2769.
94. Bhalerao, V.; Varghese, S.; Lele, A.; Badiger, M., Thermoreversible hydrogel based on radiation induced copolymerisation of poly (N-isopropyl acrylamide) and poly (ethylene oxide). *Polymer* **1998,** *39* (11), 2255-2260.
95. Li, C.; Alam, M. M.; Bolisetty, S.; Adamcik, J.; Mezzenga, R., New biocompatible thermo-reversible hydrogels from PNiPAM-decorated amyloid fibrils. *Chemical Communications* **2011,** *47* (10), 2913-2915.
96. Huang, Y.; Qiu, Z.; Xu, Y.; Shi, J.; Lin, H.; Zhang, Y., Supramolecular hydrogels based on short peptides linked with conformational switch. *Organic & biomolecular chemistry* **2011,** *9* (7), 2149-2155.
97. Raeburn, J.; McDonald, T. O.; Adams, D. J., Dipeptide hydrogelation triggered via ultraviolet light. *Chemical Communications* **2012,** *48* (75), 9355-9357.
98. Shi, J.; Gao, Y.; Yang, Z.; Xu, B., Exceptionally small supramolecular hydrogelators based on aromatic–aromatic interactions. *Beilstein journal of organic chemistry* **2011,** *7* (1), 167-172.
99. Sahoo, J. K.; Nalluri, S. K. M.; Javid, N.; Webb, H.; Ulijn, R. V., Biocatalytic amide condensation and gelation controlled by light. *Chemical Communications* **2014,** *50* (41), 5462-5464.
100. Williams, R. J.; Mart, R. J.; Ulijn, R. V., Exploiting biocatalysis in peptide self‐assembly. *Peptide Science* **2010,** *94* (1), 107-117.
101. Das, A. K.; Collins, R.; Ulijn, R. V., Exploiting Enzymatic (Reversed) Hydrolysis in Directed Self‐Assembly of Peptide Nanostructures. *Small* **2008,** *4* (2), 279-287.

102. Leckie, J.; Hope, A.; Hughes, M.; Debnath, S.; Fleming, S.; Wark, A. W.; Ulijn, R. V.; Haw, M. D., Nanopropulsion by biocatalytic self-assembly. *ACS nano* **2014,** *8* (9), 9580-9589.
103. Zelzer, M.; Todd, S. J.; Hirst, A. R.; McDonald, T. O.; Ulijn, R. V., Enzyme responsive materials: design strategies and future developments. *Biomaterials Science* **2013,** *1* (1), 11-39.
104. Yang, Z.; Xu, B., Supramolecular hydrogels based on biofunctional nanofibers of self-assembled small molecules. *Journal of Materials Chemistry* **2007,** *17* (23), 2385-2393.
105. Debnath, S.; Ulijn, R. V., Enzyme-Responsive Molecular Gels. *Functional Molecular Gels* **2013,** *1*, 95.
106. Abul-Haija, Y. M.; Roy, S.; Frederix, P. W. J. M.; Javid, N.; Jayawarna, V.; Ulijn, R. V., Biocatalytically Triggered Co-Assembly of Two-Component Core/Shell Nanofibers. *Small* **2014,** *10* (5), 973-979.
107. Wang, W.; Yang, Z.; Patanavanich, S.; Xu, B.; Chau, Y., Controlling self-assembly within nanospace for peptide nanoparticle fabrication. *Soft Matter* **2008,** *4* (8), 1617-1620.
108. Gao, Y.; Yang, Z.; Kuang, Y.; Ma, M. L.; Li, J.; Zhao, F.; Xu, B., Enzyme‐instructed self‐assembly of peptide derivatives to form nanofibers and hydrogels. *Peptide Science* **2010,** *94* (1), 19-31.
109. Yang, Z.; Liang, G.; Xu, B., Enzymatic control of the self-assembly of small molecules: a new way to generate supramolecular hydrogels. *Soft Matter* **2007,** *3* (5), 515-520.
110. Chronopoulou, L.; Sennato, S.; Bordi, F.; Giannella, D.; Di Nitto, A.; Barbetta, A.; Dentini, M.; Togna, A. R.; Togna, G. I.; Moschini, S., Designing unconventional Fmoc-peptide-based biomaterials: structure and related properties. *Soft matter* **2014,** *10* (12), 1944-1952.
111. Nalluri, S. K. M.; Berdugo, C.; Javid, N.; Frederix, P. W.; Ulijn, R. V., Biocatalytic Self‐Assembly of Supramolecular Charge‐Transfer Nanostructures Based on n‐Type Semiconductor‐Appended Peptides. *Angewandte Chemie International Edition* **2014,** *53* (23), 5882-5887.
112. Li, J.; Nowak, P.; Otto, S., Dynamic combinatorial libraries: From exploring molecular recognition to systems chemistry. *Journal of the American Chemical Society* **2013,** *135* (25), 9222-9239.
113. Corbett, P. T.; Leclaire, J.; Vial, L.; West, K. R.; Wietor, J.-L.; Sanders, J. K.; Otto, S., Dynamic combinatorial chemistry. *Chem Rev* **2006,** *106* (9), 3652-3711.
114. Rowan, S. J.; Cantrill, S. J.; Cousins, G. R.; Sanders, J. K.; Stoddart, J. F., Dynamic covalent chemistry. *Angewandte Chemie International Edition* **2002,** *41* (6), 898-952.
115. Mattia, E.; Otto, S., Supramolecular systems chemistry. *Nat Nanotechnol* **2015,** *10* (2), 111-119.
116. Roy, S.; Ulijn, R. V., Exploiting biocatalysis in the synthesis of supramolecular polymers. In *Enzymatic Polymerisation*, Springer: Berlin, 2010; pp 127-143.
117. Wang, J.; Liu, K.; Xing, R.; Yan, X., Peptide self-assembly: thermodynamics and kinetics. *Chemical Society Reviews* **2016,** *45* (20), 5589-5604.
118. Toledano, S.; Williams, R. J.; Jayawarna, V.; Ulijn, R. V., Enzyme-triggered self-assembly of peptide hydrogels via reversed hydrolysis. *Journal of the American Chemical Society* **2006,** *128* (4), 1070-1071.

119. Guilbaud, J.-B.; Rochas, C.; Miller, A. F.; Saiani, A., Effect of enzyme concentration of the morphology and properties of enzymatically triggered peptide hydrogels. *Biomacromolecules* **2013,** *14* (5), 1403-1411.
120. Boekhoven, J.; Poolman, J. M.; Maity, C.; Li, F.; van der Mee, L.; Minkenberg, C. B.; Mendes, E.; van Esch, J. H.; Eelkema, R., Catalytic control over supramolecular gel formation. *Nature chemistry* **2013,** *5* (5), 433-437.
121. Javid, N.; Vogtt, K.; Roy, S.; Hirst, A. R.; Hoell, A.; Hamley, I. W.; Ulijn, R. V.; Sefcik, J., Supramolecular structures of enzyme clusters. *The journal of physical chemistry letters* **2011,** *2* (12), 1395-1399.
122. Debnath, S.; Roy, S.; Ulijn, R. V., Peptide Nanofibers with Dynamic Instability through Nonequilibrium Biocatalytic Assembly. *Journal of the American Chemical Society* **2013,** *135* (45), 16789-16792.
123. Pappas, C. G.; Mutasa, T.; Frederix, P. W. J. M.; Fleming, S.; Bai, S.; Debnath, S.; Kelly, S. M.; Gachagan, A.; Ulijn, R. V., Transient supramolecular reconfiguration of peptide nanostructures using ultrasound. *Materials Horizons* **2015,** *2* (2), 198-202.
124. Cosgrove, T., *Colloid science: principles, methods and applications*. John Wiley & Sons: 2010.
125. Tadros, T., Formulation of Liquid/Liquid Dispersions (Emulsions). In *Formulation of Disperse Systems*, Tadros, T., Ed. Wiley-VCH Verlag GmbH & Co. KGaA: 2014; pp 161-202.
126. Vincent, B., Emulsions. In *Colloid Science: Principles, Methods and Applications*, Second ed.; Cosgrove, T., Ed. Wiley-VCH Verlag GmbH & Co. KGaA: 2014; pp 117-133.
127. Holmberg, K.; Jönsson, B.; Kronberg, B.; Lindman, B., Surfactants and polymers in aqueous solution. *Journal of Synthetic Lubrication* **2004,** *20* (4), 367-370.
128. Jonsson, B., *Surfactants and polymers in aqueous solution*. John Wiley & Sons: New York, U.S.A., 1998.
129. Eastoe, J., Microemulsions. In *Colloid Science: Principles, Methods and Applications*, Second ed.; Cosgrove, T., Ed. Wiley-VCH Verlag GmbH & Co. KGaA: 2014; pp 91-115.
130. Tadros, T., Formulation of Microemulsions. In *Formulation of Disperse Systems*, Wiley-VCH Verlag GmbH & Co. KGaA: 2014; pp 301-324.
131. Liu, Y.; Jessop, P. G.; Cunningham, M.; Eckert, C. A.; Liotta, C. L., Switchable surfactants. *Science* **2006,** *313* (5789), 958-960.
132. Xu, J.; Zhang, Y.; Chen, H.; Wang, P.; Xie, Z.; Yao, Y.; Yan, Y.; Zhang, J., Effect of surfactant headgroups on the oil/water interface: An interfacial tension measurement and simulation study. *Journal of Molecular Structure* **2013,** *1052* (0), 50-56.
133. Chappat, M., Some applications of emulsions. *Colloids and Surfaces A: Physicochemical and Engineering Aspects* **1994,** *91*, 57-77.
134. Kronberg, B.; Holmberg, K.; Lindman, B., *Surface chemistry of surfactants and polymers*. John Wiley & Sons: Queensland, Australia, 2014.
135. Bancroft, W. D., The theory of emulsification, V. *The Journal of Physical Chemistry* **1913,** *17* (6), 501-519.
136. McClements, D. J., *Food emulsions: principles, practices, and techniques*. 4th ed.; CRC press: London, England, 2015.

137. Jafari, S. M.; Assadpoor, E.; He, Y.; Bhandari, B., Re-coalescence of emulsion droplets during high-energy emulsification. *Food hydrocolloids* **2008,** *22* (7), 1191-1202.
138. Lobo, L.; Svereika, A.; Nair, M., Coalescence during emulsification: 1. Method development. *Journal of colloid and interface science* **2002,** *253* (2), 409-418.
139. Lobo, L.; Svereika, A., Coalescence during emulsification: 2. Role of small molecule surfactants. *Journal of colloid and interface science* **2003,** *261* (2), 498-507.
140. Sjoblom, J., *Emulsions and Emulsion Stability: Surfactant Science Series*. 2nd ed.; CRC Press: London, England, 2005; Vol. 132.
141. Soares, A.; Guieysse, B.; Jefferson, B.; Cartmell, E.; Lester, J., Nonylphenol in the environment: a critical review on occurrence, fate, toxicity and treatment in wastewaters. *Environment international* **2008,** *34* (7), 1033-1049.
142. Guzey, D.; McClements, D. J., Formation, stability and properties of multilayer emulsions for application in the food industry. *Advances in Colloid and Interface Science* **2006,** *128–130*, 227-248.
143. Holmberg, K., Natural surfactants. *Current Opinion in Colloid & Interface Science* **2001,** *6* (2), 148-159.
144. Nesterenko, A.; Drelich, A.; Lu, H.; Clausse, D.; Pezron, I., Influence of a mixed particle/surfactant emulsifier system on water-in-oil emulsion stability. *Colloids and Surfaces A: Physicochemical and Engineering Aspects* **2014**.
145. Chevalier, Y.; Bolzinger, M.-A., Emulsions stabilized with solid nanoparticles: Pickering emulsions. *Colloids and Surfaces A: Physicochemical and Engineering Aspects* **2013,** *439*, 23-34.
146. Pickering, S. U. M., Pickering emulsions. *Journal of the Chemical Society Transactions* **1907,** *91* (23), 2001-2021.
147. Liu, P.; Lu, W.; Wang, W.-J.; Li, B.-G.; Zhu, S., Highly CO2/N2-Switchable Zwitterionic Surfactant for Pickering Emulsions at Ambient Temperature. *Langmuir* **2014,** *30* (34), 10248-10255.
148. Scott, G.; Roy, S.; Abul-Haija, Y. M.; Fleming, S.; Bai, S.; Ulijn, R. V., Pickering Stabilized Peptide Gel Particles as Tunable Microenvironments for Biocatalysis. *Langmuir* **2013,** *29* (46), 14321-14327.
149. Tang, C.; Qiu, F.; Zhao, X., Molecular Design and Applications of Self-Assembling Surfactant-Like Peptides. *Journal of Nanomaterials* **2013,** *2013*, 9.
150. Hanson, J. A.; Chang, C. B.; Graves, S. M.; Li, Z.; Mason, T. G.; Deming, T. J., Nanoscale double emulsions stabilized by single-component block copolypeptides. *Nature* **2008,** *455* (7209), 85-88.
151. Antipov, A. A.; Sukhorukov, G. B.; Donath, E.; Möhwald, H., Sustained release properties of polyelectrolyte multilayer capsules. *The Journal of Physical Chemistry B* **2001,** *105* (12), 2281-2284.
152. Zou, S.; Yang, Y.; Liu, H.; Wang, C., Synergistic stabilization and tunable structures of Pickering high internal phase emulsions by nanoparticles and surfactants. *Colloids and Surfaces A: Physicochemical and Engineering Aspects* **2013,** *436*, 1-9.
153. Binks, B. P.; Desforges, A.; Duff, D. G., Synergistic Stabilization of Emulsions by a Mixture of Surface-Active Nanoparticles and Surfactant. *Langmuir* **2006,** *23* (3), 1098-1106.

154. Heeres, A.; van der Pol, C.; Stuart, M.; Friggeri, A.; Feringa, B. L.; van Esch, J., Orthogonal self-assembly of low molecular weight hydrogelators and surfactants. *Journal of the American Chemical Society* **2003,** *125* (47), 14252-14253.
155. Brizard, A. M.; Stuart, M. C.; van Esch, J. H., Self-assembled interpenetrating networks by orthogonal self assembly of surfactants and hydrogelators. *Faraday discussions* **2009,** *143*, 345-357.
156. Laupheimer, M.; Sottmann, T.; Schweins, R.; Stubenrauch, C., Studying orthogonal self-assembled systems: microstructure of gelled bicontinuous microemulsions. *Soft matter* **2014,** *10* (43), 8744-8757.
157. Laupheimer, M.; Jovic, K.; Antunes, F. E.; Miguel, M. d. G. M.; Stubenrauch, C., Studying orthogonal self-assembled systems: phase behaviour and rheology of gelled microemulsions. *Soft Matter* **2013,** *9* (13), 3661-3670.
158. Benna-Zayani, M.; Kbir-Ariguib, N.; Trabelsi-Ayadi, M.; Grossiord, J.-L., Stabilisation of W/O/W double emulsion by polysaccharides as weak gels. *Colloids and Surfaces A: Physicochemical and Engineering Aspects* **2008,** *316* (1), 46-54.
159. Sala, G.; de Wijk, R. A.; van de Velde, F.; van Aken, G. A., Matrix properties affect the sensory perception of emulsion-filled gels. *Food Hydrocolloids* **2008,** *22* (3), 353-363.
160. Kim, K.-H.; Renkema, J.; Van Vliet, T., Rheological properties of soybean protein isolate gels containing emulsion droplets. *Food Hydrocolloids* **2001,** *15* (3), 295-302.
161. Van Vliet, T., Rheological properties of filled gels. Influence of filler matrix interaction. *Colloid and Polymer Science* **1988,** *266* (6), 518-524.
162. Xiong, Y. L.; Aguilera, J. M.; Kinsella, J. E., Emulsified Milkfat Effects on Rheology of Acid‐Induced Milk Gels. *Journal of Food Science* **1991,** *56* (4), 920-925.
163. Zhao, X.-Y.; Xu, J.; Zheng, L.-Q.; Li, X.-W., Preparation of temperature-sensitive microemulsion-based gels formed from a triblock copolymer. *Colloids and Surfaces A: Physicochemical and Engineering Aspects* **2007,** *307* (1), 100-107.
164. Zhang, Z.; Liu, G.; Bell, S., Synthesis of Poly (solketal methacrylate)-b lock-poly (2-(dimethylamino) ethyl methacrylate) and Preparation of Nanospheres with Cross-Linked Shells. *Macromolecules* **2000,** *33* (21), 7877-7883.
165. Brenner, H., *Interfacial transport processes and rheology*. 1st ed.; Butterworth-Heinman: Boston, 1991.
166. Hailing, P. J.; Walstra, P., Protein‐stabilized foams and emulsions. *C R C Critical Reviews in Food Science and Nutrition* **1981,** *15* (2), 155-203.
167. Hermanson, K. D.; Huemmerich, D.; Scheibel, T.; Bausch, A. R., Engineered microcapsules fabricated from reconstituted spider silk. *Advanced Materials* **2007,** *19* (14), 1810-1815.
168. Yeh, J. I.; Du, S.; Tortajada, A.; Paulo, J.; Zhang, S., Peptergents: peptide detergents that improve stability and functionality of a membrane protein, glycerol-3-phosphate dehydrogenase. *Biochemistry* **2005,** *44* (51), 16912-16919.
169. Zhao, X., Design of self-assembling surfactant-like peptides and their applications. *Current Opinion in Colloid & Interface Science* **2009,** *14* (5), 340-348.
170. Rozkiewicz, D. I.; Myers, B. D.; Stupp, S. I., Interfacial Self-Assembly of Cell-like Filamentous Microcapsules. *Angew. Chem.-Int. Edit.* **2011,** *50* (28), 6324-6327.

171. Vauthey, S.; Santoso, S.; Gong, H.; Watson, N.; Zhang, S., Molecular self-assembly of surfactant-like peptides to form nanotubes and nanovesicles. *Proceedings of the National Academy of Sciences* **2002,** *99* (8), 5355-5360.
172. Adams, D. J.; Holtzmann, K.; Schneider, C.; Butler, M. F., Self-assembly of surfactant-like peptides. *Langmuir* **2007,** *23* (25), 12729-12736.
173. Yang, S. J.; Zhang, S., Self-assembling behavior of designer lipid-like peptides. *Supramolecular Chemistry* **2006,** *18* (5), 389-396.
174. Morikawa, M.-a.; Yoshihara, M.; Endo, T.; Kimizuka, N., α-Helical Polypeptide Microcapsules Formed by Emulsion-Templated Self-Assembly. *Chemistry – A European Journal* **2005,** *11* (5), 1574-1578.
175. Dexter, A. F.; Middelberg, A. P., Peptides as functional surfactants. *Industrial & Engineering Chemistry Research* **2008,** *47* (17), 6391-6398.
176. Malcolm, A. S.; Dexter, A. F.; Middelberg, A. P. J., Foaming properties of a peptide designed to form stimuli-responsive interfacial films. *Soft Matter* **2006,** *2* (12), 1057-1066.
177. Middelberg, A. P. J.; He, L.; Dexter, A. F.; Shen, H. H.; Holt, S. A.; Thomas, R. K., The interfacial structure and Young's modulus of peptide films having switchable mechanical properties. *Journal of The Royal Society Interface* **2008,** *5* (18), 47-54.
178. Dexter, A. F.; Middelberg, A. P. J., Switchable peptide surfactants with designed metal binding capacity. *The Journal of Physical Chemistry C* **2007,** *111* (28), 10484-10492.
179. Jones, D. B.; Middelberg, A. P. J., Interfacial protein networks and their impact on droplet breakup. *AIChE journal* **2003,** *49* (6), 1533-1541.
180. Middelberg, A. P. J.; Radke, C. J.; Blanch, H. W., Peptide interfacial adsorption is kinetically limited by the thermodynamic stability of self association. *Proceedings of the National Academy of Sciences* **2000,** *97* (10), 5054-5059.
181. Vijay, R.; Polavarapu, P. L., FMOC-amino acid surfactants: discovery, characterization and chiroptical spectroscopy. *The Journal of Physical Chemistry A* **2012,** *116* (44), 10759-10769.
182. Scott, G. G.; McKnight, P. J.; Tuttle, T.; Ulijn, R. V., Tripeptide Emulsifiers. *Advanced Materials* **2016,** *28* (7), 1329-1329.
183. Texter, J., *Reactions and synthesis in surfactant systems*. CRC Press: London, England, 2001.
184. Zhu, Y.; Jiang, J.; Cui, Z.; Binks, B. P., Responsive aqueous foams stabilised by silica nanoparticles hydrophobised in situ with a switchable surfactant. *Soft matter* **2014,** *10* (48), 9739-9745.
185. Schramm, L. L., *Surfactants: fundamentals and applications in the petroleum industry*. Cambridge University Press: Cambridge, England, 2000.
186. Austad, T.; Milter, J., Surfactant flooding in enhanced oil recovery. *Surfactants: Fundamentals and Applications in the Petroleum Industry* **2000**, 203-249.
187. Cheng, C. C.; Lin, I.; Chen, J. K.; Liao, Z. S.; Huang, J. J.; Lee, D. J.; Xin, Z., Nucleobase‐Functionalized Supramolecular Micelles with Tunable Physical Properties for Efficient Controlled Drug Release. *Macromolecular Bioscience* **2016,** *16* (10), 1415-1421.
188. Lochhead, R. Y.; Hemker, W. J.; Castaneda, J. Y., Hydrophobically modified Carbopol resins. *Soap cosmetics chemical specialties* **1987,** *63* (5), 28.

189. Jessop, P. G.; Mercer, S. M.; Heldebrant, D. J., CO 2-triggered switchable solvents, surfactants, and other materials. *Energy & Environmental Science* **2012,** *5* (6), 7240-7253.
190. Chevallier, E.; Monteux, C.; Lequeux, F.; Tribet, C., Photofoams: remote control of foam destabilization by exposure to light using an azobenzene surfactant. *Langmuir* **2012,** *28* (5), 2308-2312.
191. Khoukh, S.; Perrin, P.; Bes de Berc, F.; Tribet, C., Reversible Light ‐ Triggered Control of Emulsion Type and Stability. *ChemPhysChem* **2005,** *6* (10), 2009-2012.
192. Sakai, H.; Matsumura, A.; Yokoyama, S.; Saji, T.; Abe, M., Photochemical switching of vesicle formation using an azobenzene-modified surfactant. *The Journal of Physical Chemistry B* **1999,** *103* (49), 10737-10740.
193. Alava, C.; Saunders, B. R., Temperature-responsive emulsions: The effect of added surfactant. *Colloids and Surfaces A: Physicochemical and Engineering Aspects* **2005,** *270–271*, 18-25.
194. Binks, B. P.; Murakami, R.; Armes, S. P.; Fujii, S., Temperature ‐ Induced Inversion of Nanoparticle ‐ Stabilized Emulsions. *Angewandte Chemie* **2005,** *117* (30), 4873-4876.
195. Koh, A. Y.; Saunders, B. R., Thermally induced gelation of an oil-in-water emulsion stabilised by a graft copolymer. *Chemical Communications* **2000,** (24), 2461-2462.
196. Patel, A. R.; Drost, E.; ten Hoorn, J. S.; Velikov, K. P., Fabrication and characterization of emulsions with pH responsive switchable behavior. *Soft Matter* **2013,** *9* (29), 6747-6751.
197. Minkenberg, C. B.; Florusse, L.; Eelkema, R.; Koper, G. J. M.; van Esch, J. H., Triggered Self-Assembly of Simple Dynamic Covalent Surfactants. *Journal of the American Chemical Society* **2009,** *131* (32), 11274-11275.
198. Malcolm, A. S.; Dexter, A. F.; Middelberg, A. P., Foaming properties of a peptide designed to form stimuli-responsive interfacial films. *Soft Matter* **2006,** *2* (12), 1057-1066.
199. Huang, X.-F.; Xiong, Y.; Yin, W.; Lu, L.; Liu, J.; Peng, K., Demulsification of a new magnetically responsive bacterial demulsifier for water-in-oil emulsions. *Energy & Fuels* **2016,** *30* (6), 5190-5197.
200. Besnard, L.; Marchal, F.; Paredes, J. F.; Daillant, J.; Pantoustier, N.; Perrin, P.; Guenoun, P., Multiple Emulsions Controlled by Stimuli ‐ Responsive Polymers. *Advanced Materials* **2013,** *25* (20), 2844-2848.
201. Bai, S.; Debnath, S.; Gibson, K.; Schlicht, B.; Bayne, L.; Zagnoni, M.; Ulijn, R. V., Biocatalytic Self-Assembly of Nanostructured Peptide Microparticles using Droplet Microfluidics. *Small* **2014,** *10* (2), 285-93.
202. Dexter, A. F.; Malcolm, A. S.; Middelberg, A. P., Reversible active switching of the mechanical properties of a peptide film at a fluid–fluid interface. *Nature materials* **2006,** *5* (6), 502-506.
203. van Gunsteren, W. F.; Bakowies, D.; Baron, R.; Chandrasekhar, I.; Christen, M.; Daura, X.; Gee, P.; Geerke, D. P.; Glättli, A.; Hünenberger, P. H., Biomolecular modeling: goals, problems, perspectives. *Angewandte Chemie International Edition* **2006,** *45* (25), 4064-4092.
204. McCammon, J., Molecular dynamics study of the bovine pancreatic trypsin inhibitor. *Models for Protein Dynamics* **1976**, 137.

205. Adcock, S. A.; McCammon, J. A., Molecular dynamics: survey of methods for simulating the activity of proteins. *Chem Rev* **2006,** *106* (5), 1589-1615.
206. Karplus, M.; Kuriyan, J., Molecular dynamics and protein function. *Proceedings of the National Academy of Sciences of the United States of America* **2005,** *102* (19), 6679-6685.
207. Mu, X.; Eckes, K. M.; Nguyen, M. M.; Suggs, L. J.; Ren, P., Experimental and computational studies reveal an alternative supramolecular structure for Fmoc-dipeptide self-assembly. *Biomacromolecules* **2012,** *13* (11), 3562-3571.
208. Born, M.; Oppenheimer, R., Zur quantentheorie der molekeln. *Annalen der Physik* **1927,** *389* (20), 457-484.
209. Jensen, F., *Introduction to computational chemistry*. 2nd ed.; John Wiley & Sons: Queensland, Australia, 2013.
210. Leach, A. R., *Molecular modelling: principles and applications*. 2nd ed.; Pearson Education: Oxford, England, 2001.
211. Brooks, B. R.; Brooks, C. L.; MacKerell, A. D.; Nilsson, L.; Petrella, R. J.; Roux, B.; Won, Y.; Archontis, G.; Bartels, C.; Boresch, S., CHARMM: the biomolecular simulation program. *Journal of computational chemistry* **2009,** *30* (10), 1545-1614.
212. Vanommeslaeghe, K.; Hatcher, E.; Acharya, C.; Kundu, S.; Zhong, S.; Shim, J.; Darian, E.; Guvench, O.; Lopes, P.; Vorobyov, I., CHARMM general force field: A force field for drug‐like molecules compatible with the CHARMM all‐atom additive biological force fields. *Journal of computational chemistry* **2010,** *31* (4), 671-690.
213. Marrink, S. J.; De Vries, A. H.; Mark, A. E., Coarse grained model for semiquantitative lipid simulations. *The Journal of Physical Chemistry B* **2004,** *108* (2), 750-760.
214. Marrink, S. J.; Risselada, H. J.; Yefimov, S.; Tieleman, D. P.; De Vries, A. H., The MARTINI force field: coarse grained model for biomolecular simulations. *The Journal of Physical Chemistry B* **2007,** *111* (27), 7812-7824.
215. Monticelli, L.; Kandasamy, S. K.; Periole, X.; Larson, R. G.; Tieleman, D. P.; Marrink, S.-J., The MARTINI coarse-grained force field: extension to proteins. *Journal of chemical theory and computation* **2008,** *4* (5), 819-834.
216. Zhang, H.; Wang, H.; Xu, G.; Yuan, S., A molecular dynamics simulation of N-(fluorenyl-9-methoxycarbonyl)-dipeptides supramolecular hydrogel. *Colloids and Surfaces A: Physicochemical and Engineering Aspects* **2013,** *417* (0), 217-223.
217. Marrink, S. J.; Tieleman, D. P., Perspective on the Martini model. *Chemical Society Reviews* **2013,** *42* (16), 6801-6822.
218. de Jong, D. H.; Singh, G.; Bennett, W. D.; Arnarez, C.; Wassenaar, T. A.; Schäfer, L. V.; Periole, X.; Tieleman, D. P.; Marrink, S. J., Improved parameters for the martini coarse-grained protein force field. *Journal of Chemical Theory and Computation* **2012,** *9* (1), 687-697.
219. Palma, C.-A.; Cecchini, M.; Samori, P., Predicting self-assembly: from empirism to determinism. *Chemical Society Reviews* **2012,** *41* (10), 3713-3730.
220. Bellesia, G.; Shea, J.-E., What determines the structure and stability of KFFE monomers, dimers, and protofibrils? *Biophysical journal* **2009,** *96* (3), 875-886.
221. Hauser, C. A.; Deng, R.; Mishra, A.; Loo, Y.; Khoe, U.; Zhuang, F.; Cheong, D. W.; Accardo, A.; Sullivan, M. B.; Riekel, C., Natural tri-to hexapeptides self-assemble in

water to amyloid β-type fiber aggregates by unexpected α-helical intermediate structures. *Proceedings of the National Academy of Sciences* **2011,** *108* (4), 1361-1366.
222. López-Pérez, D. E.; Revilla-López, G.; Hamley, I.; Alemán, C., Molecular insights into aggregates made of amphiphilic Fmoc-tetrapeptides. *Soft Matter* **2013,** *9* (46), 11021-11032.
223. Fletcher, J. M.; Harniman, R. L.; Barnes, F. R.; Boyle, A. L.; Collins, A.; Mantell, J.; Sharp, T. H.; Antognozzi, M.; Booth, P. J.; Linden, N., Self-assembling cages from coiled-coil peptide modules. *Science* **2013,** *340* (6132), 595-599.
224. Castelletto, V.; Moulton, C. M.; Cheng, G.; Hamley, I. W.; Hicks, M. R.; Rodger, A.; López-Pérez, D. E.; Revilla-López, G.; Alemán, C., Self-assembly of Fmoc-tetrapeptides based on the RGDS cell adhesion motif. *Soft Matter* **2011,** *7* (24), 11405-11415.
225. Caruso, M.; Gatto, E.; Placidi, E.; Ballano, G.; Formaggio, F.; Toniolo, C.; Zanuy, D.; Alemán, C.; Venanzi, M., A single-residue substitution inhibits fibrillization of Ala-based pentapeptides. A spectroscopic and molecular dynamics investigation. *Soft matter* **2014,** *10* (15), 2508-2519.
226. Xu, H.; Das, A. K.; Horie, M.; Shaik, M. S.; Smith, A. M.; Luo, Y.; Lu, X.; Collins, R.; Liem, S. Y.; Song, A., An investigation of the conductivity of peptide nanotube networks prepared by enzyme-triggered self-assembly. *Nanoscale* **2010,** *2* (6), 960-966.
227. Yu, T.; Schatz, G. C., Free energy profile and mechanism of self-assembly of peptide amphiphiles based on a collective assembly coordinate. *The Journal of Physical Chemistry B* **2013,** *117* (30), 9004-9013.
228. Guo, C.; Luo, Y.; Zhou, R.; Wei, G., Probing the self-assembly mechanism of diphenylalanine-based peptide nanovesicles and nanotubes. *ACS nano* **2012,** *6* (5), 3907-3918.
229. Lee, O.-S.; Cho, V.; Schatz, G. C., Modeling the self-assembly of peptide amphiphiles into fibers using coarse-grained molecular dynamics. *Nano letters* **2012,** *12* (9), 4907-4913.
230. Khalfa, A.; Treptow, W.; Maigret, B.; Tarek, M., Self assembly of peptides near or within membranes using coarse grained MD simulations. *Chemical Physics* **2009,** *358* (1), 161-170.
231. Villa, A.; Peter, C.; van der Vegt, N. F., Self-assembling dipeptides: conformational sampling in solvent-free coarse-grained simulation. *Physical Chemistry Chemical Physics* **2009,** *11* (12), 2077-2086.
232. Zheng, X.; Wang, D.; Shuai, Z., Coarse-grained molecular dynamics simulations of photoswitchable assembly and disassembly. *Nanoscale* **2013,** *5* (9), 3681-3689.
233. Yu, T.; Schatz, G. C., Free-energy landscape for peptide amphiphile self-assembly: stepwise versus continuous assembly mechanisms. *The Journal of Physical Chemistry B* **2013,** *117* (45), 14059-14064.
234. Sasselli, I. R.; Pappas, C. G.; Matthews, E.; Wang, T.; Hunt, N. T.; Ulijn, R. V.; Tuttle, T., Using experimental and computational energy equilibration to understand hierarchical self-assembly of Fmoc-dipeptide amphiphiles. *Soft Matter* **2016,** *12* (40), 8307-8315.

235. Nesterenko, A.; Drelich, A.; Lu, H.; Clausse, D.; Pezron, I., Influence of a mixed particle/surfactant emulsifier system on water-in-oil emulsion stability. *Colloids and Surfaces A: Physicochemical and Engineering Aspects* **2014,** *457*, 49-57.
236. Tang, C.; Qiu, F.; Zhao, X., Molecular design and applications of self-assembling surfactant-like peptides. *Journal of Nanomaterials* **2013,** *2013*, 15.
237. Morikawa, M. a.; Yoshihara, M.; Endo, T.; Kimizuka, N., α - Helical Polypeptide Microcapsules Formed by Emulsion - Templated Self - Assembly. *Chemistry-A European Journal* **2005,** *11* (5), 1574-1578.
238. Qian, Y.; Zhang, Q.; Qiu, X.; Zhu, S., CO2-responsive diethylaminoethyl-modified lignin nanoparticles and their application as surfactants for CO2/N2-switchable Pickering emulsions. *Green Chemistry* **2014,** *16* (12), 4963-4968.
239. Appel, E. A.; del Barrio, J.; Loh, X. J.; Scherman, O. A., Supramolecular polymeric hydrogels. *Chemical Society Reviews* **2012,** *41* (18), 6195-6214.
240. van Esch, J. H., We Can Design Molecular Gelators, But Do We Understand Them? *Langmuir* **2009,** *25* (15), 8392-8394.
241. Hirst, A. R.; Escuder, B.; Miravet, J. F.; Smith, D. K., High - Tech Applications of Self - Assembling Supramolecular Nanostructured Gel - Phase Materials: From Regenerative Medicine to Electronic Devices. *Angewandte Chemie International Edition* **2008,** *47* (42), 8002-8018.
242. Wang, W.; Chau, Y., Self-assembled peptide nanorods as building blocks of fractal patterns. *Soft Matter* **2009,** *5* (24), 4893-4898.
243. Sadownik, J. W.; Leckie, J.; Ulijn, R. V., Micelle to fibre biocatalytic supramolecular transformation of an aromatic peptide amphiphile. *Chemical Communications* **2011,** *47* (2), 728-730.
244. Klionsky, D. J.; Emr, S. D., Membrane protein sorting: biosynthesis, transport and processing of yeast vacuolar alkaline phosphatase. *The EMBO Journal* **1989,** *8* (8), 2241.
245. Klibanov, A. M., Improving enzymes by using them in organic solvents. *Nature* **2001,** *409* (6817), 241-246.
246. Bell, G.; Halling, P. J.; Moore, B. D.; Partridge, J.; Rees, D. G., Biocatalyst behaviour in low-water systems. *Trends in Biotechnology* **1995,** *13* (11), 468-473.
247. Laane, C.; Boeren, S.; Vos, K.; Veeger, C., Rules for optimization of biocatalysis in organic solvents. *Biotechnology and Bioengineering* **1987,** *30* (1), 81-87.
248. Yan, C.; Pochan, D. J., Rheological properties of peptide-based hydrogels for biomedical and other applications. *Chemical Society Reviews* **2010,** *39* (9), 3528-3540.
249. Cheng, G.; Castelletto, V.; Moulton, C.; Newby, G.; Hamley, I., Hydrogelation and self-assembly of Fmoc-tripeptides: unexpected influence of sequence on self-assembled fibril structure, and hydrogel modulus and anisotropy. *Langmuir* **2010,** *26* (7), 4990-4998.
250. Chen, L.; Morris, K.; Laybourn, A.; Elias, D.; Hicks, M. R.; Rodger, A.; Serpell, L.; Adams, D. J., Self-assembly mechanism for a naphthalene– dipeptide leading to hydrogelation. *Langmuir* **2009,** *26* (7), 5232-5242.
251. Ghose, A. K.; Viswanadhan, V. N.; Wendoloski, J. J., Prediction of hydrophobic (lipophilic) properties of small organic molecules using fragmental methods: an analysis of ALOGP and CLOGP methods. *The Journal of Physical Chemistry A* **1998,** *102* (21), 3762-3772.

252. Pallen, C. J.; Wang, J. H., Calmodulin-stimulated dephosphorylation of p-nitrophenyl phosphate and free phosphotyrosine by calcineurin. *Journal of Biological Chemistry* **1983,** *258* (14), 8550-8553.
253. Butler, L. G., Enzymes in non-aqueous solvents. *Enzyme and microbial technology* **1979,** *1* (4), 253-259.
254. Batra, R.; Gupta, M. N., Enhancement of enzyme activity in aqueous-organic solvent mixtures. *Biotechnology letters* **1994,** *16* (10), 1059-1064.
255. Simopoulos, T. T.; Jencks, W. P., Alkaline phosphatase is an almost perfect enzyme. *Biochemistry* **1994,** *33* (34), 10375-10380.
256. Raeburn, J.; Chen, L.; Awhida, S.; Deller, R. C.; Vatish, M.; Gibson, M. I.; Adams, D. J., Using molecular rotors to probe gelation. *Soft matter* **2015,** *11* (18), 3706-3713.
257. Kirk, O.; Borchert, T. V.; Fuglsang, C. C., Industrial enzyme applications. *Current Opinion in Biotechnology* **2002,** *13* (4), 345-351.
258. Lods, L.; Dres, C.; Johnson, C.; Scholz, D.; Brooks, G., The future of enzymes in cosmetics. *International journal of cosmetic science* **2000,** *22* (2), 85-94.
259. Wildman, S. A.; Crippen, G. M., Prediction of physicochemical parameters by atomic contributions. *Journal of chemical information and computer sciences* **1999,** *39* (5), 868-873.
260. Broto, P.; Moreau, G.; Vandycke, C., Molecular structures: perception, autocorrelation descriptor and sar studies: system of atomic contributions for the calculation of the n-octanol/water partition coefficients. *European journal of medicinal chemistry* **1984,** *19* (1), 71-78.
261. Phillips, J. C.; Braun, R.; Wang, W.; Gumbart, J.; Tajkhorshid, E.; Villa, E.; Chipot, C.; Skeel, R. D.; Kale, L.; Schulten, K., Scalable molecular dynamics with NAMD. *Journal of computational chemistry* **2005,** *26* (16), 1781-1802.
262. Sasselli, I. R.; Ulijn, R.; Tuttle, T., CHARMM force field parameterization protocol for self-assembling peptide amphiphiles: the Fmoc moiety. *Physical Chemistry Chemical Physics* **2016,** *18* (6), 4659-4667.
263. de Souza, O. N.; Ornstein, R. L., Effect of periodic box size on aqueous molecular dynamics simulation of a DNA dodecamer with particle-mesh Ewald method. *Biophysical journal* **1997,** *72* (6), 2395.
264. Feller, S. E.; Zhang, Y.; Pastor, R. W.; Brooks, B. R., Constant pressure molecular dynamics simulation: the Langevin piston method. *The Journal of chemical physics* **1995,** *103* (11), 4613-4621.
265. Hub, J. S.; De Groot, B. L.; Van Der Spoel, D., g_wham □ A Free Weighted Histogram Analysis Implementation Including Robust Error and Autocorrelation Estimates. *Journal of Chemical Theory and Computation* **2010,** *6* (12), 3713-3720.
266. Humphrey, W.; Dalke, A.; Schulten, K., VMD: visual molecular dynamics. *Journal of molecular graphics* **1996,** *14* (1), 33-38.
267. Balasuriya, T. S.; Dagastine, R. R., Interaction forces between bubbles in the presence of novel responsive peptide surfactants. *Langmuir* **2012,** *28* (50), 17230-17237.
268. Fameau, A. L.; Saint‐Jalmes, A.; Cousin, F.; Houinsou Houssou, B.; Novales, B.; Navailles, L.; Nallet, F.; Gaillard, C.; Boué, F.; Douliez, J. P., Smart foams: switching reversibly between ultrastable and unstable foams. *Angewandte Chemie International Edition* **2011,** *50* (36), 8264-8269.

269. Mart, R. J.; Osborne, R. D.; Stevens, M. M.; Ulijn, R. V., Peptide-based stimuli-responsive biomaterials. *Soft Matter* **2006,** *2* (10), 822-835.
270. Zhang, S., Fabrication of novel biomaterials through molecular self-assembly. *Nature biotechnology* **2003,** *21* (10), 1171-1178.
271. Tao, K.; Levin, A.; Adler-Abramovich, L.; Gazit, E., Fmoc-modified amino acids and short peptides: simple bio-inspired building blocks for the fabrication of functional materials. *Chemical Society Reviews* **2016,** *45* (14), 3935-3953.
272. Cui, H.; Webber, M. J.; Stupp, S. I., Self-assembly of peptide amphiphiles: From molecules to nanostructures to biomaterials. *Peptide Science* **2010,** *94* (1), 1-18.
273. Ryan, D. M.; Nilsson, B. L., Self-assembled amino acids and dipeptides as noncovalent hydrogels for tissue engineering. *Polymer Chemistry* **2012,** *3* (1), 18-33.
274. Roberts, D.; Rochas, C.; Saiani, A.; Miller, A., Effect of peptide and guest charge on the structural, mechanical and release properties of β-sheet forming peptides. *Langmuir* **2012,** *28* (46), 16196-16206.
275. Webber, M. J.; Newcomb, C. J.; Bitton, R.; Stupp, S. I., Switching of self-assembly in a peptide nanostructure with a specific enzyme. *Soft Matter* **2011,** *7* (20), 9665-9672.
276. Yucel, T.; Micklitsch, C. M.; Schneider, J. P.; Pochan, D. J., Direct observation of early-time hydrogelation in β-hairpin peptide self-assembly. *Macromolecules* **2008,** *41* (15), 5763-5772.
277. Ozbas, B.; Kretsinger, J.; Rajagopal, K.; Schneider, J. P.; Pochan, D. J., Salt-triggered peptide folding and consequent self-assembly into hydrogels with tunable modulus. *Macromolecules* **2004,** *37* (19), 7331-7337.
278. Veerman, C.; Rajagopal, K.; Palla, C. S.; Pochan, D. J.; Schneider, J. P.; Furst, E. M., Gelation kinetics of β-hairpin peptide hydrogel networks. *Macromolecules* **2006,** *39* (19), 6608-6614.
279. Niece, K. L.; Czeisler, C.; Sahni, V.; Tysseling-Mattiace, V.; Pashuck, E. T.; Kessler, J. A.; Stupp, S. I., Modification of gelation kinetics in bioactive peptide amphiphiles. *Biomaterials* **2008,** *29* (34), 4501-4509.
280. Tena-Solsona, M.; Escuder, B.; Miravet, J. F.; Casttelleto, V.; Hamley, I. W.; Dehsorkhi, A., Thermodynamic and Kinetic Study of the Fibrillization of a Family of Tetrapeptides and Its Application to Self-Sorting. What Takes So Long? *Chemistry of Materials* **2015,** *27* (9), 3358-3365.
281. Ramos Sasselli, I.; Halling, P. J.; Ulijn, R. V.; Tuttle, T., Supramolecular Fibers in Gels Can Be at Thermodynamic Equilibrium: A Simple Packing Model Reveals Preferential Fibril Formation versus Crystallization. *ACS nano* **2016,** *10* (2), 2661-2668.
282. Yang, Z.; Liang, G.; Ma, M.; Gao, Y.; Xu, B., In Vitro and In Vivo Enzymatic Formation of Supramolecular Hydrogels Based on Self‐Assembled Nanofibers of a β‐Amino Acid Derivative. *Small* **2007,** *3* (4), 558-562.
283. Decker, L. A.; Corporation, W. B., *Worthington Enzyme Manual: Enzymes, Enzyme Reagents, Related Biochemicals*. Worthington Biochemical Corporation: 1977.
284. Moreira, I. P.; Sasselli, I. R.; Cannon, D. A.; Hughes, M.; Lamprou, D. A.; Tuttle, T.; Ulijn, R. V., Enzymatically activated emulsions stabilised by interfacial nanofibre networks. *Soft Matter* **2016,** *12* (9), 2623-2631.

285. Solans, C.; Pons, R.; Zhu, S.; Davis, H. T.; Evans, D. F.; Nakamura, K.; Kunieda, H., Studies on macro-and microstructures of highly concentrated water-in-oil emulsions (gel emulsions). *Langmuir* **1993,** *9* (6), 1479-1482.
286. Li, Z.; Ming, T.; Wang, J.; Ngai, T., High internal phase emulsions stabilized solely by microgel particles. *Angewandte Chemie International Edition* **2009,** *48* (45), 8490-8493.
287. Izmailova, V.; Yampolskaya, G.; Tulovskaya, Z., Development of the Rehbinder's concept on structure-mechanical barrier in stability of dispersions stabilized with proteins. *Colloids and Surfaces A: Physicochemical and Engineering Aspects* **1999,** *160* (2), 89-106.
288. Wilde, P., Interfaces: their role in foam and emulsion behaviour. *Current Opinion in Colloid & Interface Science* **2000,** *5* (3), 176-181.
289. Hess, B.; Kutzner, C.; Van Der Spoel, D.; Lindahl, E., GROMACS 4: algorithms for highly efficient, load-balanced, and scalable molecular simulation. *Journal of chemical theory and computation* **2008,** *4* (3), 435-447.
290. Berendsen, H. J.; Postma, J. v.; van Gunsteren, W. F.; DiNola, A.; Haak, J., Molecular dynamics with coupling to an external bath. *The Journal of chemical physics* **1984,** *81* (8), 3684-3690.
291. http://www.cgmartini.nl/index.php/downloads/tools/204-martinize. *martinize.py*.
292. Torrie, G. M.; Valleau, J. P., Nonphysical sampling distributions in Monte Carlo free-energy estimation: Umbrella sampling. *Journal of Computational Physics* **1977,** *23* (2), 187-199.
293. Souaille, M.; Roux, B. t., Extension to the weighted histogram analysis method: combining umbrella sampling with free energy calculations. *Computer Physics Communications* **2001,** *135* (1), 40-57.
294. Verschueren, K., Handbook of environmental data on organic chemicals. **1983**.
295. Edelbach, D. J.; Lodge, K. B., Insights into the measurement of the octanol–water partition coefficient from experiments with acrylate esters. *Physical Chemistry Chemical Physics* **2000,** *2* (8), 1763-1771.
296. Adler-Abramovich, L.; Marco, P.; Arnon, Z. A.; Creasey, R. C. G.; Michaels, T. C. T.; Levin, A.; Scurr, D. J.; Roberts, C. J.; Knowles, T. P. J.; Tendler, S. J. B.; Gazit, E., Controlling the Physical Dimensions of Peptide Nanotubes by Supramolecular Polymer Coassembly. *ACS nano* **2016,** *10* (8), 7436-7442.
297. Liyanage, W.; Nilsson, B. L., Substituent Effects on the Self-Assembly/Coassembly and Hydrogelation of Phenylalanine Derivatives. *Langmuir* **2016,** *32* (3), 787-799.
298. Adhikari, B.; Nanda, J.; Banerjee, A., Multicomponent hydrogels from enantiomeric amino acid derivatives: helical nanofibers, handedness and self-sorting. *Soft Matter* **2011,** *7* (19), 8913-8922.
299. Colquhoun, C.; Draper, E. R.; Eden, E. G.; Cattoz, B. N.; Morris, K. L.; Chen, L.; McDonald, T. O.; Terry, A. E.; Griffiths, P. C.; Serpell, L. C., The effect of self-sorting and co-assembly on the mechanical properties of low molecular weight hydrogels. *Nanoscale* **2014,** *6* (22), 13719-13725.
300. Morris, K. L.; Chen, L.; Raeburn, J.; Sellick, O. R.; Cotanda, P.; Paul, A.; Griffiths, P. C.; King, S. M.; O'Reilly, R. K.; Serpell, L. C., Chemically programmed self-sorting of gelator networks. *Nature communications* **2013,** *4*, 1480.

301. Draper, E. R.; Eden, E. G.; McDonald, T. O.; Adams, D. J., Spatially resolved multicomponent gels. *Nature chemistry* **2015,** *7* (10), 848-852.
302. Brizard, A.; Stuart, M.; van Bommel, K.; Friggeri, A.; de Jong, M.; van Esch, J., Preparation of Nanostructures by Orthogonal Self‐Assembly of Hydrogelators and Surfactants. *Angewandte Chemie International Edition* **2008,** *47* (11), 2063-2066.
303. White, S. H.; Wimley, W. C., Hydrophobic interactions of peptides with membrane interfaces. *Biochimica et Biophysica Acta (BBA)-Reviews on Biomembranes* **1998,** *1376* (3), 339-352.
304. Banwell, E. F.; Abelardo, E. S.; Adams, D. J.; Birchall, M. A.; Corrigan, A.; Donald, A. M.; Kirkland, M.; Serpell, L. C.; Butler, M. F.; Woolfson, D. N., Rational design and application of responsive α-helical peptide hydrogels. *Nature materials* **2009,** *8* (7), 596-600.

I. Appendices

Appendix 1. Characterisation of non-enzymatically self-assembled Fmoc-YL in aqueous buffer

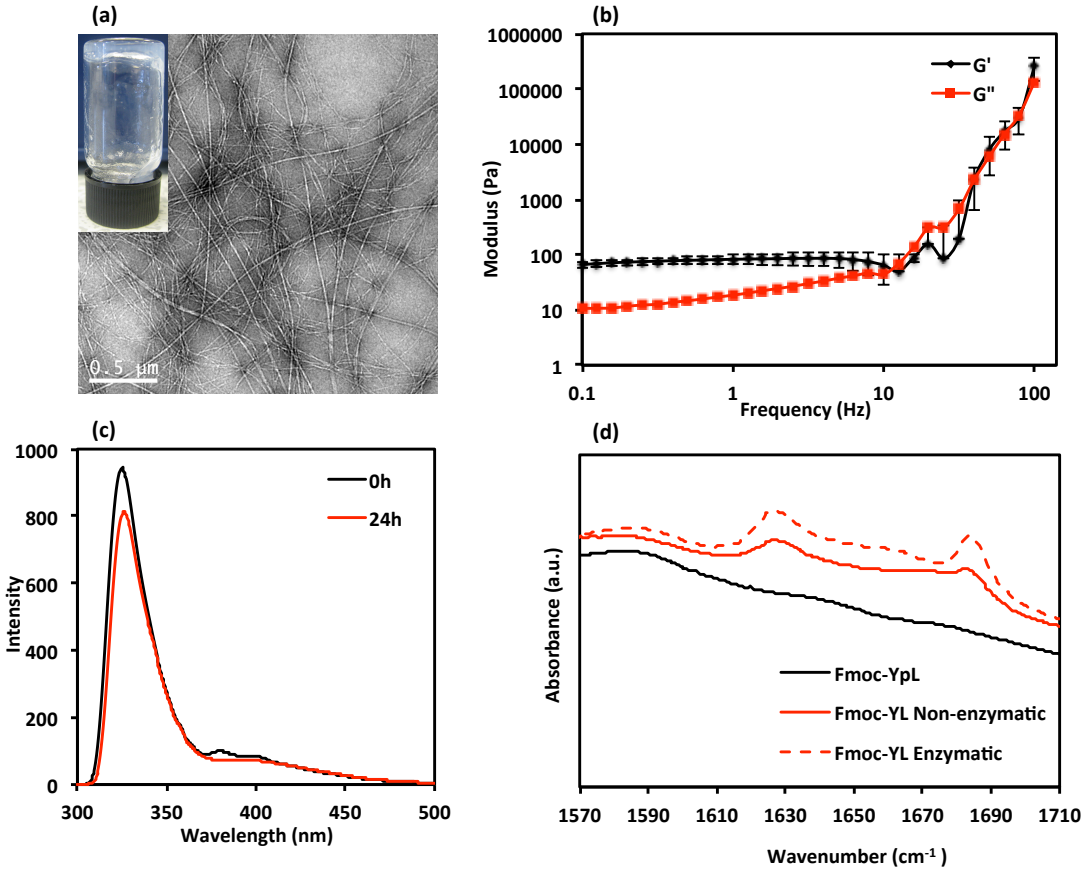

Figure I.1. Characterisation of non-enzymatically formed 10 mM Fmoc-YL in pH 8 0.6 M phosphate buffer, when heated to 80°C and gradually cooled down overnight: (a) TEM image showing thicker and less entangled nanofibres. Inset presents the macroscopic aspect of this hydrogel, as per vial inversion; (b) Rheological dynamic frequency sweep; (c) Fluorescence spectra of Fmoc-YL when compared with time zero, showing there is a small 1 nm red-shift occurring, however showing the disappearance of the peak related to the micellar aggregates; (d) FTIR spectrum when compared with the previously presented samples, showing it forms a less well-ordered H-bonding network than the enzymatically-triggered Fmoc-YL.

Appendix 2. TEM imaging of biphasic aqueous/chloroform samples

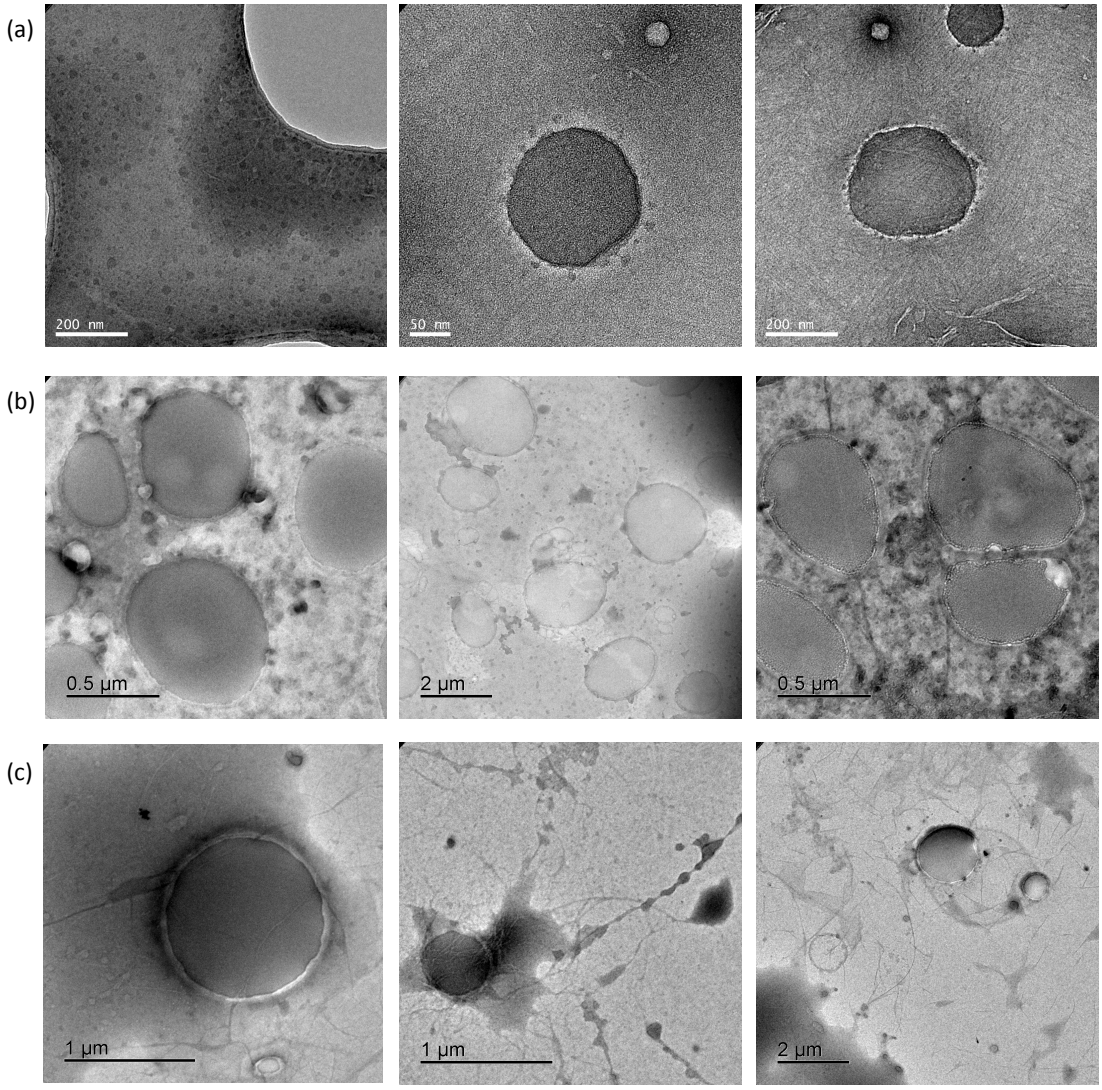

Figure I.2. TEM images obtained 24 h after preparation: (a) Fmoc-YpL control with no alkaline phosphatase; (b) 2.5 mM Fmoc-YpL in aqueous buffer added AP, left for 24 h and then added chloroform and hand-shaked; (c) Fmoc-YpL de-emulsified mixture added AP after 1 month storage.

Appendix 3. Fluorescence microscopy images of Fmoc-YL produced enzymatically

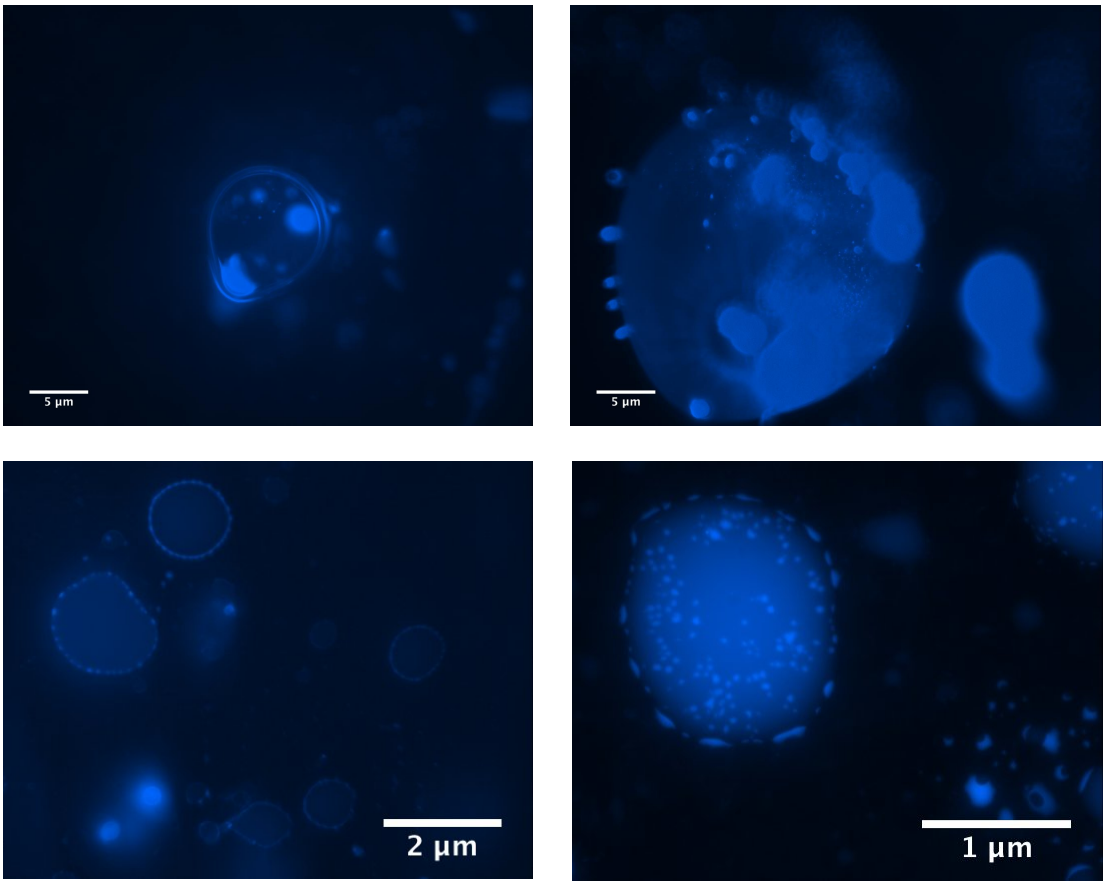

Figure I.3. Fluorescence microscopy images of chloroform-in water emulsion stabilised by Fmoc-YL when enzymatically formed.

Appendix 4. Characterisation of non-enzymatically self-assembled Fmoc-YL in a biphasic system

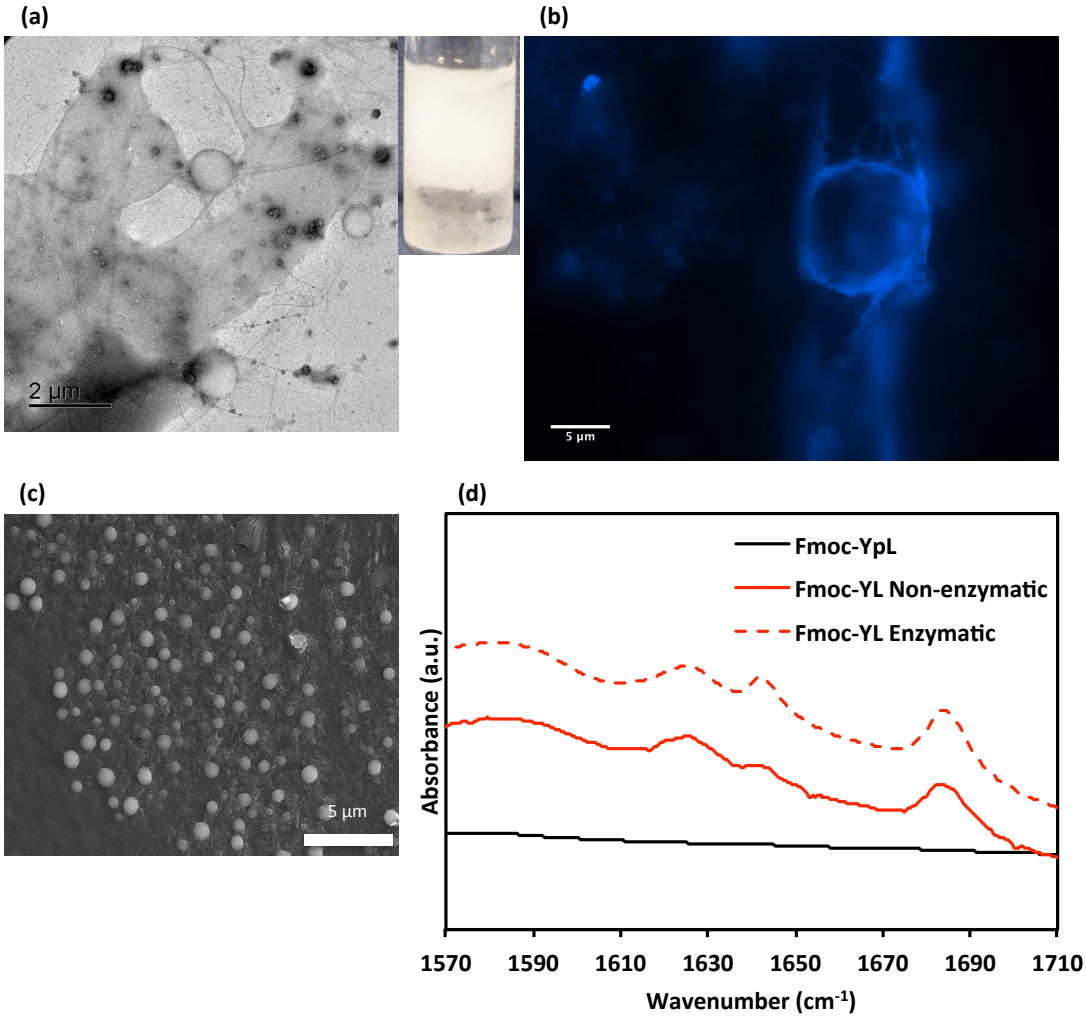

Figure I.4. Characterisation of non-enzymatically formed 5 mM Fmoc-YL emulsion when prepared in 0.5 mL pH 8 0.6 M phosphate buffer, heated to 80°C and gradually cooled down overnight, added 0.5 mL chloroform and hand-shaken for 5 seconds: (a) TEM image showing droplets stabilised by nanofibres. Inset presents the macroscopic aspect of this emulsion; (b) Fluorescence microscopy of a droplet stabilised by nanofibres, labelled with ThT; (c) SEM image showing many droplets; (d) FTIR spectrum when compared with the previously presented biphasic samples, showing it forms a slightly less well-ordered H-bonding network than the enzymatically-triggered Fmoc-YL.

Appendix 5. Fluorescence of controls

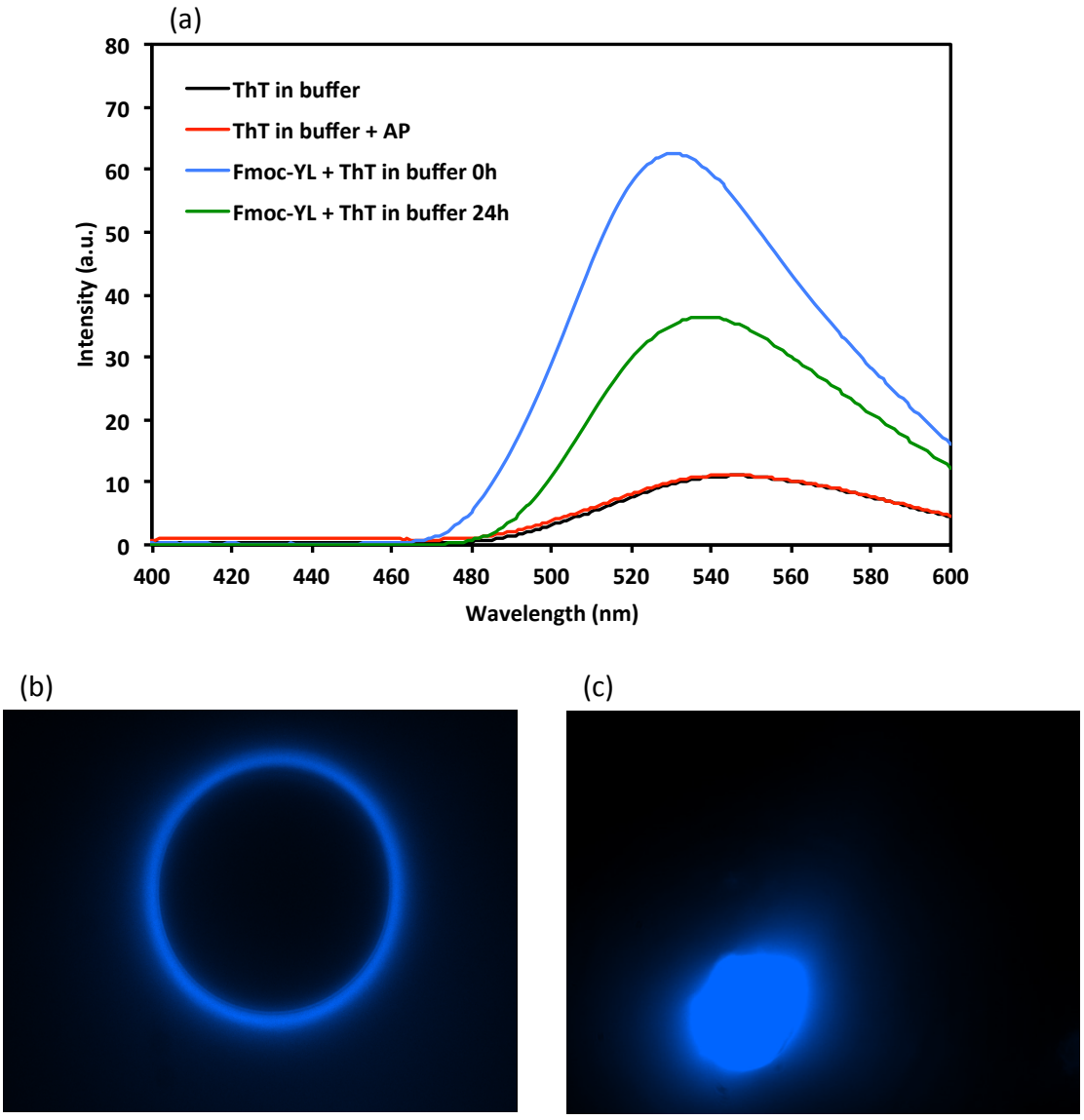

Figure I.5. (a) Fluorescence spectra of ThT in buffer with and without alkaline phosphatase, showing that the presence of AP does not change the fluorescence emission of ThT at 460-600 nm (using a 365 nm excitation wavelength), Fmoc-YL in buffer after gelation shows the emission changes when ThT intercalates with the self-assembled fibres; (b) Fluorescence microscopy image of ThT in buffer + AP, showing the fluorescence is only given by the ThT, in the same WL range; (c) Fluorescence microscopy image of ThT in buffer + AP + chloroform, showing the fluorescence emission is stronger.

Appendix 6. NMR spectra of synthesised peptides (Fmoc-YL and Fmoc-YpL)

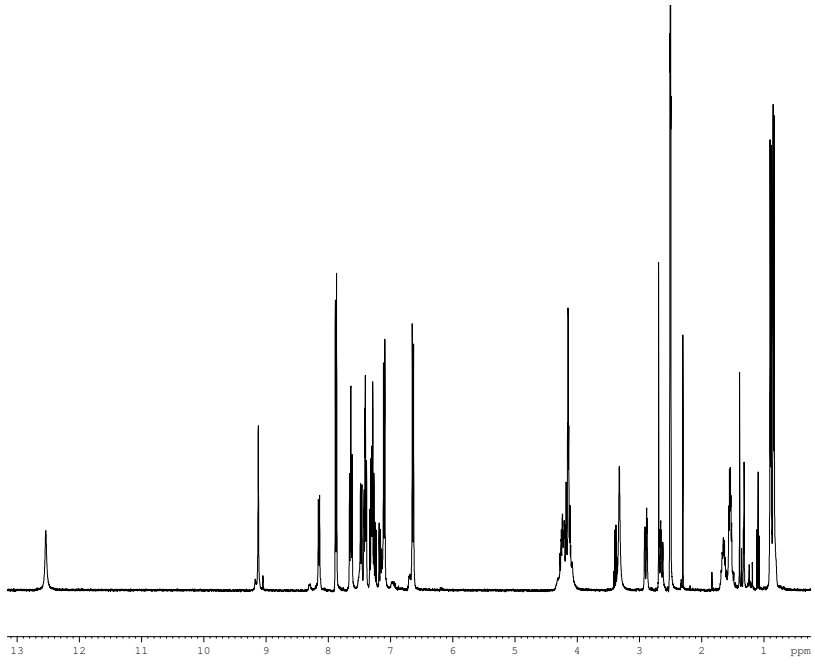

Figure I.6. ^{1}H NMR spectrum of Fmoc-YL.

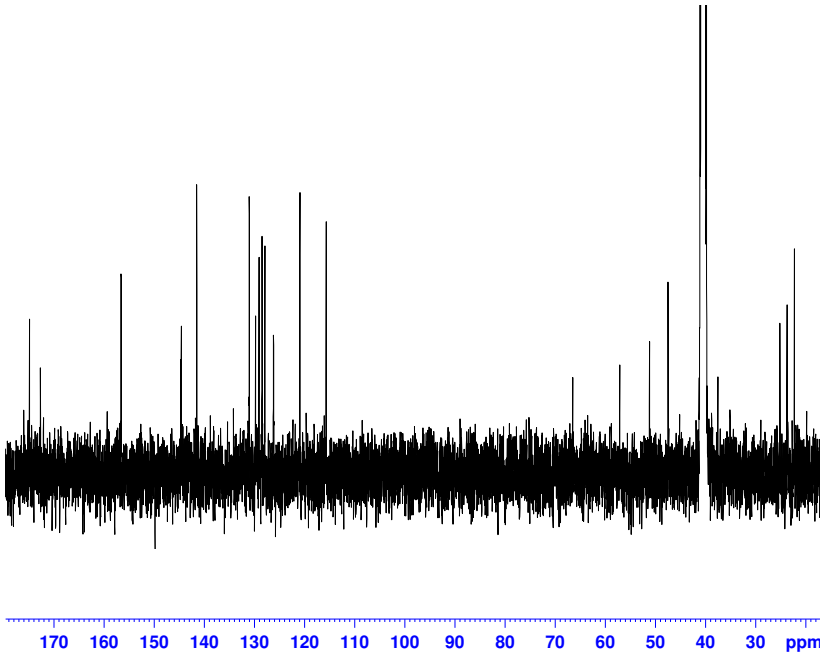

Figure I.7. ^{13}C NMR spectrum of Fmoc-YL.

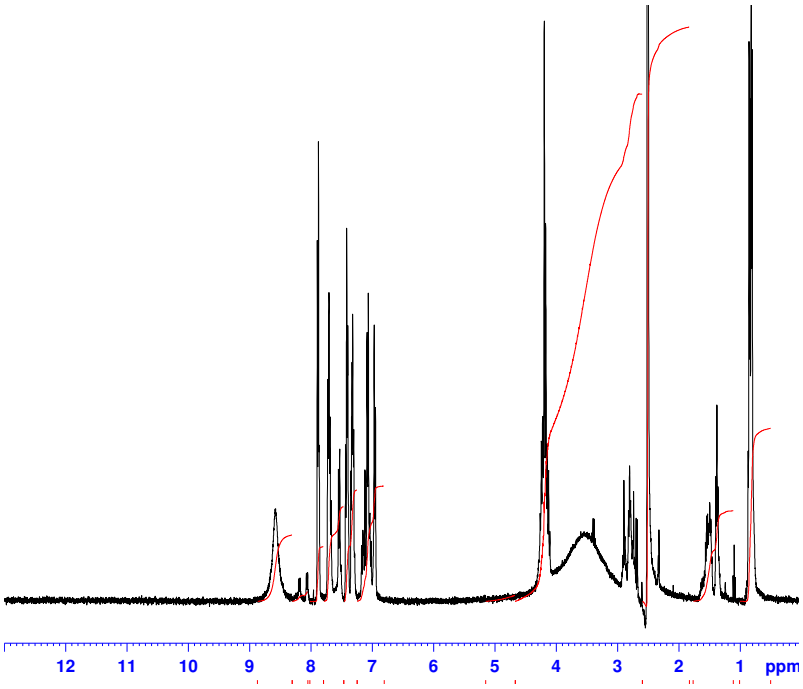

Figure I.8. ^{1}H NMR spectrum of Fmoc-YpL.

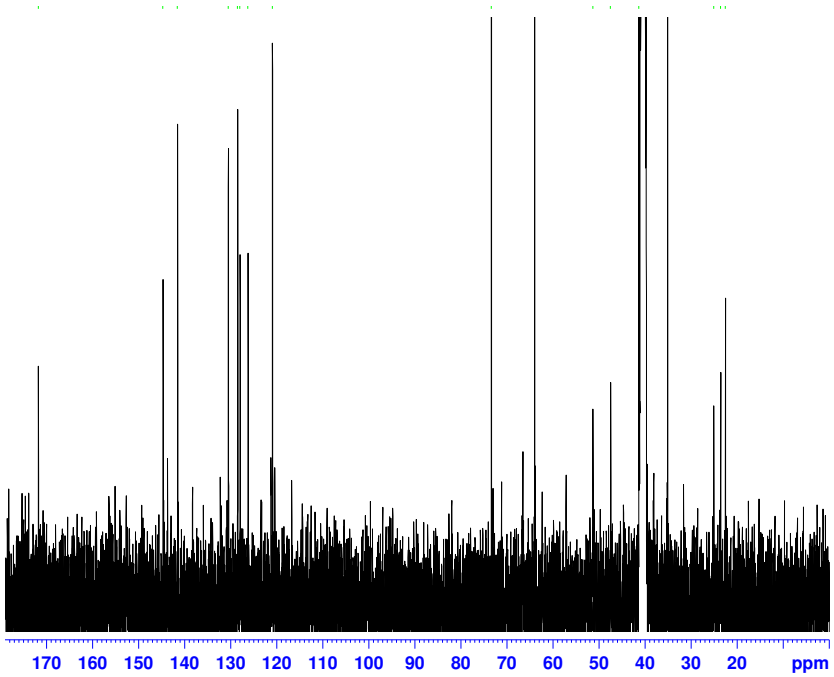

Figure I.9. ^{13}C NMR spectrum of Fmoc-YpL.

Appendix 7. Negative controls of 1:1 aqueous buffer 0.6 M : chloroform volume ratio with different emulsifiers (or none) and briefly hand-shaken

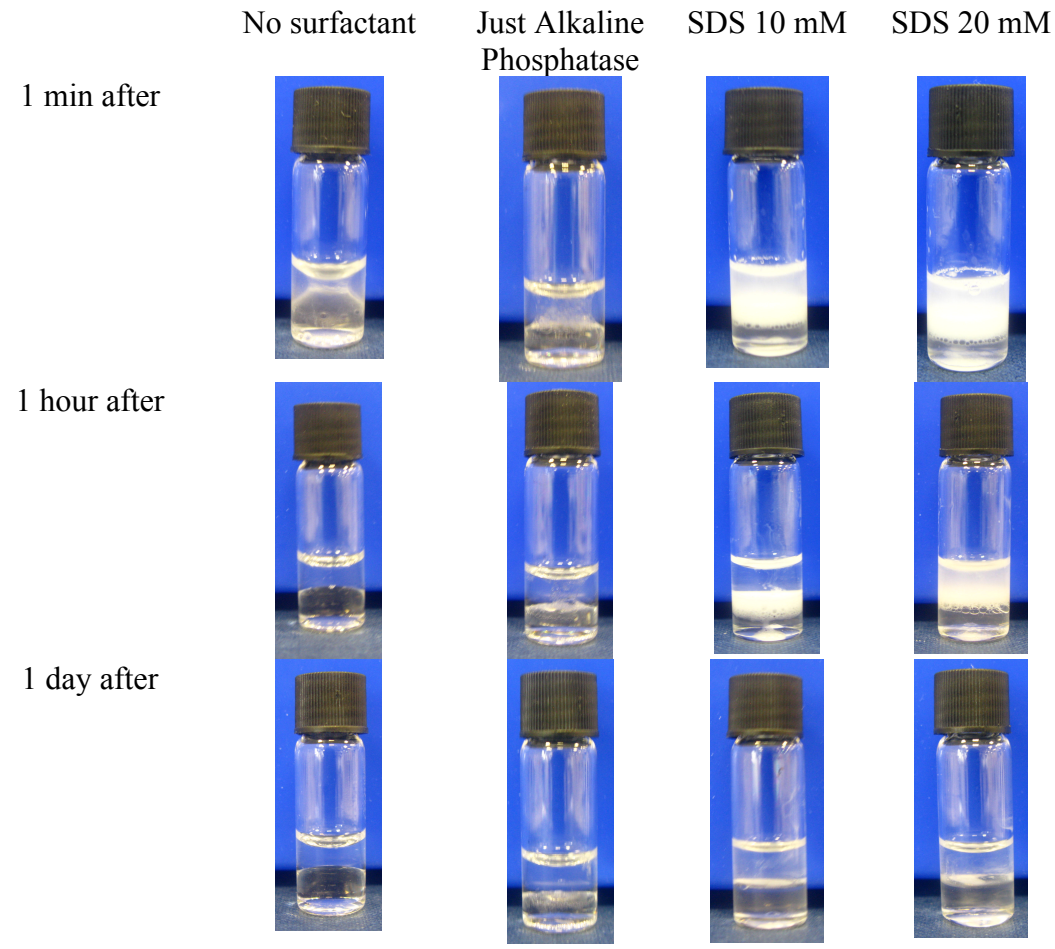

Appendix 8. NAMD Example of Minimisation Input file

```
#############################################################
## JOB DESCRIPTION                                         ##
#############################################################

# This is what this job does


#############################################################
## ADJUSTABLE PARAMETERS                                   ##
#############################################################

structure          solvate.psf
coordinates        solvate.pdb
OutputName         name_min

set temperature    300


firsttimestep      0


#############################################################
## SIMULATION PARAMETERS                                   ##
#############################################################

# Input
paraTypeCharmm      on
parameters          /users/ines/scripts/par_all22_36_Pim.prm

# NOTE: Do not set the initial velocity temperature if you
# have also specified a .vel restart file!
temperature         $temperature


#Periodic Boundary conditions
# NOTE: Do not set the periodic cell basis if you have also
# specified an .xsc restart file!
cellBasisVector1    80.0  0.0   0.00
cellBasisVector2     0.0  80.0  0.0
cellBasisVector3     0.0   0.0  80.0
cellOrigin          38.52 35.16 36.52

wrapWater           on
wrapAll             on

margin  2.0

# Force-Field Parameters
exclude             scaled1-4
1-4scaling          1.0
cutoff              12
switching           on
switchdist          10
pairlistdist        13.5


# Integrator Parameters
timestep            2.0    ;# fs
rigidBonds          all    ;# larger steps require 'all'
nonbondedFreq       1
```

```
fullElectFrequency  2
stepspercycle       100


#PME (for full-system periodic electrostatics)
if {1} {
PME                 yes
PMEGridSpacing      1.0
}

# Constant Temperature Control
langevin            on    ;# do langevin dynamics
langevinDamping     5     ;# damping coefficient (gamma) of 5/ps
langevinTemp        $temperature
langevinHydrogen    off    ;# don't couple langevin bath to hydrogens


# Constant Pressure Control (variable volume)
if {1} {
useGroupPressure      yes ;# needed for 2fs steps
useFlexibleCell       no  ;# no for water box, yes for membrane
useConstantArea       no  ;# no for water box, yes for membrane

langevinPiston        on
langevinPistonTarget  1.01325 ;#  in bar -> 1 atm
langevinPistonPeriod  100
langevinPistonDecay   50
langevinPistonTemp    $temperature
}


restartfreq         1000     ;# 500steps = every 0.5ps
dcdfreq             1000
xstFreq             5000
outputEnergies      500
outputPressure      500

# reassignTemp        18
# reassignIncr        5
# reassignHold        293
# reassignFreq        500

#############################################################
## EXECUTION SCRIPT                                        ##
#############################################################

# Minimization
if {1} {
minimize             10000 ;#more than enough because it was constant
after 1000 steps already
reinitvels          18
}

# run 30000 ;# 30 ps heating phase
```

Appendix 9. NAMD Example of Equilibration Input file

```
#############################################################
## JOB DESCRIPTION                                         ##
#############################################################

# This is what this job does


#############################################################
## ADJUSTABLE PARAMETERS                                   ##
#############################################################

structure          solvate.psf
coordinates        solvate.pdb
outputName         name_eq

set temperature    300

# Continuing a job from the restart files
if {1} {
set inputname      name_min
binCoordinates     $inputname.restart.coor
binVelocities              $inputname.restart.vel     ;#  remove  the
"temperature" entry if you use this!
extendedSystem     $inputname.xsc
}

firsttimestep      0


#############################################################
## SIMULATION PARAMETERS                                   ##
#############################################################

# Input
paraTypeCharmm      on
parameters          /users/ines/scripts/par_all22_36_Pim.prm

# NOTE: Do not set the initial velocity temperature if you
# have also specified a .vel restart file!
# temperature         $temperature


# Periodic Boundary conditions
# NOTE: Do not set the periodic cell basis if you have also
# specified an .xsc restart file!
if {0} {
cellBasisVector1    80.0  0.0   0.00
cellBasisVector2     0.0  80.0  0.0
cellBasisVector3     0.0   0.0  80.0
cellOrigin          38.52 35.16 36.52
}
wrapWater           on
wrapAll             on

margin  2.0

# Force-Field Parameters
exclude             scaled1-4
1-4scaling          1.0
```

```
cutoff              12
switching           on
switchdist          10
pairlistdist        13.5


# Integrator Parameters
timestep            2.0    ;# fs
rigidBonds          all  ;# larger steps require 'all' #try this
nonbondedFreq       1
fullElectFrequency  2
stepspercycle       100


#PME (for full-system periodic electrostatics)
if {1} {
PME                 yes
PMEGridSpacing      1.0
}

# Constant Temperature Control
langevin            on    ;# do langevin dynamics
langevinDamping     5     ;# damping coefficient (gamma) of 5/ps
langevinTemp        $temperature
langevinHydrogen    off    ;# don't couple langevin bath to hydrogens


# Constant Pressure Control (variable volume)
if {1} {
useGroupPressure      yes ;# needed for 2fs steps
useFlexibleCell       no  ;# no for water box, yes for membrane
useConstantArea       no  ;# no for water box, yes for membrane

langevinPiston        on
langevinPistonTarget  1.01325 ;#  in bar -> 1 atm
langevinPistonPeriod  100
langevinPistonDecay   50
langevinPistonTemp    $temperature
}


restartfreq         5000     ;# 5000steps = every 10.0ps
dcdfreq             5000
xstFreq             5000
outputEnergies      2500
outputPressure      2500

reassignTemp        18
reassignIncr        5
reassignHold        293
reassignFreq        500

#constraints         on
#consref             reference.pdb
#conskfile           reference.pdb
#conskcol            B
#constraintScaling   10.0
#selectConstraints   on
#selectConstrZ       on
#Addingconstrins to the simulation, just in line Z, so C4 of OCOH can
move on x,Y plane

#############################################################
```

```
## EXECUTION SCRIPT                                                   ##
#####################################################################

# Minimization
if {0} {
minimize            10000
reinitvels          18
}

run 250000 ;# 55 ps heating phase and 445 ps equilibration
```

Appendix 10. NAMD Example of Production Input file (200 ns)

```
#############################################################
## JOB DESCRIPTION                                         ##
#############################################################

# This is what this job does


#############################################################
## ADJUSTABLE PARAMETERS                                   ##
#############################################################

structure          solvate.psf
coordinates        solvate.pdb
OutputName         name_200ns

set temperature    300

# Continuing a job from the restart files
if {1} {
set inputname      name_eq
binCoordinates     $inputname.restart.coor
binVelocities     $inputname.restart.vel  ;# remove the "temperature"
entry if you use this!
extendedSystem     $inputname.restart.xsc
}

firsttimestep      0


#############################################################
## SIMULATION PARAMETERS                                   ##
#############################################################

# Input
paraTypeCharmm      on
parameters          /users/ines/scripts/par_all22_36_Pim.prm

# NOTE: Do not set the initial velocity temperature if you
# have also specified a .vel restart file!
#temperature         $temperature


# Periodic Boundary conditions
# NOTE: Do not set the periodic cell basis if you have also
# specified an .xsc restart file!
if {0} {
cellBasisVector1    80.0  0.0   0.00
cellBasisVector2     0.0  80.0  0.0
cellBasisVector3     0.0   0.0  80.0
cellOrigin          38.52 35.16 36.52
}
wrapWater           on
wrapAll             on

margin  2.0

# Force-Field Parameters
exclude             scaled1-4
1-4scaling          1.0
```

```
cutoff              12
switching           on
switchdist          10
pairlistdist        13.5


# Integrator Parameters
timestep            2.0    ;# fs
rigidBonds          all  ;#larger steps require 'all' #try this
nonbondedFreq       1
fullElectFrequency  2
stepspercycle       100


#PME (for full-system periodic electrostatics)
if {1} {
PME                 yes
PMEGridSpacing      1.0
}

# Slow heating after minimization
# reassignFreq 1000
# reassignTemp 10
# reassignIncr 10
# reassignhold 300

# Constant Temperature Control
langevin            on    ;# do langevin dynamics
langevinDamping     5     ;# damping coefficient (gamma) of 5/ps
langevinTemp        $temperature
langevinHydrogen    off    ;# don't couple langevin bath to hydrogens


# Constant Pressure Control (variable volume)
if {1} {
useGroupPressure      yes ;# needed for 2fs steps
useFlexibleCell       no  ;# no for water box, yes for membrane
useConstantArea       no  ;# no for water box, yes for membrane

langevinPiston        on
langevinPistonTarget  1.01325 ;#  in bar -> 1 atm
langevinPistonPeriod  100
langevinPistonDecay   50
langevinPistonTemp    $temperature
}


restartfreq         5000     ;# 500steps = every 0.5ps
dcdfreq             5000
xstFreq             5000
outputEnergies      2500
outputPressure      2500

#constraints         on
#consref             reference.pdb
#conskfile           reference.pdb
#conskcol            B
#constraintScaling   10.0
#selectConstraints   on
#selectConstrZ       on
#Addingconstrins to the simulation, just in line Z, so C4 of OCOH can
move on x,Y plane
```

```
#####################################################################
## EXECUTION SCRIPT                                                ##
#####################################################################
# Minimization
if {0} {
minimize            10000
reinitvels          25
}

run 100000000 ;# 200 ns run
```

Appendix 11. Script for Proximity Analysis

"proximity-count.tcl"

```
mol new count-bang.dcd waitfor all
mol addfile dry.psf waitfor all

set nf [molinfo top get numframes]

for {set i bang} {$i <= what} {incr i} {
    set countFF 0
    set countFY 0
    set countFL 0
    for {set F 1} {$F <= 175} {incr F 3} {
        for {set F2 [expr {$F + 3}]} {$F2 <= 178} {incr F2 3} {
            set Y2 [expr {$F2 + 1}]
            set L2 [expr {$F2 + 2}]
            set sel1a [atomselect top "resid $F and not backbone and
noh and within 5.5 of (resid $F2 and not backbone and noh)" frame $i]
          set sel2a [atomselect top "resid $F and not backbone and
noh and within 5.5 of (resid $Y2 and not backbone and noh)" frame $i]
            set sel3a [atomselect top "resid $F and not backbone and
noh and within 5.5 of (resid $L2 and not backbone and noh)" frame $i]

          if {[$sel1a num] > 0} {
            set countFF [expr {$countFF + 1}]
          }
          if {[$sel2a num] > 0} {
            set countFY [expr {$countFY + 1}]
          }
          if {[$sel3a num] > 0} {
            set countFL [expr {$countFL + 1}]
            }
        }
    }
    set countYY 0
    set countYL 0
    for {set Y 2} {$Y <= 176} {incr Y 3} {
        for {set F2 [expr {$Y + 2}]} {$F2 <= 178} {incr F2 3} {
            set Y2 [expr {$F2 + 1}]
            set L2 [expr {$F2 + 2}]
          set sel1a [atomselect top "resid $Y and not backbone and
noh and within 5.5 of (resid $F2 and not backbone and noh)" frame $i]
            set sel2a [atomselect top "resid $Y and not backbone and
noh and within 5.5 of (resid $Y2 and not backbone and noh)" frame $i]
            set sel3a [atomselect top "resid $Y and not backbone and
noh and within 5.5 of (resid $L2 and not backbone and noh)" frame $i]

            if {[$sel1a num] > 0} {
                set countFY [expr {$countFY + 1}]
            }
            if {[$sel2a num] > 0} {
                set countYY [expr {$countYY + 1}]
            }
            if {[$sel3a num] > 0} {
                set countYL [expr {$countYL + 1}]
            }
        }
    }

    set countLL 0
    for {set L 3} {$L <= 177} {incr L 3} {
```

```
        for {set F2 [expr {$L + 1}]} {$F2 <= 178} {incr F2 3} {
            set Y2 [expr {$F2 + 1}]
            set L2 [expr {$F2 + 2}]
            set sel1a [atomselect top "resid $L and not backbone and
noh and within 5.5 of (resid $F2 and not backbone and noh)" frame $i]
            set sel2a [atomselect top "resid $L and not backbone and
noh and within 5.5 of (resid $Y2 and not backbone and noh)" frame $i]
            set sel3a [atomselect top "resid $L and not backbone and
noh and within 5.5 of (resid $L2 and not backbone and noh)" frame $i]

            if {[$sel1a num] > 0} {
                set countFL [expr {$countFL + 1}]
            }
            if {[$sel2a num] > 0} {
                set countYL [expr {$countYL + 1}]
            }
            if {[$sel3a num] > 0} {
                set countLL [expr {$countLL + 1}]
            }
        }
    }

    set outfile [open alles-bang a+]
    puts                                                        $outfile
"${countFF},${countFY},${countFL},${countYY},${countYL},${countLL}"
    close $outfile
    unset countFF
    unset countFY
    unset countFL
    unset countYY
    unset countYL
    unset countLL
}

exit
```

Script for Submission of Proximity Analysis Script
"batchcatdcd.tcsh"

```
#!/bin/tcsh

@ i = 0
while ($i <= 4990)
   @ j = $i + 9
   catdcd -o count-$i.dcd -first $i -last $j -stride 1 dry.dcd
   echo $i
   sed "s/bang/"$i"/" < proximity-count.tcl > temp1.tcl
   sed "s/what/"$j"/" < temp1.tcl > count-$i.tcl
   vmdrun count-$i
   @ i = $i + 10
   rm temp1.tcl
end
```

Appendix 12. TEM images of aqueous buffer samples

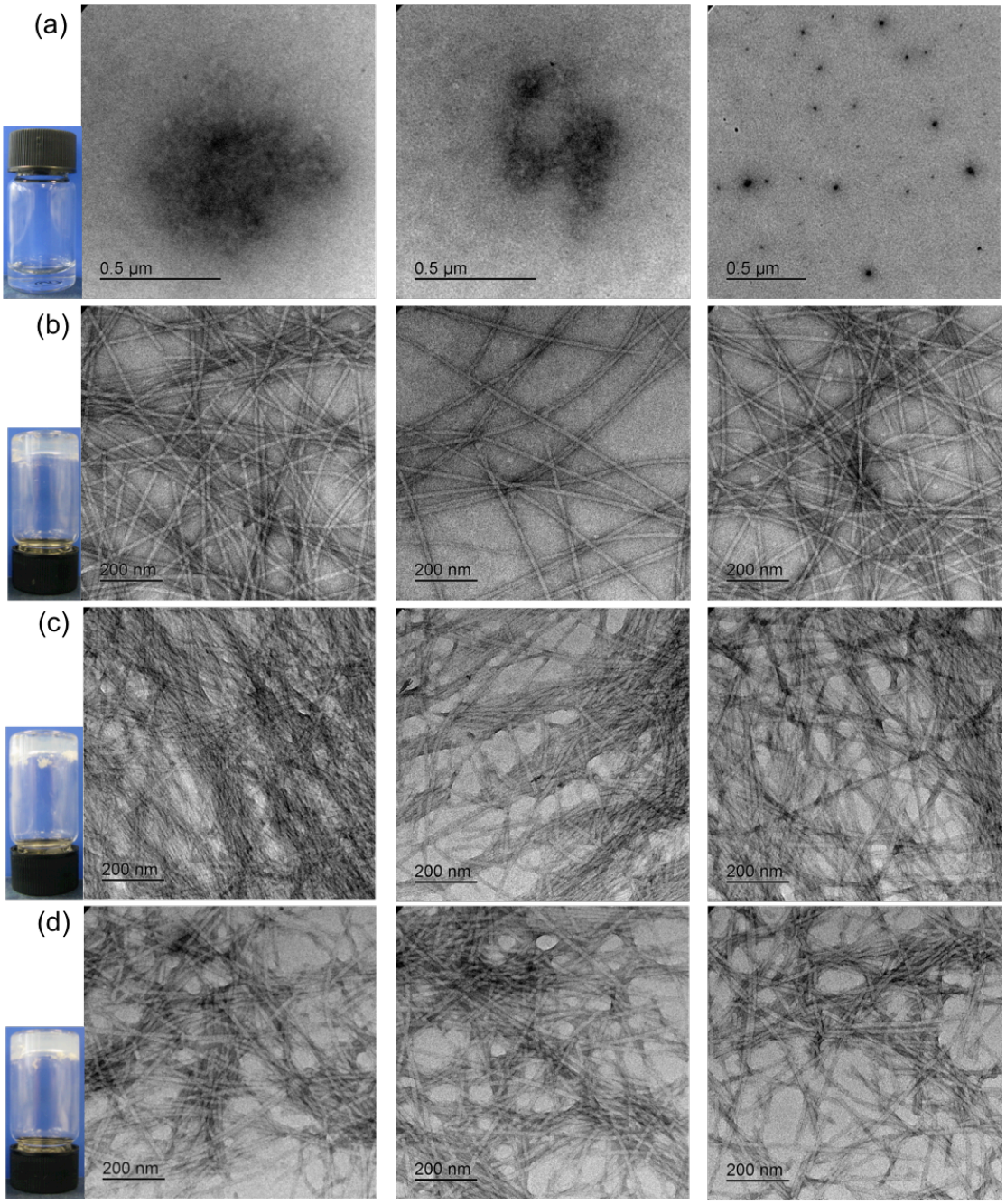

Figure I.10. Photographs of macroscopic aspect and TEM images obtained after 24 hours of the aqueous buffer samples: (a) KY*p*F control with no alkaline phosphatase; (b) KY*p*F added 0.07 µM AP; (c) 1.3 µM AP; (d) 3.3 µM AP. Continues on the next page.

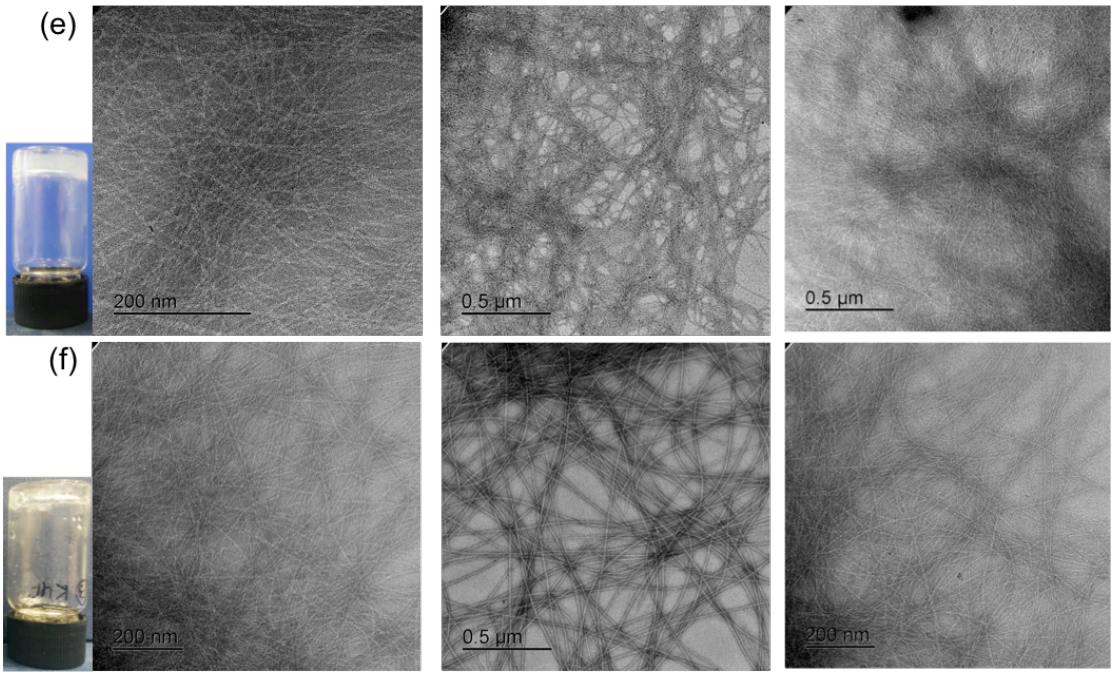

Continuation of Figure I.10. Photographs of macroscopic aspect and TEM images obtained after 24 hours of the aqueous buffer samples: (E) KY*p*F added 6.6 µM AP; (F) KYF formed non-enzymatically.

Appendix 13. Rheology strain sweeps

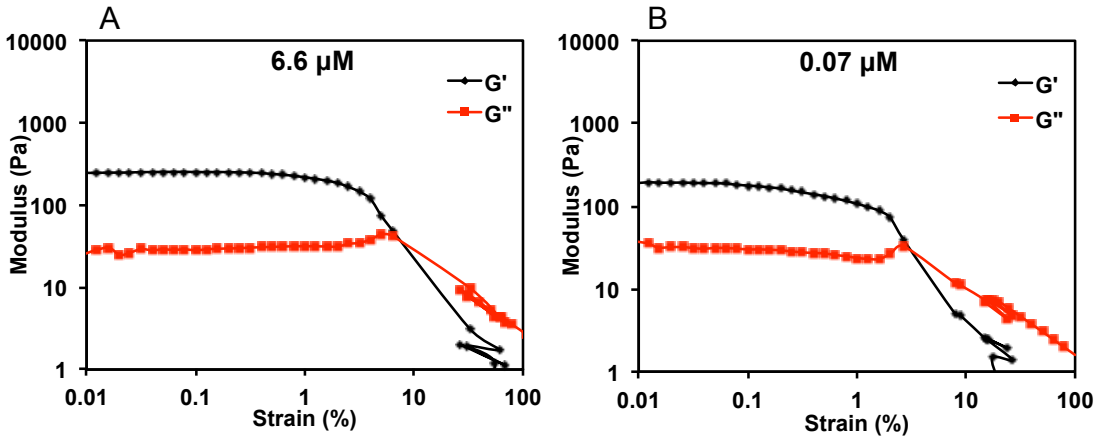

Figure I.11. Strain sweep measurements showing viscoelastic behaviour of the hydrogels produced when the highest and lowest enzyme concentrations are used: (A) KY*p*F + 6.6 µM AP; (B) KY*p*F + 0.07 µM AP.

Appendix 14. FTIR spectra controls in aqueous buffer

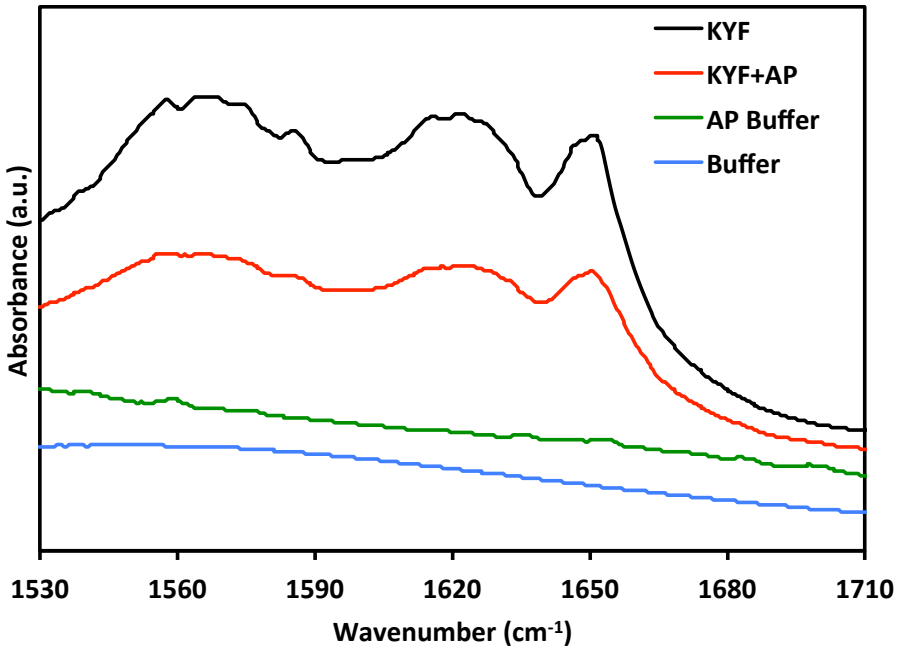

Figure I.12. FTIR spectra of the controls in aqueous buffer, showing the non-enzymatically formed KYF (black curve) presents less well-organised bonded networks when compared with KYF formed biocatalytically, that alkaline phosphatase does not have a significant disturbance on non-enzymatically formed KYF hydrogel (red curve), also shown by the only AP curve (green), similar to the buffer blank (blue).

Appendix 15. Blanks of UV-Vis enzymatic assay

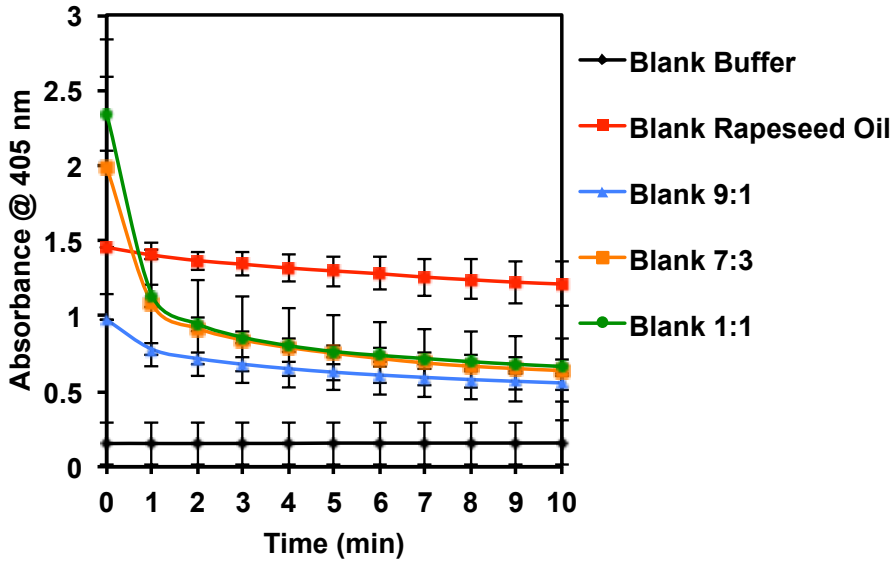

Figure I.13. Blank measurements of the samples, in the absence of enzyme but in the presence of its substrate pNPP, showing there was a measurement artifact at time zero when rapeseed oil was present.

Appendix 16. TEM images of biphasic aqueous buffer/rapeseed oil samples

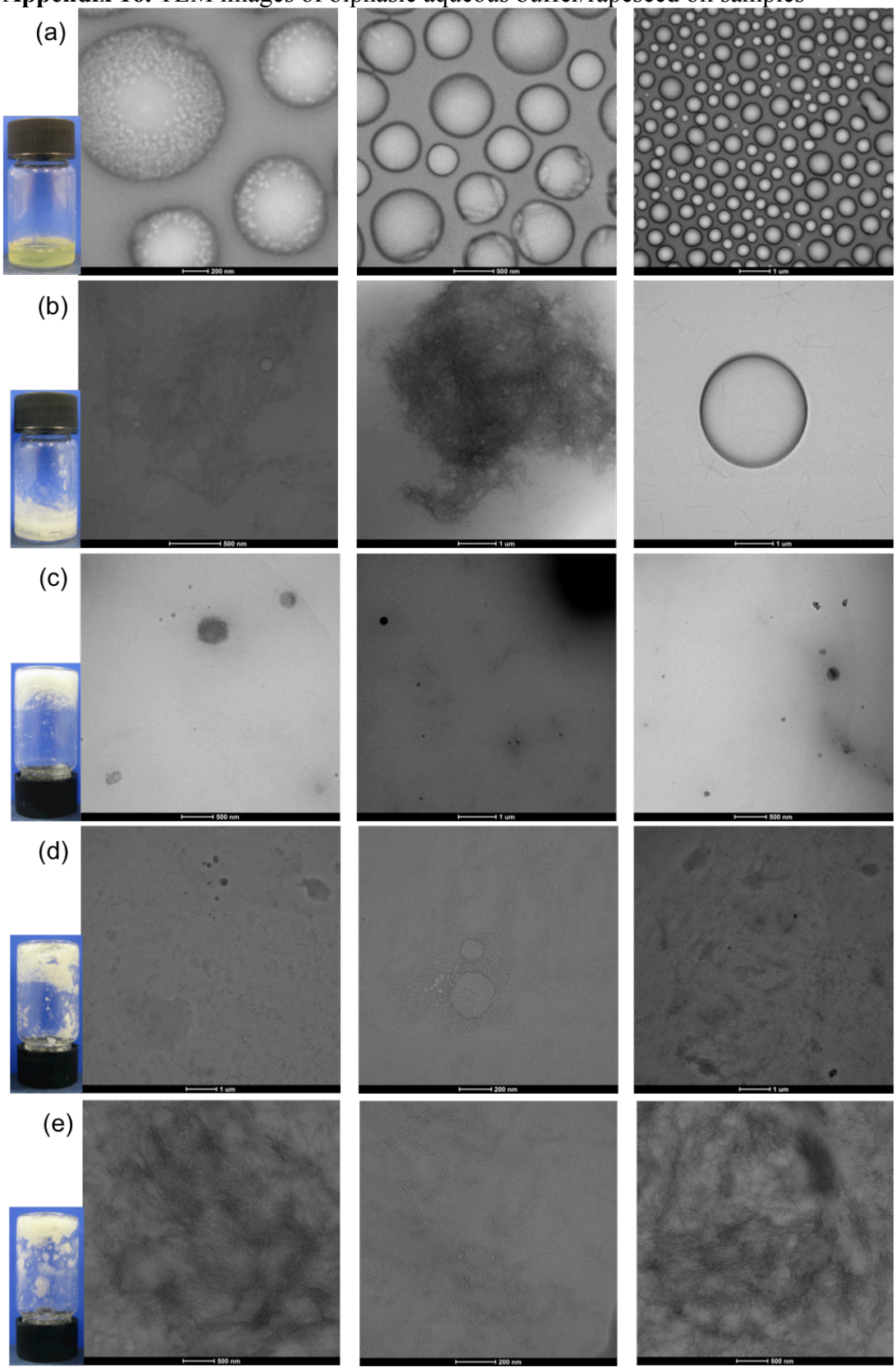

Figure I.14. Photographs of macroscopic aspect and TEM images obtained after 24 hours of the 9:1 buffer:rapeseed oil samples: (a) KY*p*F control with no alkaline phosphatase; (b) KY*p*F added 0.07 µM AP; (c) 1.3 µM AP; (d) 3.3 µM AP; (e) 6.6 µM AP upon preparation.

Appendix 17. FTIR spectra controls in biphasic systems

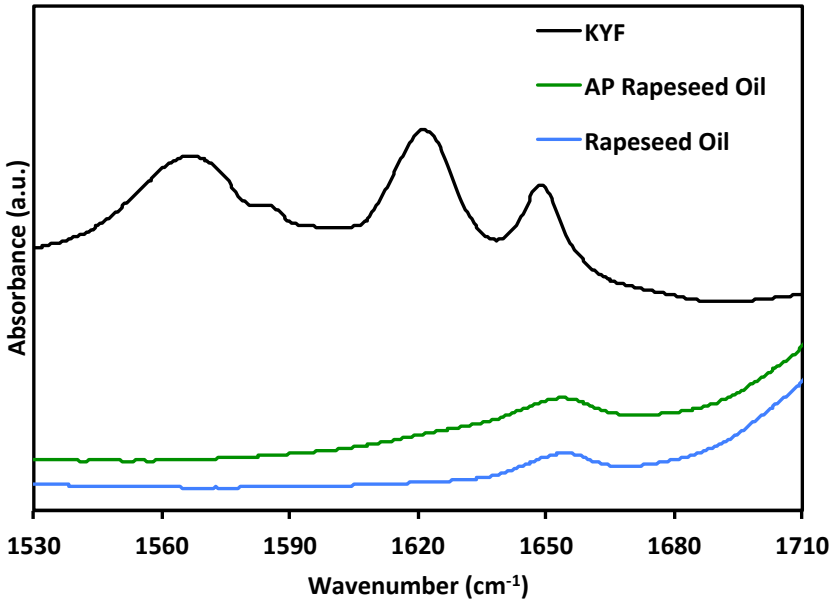

Figure I.15. FTIR spectra of the control non-enzymatically formed KYF (black curve) in 9:1 buffer:rapeseed oil biphasic system, showing less well-organised bonded networks when compared with KYF formed biocatalytically. The rapeseed oil control curve presents a peak at around 1652 cm^{-1}, which is also observed for the alkaline phosphatase in rapeseed oil control.

Appendix 18. Gromacs Example of Minimisation Input file

```
;
; STANDARD MD INPUT OPTIONS FOR MARTINI 2.0
;
; for use with GROMACS 3.3
;

; RUN CONTROL PARAMETERS =
; MARTINI - Most simulations are stable with dt=40 fs,
; some (especially rings) require 20-30 fs.
; The range of time steps used for parametrization
; is 20-40 fs, using smaller time steps is therefore not recommended.

integrator               = steep
; start time and timestep in ps
tinit                    = 0.0
dt                       = 0.025
nsteps                   = 5000
; number of steps for center of mass motion removal =
nstcomm                  = 1
comm-grps                =
emtol                    = 2000

; OUTPUT CONTROL OPTIONS =
; Output frequency for coords (x), velocities (v) and forces (f) =
nstxout                  = 1
nstvout                  = 1
nstfout                  = 0
; Output frequency for energies to log file and energy file =
nstlog                   = 100
nstenergy                = 100
; Output frequency and precision for xtc file =
nstxtcout                = 0
xtc_precision            = 0
; This selects the subset of atoms for the xtc file. You can =
; select multiple groups. By default all atoms will be written. =
xtc-grps                 =
; Selection of energy groups =
energygrps               =

; NEIGHBORSEARCHING PARAMETERS =
; MARTINI - no need for more frequent updates
; or larger neighborlist cut-off due
; to the use of shifted potential energy functions.

; nblist update frequency =
nstlist                  = 10
; ns algorithm (simple or grid) =
ns_type                  = grid
; Periodic boundary conditions: xyz or no =
pbc                      = xyz
; nblist cut-off         =
rlist                    = 1.5

; OPTIONS FOR ELECTROSTATICS AND VDW =
; MARTINI - vdw and electrostatic interactions are used
; in their shifted forms. Changing to other types of
; electrostatics will affect the general performance of
; the model.

; Method for doing electrostatics =
coulombtype              = Shift
```

```
rcoulomb_switch          = 0.0
rcoulomb                 = 1.2
; Dielectric constant (DC) for cut-off or DC of reaction field =
epsilon_r                = 15
; Method for doing Van der Waals =
vdw_type                 = Shift
; cut-off lengths        =
rvdw_switch              = 0.9
rvdw                     = 1.2
; Apply long range dispersion corrections for Energy and Pressure =
DispCorr                 = No

; OPTIONS FOR WEAK COUPLING ALGORITHMS =
; MARTINI - normal temperature and pressure coupling schemes
; can be used. It is recommended to couple individual groups
; in your system seperately.

; Temperature coupling   =
tcoupl                   = no
tau_t                    = 0.1 0.1
tc-grps                  = peptide non-peptide
ref_t                    = 303 303
Pcoupl                   = no
Pcoupltype               = isotropic
tau_p                    = 3.0 3.0
compressibility          = 4.6e-3 4.6e-3
ref_p                    = 1.0 1.0

; GENERATE VELOCITIES FOR STARTUP RUN =
gen_vel                  = no
gen_temp                 = 303
gen_seed                 = 474529

; OPTIONS FOR BONDS     =
; MARTINI - for ring systems constraints are defined
; which are best handled using Lincs.

constraints              = none
; Type of constraint algorithm =
constraint_algorithm     = Lincs
; Do not constrain the start configuration =
unconstrained_start      = no
; Highest order in the expansion of the constraint coupling matrix =
lincs_order              = 4
; Lincs will write a warning to the stderr if in one step a bond =
; rotates over more degrees than =
lincs_warnangle          = 90
```

Appendix 19. Gromacs Example of Equilibration/Production Input file (10 μs)

```
;
; STANDARD MD INPUT OPTIONS FOR MARTINI 2.0
;
; for use with GROMACS 3.3
;

; RUN CONTROL PARAMETERS =
; MARTINI - Most simulations are stable with dt=40 fs,
; some (especially rings) require 20-30 fs.
; The range of time steps used for parametrization
; is 20-40 fs, using smaller time steps is therefore not recommended.

integrator               = md
; start time and timestep in ps
tinit                    = 0.0
dt                       = 0.02
nsteps                   = 500000000 ;to make 10 us simulation
; number of steps for center of mass motion removal =
nstcomm                  = 100
comm-grps                =

; OUTPUT CONTROL OPTIONS =
; Output frequency for coords (x), velocities (v) and forces (f) =
nstxout                  = 200000
nstvout                  = 200000
nstfout                  = 0
; Output frequency for energies to log file and energy file =
nstlog                   = 200000
nstenergy                = 200000
; Output frequency and precision for xtc file =
nstxtcout                = 0
xtc_precision            = 0
; This selects the subset of atoms for the xtc file. You can =
; select multiple groups. By default all atoms will be written. =
xtc-grps                 =
; Selection of energy groups =
energygrps               =

; NEIGHBORSEARCHING PARAMETERS =
; MARTINI - no need for more frequent updates
; or larger neighborlist cut-off due
; to the use of shifted potential energy functions.

; nblist update frequency =
nstlist                  = 10
; ns algorithm (simple or grid) =
ns_type                  = grid
; Periodic boundary conditions: xyz or no =
pbc                      = xyz
; nblist cut-off         =
rlist                    = 1.5


; OPTIONS FOR ELECTROSTATICS AND VDW =
; MARTINI - vdw and electrostatic interactions are used
; in their shifted forms. Changing to other types of
; electrostatics will affect the general performance of
; the model.

; Method for doing electrostatics =
coulombtype              = Shift
```

```
rcoulomb_switch          = 0.0
rcoulomb                 = 1.2
; Dielectric constant (DC) for cut-off or DC of reaction field =
epsilon_r                = 15
; Method for doing Van der Waals =
vdw_type                 = Shift
; cut-off lengths        =
rvdw_switch              = 0.9
rvdw                     = 1.2
; Apply long range dispersion corrections for Energy and Pressure =
DispCorr                 = No

; OPTIONS FOR WEAK COUPLING ALGORITHMS =
; MARTINI - normal temperature and pressure coupling schemes
; can be used. It is recommended to couple individual groups
; in your system seperately.

; Temperature coupling   =
tcoupl                   = Berendsen
tau_t                    = 1.25 1.25
tc-grps                  = peptide non-peptide
ref_t                    = 303 303
Pcoupl                   = Berendsen
Pcoupltype               = isotropic
tau_p                    = 3.0 3.0
compressibility          = 3e-4 3e-4
ref_p                    = 1.0 1.0

; GENERATE VELOCITIES FOR STARTUP RUN =
gen_vel                  = yes
gen_temp                 = 303
gen_seed                 = 474529

; OPTIONS FOR BONDS     =
; MARTINI - for ring systems constraints are defined
; which are best handled using Lincs.

constraints              = none
; Type of constraint algorithm =
constraint_algorithm     = Lincs
; Do not constrain the start configuration =
unconstrained_start      = no
; Highest order in the expansion of the constraint coupling matrix =
lincs_order              = 4
; Lincs will write a warning to the stderr if in one step a bond =
; rotates over more degrees than =
lincs_warnangle          = 90
```

Appendix 20. Script for bond calculation of phosphorylated tyrosine in KYpF

```
mol new KYpF_whole.trr waitfor all
mol addfile ionized.psf

set nf [molinfo top get numframes]

set BB [atomselect top "resname TYR and (name N or name HN or name CA or name HA or
name C or name O)"]
set SC4_1 [atomselect top "resname TYR and (name CB or name CG or name CD1 or name
HD1)"]
set SC4_2 [atomselect top "resname TYR and (name CD2 or name HD2 or name CE2 or name
HE2)"]
set SC4_3 [atomselect top "resname TYR and (name CE1 or name HE1 or name CZ)"]
set Qa [atomselect top "resname TYR and (name OH or name P1 or name O2 or name O3 or
name O4)"]

set outfile [open "b-bonds.out" w]

for {set i 0} {$i < $nf} {incr i} {
#       puts $i
        $BB frame $i
        $SC4_1 frame $i
        $SC4_2 frame $i
        $SC4_3 frame $i
        $Qa frame $i

        set com1 [measure center $BB weight mass]
        set com2 [measure center $SC4_1 weight mass]
        set com3 [measure center $SC4_2 weight mass]
        set com4 [measure center $SC4_3 weight mass]
        set com5 [measure center $Qa weight mass]
        set dist1($i.r) [veclength [vecsub $com1 $com2]]
        set dist2($i.r) [veclength [vecsub $com2 $com3]]
        set dist3($i.r) [veclength [vecsub $com2 $com4]]
        set dist4($i.r) [veclength [vecsub $com3 $com4]]
        set dist5($i.r) [veclength [vecsub $com4 $com5]]
        puts $outfile "$i $dist1($i.r) $dist2($i.r) $dist3($i.r) $dist4($i.r)
$dist5($i.r)"
}
close $outfile
exit
```

Appendix 21. Script for angle calculation of phosphorylated tyrosine in KYpF

```
mol new KYpF_whole.trr waitfor all
mol addfile ionized.psf

set nf [molinfo top get numframes]

set BB [atomselect top "resname TYR and (name N or name HN or name CA or name HA or
name C or name O)"]
set SC4_1 [atomselect top "resname TYR and (name CB or name CG or name CD1 or name
HD1)"]
set SC4_2 [atomselect top "resname TYR and (name CD2 or name HD2 or name CE2 or name
HE2)"]
set SP1 [atomselect top "resname TYR and (name CE1 or name HE1 or name CZ or name OH
or name HH)"]
set Qa [atomselect top "resname TYR and (name OH or name P1 or name O2 or name O3 or
name O4)"]

set outfile [open "b-angles.out" w]


for {set i 0} {$i < $nf } {incr i} {
#       puts $i
        $BB frame $i
        $SC4_1 frame $i
        $SC4_2 frame $i
        $SP1 frame $i
        $Qa frame $i

        set coma [measure center $BB weight mass]
        set comb [measure center $SC4_1 weight mass]
        set comc [measure center $SC4_2 weight mass]
        set comd [measure center $SP1 weight mass]
        set come [measure center $Qa weight mass]

        set distab [veclength [vecsub $coma $comb]]
        set distac [veclength [vecsub $coma $comc]]
        set distad [veclength [vecsub $coma $comd]]
        set distbc [veclength [vecsub $comb $comc]]
        set distbd [veclength [vecsub $comb $comd]]
        set distcd [veclength [vecsub $comc $comd]]
        set distae [veclength [vecsub $coma $come]]
        set distbe [veclength [vecsub $comb $come]]
        set distce [veclength [vecsub $comc $come]]
        set distde [veclength [vecsub $comd $come]]

        set sqab [expr pow($distab, 2)]
        set sqac [expr pow($distac, 2)]
        set sqad [expr pow($distad, 2)]
        set sqbc [expr pow($distbc, 2)]
        set sqbd [expr pow($distbd, 2)]
        set sqcd [expr pow($distcd, 2)]
        set sqae [expr pow($distae, 2)]
        set sqbe [expr pow($distbe, 2)]
        set sqce [expr pow($distce, 2)]
        set sqde [expr pow($distde, 2)]


        set preangabd [expr ($sqad - $sqab - $sqbd) / ( -2 * $distab * $distbd )]
        set preangabc [expr ($sqac - $sqab - $sqbc) / ( -2 * $distab * $distbc )]
        set preangdbc [expr ($sqcd - $sqbd - $sqbc) / ( -2 * $distbd * $distbc )]
        set preangbcd [expr ($sqbd - $sqbc - $sqcd) / ( -2 * $distbc * $distcd )]
        set preangcdb [expr ($sqbc - $sqcd - $sqbd) / ( -2 * $distcd * $distbd )]
        set preangbde [expr ($sqbe - $sqbd - $sqde) / ( -2 * $distbd * $distde )]
        set preangcde [expr ($sqce - $sqcd - $sqde) / ( -2 * $distcd * $distde )]

        set angabd [expr acos($preangabd) ]
        set angabc [expr acos($preangabc) ]
        set angdbc [expr acos($preangdbc) ]
        set angbcd [expr acos($preangbcd) ]
        set angcdb [expr acos($preangcdb) ]
        set angbde [expr acos($preangbde) ]
        set angcde [expr acos($preangcde) ]
```

```
        set angleabd [expr ($angabd / 3.1415926535897931) * 180 ]
        set angleabc [expr ($angabc / 3.1415926535897931) * 180 ]
        set angledbc [expr ($angdbc / 3.1415926535897931) * 180 ]
        set anglebcd [expr ($angbcd / 3.1415926535897931) * 180 ]
        set anglecdb [expr ($angcdb / 3.1415926535897931) * 180 ]
        set anglebde [expr ($angbde / 3.1415926535897931) * 180 ]
        set anglecde [expr ($angcde / 3.1415926535897931) * 180 ]

        puts $outfile "$i $angleabd $angleabc $angledbc $anglebcd $anglecdb $anglebde
$anglecde"

}
close $outfile
exit
```

Appendix 22. Script for dihedral angle calculation of phosphorylated tyrosine in KYpF

```
mol new KYpF_whole.trr waitfor all
mol addfile ionized.psf

set nf [molinfo top get numframes]

set BB [atomselect top "resname TYR and (name N or name HN or name CA or name HA or
name C or name O)"]
set SC4_1 [atomselect top "resname TYR and (name CB or name CG or name CD1 or name
HD1)"]
set SC4_2 [atomselect top "resname TYR and (name CD2 or name HD2 or name CE2 or name
HE2)"]
set SC4_3 [atomselect top "resname TYR and (name CE1 or name HE1 or name CZ or name OH
or name HH)"]
set Qa [atomselect top "resname TYR and (name OH or name P1 or name O2 or name O3 or
name O4)"]

set outfile [open "b-dihedrals.out" w]

for {set i 0} {$i < $nf } {incr i} {
#       puts $i
        $BB frame $i
        $SC4_1 frame $i
        $SC4_2 frame $i
        $SC4_3 frame $i
        $Qa frame $i

        set coma [measure center $BB weight mass]
        set comb [measure center $SC4_1 weight mass]
        set comc [measure center $SC4_2 weight mass]
        set comd [measure center $SC4_3 weight mass]
        set come [measure center $Qa weight mass]

        set vecba [vecsub $comb $coma]
        set vecca [vecsub $comc $coma]
        set vecda [vecsub $comd $coma]
        set veccb [vecsub $comc $comb]
        set vecdb [vecsub $comd $comb]
        set vecdc [vecsub $comd $comc]
        set vecde [vecsub $comd $come]

        set pdcda [veccross $vecdc $vecda]
        set pdcdb [veccross $vecdc $vecdb]
        set pdcde [veccross $vecdc $vecde]

        set dp1 [vecdot $pdcda $pdcdb]
        set dp2 [vecdot $pdcde $pdcdb]

        set mgpdcda [veclength $pdcda]
        set mgpdcdb [veclength $pdcdb]
        set mgpdcde [veclength $pdcde]

        set den1 [expr $mgpdcda * $mgpdcdb]
        set den2 [expr $mgpdcde * $mgpdcdb]

        set pre1 [expr $dp1 / $den1]
        set pre2 [expr $dp2 / $den2]

        set rad1 [expr acos($pre1)]
        set rad2 [expr acos($pre2)]

        set dihed1 [expr ($rad1 / 3.1415926535897931) * 180 ]
        set dihed2 [expr ($rad2 / 3.1415926535897931) * 180 ]

        puts $outfile "$i $dihed1 $dihed2"
}
close $outfile
exit
```

Appendix 23. Additional information added to martinize.py script for the conversion atomistic/coarse-grained of phosphorylated tyrosine (TYP, X)

```
#########################
## 4 # FG -> CG MAPPING ##  -> @MAP <-
#########################

# Amino acid codes:
AA3     = spl("TRP TYR TYP PHE HIS ARG LYS CYS ASP GLU ILE LEU MET
ASN PRO HYP GLN SER THR VAL ALA GLY") #@#
AA1     = spl("  W   Y   X   F   H   R   K   C   D   E   I   L   M
N   P   O   Q   S   T   V   A   G") #@#

(…)
    mapping = {
        "TYR":  nsplit(bb,"CB CG CD1 HD1","CD2 HD2 CE2 HE2","CE1 HE1
CZ OH HH"),
        "TYP":  nsplit(bb,"CB CG CD1 HD1","CD2 HD2 CE2 HE2","CE1 HE1
CZ","OH P1 O2 O3 O4"),#Added phosphorylated tyrosine (TyrP = TYP)

(…)

        #----+----------------------+
        ## B | SIDE CHAIN PARAMETERS |
        #----+----------------------+

        # To be compatible with Elnedyn, all parameters are
explicitly defined, even if they are double.
        self.sidechains = {
            #RES#   BEADS                   BONDS
ANGLES              DIHEDRALS
            #                               BB-SC          SC-SC
BB-SC-SC  SC-SC-SC
            "TYR": [spl("SC4 SC4 SP1"),    [(0.320,5000),
(0.270,None), (0.270,None),(0.270,None)],[(150,50),(150,50)],
[(0,50)]],
            "TYP": [spl("SC4 SC4 SC4 Qa"), [(0.320,5000),
(0.270,None), (0.270,None),
(0.270,None),(0.300,5000)],[(150,50),(150,50),(125,50),(125,50)],
[(0,50)]],


(…)

       # Defines the connectivity between between beads
        self.connectivity = {
        #RES       BONDS                                 ANGLES
DIHEDRALS             V-SITE
        "TYR":     [[(0,1),(1,2),(1,3),(2,3)],
[(0,1,2),(0,1,3)], [(0,2,3,1)]],
        "TYP":     [[(0,1),(1,2),(1,3),(2,3),(3,4)],
[(0,1,2),(0,1,3),(2,3,4),(1,2,4)], [(0,2,3,1)]]
```

Appendix 24. Gromacs topology file for phosphorylated tyrosine (TYP.itp)

```
; MARTINI 2.1 Coarse Grained topology file for "Protein_A"
; Sequence:
; X
; Secondary Structure:
; E

[ moleculetype ]
; Name         Exclusions
Protein_A         1

[ atoms ]
    1   P5      1   TYP    BB     1  0.0000 ; E
    2   SC4     1   TYP   SC1     2  0.0000 ; E
    3   SC4     1   TYP   SC2     3  0.0000 ; E
    4   SC4     1   TYP   SC3     4  0.0000 ; E
    5    Qa     1   TYP   SC4     5 -2.0000 ; E

[ bonds ]
; Sidechain bonds
    1     2      1   0.32000  5000 ; TYP
    4     5      1   0.30000  5000 ; TYP

[ constraints ]
    2     3      1   0.27000 ; TYP
    2     4      1   0.27000 ; TYP
    3     4      1   0.27000 ; TYP

[ angles ]
; Backbone angles
; Backbone-sidechain angles
; Sidechain angles
    1     2     3      2    150    50 ; TYP
    1     2     4      2    150    50 ; TYP
    3     4     5      2    125    50 ; TYP
    2     3     5      2    125    50 ; TYP

[ dihedrals ]
; Backbone dihedrals
; Sidechain improper dihedrals
    1     3     4     2      2      0    50 ; TYP
```

Appendix 25. Gromacs topology file for standard tyrosine (TYR.itp)

```
; MARTINI 2.1 Coarse Grained topology file for "Protein_A"
; Sequence:
; Y
; Secondary Structure:
; E

[ moleculetype ]
; Name         Exclusions
Protein_A         1

[ atoms ]
    1    P5     1   TYR    BB     1  0.0000 ; E
    2   SC4     1   TYR   SC1     2  0.0000 ; E
    3   SC4     1   TYR   SC2     3  0.0000 ; E
    4   SP1     1   TYR   SC3     4  0.0000 ; E

[ bonds ]
; Sidechain bonds
    1     2      1   0.32000  5000 ; TYR

[ constraints ]
    2     3      1   0.27000 ; TYR
    2     4      1   0.27000 ; TYR
    3     4      1   0.27000 ; TYR

[ angles ]
; Backbone angles
; Backbone-sidechain angles
; Sidechain angles
    1     2     3      2    150    50 ; TYR
    1     2     4      2    150    50 ; TYR

[ dihedrals ]
; Backbone dihedrals
; Sidechain improper dihedrals
    1     3     4     2      2      0    50 ; TYR
```

Appendix 26. Tcl script for the calculation of AP_{total}, AP_{DFF}, AP_{dip}, AP_{oct}

```
mol addfile XYZ_eq.trr waitfor all
mol addfile XYZ_eq.gro

set all1 [atomselect top "not resname W and not resname OCT and not resname ION" frame 0]
set all2 [atomselect top " not resname W and not resname OCT and not resname ION " frame last]
set all_i [measure sasa 1.4 $all1]
set all_f [measure sasa 1.4 $all2]
set AP_total [expr $all_i/$all_f]

set DFF1 [atomselect top "serial 1 to 1500 and not resname W and not resname OCT and not resname ION " frame 0]
set DFF2 [atomselect top "serial 1 to 1500 and not resname W and not resname OCT and not resname ION " frame last]
set DFF_i [measure sasa 1.4 $DFF1]
set DFF_f [measure sasa 1.4 $DFF2]
set AP_DFF [expr $DFF_i/$DFF_f]

set dip1 [atomselect top "not serial 1 to 1500 and not resname W and not resname OCT and not resname ION " frame 0]
set dip2 [atomselect top "not serial 1 to 1500 and not resname W and not resname OCT and not resname ION " frame last]
set dip_i [measure sasa 1.4 $dip1]
set dip_f [measure sasa 1.4 $dip2]
set AP_dip [expr $dip_i/$dip_f]

set oct1 [atomselect top "resname OCT" frame 0]
set oct2 [atomselect top "resname OCT" frame last]
set oct_i [measure sasa 1.4 $oct1]
set oct_f [measure sasa 1.4 $oct2]
set AP_oct [expr $oct_i/$oct_f]

set outfile [open AP_scores.dat a+]

puts $outfile "XYZ $AP_total $AP_DFF $AP_dip $AP_oct"
close $outfile
exit
```

Appendix 27. Top AP_{total}, AP_H', AP_{DFF} and AP_{dip} from co-assembled DFF with dipeptide in water medium

		AP_{total}	AP_H'	AP_{DFF}	Ap_{dip}
1	SW	2.37	0.22	1.84	1.34
2	RF	2.35	0.36	1.82	1.25
3	KW	2.30	0.37	1.76	1.25
4	FR	2.29	0.32	1.83	1.16
5	FW	2.19	0.02	1.49	1.47
6	WF	2.18	0.02	1.52	1.51
7	YF	2.17	0.10	1.70	1.34
8	VW	2.15	0.09	1.80	1.33
9	KH	2.15	0.39	2.20	1.18
10	RW	2.14	0.21	1.78	1.19
11	WK	2.14	0.26	1.75	1.21
12	PW	2.14	0.12	1.82	1.29
13	WW	2.10	0.00	1.50	1.46
14	FL	2.10	0.06	1.63	1.28
15	FF	2.09	0.04	1.47	1.57
16	IW	2.09	0.05	1.79	1.28
17	VF	2.09	0.10	1.78	1.28
18	KF	2.08	0.25	1.63	1.22
19	YW	2.07	0.06	1.68	1.32
20	FM	2.06	0.08	1.73	1.24
21	CF	2.06	0.11	1.68	1.27
22	FY	2.05	0.08	1.54	1.34
23	TF	2.04	0.12	1.69	1.28
24	LW	2.04	0.04	1.79	1.26
25	IF	2.04	0.06	1.70	1.28
26	SK	2.03	0.31	2.38	1.04
27	FS	2.03	0.12	1.62	1.24
28	WY	2.02	0.05	1.69	1.28
29	SF	2.00	0.11	1.64	1.26
30	TW	1.97	0.08	1.70	1.25
31	KS	1.97	0.26	2.21	1.05
32	MF	1.97	0.06	1.64	1.25
33	WM	1.96	0.05	1.70	1.23
34	WC	1.95	0.07	1.62	1.21
35	PF	1.95	0.08	1.71	1.25
36	RT	1.94	0.13	2.22	1.07
37	FI	1.94	0.04	1.58	1.31
38	WV	1.94	0.05	1.62	1.28
39	CW	1.94	0.07	1.67	1.22
40	HW	1.93	0.07	1.91	1.19
41	FP	1.93	0.08	1.59	1.25
42	YK	1.93	0.19	1.94	1.10
43	FC	1.93	0.08	1.57	1.24
44	FV	1.92	0.06	1.59	1.26
45	WH	1.92	0.07	1.69	1.20
46	LF	1.90	0.03	1.58	1.28
47	RC	1.89	0.16	2.10	1.02
48	FH	1.89	0.07	1.68	1.20
49	FT	1.89	0.07	1.56	1.19
50	WR	1.87	0.10	1.73	1.12
51	FK	1.86	0.13	1.49	1.16
52	KY	1.85	0.15	1.80	1.14
53	KL	1.84	0.13	1.99	1.05
54	RV	1.84	0.13	2.13	1.01
55	YR	1.84	0.12	1.90	1.07
56	MW	1.83	0.03	1.69	1.23
57	WT	1.83	0.05	1.59	1.22
58	KT	1.82	0.16	1.89	1.05
59	WI	1.81	0.02	1.64	1.25
60	WL	1.81	0.02	1.60	1.23
61	RH	1.80	0.12	1.91	1.14
62	ST	1.80	0.10	2.25	1.08
63	WS	1.80	0.05	1.53	1.20
64	II	1.79	0.04	2.02	1.10
65	WP	1.77	0.04	1.65	1.15
66	IK	1.77	0.10	2.08	1.02
67	SR	1.77	0.11	2.02	1.03
68	RS	1.76	0.11	2.02	1.03
69	HK	1.76	0.12	1.93	1.10
70	TY	1.76	0.06	1.95	1.09
71	AW	1.76	0.04	1.97	1.07
72	KP	1.76	0.12	2.00	1.01
73	YI	1.76	0.04	1.92	1.11
74	RP	1.75	0.10	2.13	1.01
75	KI	1.75	0.10	1.89	1.03
76	KV	1.75	0.11	1.93	1.02
77	PK	1.75	0.12	2.10	0.99
78	RM	1.74	0.08	2.11	1.02
79	VR	1.73	0.08	2.10	1.01
80	VY	1.73	0.05	2.11	1.05
81	HF	1.73	0.04	1.58	1.17
82	SH	1.73	0.10	1.98	1.16
83	LI	1.72	0.03	1.86	1.08
84	LK	1.72	0.08	1.99	1.01
85	RI	1.72	0.07	1.92	1.04
86	GF	1.72	0.05	1.84	1.05

87	FQ	1.71	0.04	1.71	1.11
88	VV	1.71	0.04	2.22	1.03
89	SY	1.71	0.05	1.87	1.13
90	NW	1.71	0.04	1.87	1.10
91	RY	1.71	0.07	1.72	1.11
92	RL	1.71	0.06	1.95	1.01
93	LL	1.70	0.02	2.01	1.07
94	QF	1.70	0.04	1.84	1.09
95	HI	1.70	0.04	2.17	1.06
96	WG	1.69	0.04	1.72	1.07
97	RG	1.69	0.09	2.05	0.98
98	GA	1.69	0.07	2.36	0.94
99	KM	1.69	0.08	1.88	1.01
100	GW	1.68	0.04	1.85	1.08
101	VK	1.68	0.08	1.98	1.01
102	CR	1.68	0.07	1.96	1.00
103	SS	1.68	0.06	1.97	1.08
104	CL	1.68	0.03	2.09	1.02
105	NF	1.67	0.04	1.87	1.06
106	VI	1.67	0.03	2.03	1.03
107	TR	1.66	0.07	1.94	1.03
108	YY	1.66	0.03	1.79	1.14
109	CI	1.66	0.03	2.04	1.03
110	FA	1.66	0.03	1.66	1.09
111	PL	1.65	0.03	2.05	1.03
112	KR	1.65	0.09	2.11	0.98
113	YM	1.65	0.03	1.85	1.10
114	MR	1.65	0.05	2.01	0.99
115	SC	1.65	0.05	1.99	1.02
116	MY	1.64	0.03	1.85	1.06
117	IP	1.64	0.03	2.03	1.03
118	HS	1.64	0.05	1.94	1.08
119	YC	1.64	0.03	1.91	1.05
120	FN	1.64	0.03	1.66	1.07
121	WA	1.64	0.02	1.64	1.08
122	IR	1.64	0.05	1.83	0.99
123	KQ	1.64	0.07	1.99	1.01
124	LY	1.63	0.02	1.91	1.08
125	KA	1.63	0.07	1.97	0.98
126	CM	1.63	0.03	2.15	1.01
127	TS	1.63	0.04	1.87	1.09
128	TK	1.63	0.06	1.95	1.02
129	RR	1.63	0.07	2.09	0.98
130	MK	1.63	0.06	1.88	1.00
131	CT	1.63	0.04	2.01	1.02
132	IS	1.62	0.03	2.01	1.02
133	HC	1.62	0.04	2.04	1.05
134	HY	1.62	0.03	1.86	1.10
135	WQ	1.62	0.02	1.59	1.10
136	PY	1.62	0.03	1.90	1.08
137	YP	1.62	0.03	1.85	1.03
138	SL	1.62	0.03	2.03	1.03
139	PI	1.61	0.03	1.92	1.04
140	LH	1.61	0.02	2.09	1.04
141	CV	1.61	0.03	2.03	1.01
142	GK	1.61	0.06	2.03	0.96
143	LP	1.61	0.02	1.98	1.01
144	TH	1.61	0.04	1.94	1.08
145	TI	1.61	0.03	2.10	1.01
146	LR	1.61	0.04	1.88	1.00
147	RK	1.60	0.07	1.98	0.99
148	AF	1.60	0.02	1.72	1.03
149	KG	1.60	0.06	1.88	0.98
150	LC	1.60	0.02	1.91	1.02
151	LA	1.60	0.03	2.26	0.98
152	CH	1.60	0.03	2.06	1.05
153	IV	1.60	0.02	1.94	1.04
154	FG	1.59	0.03	1.60	1.07
155	ML	1.59	0.02	2.04	1.01
156	CS	1.59	0.03	1.96	1.01
157	CY	1.59	0.02	1.70	1.09
158	IT	1.59	0.02	1.94	1.02
159	KN	1.59	0.05	1.95	1.00
160	SM	1.59	0.03	2.07	0.97
161	KC	1.59	0.05	1.67	1.02
162	AK	1.58	0.05	1.96	0.98
163	YT	1.58	0.03	1.75	1.08
164	VL	1.58	0.02	1.90	1.02
165	TT	1.58	0.03	1.94	1.04
166	IC	1.58	0.02	1.88	1.02
167	CK	1.58	0.05	1.79	1.00
168	YH	1.58	0.02	1.67	1.09
169	VT	1.58	0.03	1.96	1.01
170	KK	1.58	0.06	1.79	0.99
171	TM	1.57	0.02	2.08	0.99
172	WN	1.57	0.02	1.64	1.09
173	TC	1.57	0.03	1.90	1.01
174	LV	1.57	0.02	1.92	1.02
175	TV	1.57	0.02	1.95	1.03
176	YL	1.57	0.01	1.72	1.06
177	LT	1.57	0.02	1.98	1.01
178	MA	1.56	0.02	2.19	0.96

179	TP	1.56	0.03	2.06	1.01	**225**	PG	1.51	0.02	2.05	0.97
180	KD	1.56	0.06	2.07	1.06	**226**	GG	1.51	0.03	1.94	0.93
181	YV	1.56	0.02	1.78	1.06	**227**	MI	1.51	0.01	1.90	0.99
182	RA	1.56	0.04	1.85	0.98	**228**	MV	1.51	0.01	2.05	0.98
183	HR	1.56	0.04	1.73	1.05	**229**	PM	1.51	0.01	1.97	0.98
184	NK	1.56	0.05	2.02	0.99	**230**	QC	1.51	0.02	2.12	0.99
185	YG	1.56	0.03	1.97	1.01	**231**	YA	1.51	0.02	1.86	1.01
186	QS	1.56	0.03	2.37	0.99	**232**	YS	1.51	0.02	1.59	1.09
187	GP	1.56	0.03	2.12	0.99	**233**	VM	1.51	0.01	1.91	0.99
188	LM	1.56	0.01	1.92	1.01	**234**	YQ	1.50	0.02	1.90	1.02
189	IA	1.56	0.02	2.08	0.98	**235**	AM	1.50	0.01	2.04	0.97
190	WE	1.56	0.03	1.74	1.06	**236**	QT	1.50	0.02	2.13	1.00
191	MM	1.55	0.02	2.02	1.01	**237**	HH	1.50	0.02	1.80	1.06
192	TA	1.55	0.03	2.05	0.99	**238**	RQ	1.50	0.02	1.86	1.01
193	PC	1.55	0.02	1.92	1.00	**239**	GT	1.50	0.02	1.98	1.00
194	PT	1.55	0.02	2.05	1.01	**240**	SN	1.49	0.02	1.96	1.02
195	QW	1.55	0.02	1.83	1.05	**241**	AG	1.49	0.02	1.89	0.96
196	MH	1.55	0.02	2.09	1.03	**242**	HA	1.49	0.02	1.92	1.00
197	IL	1.55	0.01	1.78	1.03	**243**	AI	1.49	0.01	1.99	0.97
198	MP	1.54	0.02	2.10	0.99	**244**	HG	1.49	0.02	1.90	1.01
199	TG	1.54	0.03	2.05	1.00	**245**	LQ	1.49	0.01	2.05	0.99
200	AC	1.54	0.02	2.07	0.97	**246**	QG	1.49	0.02	2.10	0.98
201	VP	1.54	0.02	1.94	1.01	**247**	NL	1.49	0.01	2.10	0.99
202	IM	1.54	0.01	1.93	1.02	**248**	IH	1.49	0.01	1.77	1.04
203	AQ	1.54	0.03	2.24	0.97	**249**	FD	1.49	0.02	1.62	1.06
204	WD	1.54	0.03	1.66	1.10	**250**	KE	1.49	0.03	1.91	1.05
205	RD	1.54	0.05	2.07	1.07	**251**	AL	1.48	0.01	1.95	0.98
206	SV	1.54	0.02	1.94	1.01	**252**	VS	1.48	0.01	1.77	1.01
207	CG	1.54	0.03	1.97	0.98	**253**	VC	1.48	0.01	1.82	1.00
208	GC	1.54	0.03	2.08	0.98	**254**	YN	1.48	0.01	1.89	1.01
209	VH	1.53	0.02	1.93	1.06	**255**	AP	1.48	0.01	1.96	0.99
210	MS	1.53	0.02	1.97	0.98	**256**	LS	1.48	0.01	1.74	1.01
211	CC	1.53	0.02	1.77	1.01	**257**	GL	1.48	0.01	1.93	0.97
212	PS	1.53	0.02	1.93	1.01	**258**	CQ	1.48	0.01	2.05	0.99
213	IY	1.53	0.01	1.73	1.06	**259**	SP	1.48	0.01	1.80	1.00
214	HL	1.53	0.01	2.02	1.03	**260**	CA	1.48	0.01	1.88	0.98
215	TQ	1.53	0.02	2.11	1.00	**261**	NI	1.48	0.01	2.04	1.00
216	QK	1.53	0.03	1.97	1.00	**262**	TL	1.47	0.01	1.76	1.00
217	RE	1.53	0.04	2.10	1.06	**263**	AH	1.47	0.01	2.01	1.01
218	PV	1.52	0.02	1.95	1.02	**264**	AD	1.47	0.02	2.16	0.98
219	PP	1.52	0.02	1.90	1.01	**265**	GI	1.47	0.01	1.90	0.99
220	SI	1.52	0.02	1.79	1.01	**266**	SA	1.47	0.01	1.81	1.00
221	CP	1.52	0.02	1.90	1.01	**267**	MC	1.47	0.01	1.83	0.98
222	AA	1.52	0.02	1.99	0.94	**268**	AV	1.47	0.01	1.89	0.98
223	AR	1.52	0.03	1.89	0.98	**269**	QY	1.47	0.01	2.05	1.01
224	PR	1.52	0.03	1.83	0.98	**270**	PQ	1.47	0.01	2.03	1.00

271	HT	1.47	0.01	1.76	1.03
272	GS	1.47	0.01	1.86	1.00
273	VA	1.47	0.01	1.89	0.98
274	NG	1.46	0.02	1.98	0.99
275	LG	1.46	0.01	1.83	0.98
276	AY	1.46	0.01	1.87	1.00
277	GR	1.46	0.02	1.80	0.97
278	TN	1.46	0.01	1.96	1.00
279	NY	1.46	0.01	1.98	1.02
280	RN	1.46	0.02	1.80	0.99
281	NR	1.46	0.02	1.88	0.98
282	HM	1.46	0.01	1.77	1.04
283	GQ	1.46	0.01	2.00	0.97
284	DA	1.46	0.02	2.17	0.97
285	HP	1.45	0.01	1.83	0.99
286	DF	1.45	0.01	1.81	1.02
287	GN	1.45	0.01	1.96	0.98
288	GV	1.45	0.01	1.86	0.99
289	EA	1.45	0.02	2.23	0.95
290	MT	1.45	0.01	1.83	0.99
291	QH	1.45	0.01	2.05	1.02
292	QP	1.45	0.01	2.08	0.99
293	LD	1.45	0.01	2.09	1.00
294	PE	1.45	0.02	2.22	0.97
295	QA	1.44	0.01	1.95	0.97
296	PN	1.44	0.01	1.93	0.99
297	HN	1.44	0.01	1.89	1.02
298	MN	1.44	0.01	2.00	0.97
299	HV	1.44	0.01	1.72	1.04
300	QN	1.44	0.01	2.06	1.00
301	NS	1.44	0.01	1.87	1.01
302	QR	1.44	0.01	1.83	0.98
303	VQ	1.44	0.01	1.99	0.98
304	NA	1.44	0.01	1.92	0.97
305	PA	1.44	0.01	1.86	0.98
306	QI	1.43	0.01	1.98	0.99
307	IN	1.43	0.01	1.93	0.99
308	CE	1.43	0.01	2.11	0.98
309	HQ	1.43	0.01	1.83	1.04
310	NV	1.43	0.01	1.92	0.99
311	VN	1.43	0.01	1.94	0.98
312	NM	1.43	0.01	2.00	0.97
313	SD	1.43	0.01	1.98	1.02
314	VG	1.43	0.01	1.78	0.98
315	VD	1.43	0.01	1.98	0.99
316	AT	1.42	0.01	1.79	1.00
317	QM	1.42	0.01	2.00	0.99
318	IQ	1.42	0.01	1.90	0.99
319	FE	1.42	0.01	1.52	1.06
320	PH	1.42	0.01	1.66	1.06
321	NN	1.42	0.01	1.97	1.00
322	CN	1.42	0.01	1.86	0.98
323	QD	1.42	0.01	2.09	1.01
324	TE	1.41	0.01	1.99	1.02
325	GM	1.41	0.01	1.83	0.97
326	SG	1.41	0.01	1.72	1.00
327	TD	1.41	0.01	1.89	1.02
328	QV	1.41	0.01	1.91	1.00
329	GH	1.41	0.01	1.81	1.01
330	AE	1.41	0.01	1.98	0.97
331	AN	1.41	0.01	1.80	0.98
332	HD	1.40	0.01	1.96	1.04
333	EM	1.40	0.01	2.20	0.97
334	HE	1.40	0.01	1.97	1.03
335	LN	1.40	0.00	1.85	0.98
336	GD	1.40	0.01	1.91	0.98
337	NC	1.40	0.01	1.86	0.99
338	DL	1.40	0.01	2.09	0.99
339	ER	1.40	0.01	1.91	1.00
340	GY	1.40	0.00	1.72	0.99
341	EV	1.39	0.01	2.07	0.98
342	DW	1.39	0.01	1.72	1.03
343	DV	1.39	0.01	2.00	0.99
344	ES	1.39	0.01	2.03	0.98
345	EF	1.39	0.01	1.71	0.99
346	NE	1.39	0.01	2.09	0.97
347	QQ	1.39	0.01	1.96	0.99
348	QL	1.39	0.00	1.84	0.99
349	EG	1.39	0.01	2.01	0.96
350	YD	1.39	0.01	1.75	1.02
351	SQ	1.38	0.00	1.76	1.00
352	ND	1.38	0.01	1.99	1.00
353	QE	1.38	0.01	2.00	1.02
354	NH	1.38	0.00	1.83	1.04
355	DP	1.38	0.01	2.00	0.96
356	EW	1.38	0.00	1.76	1.01
357	AS	1.37	0.00	1.67	1.00
358	YE	1.37	0.00	1.69	1.03
359	NT	1.37	0.00	1.76	1.01
360	VE	1.37	0.00	1.90	0.98
361	MG	1.37	0.00	1.70	0.95
362	MQ	1.37	0.00	1.77	0.99

363	DD	1.36	0.01	2.04	0.98
364	LE	1.36	0.00	1.85	1.00
365	IE	1.36	0.00	1.85	0.98
366	EY	1.36	0.00	1.95	1.00
367	PD	1.36	0.00	1.78	0.99
368	MD	1.35	0.00	1.85	0.98
369	IG	1.35	0.00	1.64	0.97
370	DR	1.35	0.00	1.80	1.00
371	EL	1.35	0.00	1.98	0.98
372	DS	1.35	0.00	1.86	1.00
373	ED	1.35	0.00	2.03	0.97
374	ID	1.34	0.00	1.70	1.00
375	DI	1.34	0.00	1.88	0.98
376	DN	1.34	0.00	1.98	0.96
377	DT	1.34	0.00	1.80	1.00
378	DK	1.34	0.00	1.73	1.01
379	DH	1.34	0.00	1.93	1.01
380	NP	1.34	0.00	1.73	0.95
381	DC	1.34	0.00	1.88	0.99
382	EI	1.33	0.00	1.87	0.98
383	NQ	1.33	0.00	1.75	0.99
384	DY	1.33	0.00	1.85	1.00
385	EH	1.33	0.00	1.91	1.01
386	DM	1.33	0.00	1.87	0.96
387	DG	1.33	0.00	1.74	0.98
388	GE	1.33	0.00	1.75	0.97
389	CD	1.33	0.00	1.74	0.99
390	ET	1.32	0.00	1.76	0.98
391	EQ	1.31	0.00	1.82	0.99
392	EE	1.31	0.00	1.92	0.98
393	DQ	1.31	0.00	1.81	0.99
394	SE	1.31	0.00	1.71	1.01
395	EP	1.31	0.00	1.80	0.96
396	DE	1.29	0.00	1.86	0.96
397	EN	1.28	0.00	1.74	0.97
398	EC	1.28	0.00	1.76	0.95
399	ME	1.28	0.00	1.66	0.98
400	EK	1.28	0.00	1.61	0.99

Appendix 28. Top AP_{total}, AP_{oct}, AP_{DFF} and AP_{dip} from co-assembled DFF with dipeptide in biphasic medium

	Dip	AP_{total}	AP_{oct}	AP_{DFF}	AP_{dip}
1	KW	1.85	1.25	1.34	1.23
2	TW	1.83	1.30	1.34	1.24
3	WW	1.80	1.28	1.29	1.34
4	SW	1.78	1.30	1.38	1.25
5	WS	1.77	1.29	1.31	1.24
6	KF	1.76	1.31	1.36	1.17
7	WF	1.76	1.28	1.28	1.32
8	FW	1.73	1.29	1.28	1.30
9	FY	1.73	1.29	1.30	1.25
10	FF	1.72	1.26	1.33	1.30
11	RF	1.70	1.28	1.36	1.14
12	IW	1.70	1.33	1.38	1.24
13	WI	1.69	1.29	1.35	1.22
14	WL	1.69	1.31	1.33	1.21
15	FI	1.68	1.31	1.36	1.22
16	VW	1.68	1.33	1.34	1.22
17	YY	1.68	1.30	1.29	1.25
18	HW	1.67	1.28	1.30	1.26
19	SF	1.67	1.34	1.33	1.19
20	YR	1.67	1.32	1.42	1.09
21	CF	1.66	1.33	1.40	1.22
22	WC	1.66	1.32	1.30	1.18
23	WT	1.66	1.25	1.29	1.20
24	WY	1.65	1.28	1.25	1.25
25	RW	1.65	1.25	1.30	1.17
26	HF	1.65	1.29	1.30	1.21
27	YW	1.65	1.26	1.29	1.25
28	WR	1.64	1.27	1.31	1.15
29	FL	1.63	1.30	1.38	1.20
30	FM	1.63	1.29	1.37	1.18
31	YV	1.63	1.30	1.33	1.15
32	YF	1.63	1.25	1.27	1.26
33	CW	1.62	1.29	1.28	1.20
34	WD	1.62	1.33	1.39	1.11
35	FH	1.61	1.27	1.26	1.18
36	KY	1.61	1.25	1.35	1.13
37	TY	1.60	1.28	1.35	1.16
38	WV	1.60	1.25	1.30	1.19
39	FC	1.60	1.28	1.32	1.16
40	LY	1.60	1.28	1.34	1.15
41	YT	1.59	1.27	1.33	1.13
42	WA	1.59	1.31	1.36	1.09
43	FS	1.58	1.26	1.24	1.12
44	IF	1.58	1.27	1.34	1.20
45	CY	1.58	1.26	1.35	1.14
46	SY	1.58	1.29	1.36	1.16
47	PW	1.57	1.23	1.28	1.16
48	WM	1.57	1.24	1.30	1.18
49	PY	1.57	1.27	1.37	1.17
50	MW	1.57	1.29	1.32	1.18
51	LK	1.57	1.33	1.40	1.04
52	YK	1.56	1.25	1.40	1.09
53	WG	1.56	1.29	1.31	1.08
54	VF	1.56	1.27	1.30	1.18
55	FR	1.56	1.25	1.30	1.07
56	PF	1.56	1.29	1.32	1.19
57	TF	1.56	1.27	1.29	1.16
58	HI	1.56	1.31	1.37	1.14
59	WH	1.56	1.24	1.26	1.14
60	YI	1.55	1.23	1.30	1.18
61	QW	1.54	1.30	1.34	1.12
62	YS	1.54	1.22	1.34	1.13
63	KH	1.54	1.27	1.52	1.13
64	WK	1.54	1.25	1.26	1.13
65	KI	1.54	1.31	1.36	1.07
66	MF	1.53	1.32	1.33	1.19
67	RL	1.53	1.25	1.40	1.04
68	LW	1.53	1.27	1.31	1.18
69	TT	1.53	1.33	1.54	1.07
70	FT	1.53	1.25	1.28	1.14
71	KV	1.52	1.31	1.40	1.04
72	HV	1.52	1.30	1.37	1.10
73	VY	1.52	1.32	1.34	1.15
74	AW	1.51	1.22	1.32	1.10
75	YP	1.51	1.29	1.29	1.10
76	FK	1.51	1.27	1.30	1.08
77	WP	1.51	1.22	1.28	1.12
78	RY	1.51	1.26	1.37	1.10
79	IY	1.51	1.28	1.34	1.15
80	RT	1.51	1.28	1.55	1.04
81	LL	1.51	1.29	1.42	1.14
82	YL	1.51	1.25	1.34	1.15
83	SH	1.50	1.25	1.43	1.15
84	MP	1.50	1.32	1.40	1.08
85	IV	1.50	1.30	1.35	1.10

86	NW	1.50	1.27	1.32	1.17	**132**	KS	1.45	1.28	1.45	1.04
87	FN	1.50	1.32	1.33	1.07	**133**	LP	1.45	1.22	1.36	1.13
88	IH	1.50	1.29	1.35	1.12	**134**	PI	1.45	1.21	1.35	1.12
89	SI	1.50	1.29	1.38	1.07	**135**	TH	1.45	1.28	1.49	1.09
90	VV	1.50	1.27	1.40	1.12	**136**	CI	1.45	1.27	1.31	1.08
91	ST	1.50	1.29	1.50	1.08	**137**	PM	1.45	1.24	1.33	1.06
92	FV	1.49	1.28	1.26	1.12	**138**	NF	1.45	1.30	1.32	1.08
93	AF	1.49	1.24	1.36	1.08	**139**	SK	1.45	1.23	1.45	1.04
94	TS	1.49	1.26	1.49	1.07	**140**	MY	1.45	1.28	1.29	1.12
95	SL	1.49	1.30	1.35	1.08	**141**	YC	1.45	1.28	1.28	1.11
96	RI	1.49	1.28	1.38	1.03	**142**	FA	1.44	1.28	1.31	1.06
97	HY	1.49	1.27	1.36	1.10	**143**	CL	1.44	1.29	1.33	1.08
98	LC	1.49	1.27	1.35	1.08	**144**	IC	1.44	1.24	1.30	1.07
99	RC	1.49	1.31	1.43	1.02	**145**	HR	1.44	1.29	1.46	1.07
100	HT	1.49	1.33	1.49	1.08	**146**	FP	1.44	1.25	1.29	1.07
101	PS	1.49	1.29	1.37	1.05	**147**	HC	1.44	1.28	1.37	1.07
102	WQ	1.48	1.27	1.29	1.09	**148**	VS	1.44	1.28	1.32	1.06
103	YM	1.48	1.27	1.30	1.12	**149**	CC	1.44	1.29	1.33	1.06
104	LI	1.48	1.28	1.35	1.14	**150**	IS	1.44	1.31	1.33	1.07
105	SS	1.48	1.29	1.46	1.09	**151**	GY	1.44	1.31	1.46	1.02
106	PC	1.48	1.27	1.33	1.07	**152**	MV	1.44	1.27	1.32	1.07
107	WN	1.48	1.24	1.31	1.08	**153**	KM	1.44	1.29	1.39	1.02
108	VT	1.48	1.28	1.39	1.05	**154**	VC	1.43	1.24	1.35	1.07
109	CH	1.48	1.29	1.38	1.06	**155**	LH	1.43	1.26	1.31	1.09
110	RH	1.48	1.26	1.51	1.09	**156**	KT	1.43	1.23	1.43	1.05
111	TK	1.47	1.30	1.51	1.03	**157**	CM	1.43	1.26	1.36	1.07
112	HP	1.47	1.27	1.40	1.05	**158**	LR	1.43	1.29	1.37	1.00
113	KL	1.47	1.22	1.33	1.06	**159**	TR	1.43	1.29	1.47	1.02
114	RS	1.47	1.29	1.51	1.04	**160**	TL	1.42	1.24	1.34	1.06
115	LF	1.47	1.31	1.33	1.16	**161**	VH	1.42	1.25	1.30	1.08
116	MH	1.47	1.28	1.42	1.08	**162**	PV	1.42	1.29	1.35	1.09
117	YH	1.47	1.25	1.30	1.13	**163**	GF	1.42	1.27	1.32	1.08
118	GW	1.47	1.23	1.31	1.05	**164**	HL	1.42	1.27	1.30	1.07
119	FQ	1.47	1.29	1.32	1.09	**165**	PR	1.42	1.25	1.34	1.00
120	PT	1.46	1.33	1.41	1.04	**166**	VM	1.42	1.28	1.32	1.08
121	FG	1.46	1.28	1.29	1.07	**167**	VL	1.42	1.27	1.34	1.11
122	RV	1.46	1.31	1.39	1.03	**168**	LT	1.42	1.27	1.34	1.05
123	CP	1.46	1.24	1.33	1.07	**169**	PH	1.42	1.27	1.30	1.08
124	KC	1.46	1.24	1.37	1.04	**170**	LM	1.42	1.29	1.38	1.06
125	PP	1.46	1.23	1.36	1.10	**171**	TI	1.42	1.33	1.33	1.04
126	ML	1.46	1.27	1.36	1.09	**172**	II	1.42	1.28	1.34	1.10
127	SV	1.46	1.28	1.34	1.06	**173**	SR	1.42	1.26	1.44	1.02
128	RM	1.46	1.31	1.39	1.03	**174**	PK	1.41	1.24	1.33	1.02
129	KP	1.46	1.28	1.37	1.03	**175**	SC	1.41	1.26	1.35	1.03
130	MM	1.46	1.31	1.38	1.05	**176**	WE	1.41	1.26	1.32	1.08
131	LS	1.46	1.27	1.35	1.05	**177**	CV	1.41	1.28	1.31	1.06

178	VI	1.41	1.25	1.34	1.11	**224**	CK	1.36	1.24	1.34	1.01
179	IR	1.41	1.25	1.32	1.02	**225**	YA	1.36	1.28	1.32	1.03
180	MK	1.41	1.25	1.37	1.00	**226**	VG	1.36	1.25	1.41	1.00
181	IL	1.41	1.22	1.32	1.08	**227**	RR	1.36	1.24	1.50	0.99
182	MS	1.40	1.26	1.38	1.02	**228**	AL	1.36	1.26	1.41	1.00
183	CS	1.40	1.27	1.35	1.05	**229**	SA	1.36	1.30	1.50	1.01
184	TP	1.40	1.23	1.33	1.05	**230**	CT	1.35	1.27	1.30	1.03
185	RP	1.40	1.26	1.39	1.00	**231**	KG	1.35	1.27	1.45	0.98
186	GI	1.40	1.28	1.41	1.00	**232**	KD	1.35	1.28	1.49	1.08
187	TV	1.40	1.24	1.36	1.05	**233**	RA	1.35	1.30	1.47	0.99
188	SM	1.39	1.26	1.39	1.01	**234**	CR	1.35	1.28	1.32	0.98
189	SP	1.39	1.26	1.31	1.04	**235**	KN	1.35	1.28	1.48	1.01
190	KA	1.39	1.31	1.49	0.99	**236**	YQ	1.35	1.24	1.30	1.05
191	KQ	1.39	1.29	1.55	1.01	**237**	TD	1.35	1.32	1.53	1.02
192	IP	1.39	1.29	1.30	1.07	**238**	LN	1.34	1.24	1.39	1.00
193	IM	1.38	1.27	1.32	1.08	**239**	TA	1.34	1.24	1.49	1.00
194	FD	1.38	1.25	1.32	1.07	**240**	IA	1.34	1.26	1.40	0.99
195	QF	1.38	1.27	1.29	1.08	**241**	GL	1.34	1.25	1.41	0.99
196	MC	1.38	1.23	1.31	1.03	**242**	KR	1.34	1.30	1.46	1.00
197	EW	1.38	1.31	1.34	1.03	**243**	DF	1.34	1.26	1.34	1.03
198	PL	1.38	1.27	1.32	1.13	**244**	ID	1.34	1.27	1.40	1.00
199	MI	1.38	1.28	1.31	1.07	**245**	MG	1.34	1.30	1.44	0.97
200	CG	1.38	1.28	1.42	0.99	**246**	SN	1.34	1.28	1.48	1.02
201	TM	1.38	1.27	1.37	1.02	**247**	NM	1.34	1.33	1.47	0.99
202	IT	1.37	1.28	1.31	1.04	**248**	AV	1.34	1.24	1.43	0.99
203	QL	1.37	1.28	1.44	1.01	**249**	QV	1.34	1.29	1.42	1.00
204	HM	1.37	1.25	1.34	1.07	**250**	CE	1.34	1.34	1.54	0.99
205	FE	1.37	1.23	1.33	1.06	**251**	IE	1.34	1.29	1.45	0.99
206	NI	1.37	1.32	1.45	1.01	**252**	VR	1.33	1.23	1.33	1.01
207	YN	1.37	1.30	1.40	1.01	**253**	GA	1.33	1.29	1.50	0.94
208	IK	1.37	1.26	1.28	1.01	**254**	IQ	1.33	1.24	1.35	1.03
209	LV	1.37	1.23	1.33	1.06	**255**	AK	1.33	1.27	1.49	0.98
210	VK	1.37	1.23	1.31	1.01	**256**	YG	1.33	1.24	1.30	1.02
211	KK	1.37	1.25	1.46	1.00	**257**	NR	1.33	1.29	1.53	0.99
212	SD	1.37	1.31	1.60	1.04	**258**	QY	1.33	1.30	1.38	1.03
213	RG	1.36	1.28	1.47	0.99	**259**	VE	1.33	1.29	1.45	1.01
214	NY	1.36	1.25	1.41	1.04	**260**	IG	1.33	1.25	1.36	1.00
215	MT	1.36	1.24	1.34	1.01	**261**	TN	1.33	1.32	1.46	1.02
216	DW	1.36	1.28	1.29	1.04	**262**	NV	1.33	1.28	1.43	1.00
217	AG	1.36	1.30	1.55	0.95	**263**	PG	1.33	1.22	1.39	0.99
218	HK	1.36	1.24	1.36	1.06	**264**	GK	1.33	1.27	1.49	0.97
219	TG	1.36	1.30	1.52	1.00	**265**	AD	1.32	1.30	1.54	0.99
220	VP	1.36	1.25	1.28	1.07	**266**	HH	1.32	1.28	1.41	1.06
221	HS	1.36	1.30	1.44	1.07	**267**	GP	1.32	1.27	1.41	0.99
222	TC	1.36	1.24	1.31	1.02	**268**	GS	1.32	1.24	1.47	0.99
223	MR	1.36	1.25	1.38	0.99	**269**	AP	1.32	1.23	1.39	1.00

270	AY	1.32	1.26	1.35	1.02	**316**	AA	1.29	1.25	1.44	0.94
271	LG	1.32	1.23	1.34	0.99	**317**	CQ	1.29	1.24	1.38	0.98
272	HA	1.32	1.21	1.46	1.01	**318**	PQ	1.29	1.26	1.35	1.00
273	VN	1.32	1.28	1.40	1.02	**319**	MD	1.29	1.27	1.46	0.99
274	VA	1.32	1.27	1.39	0.99	**320**	HD	1.29	1.29	1.49	1.04
275	KE	1.31	1.26	1.44	1.07	**321**	VD	1.29	1.26	1.38	1.00
276	EF	1.31	1.24	1.33	1.04	**322**	EV	1.28	1.31	1.50	0.97
277	LA	1.31	1.24	1.35	0.99	**323**	YE	1.28	1.28	1.31	1.03
278	AI	1.31	1.28	1.35	1.01	**324**	AH	1.28	1.25	1.45	1.00
279	NT	1.31	1.30	1.51	1.02	**325**	RD	1.28	1.22	1.39	1.05
280	CA	1.31	1.27	1.39	0.98	**326**	QS	1.28	1.27	1.45	1.01
281	GV	1.31	1.23	1.39	0.98	**327**	RQ	1.28	1.25	1.39	1.02
282	NL	1.31	1.30	1.38	1.01	**328**	HG	1.28	1.24	1.44	1.00
283	QC	1.31	1.27	1.46	0.99	**329**	AS	1.28	1.23	1.42	0.98
284	TE	1.31	1.28	1.52	1.02	**330**	NC	1.28	1.25	1.38	0.98
285	AC	1.31	1.24	1.42	0.98	**331**	GC	1.28	1.25	1.36	0.98
286	YD	1.31	1.25	1.32	1.03	**332**	GN	1.28	1.29	1.46	0.99
287	QM	1.30	1.28	1.48	0.99	**333**	MQ	1.28	1.24	1.37	1.01
288	PN	1.30	1.25	1.38	1.00	**334**	NP	1.28	1.23	1.37	0.98
289	RK	1.30	1.26	1.41	0.99	**335**	QI	1.28	1.23	1.33	1.01
290	AT	1.30	1.23	1.45	1.01	**336**	AN	1.28	1.26	1.46	0.98
291	GG	1.30	1.25	1.45	0.93	**337**	DS	1.27	1.27	1.51	1.00
292	RN	1.30	1.30	1.43	1.00	**338**	QD	1.27	1.26	1.48	1.03
293	GR	1.30	1.25	1.44	0.98	**339**	MN	1.27	1.25	1.39	0.98
294	LD	1.30	1.23	1.36	1.01	**340**	DQ	1.27	1.32	1.54	1.00
295	GT	1.30	1.27	1.43	1.00	**341**	QT	1.27	1.27	1.46	1.00
296	GM	1.30	1.28	1.42	0.98	**342**	DY	1.27	1.27	1.44	0.99
297	NA	1.30	1.27	1.48	1.00	**343**	ES	1.27	1.26	1.49	0.99
298	CN	1.30	1.23	1.42	0.99	**344**	PE	1.27	1.26	1.37	0.98
299	RE	1.30	1.27	1.44	1.06	**345**	HQ	1.27	1.28	1.42	1.02
300	AQ	1.30	1.26	1.51	0.97	**346**	SG	1.26	1.23	1.35	1.00
301	NH	1.29	1.27	1.49	1.05	**347**	EG	1.26	1.26	1.49	0.96
302	AM	1.29	1.27	1.40	0.99	**348**	DD	1.26	1.28	1.53	0.98
303	QP	1.29	1.28	1.39	0.99	**349**	CD	1.26	1.28	1.37	0.99
304	HN	1.29	1.30	1.43	1.04	**350**	GH	1.26	1.27	1.42	0.99
305	MA	1.29	1.25	1.40	0.96	**351**	IN	1.26	1.24	1.30	1.00
306	NS	1.29	1.25	1.45	1.03	**352**	EC	1.26	1.26	1.48	0.99
307	LQ	1.29	1.25	1.33	1.00	**353**	EP	1.26	1.28	1.43	0.97
308	LE	1.29	1.27	1.37	1.00	**354**	QK	1.26	1.25	1.41	0.99
309	NK	1.29	1.27	1.45	0.99	**355**	QA	1.26	1.28	1.43	0.98
310	QR	1.29	1.32	1.48	0.98	**356**	GQ	1.26	1.24	1.44	0.97
311	PD	1.29	1.25	1.36	0.99	**357**	EL	1.26	1.28	1.42	0.97
312	SE	1.29	1.25	1.49	1.03	**358**	VQ	1.26	1.27	1.34	1.00
313	PA	1.29	1.24	1.39	0.97	**359**	DL	1.25	1.27	1.38	0.99
314	SQ	1.29	1.24	1.43	1.01	**360**	DK	1.25	1.27	1.45	1.01
315	TQ	1.29	1.25	1.44	1.01	**361**	AE	1.25	1.25	1.44	0.97

362	NQ	1.25	1.25	1.46	1.01
363	EK	1.25	1.32	1.50	0.99
364	NN	1.25	1.28	1.44	1.00
365	QQ	1.25	1.30	1.47	1.00
366	DI	1.25	1.23	1.40	0.98
367	DR	1.25	1.31	1.48	1.01
368	DH	1.24	1.29	1.48	1.01
369	HE	1.24	1.24	1.41	1.03
370	ND	1.24	1.29	1.43	1.02
371	ER	1.24	1.29	1.47	1.01
372	NG	1.24	1.27	1.40	0.99
373	DG	1.24	1.25	1.42	0.97
374	DT	1.23	1.24	1.43	1.01
375	EI	1.23	1.23	1.37	0.97
376	EM	1.23	1.23	1.45	0.97
377	QH	1.23	1.23	1.41	1.02
378	DV	1.23	1.29	1.39	0.99
379	DM	1.23	1.26	1.43	0.96
380	QE	1.23	1.22	1.45	1.01
381	DC	1.23	1.27	1.42	0.98
382	DN	1.23	1.27	1.47	0.98
383	GD	1.23	1.29	1.38	0.99
384	GE	1.23	1.23	1.39	0.98
385	AR	1.23	1.25	1.38	0.97
386	ME	1.23	1.22	1.37	0.98
387	DA	1.22	1.24	1.39	0.98
388	EA	1.22	1.27	1.41	0.96
389	ED	1.22	1.25	1.46	0.97
390	QN	1.22	1.26	1.41	1.00
391	QG	1.22	1.26	1.36	0.97
392	DP	1.22	1.24	1.36	0.97
393	NE	1.21	1.24	1.40	1.01
394	DE	1.21	1.26	1.45	0.96
395	EE	1.21	1.31	1.45	0.98
396	EQ	1.21	1.24	1.42	1.00
397	EY	1.21	1.26	1.32	0.99
398	ET	1.21	1.28	1.40	0.97
399	EN	1.20	1.23	1.42	0.96
400	EH	1.19	1.22	1.38	1.00